UNIVERSITY OF SOUTHAMPTON
FACULTY OF PHYSICAL SCIENCES AND ENGINEERING
SCHOOL OF ELECTRONICS AND COMPUTER SCIENCE

Cooperative Communication for Cognitive Radio Networks

by

Wei Liang
B.Sc., M.Sc.

A doctoral thesis submitted in partial fulfilment of the
requirements for the award of Doctor of Philosophy
at the University of Southampton

May 2015

SUPERVISOR:
Dr. Soon Xin NG
PHD, SMIEEE, MIET, CEng, FHEA
and
Professor Lajos Hanzo
FREng, FIEEE, FIEE, DSc, EIC of IEEE Press
Chair of Southampton Wirelss Group
School of Electronics and Computer Science
University of Southampton
Southampton SO17 1BJ
United Kingdom

Dedicated to my family

UNIVERSITY OF SOUTHAMPTON

ABSTRACT

FACULTY OF PHYSICAL SCIENCES AND ENGINEERING
SCHOOL OF ELECTRONICS AND COMPUTER SCIENCE

Doctor of Philosophy

Cooperative Communication for Cognitive Radio Networks

by Wei Liang

A Cooperative Cognitive Radio (CCR) network, which integrates a conventional cooperative system and cognitive radios (CRs) into a holistic system, is a promising paradigm for the next generation mobile communication systems. The spectral efficiency, power efficiency, bandwidth reduction and system complexity in CCR networks are the fundamental parameters of our system design and optimization. In this thesis, we focus our attention on opportunistically exploiting the underutilized spectrum band in the CR network with the aid of cooperative protocols. Furthermore, we invoke channel coding schemes in our CCR system in order to improve the overall system throughput. In our CCR system, the overlay based cooperation scheme of Primary Users (PUs) and Cognitive Users (CUs) is considered, which has the potential of leading to a transmission power reduction and transmission rate improvement for both the PU and the CU. More explicitly, our cooperative protocol allows a group of CUs to serve as Relay Nodes (RNs) for relaying the signal of the PUs' transmitters to the PUs' intended destinations. To elaborate further, both one-way relaying and two-way relaying schemes are used in our proposed system, so that the bandwidth requirement of the PUs is reduced. Alternatively, the freed bandwidth may be leased to a group of CUs for their secondary communications. Our numerical and simulation results show that the bandwidth reduction attained by the proposed two-way relaying based CR scheme may approach as much as 80% of the PU's bandwidth. Moreover, an Adaptive Dynamic Network Coding (ADNC) scheme is also conceived for this overlay CCR system, which is designed for supporting communications between multiple PUs and a common Base Station (BS). More particularly, the near-instantaneously Adaptive Turbo Trellis Coded Modulation (ATTCM) is employed for appropriately adjusting both the modulation mode as well as the channel coding rate and the network coding rate, according to the near-instantaneous channel conditions. In order to facilitate the recovery of the source information at the BS, the CUs invoke the ADNC technique, which is assisted by our cooperative protocol operating by exchanging the CCR-based control information between the near-instantaneously ATTCM and network coding codec as well as between the CUs and the BS. Additionally, the network encoder may also be activated in its adaptive mode for supporting the CUs, depending on the Boolean value of the feedback flags generated based on the success/failure of the ATTCM decoder and of the network decoder, which is evaluated and fed back by the BS. Quantitatively, it was found that the joint holistic design of our ATTCM-ADNC-CCR scheme is either capable of freeing up an approx-

imately 40% of the PU's bandwidth in comparison to its non-cooperative counterpart, or increasing the attainable throughput by as much as 2 bit/symbol. Furthermore, a Pragmatic Distributed Algorithm (PDA) is proposed for supporting the efficient spectral access of multiple PUs and CUs in CCR networks. The novelty of our PDA is that the PUs negotiate with the CUs concerning the specific amount of relaying and transmission time, and the CU will decide either to accept or to decline this offer. These CUs relay the signal received from the PUs to the PUs' receiver, but only when both the PUs' and the CUs' minimum rate requirements are satisfied. Moreover, we show that the cooperative spectral access based on our PDA reaches an equilibrium, when it is repeated for a sufficiently long duration. These benefits are achieved, because the PUs are motivated to cooperate by the incentive of achieving a higher PU rate, whilst defecting from cooperation can be discouraged with the aid of a limited-duration punishment. Therefore, our proposed PDA outperforms the benchmark, despite its significantly lower overhead and lower complexity. Finally, we present the joint design of coding, modulation, user-cooperation and CR techniques, which may lead to significant mutual benefits for both the PUs and the CUs.

Declaration of Authorship

I, **Wei Liang**, declare that the thesis entitled **Cooperative Communication for Cognitive Radio Networks** and the work presented in it are my own and has been generated by me as the result of my own original research. I confirm that:

- This work was done wholly or mainly while in candidature for a research degree at this University;
- Where any part of this thesis has previously been submitted for a degree or any other qualification at this University or any other institution, this has been clearly stated;
- Where I have consulted the published work of others, this is always clearly attributed;
- Where I have quoted from the work of others, the source is always given. With the exception of such quotations, this thesis is entirely my own work;
- I have acknowledged all main sources of help;
- Where the thesis is based on work done by myself jointly with others, I have made clear exactly what was done by others and what I have contributed myself;
- Parts of this work have been published.

Signed: ..... Date: .....

Acknowledgements

First of all, I would like to give the greatest gratitude to both of my supervisors Dr. Soon Xin Ng and Prof. Lajos Hanzo. I really appreciate their generous and insightful guidances as well as wise advices in the past four years of my PhD study, which encourage me to insist on my own career that I passionate about. Thanks for sharing with me about their precious experiences, not only in science, but also in life.

Secondly, I would also like to thank all the other colleagues in Southampton Wireless Group for their help and supports. In particular, I wish to express my appreciation to Dr. Dandan Liang, Dr. Jing Zuo, Dr. Li Li, Dr. Shaoshi Yang and Miss Xuan Li for their kindly help and valuable ecouragement. I am very grateful for the collaboration with Dr. Jiao Feng and Dr. Hung Vietnguyen.

Thirdly, I would like to thank my parents, Dr. Peikang Liang and Ms Jing Li, as well as my parents in law, Mr Yajun Shi and Ms Fendi Yang for their endless love and full support on my PhD study.

Last but not the least, I would like to express my deepest appreciation to my husband, Dr. Jia Shi. Thanks for his love, understanding and support.

List of Publications

Journal Papers

1. **Wei Liang**, Soon Xin Ng and Lajos Hanzo, "Cooperative Communication Between Cognitive and Primary Users", *IET Communications*, Vol. 7, pp. 7-17, November 2013.

2. **Wei Liang**, Soon Xin Ng, Jiao Feng and Lajos Hanzo, "Pragmatic Distributed Algorithm for Spectral Access in Cooperative Cognitive Radio Networks", *IEEE Transactions on Communications*, Vol. 62, pp. 1188-1200, April 2014.

3. **Wei Liang**, Hung Viet nguyen, Soon Xin Ng and Lajos Hanzo, "Adaptive TTCM Aided Near-Instantaneously Dynamic Network Coding for Cooperative Cognitive Radio Networks", *IEEE Transactions on Vehicular Technology*, accepted, March 2015.

Conference Papers

1. **Wei Liang**, Soon Xin Ng and Lajos Hanzo, "TTCM-Aided SDMA-Based Two-Way Relaying", *2011 IEEE Vehicular Technology Conference (VTC2011-Fall)*, 5-8 September, San Francisco, USA.

2. **Wei Liang**, Soon Xin Ng and Lajos Hanzo, "Adaptive Turbo Trellis Coded Modulation Aided Cooperative Cognitive Radio", *2012 IEEE Wireless Communications and Networking Conference (WCNC 2012)* , 1-4 April, Paris, France.

3. **Wei Liang**, Soon Xin Ng, Siavash Bayat, Yonghui Li and Lajos Hanzo, "Opportunistic Spectral Access in Cooperative Cognitive Radio Networks", *2014 IEEE Vehicular Technology Conference (VTC2014-Fall)*, 14-17 September, Vancouver, Canada.

Contents

Glossary

AAF	Amplify-and-Forward
ACM	Adaptive Coded Modulation
ADNC	Adaptive Dynamic Network Code
ATTCM	Adaptive TTCM
AWGN	Additive White Gaussian Noise
BER	Bit Error Ratio
BICM	Bit-Interleaved Coded Modulation
BICM-ID	Iterative-Decoding assisted BICM
BPS	Bit Per Symbol
BS	Base Station
CA	Centralized Algorithm
CAF	Compress-and-Forward
CCMC	Continuous-input Continuous-output Memoryless Channel
CCR	Cooperative Cognitive Radio
CDA	Conventional Distributed Algorithm
CEF	Channel Estimation Factor
CIR	Channel Impulse Response
CM	Coded Modulation
CR	Cognitive Radio
CSI	Channel State Information
CU	Cognitive User
DAF	Decode-and-Forward
DCMC	Discrete-input Continuous-output Memoryless Channel
DMC	Discrete Memoryless Channel
DN	Destination Node

DNCs Dynamic Network Codes

EXIT Extrinsic Information Transfer

FCC Federal Communications Commission
FEC Forwarded Error Correction
FER Frame Error Ratio
FSO Free-Space Optical

GDNC Generalized Dynamic Network Codes

HD Hamming Distance

iBPS Information Bit Per Symbol
IC Interference Cancellation

KKT Karush-Luhn-Tucker

MABC Multiple-Access Broadcast Channel
MAP Maximum-A-Posteriori
MARC Multiple Access Relay Channel
MIMO Multiple-Input Multiple-Output
MISO Multiple-Input-Single-Output
ML Maximum Likelihood
MLSE maximum likelihood sequence estimation
MMSE Minimum Mean-Square Error
MS Mobile Station
MUDs Multi-User Detectors

NC Network Coding

OWR One-Way Relaying

PDA Pragmatic Distributed Algorithm
PSK Phase Shift Keying
PU Primary User

QAM Quadrature Amplitude Modulation

RA Random Algorithm
RD Relay-to-Destination
RDRPR Reduced-Distance-Related-Pathloss-Reduction
RN Relay Node
RSC Recursive Systematic Convolution

SD Source-to-Destination
SDMA Space Division Multiple Access
SER Symbol Error Ratio
SISO Single-Input-Single-Output
SN Source Node
SNR Signal to Noise power Ratio
SP Set Partition
SR Source-to-Relay

TCM Trellis Coded Modulation
TDBC Time Division Broadcast Channel
TS Time-Slot
TTCM Turbo Trellis Coded Modulation
TWR Two-Way Relaying

UL Uplink

WRAN Wireless Regional Area Network

ZF Zero Forcing

List of Symbols

General Conventions

- The superscript $\underline{(.)}$ indicates the symbol sequences.
- The superscript ^{T} is used to indicate matrix transpose operation. Therefore, $\mathbf{a}^T$ represents the transpose of the matrix **a**.
- The superscript ^{H} is used to indicate complex conjugate transpose operation. Therefore, $\mathbf{a}^H$ represents the complex conjugate transpose of the matrix **a**.
- The notation $\hat{x}$ represents the estimate of x.

Mathematical Operators and Functions

$p(\cdot)$:	The probability density function.
$\mathrm{P}(\cdot)$:	The probability.
$W(\cdot)$:	The weight matrix of multiple user detections.
G_{ab}:	The geometrical-gain between node a and node b.
$P(\cdot)$:	The transmit power of PU.
$[\cdot]_{a\times b}$:	The matrix having a rows and b columns.
$\mathcal{M}_{a\times b}$:	The transfer matrix of network decoder having a rows and b columns.
$\mathcal{I}(\cdot)$:	The identity matrix of the transfer matrix $\mathcal{M}$.
$\mathcal{P}(\cdot)$:	The parity matrix of the transfer matrix $\mathcal{M}$.
$C(\cdot)$:	The capacity.
$\eta(\cdot)$:	The average throughput.

$R(\cdot)$: The transmission rate. .

$\Upsilon(\cdot)$: The switching thresholds were designed for ensuring that the BER at the RN becomes lower than a target.

$\exp(\cdot)$: The exponential operation.

$\sum$: The sum operation.

$var[\cdot]$: The variance of a variable.

$\log_2(\cdot)$: Logarithm to base 2.

$\min(\cdot)$: The minimum value among a number of variables.

$\max(\cdot)$: The maximum value among a number of variables.

Specific Symbols

N_d: The number of bits in a dataword..

N_c: The number of bits in a codeword.

M: The modulation level.

L_m: The number of shift-register stages in the TCM encoder.

ω_A: The amplification factor of amplify and forward.

T: The time slot.

W: The Bandwidth.

σ_{ab}: The channel variance.

λ: The wavelength.

ψ: The ratio of transmission power allocated for helping the PU/SN to the total transmission power of the CUs over the bandwidth W_1.

ζ: The passband bandwidth of PSK/QAM modulation.

B_s: The Bandwidth reduction factor.

m_1: The number of information frames transmitted by each of the L PUs.

m_2: The number of parity frames transmitted by each K CUs during the transmission session.

S_f: The feedback flag send from the base station to the CUs.

L_{PU}: or [L] The number of PUs.

L_{CU}: or [K] The number of CUs.

l: The index of PUs.

k: The index of CUs.

$R_{l,req}^{PU}$: The rate requirement of lth PU.

$R_{k,req}^{CU}$: The rate requirement of kth CU.

$\beta_{l,k}$: The time allocation factor.

τ: The step size of time allocation fraction.

$m_{l,k}$: The matching matrix entry.

P_{match}: The relative frequency of successfully matched PUs.

$\epsilon_{l,k}$: The time fraction.

α: The path-loss exponent.

Chapter 1

Introduction

1.1 Historical Perspective on Cooperative Communication for Cognitive Radio

Wireless communications technologies have seen a remarkable evolution throughout the 1990s and 2000s. The new generation of wireless devices has facilitated notable improvements in terms of communication reliability, device size, data rates, battery life and network connectivity. Since the turn of the century, Cognitive Radio (CR) and cooperative communication techniques have been extensively considered in the literature for the sake of efficiently improving the exploitation of the wireless radio resources. In order to solve the spectrum shortage problem, the following two aspects have been investigated [1]:

- Exploration of hitherto unused spectrum, as in mm-wave [2] visible light [3] and Terahertz communications [4].
- Identifying and opportunistically exploiting the " *spectrum holes*[1]" that are momentarily unused by the licensed owners of the spectrum.

Our research aims for investigating a combination of CR techniques with cooperative communication schemes for improving the exploitation of the spectrum. We commence by reviewing the corresponding literature and standard, before our novel solutions are proposed.

In [6], Mitola and Maguire stated that "radio etiquette is the set of RF bands, air interfaces, protocols, and spatial-temporal patterns that moderate the use of radio spectrum. CR extends the

[1] A spectrum hole [5] represents a band of frequencies that are not being used by the primary user of that band at a particular time in a particular geographic area. Moreover, it is also one of several dimensions of a hyperspace (transmission hyperspace, radio spectrum or simply spectral space) of radio signals that is momentarily unoccupied. Note that the dimension of a hyperspace may include the space, temporal, frequency, code or angle of arrival domain [5]. A 'resource hole' may be classified as a: frequency hole, temporal hole, time-frequency hole, space-time-frequency hole, space-frequency hole, etc [5].

software radio with radio-domain model-based reasoning about such etiquette." In wireless communications, CR constitutes a design paradigm for a network or a wireless node, which could change its transmission mode efficiently in order to communicate by avoiding the interference with the licensed user/Primary User (PU) or the unlicensed user/ Cognitive User (CU). Goldsmith *et al.* [7] stated that in the terminology of information theory, the CR is a wireless communication system that intelligently utilizes any available side information about the a) channel conditions, b) codebooks, c) activity, and d) message of other nodes with which it shares the spectrum. Specifically, a CR is a specific type of spectrum sensing assisted cooperative scheme, where the cooperation efficiency critically depends on the amount of knowledge exchange between the CUs and PUs [7]. In Haykin's paper [8], it was stated that a CR constitutes a highly reliable communications device ensuring that the radio spectrum can be efficient exploited.

The radio spectrum is a precious and scarce resource. Numerous wireless communication engineers have made efforts to maximize the exploitation of the radio spectrum. Interestingly, in November 2002, the Federal Communications Commission (FCC) demonstrated that the actual licensed spectrum is largely unoccupied most of the time [9] and hence they planned to reshape the traditional models of spectral allocation and control. Clearly, the static spectrum allocation has resulted in low-efficiency exploitation of the precious spectral resources. Another recent measurement shows that the average spectrum occupancy in the band spanning from 30 MHz to 3 GHz over six cities is 5.2% and that the maximum total spectrum occupancy is 13.1 % in New York City [10]. In order to resolve the contradiction between the static spectrum allocation, and its low real exploitation, opportunistic access of the under-utilized licensed frequency bands has been proposed [10]. Additionally, the CR technique allows users to utilize and share the available spectrum, which is not *fully*[2] occupied in either space, or in time or in fact in the joint space-time domain, in an opportunistic manner. CUs are allowed to detect the available spectrum, adjust to detect the PUs present in the spectrum and to coordinate with other CUs. The architecture of a CR network including both PUs and CUs is shown in Figure 1.1.

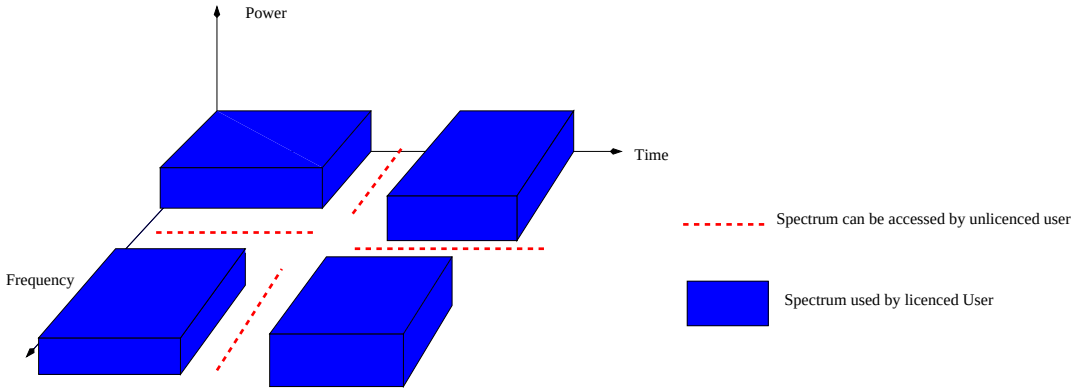

Figure 1.1: The illustration of the spectral-domain white spaces.

[2]The term 'fully' is with respect to the 'radio-temperature' or 'capacity achievable'.

As seen in Figure 1.1, in the CR terminology, PUs have a higher priority or 'legacy rights' for the usage of a specific part of the spectrum. By contrast, the CUs have a lower priority and they should exploit the spectrum without causing interference to PUs. Hence the CUs have to have CR capabilities, including the sensing of the spectrum that has not been occupied by the PUs and may exploit the unused spectrum in order to improve its exploitation. Specifically, an overview of spectrum sensing techniques has been provided in [5, 11]. Moreover, a CR is capable of using or sharing the spectrum in an opportunistic manner, with the aid of a spectrum sharing technique. The family of spectrum sharing techniques enable the CUs to coordinate their access with the primary channel [12], as detailed in Section 1.3.

Cooperative communication [13] relies on the broadcast nature of wireless communications in order to allow the nodes to help each other for the sake of attaining the same advantages as those offered by Multiple-Input Multiple-Output (MIMO) systems. As a benefit, they are capable of improving the attractive communication capacity and transmission integrity. Various cooperative techniques have been widely investigated since the turn of the century. In [14, 15], several classical cooperative protocols were evaluated in terms of their power saving, diversity order and outage probability. The diversity-multiplexing trade-off was quantified in [16]. Specifically, relay selection, optimal resource allocation, as well as network-coded cooperation have been investigated in [17–19]. More explicitly, various half-duplex two-phase cooperative techniques were proposed for recovering the 50% throughput loss experienced by conventional One-Way Relaying (OWR) scheme [20], such as Two-Way Relaying (TWR) [21] and successive relaying [22] systems.

In a nutshell, CR is a novel technology that can potentially improve the exploitation of the radio spectrum and cooperative communications plays a key role in the development of CR networks. The applications of cooperative communication approaches in the context of CR networks have been discussed in [1, 23–30, 30–37]. Cooperative relaying is widely regarded as the key technology in CR networks [38]. The applications of cooperative relaying in CR systems have also been discussed in [23–26]. At the time of writing research efforts are invested in determining the optimum power allocation and in simplifying the relay selection process in cooperative CRs [29–31]. Relay selection techniques have been employed in multiple-relay CR networks with the aim of improving the performance of the second-hop transmission [27, 28]. The main consideration in relay selection and power allocation in CR networks are related to improving the overall spectral efficiency and to the reduction of the interference [29–31]. Additionally, various resource allocation techniques have been conceived for CR-aided wireless networks over the space-, time- and frequency-domain for improving the attractive spectral efficiency [32–34]. Furthermore, diverse spectrum sharing protocols have been combined with TWR in CR networks, where two PUs communicate with each other with the assistance of the CUs acting as the relay [30, 35, 36].

Therefore, cooperative communication aided CR systems may be categorized into the following three types:

- Cooperation among the PUs;
- Cooperation between PUs and CUs [38–41];
- Cooperation among the CU peers [42, 43].

More specifically, the first type is similar to the traditional cooperative communication, while in the third type, a CU may act as a Relay Node (RN) for other CUs, which may have different available spectra [42]. For the second type, the PUs have a higher priority than the CUs, where the CUs may act as RN for the PUs [39]. Another interesting protocol involving simultaneous transmissions of the PUs and CUs has been proposed in [38] for maximizing the overall achievable rate. In this chapter, we commence by review the advances in spectrum sharing of CR networks, specifically focusing on cooperative communications. More explicitly, cooperative communication inspired a range of new design concepts capable of dramatically improving the spectral efficiency of wireless networks.

1.2 Relay Topology and Cooperative Communication Protocols

The concept of relay channels was devised by Van der Meulen in [44], while some relaying protocols were proposed in [45]. In cooperative communication, the link between the Mobile Station (MS) and the Base Station (BS) is imposed by the introduction of a relay channel. The relay node can be thought of as an auxiliary record channel in addition to the direct links between the source and destination nodes. An important aspect of cooperative communication is the processing of the signal received at the RN, which was transmitted from the Source Node (SN) [13].

1.2.1 Topology of Cooperative Communication

In recently years, various relay assisted cooperative communication scenarios have been developed and studied, such as the half-duplex relay channel [46], the relay channel relying on channel coding [47], MIMO-aided relay channel [48–50], multi-node relay channel and TWR channel [51, 52]. In the two-way and multi-way relay channels, the communications take place in more than one directions, which constitutes a new feature in cooperative communications. More explicitly, the attractive TWR scheme of [52] assists a pair of MSs in exchanging their signals with the aid of either a single or several RNs using two transmission periods. The TWR protocol aims for improving both the power efficiency, and the achievable rate with the aid of network coding, superposition coding and hierarchical cooperation [52]. A simple OWR system is shown in Figure 1.2 along with a single RN, where a SN sends its information to its Destination Node (DN) during phase 1, while this information is also received by the RN. In Phase 2, the RN forwards the source information from the SN to the DN. The two-hop communication protocols may also involve multiple RNs between SN and DN, as shown in Figure 1.3. All nodes are operated in half-duplex mode. Normally,

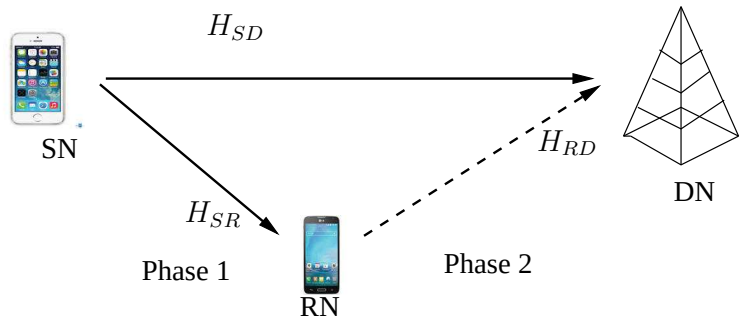

Figure 1.2: The topology of OWR transmission in a cooperative communication network. The "SN" denotes the source node, "RN" is the relay node and "DN" represents the destination node. The channel between SN and RN is represented as H_{SR}, while the SN to DN and the RN to DN channel, by H_{SD} and H_{RD}, respectively.

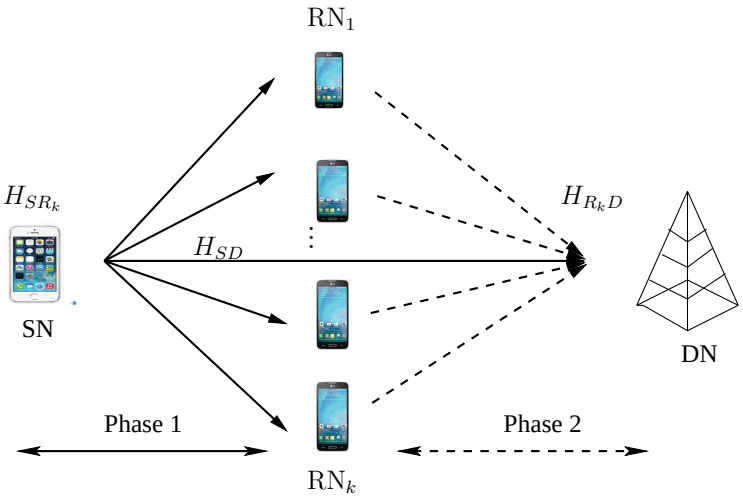

Figure 1.3: The topology of multi-relay transmission in a cooperative communication network. The number of RNs is denoted by K, where $k \in \{1, \cdots, K\}$.

the scheme will select the "best" RN to help the SN to forward its information to the DN. In Phase 1, the SN broadcasts its information to all the RNs and DNs. In particular, Aggelos [17] proposed a distributed method of selecting the best relay that requires no topology information and it only relies on the local measurements of the instantaneous channel conditions. This method requires no explicit communication among the RNs. A rich list of contributions related to single or multiple relay aided cooperative communication can be found in [20, 53–55].

Additionally, TWR may be invoked for increasing the attainable throughput. The two-way communication problem was first studied by Shannon in [56], as a part of network information theory. The achievable rate of the general full-duplex TWR channel (including the direct link) was studied in [21]. In Figure 1.4, a pair of SNs, namely SN_1 and SN_2, simultaneously transmit their individual information to the RN, during the first transmission period. During the second transmis-

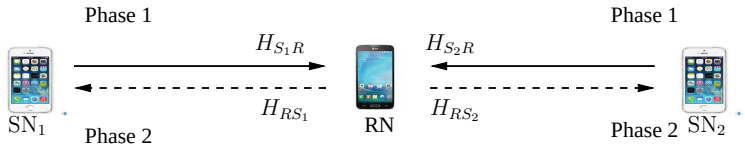

Figure 1.4: The topology of TWR during a pair of TSs in a cooperative communication network. The channel between the SN$_1$ and the RN is represented by H_{S_1R}, while the SN$_2$-RN channel is represented by H_{S_2R}. Additionally, the channel of the record hop between the RN and the SN$_1$ as well as between RN and SN$_2$ is represented as H_{RS_1} and H_{RS_2}, respectively.

sion period, the RN sends its modulo-two combined information back to these two SNs at the same time. In [57], the TWR scheme communicates over four TSs, where the source SN_1 communicates to SN_2 in the first two TSs with SN_2 remaining silent, while SN_2 communicates to SN_1 in the last two TSs, with SN_1 being idle. Specific problem of this transmission scheme is that the corresponding sum-rate is lower, since the transmissions take place over four time slots [20]. In [58], a three-Time-Slot (TS) based TWR scheme was considered. As expected, the transmissions over three TSs achieve a higher sum-rate than those over four TSs, albeit lower than the communication over two TSs.

1.2.2 Cooperative Protocols

In this research, the two most popular cooperative communication protocols, namely the Decode-and-Forward (DAF) and Amplify-and-Forward (AAF) schemes [46,59–61] have been invoked. The family of other techniques, such as Compress-and-Forward (CAF) cooperation [45, 62] and coded cooperation are beyond our current scope. In the DAF relaying protocol, the RN would decode and re-encode the signal receive from the SN, before forwarding it to the DN. The AAF relaying protocol is a simpler technique, where the RN would amplify and forward the received signal to the DN. The noise is also amplified along with the signal in this technique, but a spatial diversity gain can still be attained due to the transmission of the signal over two spatially independent channels. By contrast, the RN of CAF cooperation would not transmit a direct copy of the received signal, it rather transmits a quantized and compressed version of the received signal. Therefore, the DN will as well as combine the message received from the SN and its quantized compressed version gleaned from the RN. The AAF and DAF protocols are detailed a little further below.

A. Amplify-and-Forward

In this section, we will characterize the transmission arrangement of the AAF regime based on the TWR channel. In Figure 1.5, there is no direct communication link between these two SNs, namely S_1 and S_2, since their direct link is poor. Hence all the source messages go through the RN, R. During the first TS t_1, both S_1 and S_2 send their information to the R. We assumed that

communications take place over flat Rayleigh fading channels, where the fading coefficients of the channel between node a and node b are represented by h_{ab}. We denote the average transmit power of the node a by P_a, where $a \in \{S_1, S_2, R\}$. Then the information y_R received at the RN is given

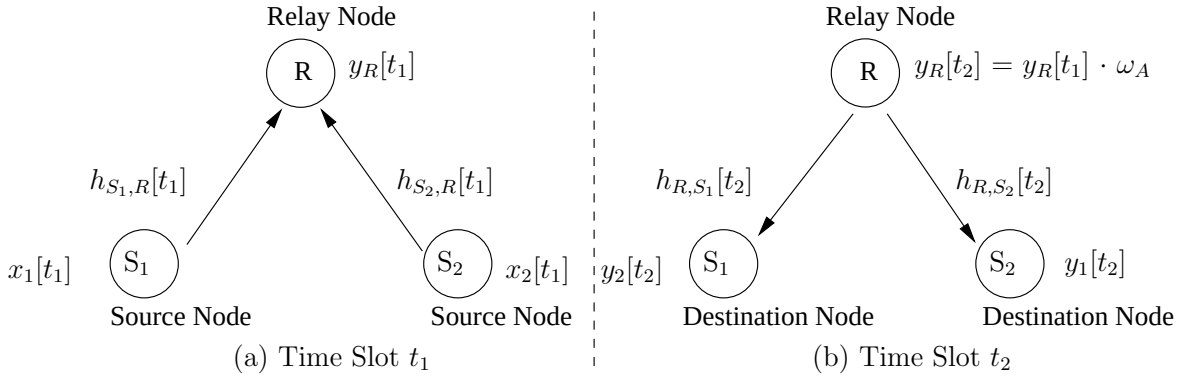

Figure 1.5: The transmission arrangement of the TWR aided half-duplex cooperative network employing the AAF protocol.

by:

$$y_R[t_1] = \sqrt{P_{S_1}} h_{S_1,R}[t_1] x_1[t_1] + \sqrt{P_{S_2}} h_{S_2,R}[t_1] + n_R[t_1] , \tag{1.1}$$

where the term $n_R[t_1]$ is the AWGN noise imposed at the RN in the TS t_1, which obeys a distribution of $\mathcal{CN}(0, N_0)$ and $\frac{N_0}{2}$ is the noise variance per dimension. The RN scales the received signal by the amplification factor ω_A, in order to meet its average transmit power constraint. The amplification factor shown in Figure 1.5 is defined as:

$$\omega_A = \sqrt{\frac{1}{P_{S_1}|h_{S_1,R}[t_1]|^2 + P_{S_2}|h_{S_2,R}[t_1]|^2 + \sigma_R^2}} . \tag{1.2}$$

Then the RN broadcasts this combined signal to two SNs, which act as the DNs. The signal received by S_1 via the $S_2 \rightarrow R \rightarrow S_1$ link is given by:

$$y_{S_1}[t_2] = \sqrt{P_R} h_{R,S_1} \omega_A y_R[t_1] + n_{S_1}[t_2] , \tag{1.3}$$

and for the $S_1 \rightarrow R \rightarrow S_2$ link, the received signal can be expressed as:

$$y_{S_2}[t_2] = \sqrt{P_R} h_{R,S_2} \omega_A y_R[t_1] + n_{S_2}[t_2] , \tag{1.4}$$

where the AWGN contribution $n_{S_1}[t_2]$ and $n_{S_2}[t_2]$ are imposed at the destination nodes S_1 and S_2, respectively, obeying a distribution of $\mathcal{CN}(0, N_0)$. Since the nodes S_1 and S_2 know their own transmitted symbols, they can subtract the back-propagating self-interference [20] formulated in Eq. (1.3) and Eq. (1.4) prior to decoding.

B. Decode-and-Forward

With reference to Figure 1.6, we consider the two-way communication between the nodes S_1 and

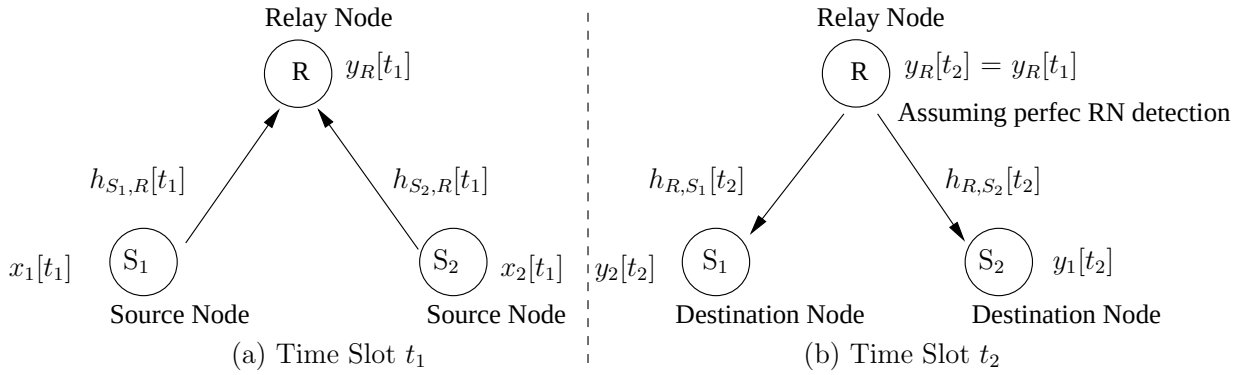

Figure 1.6: The transmission arrangement of the TWR aided half-duplex cooperative network employing the DAF protocol.

S_2 via a half-duplex DF based RN. The signal received at the RN in TS t_1 is identical to that in Eq. (1.1). Instead of amplifying the received signal, the RN decodes the symbols, $x_{S_1}[t_1]$ and $x_{S_2}[t_2]$, which were received at the first TS and then re-encodes as well as re-modulated them for transmission to the DNs. Naturally, the signal transmitted by the RN during the second TS t_2 seen Figure 1.6, will be the same as the original source information symbol when there are no decoding errors at the RN. In that case, the signals received at S_1 and S_2 are represented as:

$$y_{S_1}[t_2] = \sqrt{P_R} h_{R,S_1} x_R[t_2] + n_{S_1}[t_2] , \quad (1.5)$$

$$y_{S_2}[t_2] = \sqrt{P_R} h_{R,S_2} x_R[t_2] + n_{S_2}[t_2] . \quad (1.6)$$

1.3 Spectrum Sharing in CR networks

A range of spectrum sensing solution have been investigated by various researchers [11, 63–67, 67]. The existing work in spectrum sharing can be classified according to three aspects [68], namely the architecture, the spectrum allocation regime and the spectrum access technique, as shown in Figure 1.7. In this treatise, we have focused our attention on investigating the spectrum sharing schemes of Cooperative Cognitive Radio (CCR) networks. As seen in Figure 1.7, the architecture can be classified either as centralized or as a distributed scheme. In a centralized scheme, the spectrum allocation and access procedures are controlled by a central controller or entity. All users or nodes would send their information to the central controller. Then a spectrum allocation map is constructed by this central controller. Then, this central entity can lease spectrum to users/ nodes in a limited geographical region for a specific amount of time [69–71]. By contrast, the spectrum allocation and access is typically based on local information, which is gleaned by each distributive user/node in the distributed scheme [72, 73]. Moreover, recent contributions reveal that distributed solutions tend to closely follow the centralized philosophy, but have a lower complexity.

Moreover, the spectrum allocation regime of Figure 1.7 can be classified into non-cooperative

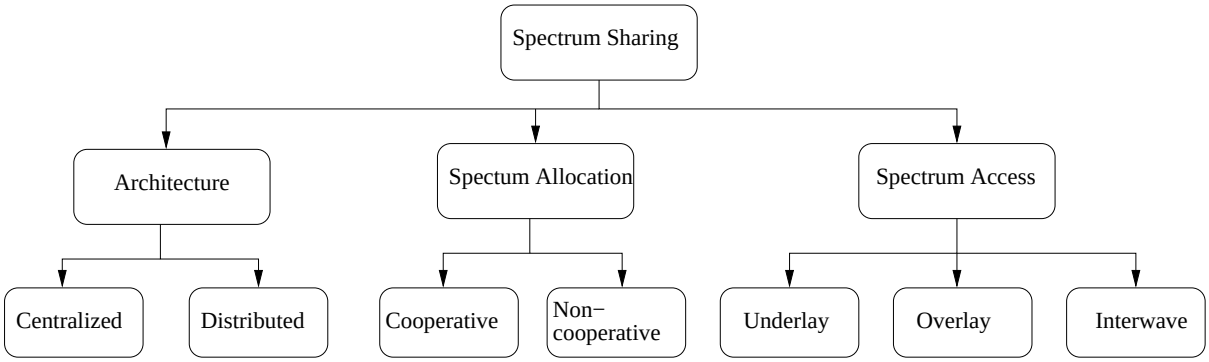

Figure 1.7: The classification of spectrum sharing in CR network.

and cooperative schemes. The non-cooperative spectrum sharing [74, 75] typically results in a reduced spectrum efficiency regime, but does not require frequent message exchanges. By contrast, in the cooperative spectrum sharing, a common technique is to form a cluster to share the users' information locally [76]. The cooperative approaches tend to outperform the non-cooperative approaches and result in a certain fairness, as well as an improved throughput. On the other hand, the non-cooperative approach imposes a lower information exchange requirement and hence requires less energy [77].

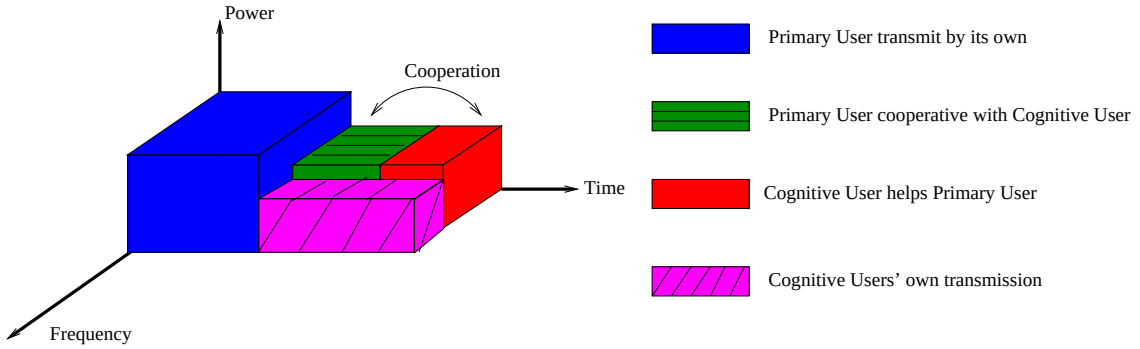

Figure 1.8: Overlay spectrum model of CR network.

Furthermore, there are three main paradigms conceived for spectrum access in CR networks [7]:

- **Underlay scheme [7]**: CUs can transmit simultaneously with PUs by using the same frequency spectrum, under the constraint that the interference inflicted by the CUs on the PUs does not degrade the PU's communication quality. In this scheme, the CUs are not required to perform spectrum sensing. However, the interference caused by the CUs' transmission must not exceed the tolerable threshold.

- **Overlay scheme [7]**: CUs can transmit simultaneously with PUs in the same frequency slot. The knowledge sharing and cooperation between the CUs and PUs is critical in the overlay model. Specifically, the interference imposed on the PUs can be offset by using part of the

CUs' power for relaying the PUs' information. As shown in Figure 1.8, some CUs assist the PUs to free up some spectrum bands. These vacant spectrum bands would then be used by other CUs for their secondary transmission.

- **Interwave scheme [7]**: The CUs would only transmit simultaneously with the PUs, when a busy spectral slot was wrongly detected as a spectral hole. Specifically, the CUs exploit the spectrum slots, which are not utilized most of the time for their secondary communication. Hence the spectrum efficiency is improved.

In the interwave technique, the knowledge sharing between the PU and CU is critical for ensuring that the CUs' transmissions do not interfere with those of the PUs. The CUs opportunistically communicate over the spectrum hole in order to minimize the interference imposed on the PUs. The underlay and overlay paradigms permit the concurrent communications of the PUs and CUs. By contrast, the main goal of the interwave paradigm is to avoid the simultaneous transmission of the PUs and CUs. Moreover, the underlay system requires accurate knowledge of the interference imposed by the CUs' transmitter on the PUs' receiver. By contrast, the overlay scheme needs a large amount of side-information, such as the non-causal knowledge of the PU's codebook. Furthermore, the interweave regime also requires considerable side-information about the PUs or the existing users and this information can be obtained from PUs' spectrum sensing action. Although these three schemes rely on distinct approaches, their advantages can be combined by constructing two hybrid schemes. For example, the underlay and overlay schemes are combined in [78, 79], where the CUs invoke the spectrum overlay technique, if spectrum holes are found. Otherwise, the spectrum underlay technique will be employed. Additionally, the authors of [80] introduced stochastic resource allocation algorithms for both the interweave and underlay paradigms, where the CUs can access the frequency band only if no PU is active in the context of the interweave and overlay paradigm. By contrast, in the underlay paradigm CUs can access the channel even when the PUs are active, provided that they adjust their transmission power so that the interference imposed on the active PUs remains below a specified threshold [81]. In our work, we have mainly considered the overlay scheme. The significant difference between the overlay scheme and the interwave regime is that the cooperation of the PUs and CUs is actively supported by the overlay scheme. In the overlay scheme of [82], the PU's performance is enhanced by exploiting the benefit of cooperative diversity with the aid of the CU acting as a RN, while CU's transmission is carefully coordinated by the PU's transmission scheduling. A "win-win" scenario has been constructed for both PU and CU which gives both the PU and CU an incentive to cooperative. Therefore, the overlay scheme constitutes an opportunistic spectrum access scheme, as discussed in [81].

1.4 Repeated Games in a CCR Network

Game theory is one of the techniques that can be beneficially used for spectrum sharing in CR networks as described in [8]. Game theoretic techniques can be divided into two types, namely non-cooperative and cooperative games. In a non-cooperative game, the players make their decisions independently and aim for maximizing their own utility. By contrast, the players in the cooperative game cooperate with each other for maximizing their total utility. Some game theoretic models that have been employed in CR networks are summarized in Table 1.1.

Game Type	Model	Author(s)	Contribution
Non-cooperative game	Auction game	Niyato *et al*. [83]	A double auction mode is invoked for analyzing the interaction among the Wireless Regional Area Network (WRAN) service providers, TV broadcasters and WRAN users.
	Repeated game	Wu *et al*. [84]	Users are given an incentive to share the spectrum in a cooperative way. To enforce user cooperation, defecting users may be asked to pay a tax.
	Stackelberg game	Haddad *et al*. [85]	A stackelberg-game was employed for controlling the user's behaviour by broadcasting the relevant information in heterogeneous cognitive networks.
Cooperative game	Coalitional game	Li *et al*. [86]	PUs and CUs form a coalitional game, where they can pay charges to each other to motivate the cooperation.
	Bargaining game	Attar [87]	A fair resource allocation method is proposed based on the Nash Bargaining solution for a problem, where a group of CUs access the resources of a primary system.

Table 1.1: Summary of game mode used in CR networks.

To elaborate further, a game is defined by a set of players, a set of actions for each player and the payoffs for the players [88]. A player chooses an action and the associated complete plan of action is referred as the *strategy* [3]. However, most of the game theory model rely on the

[3]A simple example of highlighting the difference between the action and strategy is as follows. If an individual has to

equilibrium concept, which ensures that a player could gain either a fair or an optimal pay-off under a given strategy of the other players [89–91]. More specifically, a strategy can reach equilibrium, if it becomes impossible to reward player a specific without disadvantaging other players [88]. Explicitly, in Nash equilibrium, no player has any intention to change its strategy to gain a higher payoff, provided that the other players also maintain their current strategies. In our work, we have opted for the repeated game concept in our CCR network.

A repeated game can be seen as a *static*[4] non-cooperative strategic game that is repeated over time. By repeating a game many times, the players (users) may become aware of their past behaviours and change their strategies accordingly. In the repeated game context, all players are better off, if they cooperate. More specifically, if a game is played repeatedly, then the mutually desired outcome can be reached, where each player believes that a defection for short-term personal gain will terminate the cooperation, hence resulting in a subsequent loss for the player that outweighs the potential short-term gain [88]. The threat of future 'punishments' prevents any player acting rationally from defection. In [92], a repeated game among the PUs' transceivers was formulated to show that the collusion can indeed be maintained, provided that all the PUs are aware of the potential punishment. However, if a primary service deviates from the collusion, then all the other primary services will resort to the punishment action permanently. In this case, the primary services will consider the long-term benefits for themselves. Moreover, power control strategies have been considered for the CUs in the repeated game proposed in [93, 94]. Specifically, in [94], the CUs can control the power control strategies by observing the interference imposed by them on the PUs by exploiting the feedback signals of PUs and from the transmission rates obtained in the previous step.

1.5 Outline Contributions of this Thesis

In this thesis, we will focus our investigation on the objectives shown in Figure 1.9. In Chapter 2, we primarily consider the attainable BER performance, while in Chapter 3 we focus our attention on achieving the minimum in the PUs' transmission power and bandwidth usage, while maximizing the CUs' data rate. In Chapter 4, we will analyse the achievable throughput of the PUs and compare the FER performance of different schemes at a certain transmit SNR. Finally, in Chapter 5, the sum rate of the PUs will be maximized.

Chapter 2 : TTCM Theory and Applications

decide what to eat for lunch and the options are hot soup or cold food, then a possible strategy would be "if the weather is cold, this person would select the hot soup; otherwise, he will choose the cold food." After ascertaining the weather, the person would take an action, which is to have hot soup or to eat cold food, depending on the weather information.

[4] A game is static, if the players carry out their actions only once and independent by each other [88]. Specifically, a static game is a one-shot game, where all players make decisions without any knowledge of the strategies chosen by the other players [89].

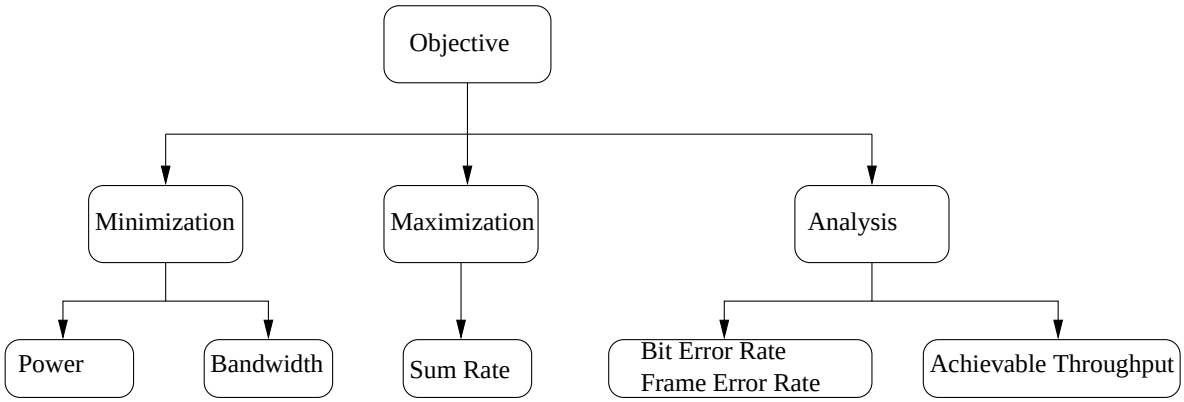

Figure 1.9: The objectives of this thesis.

In this chapter, we introduced the underlying theory and application of Turbo Trellis Coded Modulation (TTCM). We investigated both the fix and near-instantaneously adaptive mode of TTCM. TTCM schemes are capable of increasing the system's effective throughput by increasing the code rate and the number of modulation levels, when the channel-quality improves [95–97]. In Section 2.3, we have discussed the applications of fixed mode TTCM scheme. Explicitly, we have proposed a novel power- and bandwidth-efficient TTCM assisted Space Division Multiple Access (SDMA) based TWR scheme. The scheme advocated was designed for enhancing the throughput, reliability and coverage area in a cooperative communication system. A twin-antenna RN was employed for assisting a pair of users, where each user was equipped with a single-antenna aided mobile unit. During the first transmission period, both users transmit their TTCM-encoded signals to the RN. The twin-antenna RN then detects these signals using various SDMA-based detection algorithms. Iterative SDMA and TTCM detection is invoked at the RN, which then broadcasts the re-encoded TTCM signals to both users during the second transmission period. Finally, each user retrieves the opposite user's signals received from the RN. We found that the proposed scheme outperforms the non-cooperative TTCM scheme by approximately 5.3 dBs at a BER of 10^{-6}, when communicating over uncorrelated Rayleigh fading channels. Additionally, in Section 2.3.3 we extended this scheme to the scenario, when the CSI estimation is impaired by channel estimation errors. Moreover, in Section 2.3.4 we investigated the adaptive mode based TTCM scheme , where a higher-throughput TTCM scheme is employed, when the channel conditions are good, while a lower-throughput TTCM scheme or no transmission is used, when the channel conditions are poor. As shown in Figure 1.10, we treated the adaptive TTCM scheme as the main physical-layer enabling technique in Chapter 3, Chapter 4 and Chapter 5 for achieving a higher system throughput and for improving the BER/FER performance.

Chapter 3 : Cooperative Communication Between Cognitive and Primary Users

In this chapter, we considered the overlay spectrum sharing scheme among the PUs and CUs,

where the CUs serve as the RNs for relaying the information from PUs. In Section 3.2, we have considered an active cooperation between a PU and a CU, with the goal of reducing the transmission power and increasing the transmission rate for both the PU and CU. Alternatively, the required bandwidth may be reduced and the freed bandwidth may be leased to a group of CUs for their secondary communications. The more bandwidth reduction we achieved for the PU, the more benefit the CUs had. Additionally, we have considered both OWR and TWR aided CR systems, as seen in the context of Figure 1.10. In order to select the "best" CU to act as the RN among the CUs, we have employed a pair of relay selection techniques, namely the max-min and max-sum relay selection techniques. Their corresponding performance based on the OWR aided CR system was studied in Section 3.4.2.3. Furthermore, we invoked a near-instantaneously adaptive TTCM (ATTCM) scheme for appropriately adjusting both the code rate and the number of modulation levels according to the near-instantaneous channel conditions. The ATTCM switching thresholds of our OWR system were specifically adjusted for ensuring that the BER is below 10^{-5} in order to minimize the potential error propagation from the RN to the DN. Additionally, as shown in Figure 1.10 we have considered two scenarios for the switching thresholds, namely the TTCM transmissions over AWGN channels as well as over Rayleigh channels. It was shown that our proposed ATTCM aided TWR based CCR scheme maximized the CU's own data rate and improved the exploitation of the bandwidth released by the PUs to the CUs.

Chapter 4 : Adaptive Dynamic Network Coding in CCR networks

In this chapter, we considered two types of Dynamic Network Coding (DNC) schemes, namely the fixed-mode DNC and adaptive-mode DNC as seen in Figure 1.10. Specifically, We conceived an Adaptive DNC (ADNC) scheme for a CCR system, which is designed for supporting the uplink communications between multiple PUs and a common Base Station (BS). Specifically, the independent source information is transmitted from the PUs to the BS with the aid of multiple CUs acting as RNs. In order to facilitate the recovery of the source information at the BS, the CUs invoke the ADNC technique, which is assisted by our cooperative protocol operating by exchanging the CCR-based control information between the near-instantaneously ATTCM and the network coding codecs as well as between the CUs and the BS. As a result, our ADNC-CCR system constructed on the basis of a holistic approach is capable of providing an increased throughput, despite reducing the transmission-period of the PU. This reduced transmission-period can also be directly translated into an increased duration for the secondary communications of the CUs. As an additional novelty, the network encoder may also be activated in its adaptive mode for supporting the CUs, depending on the Boolean value of the feedback flags generated based on the success/failure of the ATTCM decoder and of the network decoder, which is evaluated and fed back by the BS. Explicitly, in Section 4.2.3 we have investigated an adaptive network decoder for the sake of reducing the complexity and for improving the bandwidth reduction of PUs.

Chapter 5 : Pragmatic Distributed Algorithm for Spectrum Access in CCR Networks

In this chapter, we considered four algorithms derived for spectrum trading between the multiple PUs and CUs, as shown in Figure 1.10. To elaborate further, we proposed a Pragmatic Distributed Algorithm (PDA) based on the repeated game concept in the context of an overlay scheme for maximizing the PUs' benefits. The novelty of our PDA is that the PUs negotiate with the CUs concerning the specific amount of relaying and transmission time granted for the CUs, which the CU will either accept or decline. The CUs may serve as RNs for relaying the signal received from the PUs to their destinations, while ensuring that both the PUs' and the CUs' minimum rate requirements are satisfied. This will reduce the required transmission power and/or increase the transmission rate of the PU. Moreover, we show that our proposed algorithm results in a stable pairing of a PU and CU. To elaborate further, we also compared our PDA with the Conventional Distributed Algorithm (CDA) [98] as our benchmark scheme. Our results show that the proposed scheme performs better than the benchmarker, despite its significantly lower overhead and complexity. A centralized solution based on the Centralized Algorithm (CA) was also considered for benchmarking our PDA. We found that our PDA performs close to the CA, albeit at a lower complexity. Furthermore, we also invoked our practical ATTCM scheme, which appropriately adjusts the code rate and the modulation mode according to the near-instantaneous channel conditions. It was found that the joint design of coding, modulation, user-cooperation as well as stable pairing of the PU and CU in the CR system may lead to significant mutual benefits for all PUs and CUs.

Chapter 6 : Conclusions and Further Research

In Chapter 6, we summarized our main findings and outlined a range of further potential research topics as shown in Section 6.2.

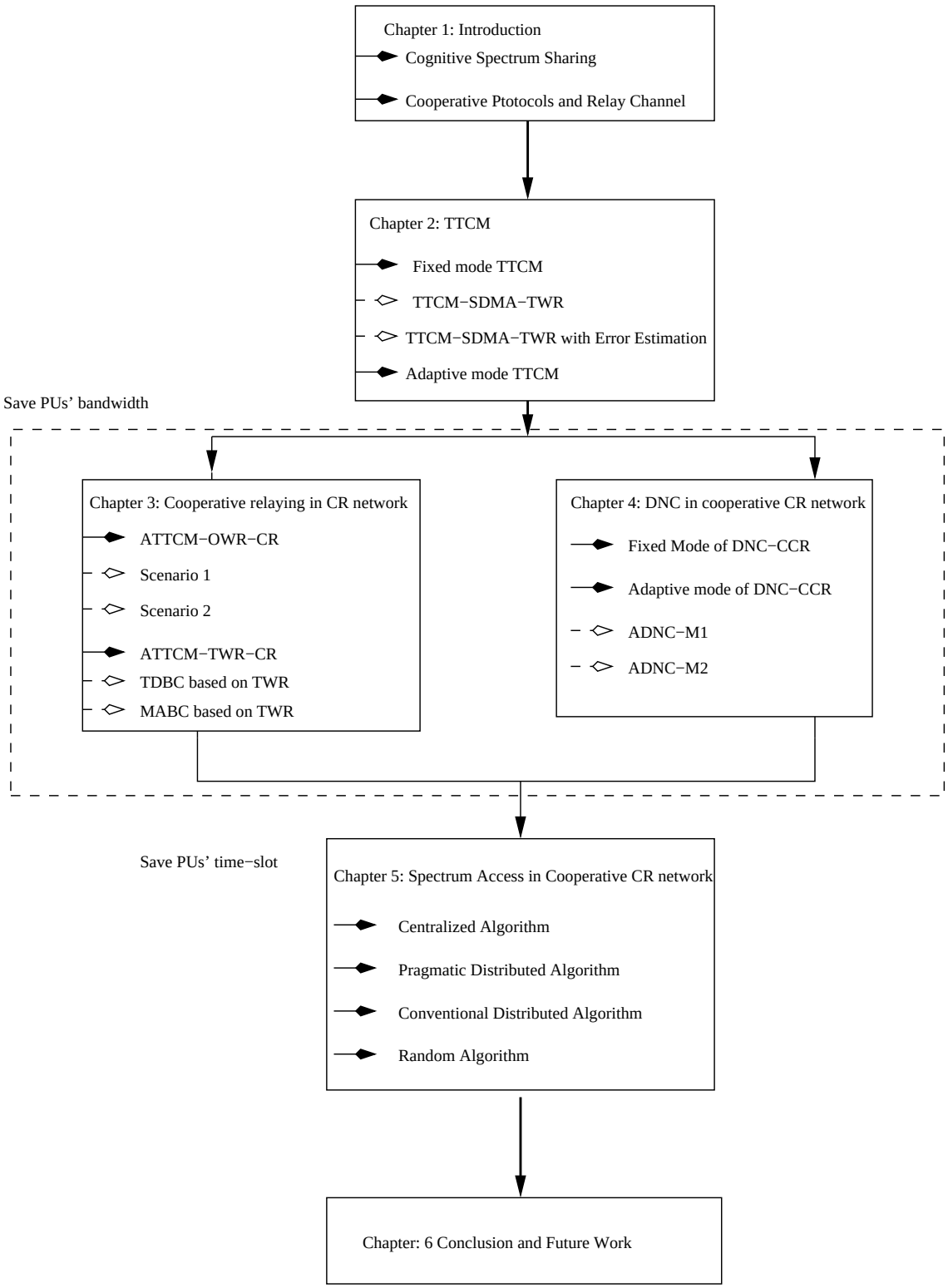

Figure 1.10: The structure of this thesis.

Chapter 2

Turbo Trellis Coded Modulation: Overview and Applications

2.1 Introduction

In this chapter, we will provide an overview and investigate some applications of the power- and bandwidth-efficient Turbo Trellis Coded Modulation (TTCM) scheme [95]. Specifically, TTCM is a joint coding and modulation scheme that has a structure similar to binary turbo codes, where two identical parallel-concatenated Trellis Coded Modulation (TCM) [99] schemes are employed as component codes. In Chapter 1, we have briefly viewed the evolution of a cooperative communication and the protocols of the relay channel. In Section 2.3.2, we will employ the fixed-mode TTCM scheme for cooperative communication. More specifically, a novel power- and bandwidth-efficient TTCM assisted Space Division Multiple Access (SDMA) based Two-Way Relaying (TWR) scheme is conceived for enhancing the attainable throughput, reliability and coverage area of cooperative communication system. A twin-antenna aided Relay Node (RN) is employed for assisting a pair of users, where each user is equipped with a single-antenna assisted mobile unit. During the first transmission period, both users transmit their TTCM-encoded signals to the RN. The twin-antenna RN then detects these signals using various SDMA-based detection algorithms. Iterative SDMA and TTCM detection is invoked at the RN, for exchanging extrinsic information between these two components. The RN then broadcasts the re-encoded TTCM signals to both users during the second transmission period. Finally, each user retrieves the opposite user's signals received from the RN. In Section 2.3.4, the sophisticated adaptive mode of TTCM scheme is investigated, where a higher order or/and higher rate modulation mode will be employed, when the instantaneous estimated channel quality is high in order to increase the number of Bit Per Symbol (BPS) transmitted. Conversely, a more robust lower rate code or/and a lower order modulation mode will be employed, when the instantaneous channel quality is low, in order to improve the Bit Error Ratio (BER) performance. Moreover, the 4-ary Phase Shift Keying (PSK), 8-ary PSK, 16-ary Quadrature Amplitude

Modulation (QAM) and 64-ary QAM modulation schemes are invoked for both the fixed and adaptive mode of TTCM.

2.2 TTCM Overview

The TTCM schemes in [95] were designed based on the search for the best component TCM codes using the so-called 'punctured' minimal distance criterion for communicating over the Additive White Gaussian Noise (AWGN) channel. Employing TTCM has the advantage that the system's effective throughput can be increased upon increasing the code rate, when the channel-quality improves. Additionally, both the BER and the Frame Error Ratio (FER) performance of the system may be improved when TTCM is used [96]. Recently, various TTCM schemes were designed in [97] with the aid of carefully concerning the tools of the Extrinsic Information Transfer (EXIT) charts [100, 101] and union bounds for the sake of approaching the capacity of the Rayleigh fading channel. The TTCM encoder comprises two identical parallel-concatenated TCM encoders [99] linked by a symbol interleaver. The first TCM encoder directly processes the original input bit sequence, while the second TCM encoder manipulates the interleaved version of the input bit sequence. Then the bit-to-symbol mapper maps the input bits to complex-valued symbols using the Set Partition (SP) based labelling method [96]. The structure of the TTCM decoder is similar to that of binary turbo codes, but each decoder alternately processes its corresponding encoder's channel-impaired output symbol, and then the other encoder's channel-impaired output symbol [pg.764] [96].

2.2.1 TCM Principle

Coded Modulation (CM) constitutes a bandwidth-efcient communication scheme that combines the functions of coding and modulation by absorbing the channel-coded bits with the aid of extending the symbol-constellation [96, 102]. They can be designed by employing relatively high-rate channel coding schemes in conjunction with multi-dimensional modulation schemes. More importantly, a coding gain may be achieved without bandwidth expansion. The history of coded modulation dates back to Shannons pioneering work [103], which founded information theory and motivated the search for codes that are capable of producing an arbitrarily low probability of error, despite operating in the vicinity of the capacity. Ungerböck [99] conceive the TCM technique, which constitutes a family of CM schemes where both coding and modulation are jointly designed. This section is based on his seminal paper [99]. TCM scheme employs non-binary modulation in conjunction with a finite-state Forwarded Error Correction (FEC) encoder, which governs the selection of FEC coded signal sequences. Basically, the expansion of the original symbol set absorbs more BPS than that required by the data rate and these extra bits are used by a convolution encoder, in order to restrict the legitimate state transition amongst the consecutive phases to certain legitimate constellation

points. In the receiver, the noisy signals can be decoded by a soft-decision maximum-likelihood sequence decoder. Explicitly, CM schemes having different coding rates and different number of modulation levels are shown in Figure 2.1. More specifically, the coding rate of CM is defined as:

$$R_c = \frac{N_d}{N_c} = \frac{N_d}{N_d + 1}, \tag{2.1}$$

where the number of bits in a non-binary symbol and the codeword are given by N_d and N_c, respectively. Therefore, the corresponding number of modulation level is given by: $M = 2^{N_c}$ and the number of Information Bit Per Symbol (iBPS) equals N_d.

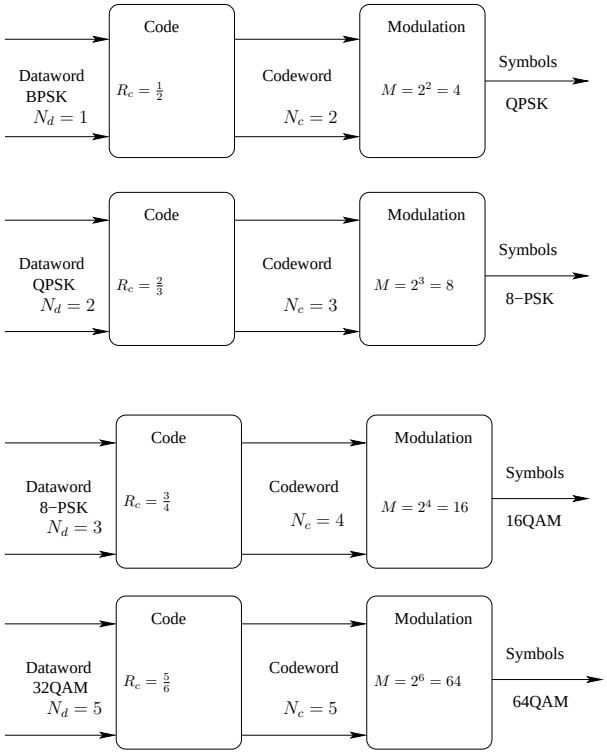

Figure 2.1: The block diagram of coded modulation schemes with different coding rates.

In Figure 2.1, the number of modulation levels M is increased for transmitting a higher number of iBPS. Ungerböck's specific TCM encoder is a conventional encoder selected from the family of Recursive Systematic Convolution (RSC) codes. The block diagram of a TCM scheme is shown in Figure 2.2, where a single parity bit is attached to each information symbol. In addition, m out of n information bits are encoded by the RSC encoder, where n represents the number of RSC-encoded bits. Hence 2^m branches may merge into each trellis state since we have $m < n$, not all the original information bits are encoded by the RSC encoder. Hence there are 2^{n-m} parallel transitions associated with each of the 2^m branches. Then the total number of transitions occurring at each trellis stage is $2^m \times 2^{n-m} = 2^n$. Additionally, the encoder memory length L_m of a code defines the number of shift-register stages in the encoder. Figure 2.2 shows a sixteen-state RSC, where the memory length (or the number of register stages) is equal to $L_m = 4$. This is a systematic encoder, which attaches an extra parity bit to the original 3-bit information. The encoded 4-bit symbol

sequence is interleaved for the sake of dispersing the bursts of symbol errors induced by the fading channel [96]. A symbol interleaver can be used to improve the code's time diversity gain, which is a benefit of dispersing the symbols over time, hence resulting in a near-uniform distribution of errors and improving the decoder's performance. The four-bit codeword is then mapped to a 16QAM constellation. The generator polynomials of the RSC encoder shown in Figure 2.2 can be described

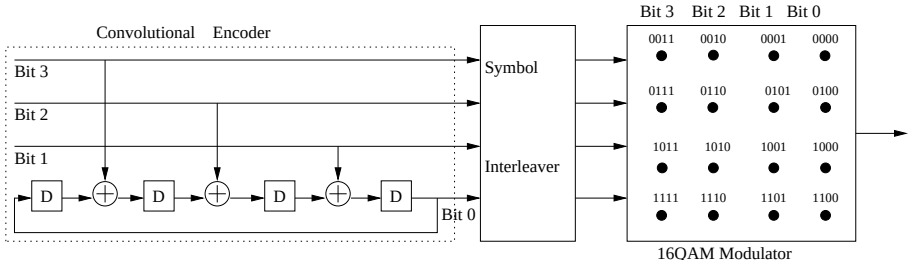

Figure 2.2: The block diagram of Ungerböck RSC encoder and modulation scheme relying on a $\frac{3}{4}$-rate code [99].

in octal format as [104]:

$$H(D) = [H^0(D)\ \ H^1(D)\ \ H^2(D)\ \ H^3(D)] = [21\ \ 02\ \ 04\ \ 10]\,, \tag{2.2}$$

where D denotes the delay due to a single shift-register stage. The polynomial coefficient $H^0(D)$ is the feedback generator polynomial. For further details on TCM please refer to [99] and [104].

2.2.2 Set Partitioning

For higher-order modulation schemes, such as 16QAM or 32QAM, Ungerböck proposed the so-called set partitioning technique for mapping the bits to QAM symbols, which is different for classic Gray Coding. As an example, the set partitioning of 16QAM is shown in Figure 2.3. Again, the phasors are not labelled by Gray encoding any more and the adjacent points may have an arbitrary Hamming Distance (HD) rather than one, as in Gray coding. Additionally, observe Figure 2.3, that the Euclidean distance is increased at each partitioning step, as we moved from level 0 to level 4 of the constellation partitioning tree in Figure 2.3. The objective of this technique is to ensure that those specific bits of the QAM-constellation, which are not protected by the conventional encoder of Figure 2.2 have a high Euclidean distance (ED). Explicitly, the specific pair of subsets seen at Level 1 of Figure 2.3 has to be protected by the RSC encoder, because the corresponding constellation points have a low ED. Hence, the level 0 subsets are labelled by the parity bit, while the remaining levels are labelled by information bits. Moreover, the corresponding bit 3 of level 4 has the lowest probability of corruption due to its highest Euclidean distance (ED). Typically, conventional TCM schemes are decoded/demodulated by using the appropriately modified Viterbi algorithm [104]. Explicitly, the Viterbi algorithm is used for finding the most likely signal path by going through the trellis having the minimum sum of squared EDs. Hence, it is a maximum

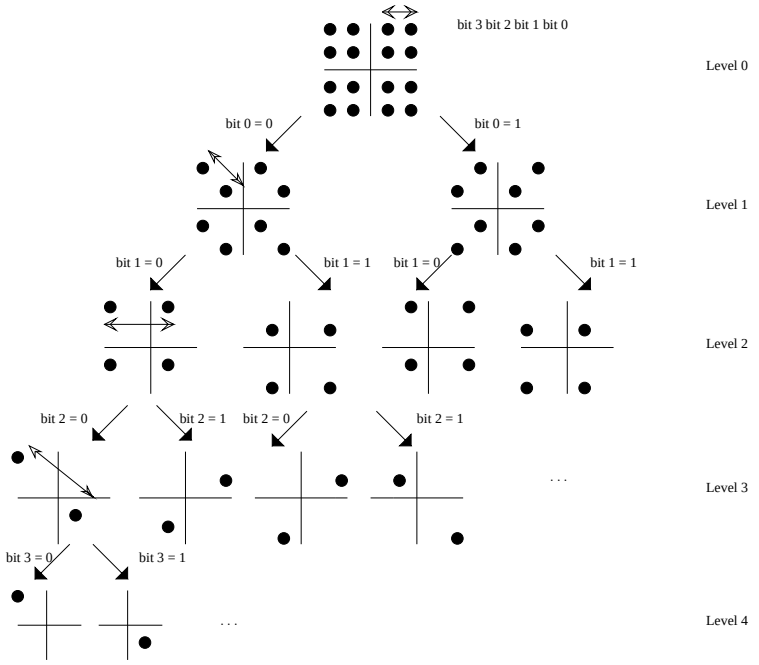

Figure 2.3: TCM 16QAM set partition © IEEE Ungerböck 1982 [99].

likelihood sequence estimation (MLSE) algorithm, which does not generate the minimum Symbol Error Ratio (SER). By contrast, the symbol-based Maximum-A-Posteriori (MAP) algorithm can be used for TCM decoding in order to directly minimise the SER. For details of the symbol-based MAP algorithm please consult Section 14.3 of [104].

2.2.3 TTCM Encoder

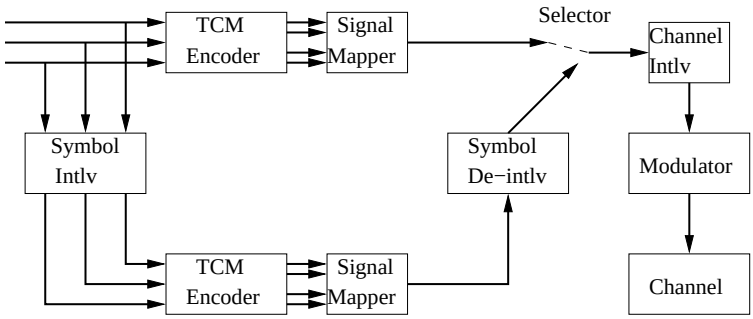

Figure 2.4: The block diagram of TTCM encoder [104]. ©IEEE, 1998, Robertson and Wörz .

Ungerböck's TCM scheme is capable of exploiting soft-decisions, but it is unable to exploit sophisticated iterative detection. Hence Robertson and Wörz further developed the TCM concept by amalgamating it with the turbo coding philosophy, which led to the conception of TTCM. The schematic of the TTCM encoder is shown in Figure 2.4, which comprises two identical TCM en-

coders, linked by a symbol interleaver. Each TCM encoder consists of a bit-to-symbol mapper and an encoder, as seen in Figure 2.4. The upper TCM encoder manipulates the original input bit sequence and the bottom one operates on the interleaved version of the input bit sequence. The output codeword of the TCM encoder (which is the input of the signal mapper) is mapped onto complex-valued QAM symbols by using the SP-based labelling method, which was discussed in Section 2.2.2. The complex-valued symbols of the bottom signal mapper of Figure 2.4 are symbol-de-interleaved according to the inverse operation of the interleaver. The TTCM codewords of both component encoders have identical information bits before entering the selector. Hence the selector that selects the symbols of the upper and lower component encoders alternatively, therefore puncturing the parity bits of the output symbols. The selector output is then further interleaved by another symbol-based interleaver, in order to disperse the bursty symbol errors during the transmission period. Finally, the output symbols are modulated and transmitted over the channel. For further details please refer to Section 14.4.1 of [104].

2.2.4 TTCM Decoder

Figure 2.5 contrasts the decoder schematic of TTCM. The structure of the TTCM decoder is similar to that of the binary turbo codes, except for the difference in the nature of the information passed from one decoder component to the other and in the treatment of the first decoding step. More specifically, each decoder alternately processes its corresponding encoder's channel-impaired output symbol and then the other encoder's channel-impaired output symbol [104]. The concept of computing the *a priori* information, the *a posteriori* information and the *extrinsic* information has been introduced in [104, 105]. The *a priori* information is known before decoding starts, while the *a posteriori* information is obtained after a decoder iteration has been competed. The difference between the *a priori* information and *a posteriori* information is the *extrinsic* information.

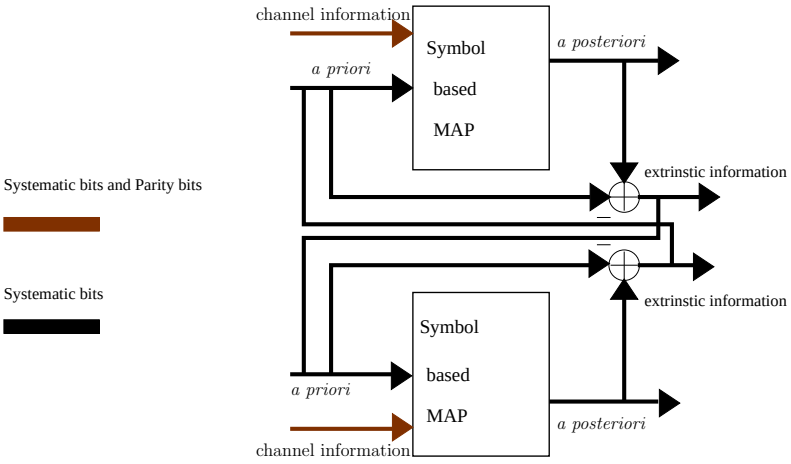

Figure 2.5: Schematic of a TTCM decoder [104].

Finally, the *extrinsic* information is fed to the other component decoders, as shown in Fig-

ure 2.5.

In a binary turbo coding scheme, the component encoder's output can be split into three additive parts for each information bit u_i at step i, which are detailed as follows:

- the systematic component (S/s), which represents the corresponding received systematic value for original information bit u_i.
- the *a priori* information, which is the information provided by the other component decoder for information bit u_i.
- the *extrinsic* information component related to the information bit u_i, which depends not only on u_i, but also on its surrounding bits.

These components are impaired by independent noise and fading effects. In order to attain iterative decoding gains, the *extrinsic* information component of non-binary turbo codes should be passed on to the other component decoder, so that the *a priori* information directly related to a bit is not reused in the other component decoder. This is because reusing it would detrimentally bias the decisions concerning this bit and hence would degrade the overall performance.

The symbol-based non-binary TTCM scheme transmits the information bits and parity bits together in the same non-binary symbol. Hence, the systematic component of the non-binary symbol, namely the original information bits, cannot be separated from the extrinsic component, since the noise and fading affect the systematic and parity components together. Therefore, the symbol-based information can be split into two components:

- the *a priori* component which is provided by the other component decoder.
- the inseparable *extrinsic* as well as systematic component of a non-binary symbol.

Each decoder passes only the latter information to the next component decoder, where the *a priori* information is removed at each component decoder's output. Again, please consult Section 14.4.2 of [104] for further details on TTCM decoding.

2.3 TTCM Applications

2.3.1 Fading Channel Model

Fading appears due to the attenuation of the radio signal, when it passes through various objects between the transmitter and the receiver, as well as owing to the destructive interference of multipath components due to the reflection and scattering of the transmitted signal. Large-scale fading [106] is more pertinent to cell-site planning, while small-scale fading [106] is more relevant to the design

of reliable communications links. Hence, small-scale fading[1] constitutes the focus of the thesis. When designing channel coded modulation, it is necessary to be aware of the correlation of the complex-valued fading over both the time and frequency-domain. The overview of small-scale fading channel manifestations is shown in Figure 2.6. The BER performance of TTCM assisted

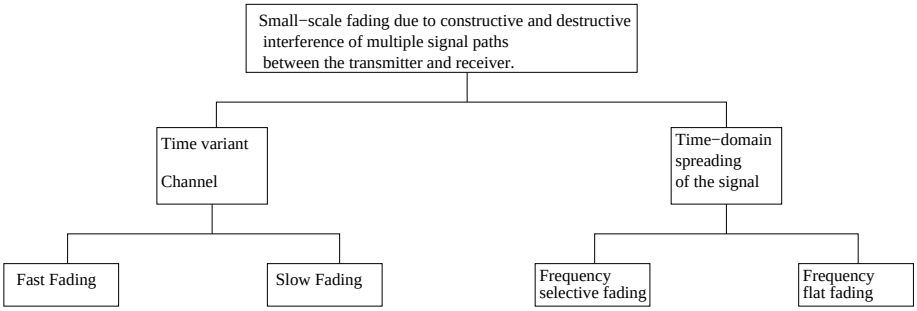

Figure 2.6: Small-scale fading channel manifestations [107, 108].

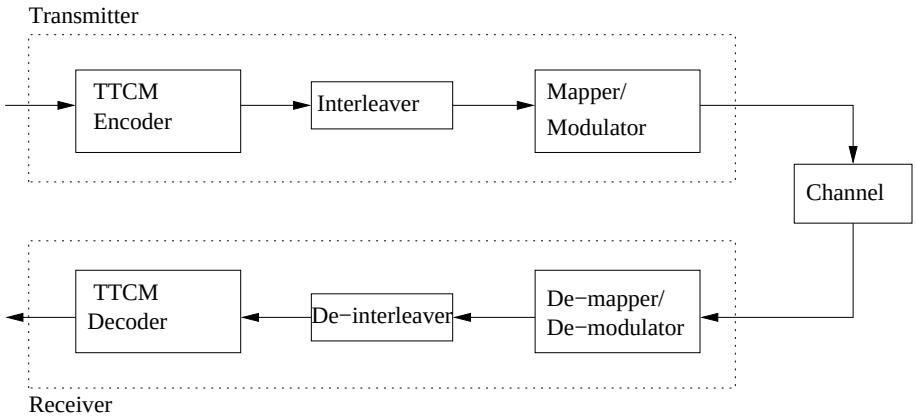

Figure 2.7: The schematic of a TTCM scheme [102].

4PSK, 8PSK, 16QAM and 64QAM schemes when communicating over AWGN and uncorrelated Rayleigh fading channels are shown in Figure 2.8 and Figure 2.9. Explicitly, Figure 2.8 present the BER performance of various TTCM schemes, when communicating over the AWGN channel. It can be seen from Figure 2.8a and Figure 2.8b that the 4PSK TTCM scheme achieves the lowest probability of errors compared to other TTCM schemes. In Figure 2.8a, the 4PSK TTCM scheme outperform the 64QAM TTCM scheme by $17.5 - 2.1 = 15.4$ dB at a target BER of 10^{-5}. Additionally, the SNR_r and E_b/N_0 thresholds of the TTCM schemes having a target BER of 10^{-5} obtained from Figure 2.8 are shown in Table 2.2. We define E_b/N_0 as the ratio of the transmitted

[1]Small-scale fading often obeys Rayleigh Distribution, since there is no line-of-sight when the number of reflected paths is high and the envelope of the received signal is statistically described by a Rayleigh pdf. When there is a dominant non-fading signal component, due to a line-of-sight propagation path, the small-scale fading envelope is described by a Rician pdf [106, 107].

Coded Modulation	TTCM
Modulation	Q-PSK, 8PSK, 16QAM, 64QAM
Mapper type	Set-Partitioned
Number of frames	$10,000$
Number of iterations	4
Code Rate	$1/2, 2/3, 3/4, 5/6$
Code Memory	3
Decoder type	Approximate Log-Map
Symbols per frame	1200, 12000
Channel	AWGN, uncorrelated Rayleigh fading channel

Table 2.1: Simulation parameters.

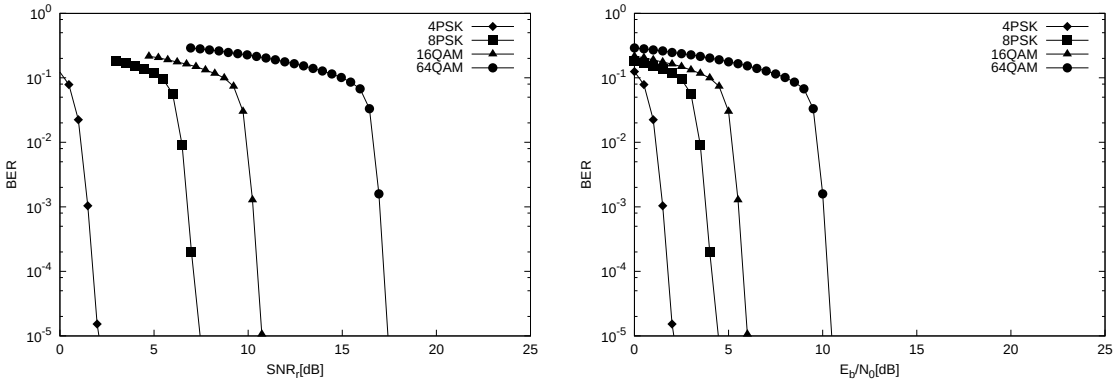

(a) BER vs SNR_r (b) BER vs $\mathrm{E}_b/\mathrm{N}_0$

Figure 2.8: BER performance of TTCM aided 4PSK, 8PSK, 16QAM and 64QAM schemes when communicating over an **AWGN channel** using four TTCM iterations. The simulation parameters are shown in Table 2.1.

Modulation scheme (target BER$= 10^{-5}$)	SNR_r [dB]	$\mathrm{E}_b/\mathrm{N}_0$ [dB]
4PSK (TTCM)	2.1	2.1
8PSK (TTCM)	7.5	4.5
16QAM (TTCM)	10.2	6
32QAM (TTCM)	17.5	11.1

Table 2.2: The value of SNR_r [dB] and $\mathrm{E}_b/\mathrm{N}_0$ [dB] of TTCM for transmission over the **AWGN channel** using a frame length of $1200,000$ symbols. The simulation parameters are shown in Table 2.1. The results were extracted from Figure 2.8

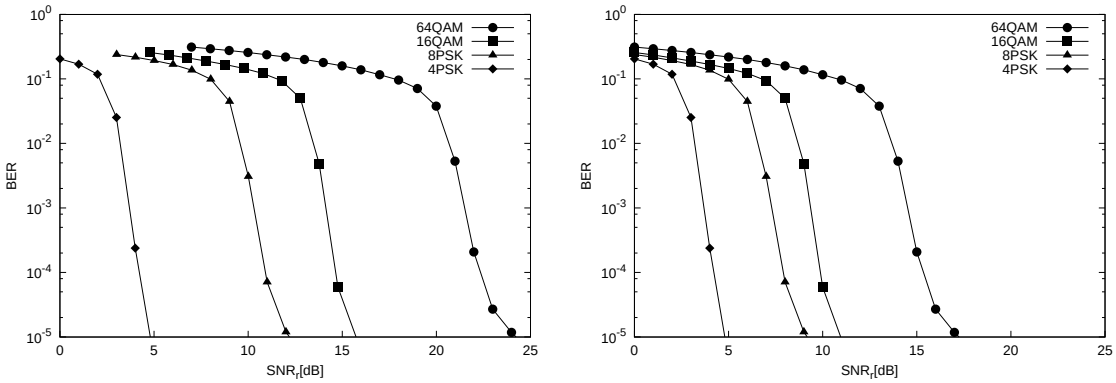

(a) BER vs SNR_r (b) BER vs $\mathrm{E}_b/\mathrm{N}_0$

Figure 2.9: BER performance of TTCM aided 4PSK, 8PSK, 16QAM and 64QAM schemes communicating over an **uncorrelated Rayleigh fading channel** using four TTCM iterations. The simulation parameters are shown in Table 2.1.

Modulation scheme (target BER$=10^{-5}$)	SNR_r [dB]	$\mathrm{E}_b/\mathrm{N}_0$ [dB]
4PSK (TTCM)	4.9	4.9
8PSK (TTCM)	12.2	9.2
16QAM (TTCM)	16.1	12.2
32QAM (TTCM)	24.8	18.5

Table 2.3: The value of SNR_r [dB] and $\mathrm{E}_b/\mathrm{N}_0$ [dB] of TTCM for transmission over the **uncorrelated Rayleigh fading channel** using a frame length of 12000 symbols. The simulation parameters are shown in Table 2.1. The results were extracted from Figure 2.9.

energy per bit to noise power:

$$\mathrm{E}_b/\mathrm{N}_0 \text{ dB} \quad = \quad \mathrm{SNR}_r \text{ dB} - 10\log_{10}(R_c)\,, \tag{2.3}$$

where the code rate R_c was defined in Eq.(2.1).

Moreover, Figure 2.9 presents the BER performance of various TTCM schemes, when communicating over uncorrelated Rayleigh fading channels. Additionally, the SNR_r and $\mathrm{E}_b/\mathrm{N}_0$ thresholds of the TTCM schemes having a target BER of 10^{-5} as shown in Figure 2.8 are tabulated in Table 2.3.

Furthermore, the FER performance curves of various TTCM schemes communicating over AWGN and uncorrelated Rayleigh fading channels are shown in Figure 2.10a and Figure 2.10b, respectively. Finally, the SNR_r thresholds of the TTCM schemes having a target FER below 10^{-3} obtained from Figure 2.10a and Figure 2.10b are shown in Table 2.4.

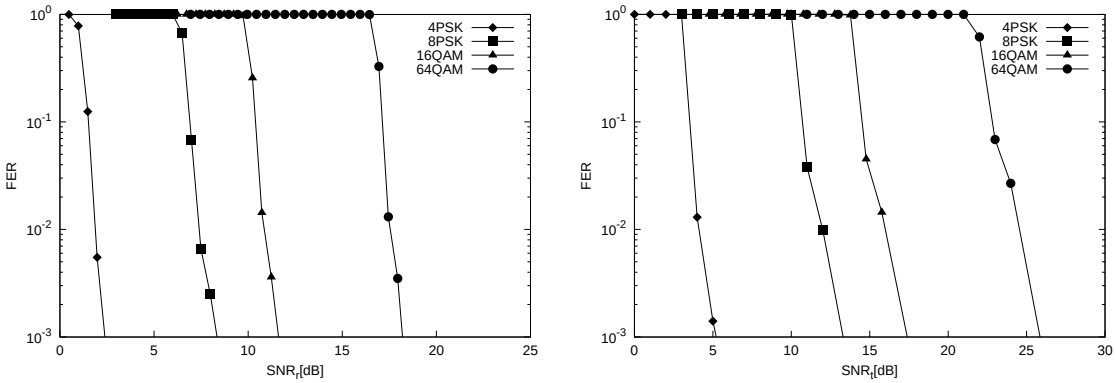

(a) AWGN channel

(b) Uncorrelated Rayleigh fading channel

Figure 2.10: FER versus SNR$_t$ performance of TTCM aided 4PSK, 8PSK, 16QAM and 64QAM schemes using four TTCM iterations. The simulation parameters are shown in Table 2.1.

2.3.2 TTCM Aided SDMA Based TWR

SDMA is a bandwidth efficient scheme, which relies on the Multiple-Input Multiple Output (MIMO) principle. Explicitly, the transmitted signal of L simultaneous (uplink) (UL) (Mobile Stations) (MSs) is received within the same frequency band and differentiated purely by their Channel Impulse Response (CIR). Each MS is equipped with a single transmitter antenna and their signals are received by the P different receiver antennas of the Base Station (BS) [59]. Again, at the BS the individual UL signals are separated with the aid of their unique, user-specific spatial signature constituted by their CIRs, which have to be accurately estimated [59]. A TTCM-aided SDMA OFDM system was studied in [59, 109]. We have investigated a variety of SDMA-based Multi-User Detectors (MUDs) [110], namely the Zero Forcing (ZF), the Minimum Mean-Square Error (MMSE), the Interference Cancellation (IC) and Maximum Likelihood (ML) MUDs. The ML MUD provides the best performance at the cost of the highest complexity. By contrast, the ZF and MMSE MUDs have a poorer performance, but impose a lower complexity. Furthermore, the TTCM-assisted IC arrangement was found to give a better performance than that of the MMSE MUD.

Relay-assisted cooperative communication schemes have been discussed in Section 1.2 of Chapter 1. More explicitly, the attractive TWR scheme of [52] assists a pair of MSs to exchange their signals with the aid of either a single or several RNs using two transmission periods. The TWR protocol aims for improving both the power efficiency as well as the achievable rate and throughput.

Against this background, in this section, we consider a new TTCM-aided SDMA-based TWR scheme constituted by a pair of users, as well as a RN. Both users transmit simultaneously to the RN during the first transmission period. Then, the RN decodes and forwards the received superposed

Modulation scheme (target FER$= 10^{-3}$)	SNR_r[dB]-AWGN channel	SNR_r[dB]-Rayleigh fading channel
4PSK (TTCM)	2.5	5.4
8PSK (TTCM)	8.6	13.6
16QAM (TTCM)	12.4	17.5
32QAM (TTCM)	17.8	26.1

Table 2.4: The value of SNR_r [dB] of TTCM for transmission over the **AWGN channel** and **uncorrelated Rayleigh fading channel** using a frame length of 12000 symbols. The simulation parameters are shown in Table 2.1. The results were extracted from Figure 2.10a and Figure 2.10b.

messages to both MSs during the second transmission period. More specifically, we propose a TTCM-aided SDMA-based TWR scheme, where each MS is equipped with a single UL transmit antenna, while the RN is equipped with two antennas. Two beneficial methods are employed for creating the bit sequence before TTCM-encoding at the RN. Finally, a power-sharing technique is employed for approaching the achievable throughput and for reducing the overall transmit power.

2.3.2.1 System Model and Analysis

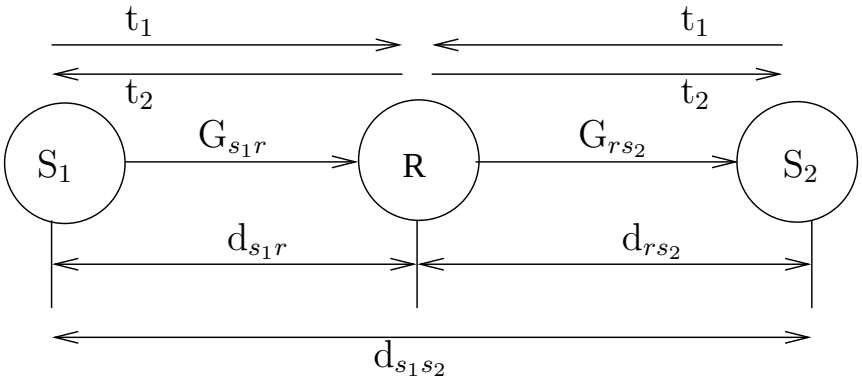

Figure 2.11: Schematic of a TWR aided system, where t_1 is the first transmission period and t_2 is the second transmission period, d_{ab} is the geographical distance between node a and node b. G_{ab} is the geometrical-gain between node a and node b.

The schematic of a TWR scheme is shown in Figure 2.11. During the first Time Slot (TS), both users transmit their information simultaneously to a RN. Then the RN decodes and forwards the received message back to the two users during the second TS [48, 49, 51]. Hence, the overall system throughput is higher than that of a one-way relaying scheme, which requires two TSs to transmit one user's information. The general schematic of the TTCM-aided SDMA-based Source-

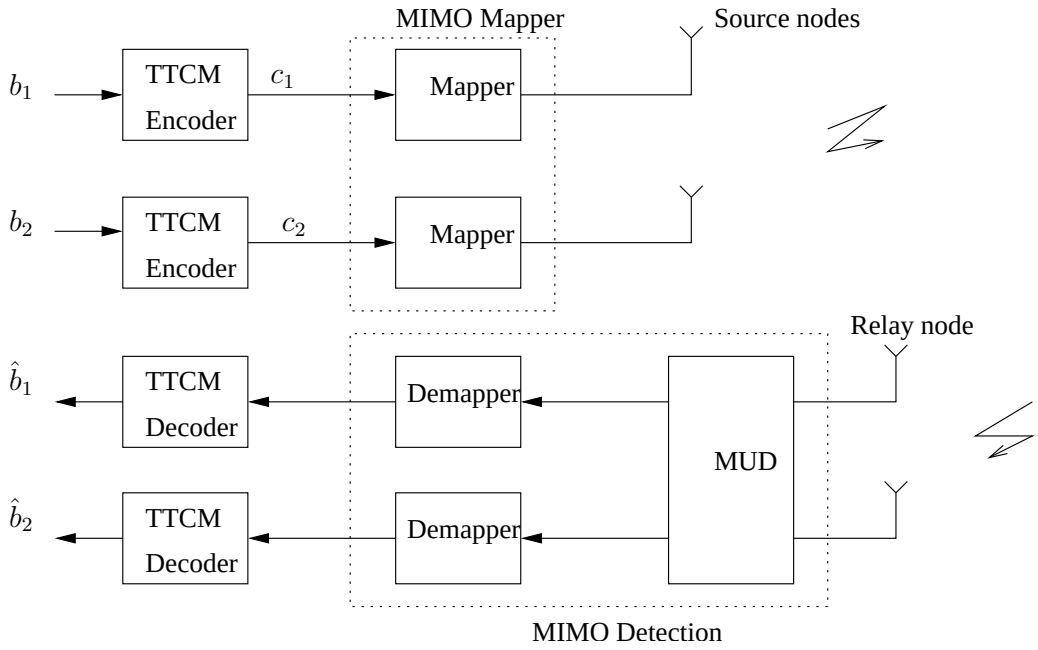

Figure 2.12: The schematic of the Source Node (SN) to RN model.

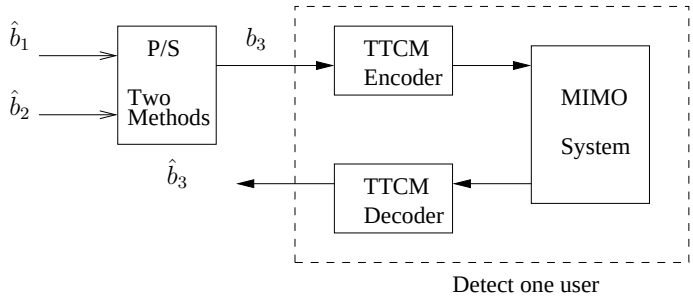

Figure 2.13: The schematic of the RN to Destination Node (DN) model.The block P/S denotes the parallel to serial converter.

to-Relay (SR) model is shown in Figure 2.12. Note that we have opted for TTCM to assist the SDMA system, since the TTCM-SDMA scheme was found to be the best arrangement from a range of coded modulation aided SDMA schemes [109].

As shown in Figure 2.12, the information bit sequences b_1 and b_2 are encoded by the TTCM encoders of MS_1 and MS_2, respectively. The two TTCM codewords c_1 and c_2 are then fed into a virtual MIMO mapper for transmission to the RN. Again, at the RN we consider four MUDs, namely the ML, MMSE, ZF and IC MUDs. The estimated information sequences $\hat{b}_1$ and $\hat{b}_2$ are obtained by the TTCM decoders.

As shown in Figure 2.13, we consider two methods for combining the estimated information sequences $\hat{b}_1$ and $\hat{b}_2$ into b_3. The RN can concatenate the two decoded N-bit sequences into a $2N$-bit sequence, i.e. we have $b_3 = [\hat{b}_1\ \hat{b}_2]$. Alternatively, the RN may combine the two sequences

into another N-bit sequence using modulo-two addition, i.e. we have $b_3 = \hat{b}_1 \oplus \hat{b}_2$, where $\oplus$ is an element-by-element modulo-two addition operator. However, the overall system throughput of the modulo-two addition aided method is higher than that of the concatenation method. The combined sequence b_3 is TTCM-encoded and broadcast from the RN to the two MSs during the second TS. This is similar to an SDMA system using two transmit antennas and one receive antenna. Each MS then detects the signal from the opposite MS based on the TTCM-decoded sequence $\hat{b}_3$. For example, at the receiver of MS_2, the information sequence of MS_1, b_1, can be retrieved from the first part of $\hat{b}_3$, if the concatenation method is used. Alternatively, it can be retrieved from $\hat{b}_1 = b_2 \oplus \hat{b}_3$ if the modulo-two addition method is employed, where b_2 is known at the receiver of MS_2.

2.3.2.1.1 SDMA Channel Model

The received signal of an SDMA system supporting L users, where each is equipped with a single-antenna, and a BS receiver equipped with N_{rx} antennas can be represented by [59, 109]:

$$Y = HX + n\,, \tag{2.4}$$

where the received signal is a $(N_{rx} \times 1)$-dimensional vector $Y = [y_0, y_1, \cdots, y_{N_{rx}-1}]^T$. Still referring to Eq. (2.4), the transmitted signal is an $(L \times 1)$-dimensional vector $X = [x_0, x_1, \cdots, x_{L-1}]^T$ and $n = [n_0, n_1, \cdots, n_{N_{rx}-1}]^T$ is a $(N_{rx} \times 1)$-dimensional Gaussian noise vector, which has a zero mean and a noise variance of $N_0/2$ per dimension.

We consider a two-user SDMA scheme, where the two MSs are considered to be a two-transmitter *virtual* SN. We also consider a two-antenna aided RN. Note that we have incorporated the reduced-pathloss-induced geometrical-gain [46, 47, 111] and the transmit power factor in the channel matrix of Eq. (2.4). Hence, the channel matrix between the two users and the two-antenna aided RN may be written as:

$$H = \begin{bmatrix} \sqrt{G_{s_1r_1}}\sqrt{P_{T,s_1}}h_{s_1r_1} & \sqrt{G_{s_2r_1}}\sqrt{P_{T,s_2}}h_{s_2r_1} \\ \sqrt{G_{s_1r_2}}\sqrt{P_{T,s_1}}h_{s_1r_2} & \sqrt{G_{s_2r_2}}\sqrt{P_{T,s_2}}h_{s_2r_2} \end{bmatrix},$$

where the subscript r_i denotes the ith receive antenna of the RN and the subscript s_j denotes the jth transmit antenna of the virtual two-antenna-aided SN, namely of the jth user. Furthermore, we denote the geometrical-gain between antenna a and antenna b as G_{ab} while $P_{T,a}$ represents the power transmitted from antenna a and h_{ab} represents the CIR coefficient between antenna a and antenna b.

2.3.2.1.2 Multi-User Detector

The MMSE, ZF and IC MUD based SDMA schemes require at least the same number of receiver antennas as that of the transmit antennas [112]. We considered the MMSE, ZF, IC and ML MUDs

in the SR link. However, only the ML MUD is used in the RD link, because there is only a single receive antenna at each DN. The weight matrix of the ZF MUD is defined as :

$$W_{\text{zf}} = H(HH^H)^{-1}\,, \tag{2.5}$$

where H^H is the Hermitian transpose of the channel matrix. The ZF-detected signal can be expressed as [109]:

$$\begin{aligned} Z_{\text{zf}} &= W_{\text{zf}}^H Y \\ &= W_{\text{zf}}^H (HX + n) \\ &= (H^H H)^{-1} H^H HX + (H^H H)^{-1} H^H n \\ &= X + (H^H H)^{-1} H^H n\,. \end{aligned} \tag{2.6}$$

By contrast, the weight matrix of the MMSE MUD is given by [109] :

$$W_{\text{mmse}} = H(HH^H + N_0 I_{N_{rx}})^{-1}\,, \tag{2.7}$$

where $I_{N_{rx}}$ is a $(N_{rx} \times N_{rx})$-element matrix having ones on its diagonal. More explicitly, the MMSE-detected signal can be written as:

$$\begin{aligned} Z_{\text{mmse}} &= W_{\text{mmse}}^H Y \\ &= (H^H H + N_0 I_{N_{rx}})^{-1} H^H HX \\ &\quad + (H^H H + N_0 I_{N_{rx}})^{-1} H^H n\,. \end{aligned} \tag{2.8}$$

Furthermore, the ML MUD is a non-linear detector, which is optimal in terms of minimizing the symbol error probability, when all possible vectors are equally likely [113]. The ML MUD has the highest complexity and it is finding the minimum difference between receiver signal and the possible transmitted symbol multiplied with the same channel transfer function, which means the estimated transmitted signal is those with the smallest difference. The conventional ML detector provides the hard decision which is given by:

$$X = \arg\min_{\tilde{X}} ||Y - H\tilde{X}||^2\,, \tag{2.9}$$

The $\tilde{X}$ is the trial vector, since X denotes all the possible transmitted symbol, so we will compare and get the minimum value of X. The ML receiver structure is simple to implement because the decision criterion depends only on vector distances. However, all possible M^L combinations of the transmitted symbols have to be considered in a ML detector, where M is the number of constellation points and L is the number of transmit antennas. By contrast, the ZF, MMSE and IC MUDs only have to consider M combinations for each. As seen from Eq. (2.8), the BER performance of the MMSE MUD is influenced by the interference introduced by the matrix $(H^H H + N_0 I_{N_{rx}})^{-1} H^H H$, which is non-diagonal. We advocated a low-complexity MMSE-based IC MUD for improving the system performance by removing the off-diagonal elements in the $(H^H H + N_0 I_{N_{rx}})^{-1} H^H H$ matrix.

It is clear from Eq. (2.6) that no residual interference persists after ZF MUD. However, some residual interference still contaminates the MMSE detected signal, as shown in Eq. (2.8). Our IC scheme is described as follows. We assume that 4PSK modulation is employed, hence we have $M = 4$. The soft estimate of a 4PSK symbol is formulated as:

$$\hat{x} = \sum_{i=1}^{J} P(x^{(i)})x^{(i)} , \tag{2.10}$$

where $x^{(i)}$ is the ith symbol in the 4PSK constellation and $P_r(x^{(i)})$ is the probability of $x^{(i)}$. More specifically, from Eq. (2.8) the MMSE-detected signal can be written in a matrix format as:

$$\begin{bmatrix} z_1 \\ z_2 \end{bmatrix} = \begin{bmatrix} a_1 & b_1 \\ c_1 & d_1 \end{bmatrix} \times \begin{bmatrix} x_1 \\ x_2 \end{bmatrix} + \begin{bmatrix} a_2 & b_2 \\ c_2 & d_2 \end{bmatrix} \times \begin{bmatrix} n_1 \\ n_2 \end{bmatrix} , \tag{2.11}$$

where $\begin{bmatrix} a_1 & b_1 \\ c_1 & d_1 \end{bmatrix}$ is the $W_{\text{mmse}}^H H$ term and $\begin{bmatrix} a_2 & b_2 \\ c_2 & d_2 \end{bmatrix}$ is the W_{mmse}^H term. The resultant noise variance in z_1 is given by:

$$\begin{aligned} var(a_2 n_1 + b_2 n_2) &= |a_2|^2 N_0 + |b_2|^2 N_0 \\ &= (|a_2|^2 + |b_2|^2) N_0, \end{aligned} \tag{2.12}$$

where $N_0/2$ is the original noise variance per dimension. We can detect the signal received from MS_1 by removing the interference from MS_2 based on Eq. (2.11), as follows:

$$\begin{aligned} \tilde{z}_1 &= z_1 - b_1 x_2 \\ &= a_1 x_1 + a_2 n_1 + b_2 n_2 . \end{aligned} \tag{2.13}$$

Similarly, the signal received from MS_2 can be detected as:

$$\begin{aligned} \tilde{z}_2 &= z_2 - c_1 x_1 \\ &= d_1 x_2 + c_2 n_1 + d_2 n_2 . \end{aligned} \tag{2.14}$$

Then, $\tilde{z}_1$ and $\tilde{z}_2$ of Eqs. (2.13) and (2.14) can be fed into the corresponding TTCM decoder for detecting the corresponding information sequences.

2.3.2.1.3 Soft Decision Based MUD

The block diagram of a TTCM-aided MIMO system using soft-decision feedback is shown in Figure 2.14. The output of the MAP decoder at the receiver is fed back to the MIMO demodulator. The MAP decoder, which was introduced in Section 2.2.4, computes the *a posteriori* probabilities for both the non-systematic channel-coded bits and for the original information bits. As seen from Figure 2.14, the information bits U are entered into the TTCM encoder and the corresponding output codeword is C. The MAP decoder is a four-port device that has $P^{apri}(X)$ and $P^{apri}(U)$ at its

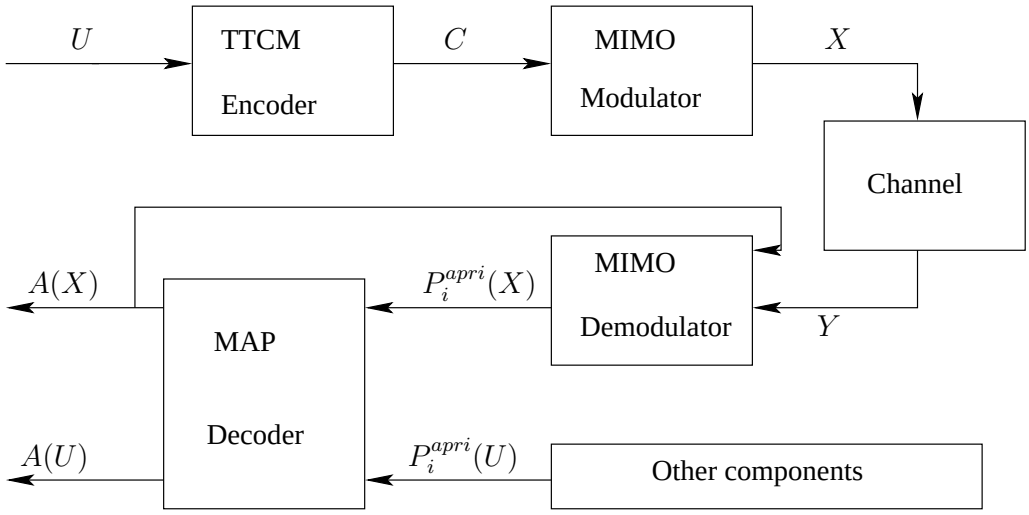

Figure 2.14: The schematic of TTCM-aided SDMA scheme using soft-decision feedback, where the notations P_i^{apri} and $A_{i,m}$ denote the *a priori* and *a posteriori* probabilities, respectively. The defination of $A_{i,m}$ is shown in Eq. (14.21) of [104].

input and produces the probabilities $A(X)$ and $A(U)$ [114]. The $P^{apri}(U)$ is the *a priori* probability of the information bits U and it is obtained from the other component decoder of the parallel concatenated turbo coding scheme. By contrast, $P^{apri}(X)$ is obtained by the soft-decision MIMO demodulator, where X is transmitted directly over the channel. The conditional probability of receiving a signal vector y, given an M-ary PSK/QAM signal vector $X = \{x^{(m)}\}$ was transmitted, where $m \in \{0, \cdots, M-1\}$ is given by:

$$\mathrm{P}(y_k|x = x^{(m)}) = \frac{1}{\pi N_0} \exp\left(-\frac{|y_k - H^{(m)}W^{(m)}x_i^{(m)}|^2}{N_0}\right), \quad (2.15)$$

where the $W^{(m)}$ denotes the weight matrix of the MUD applied to the input signal vector $x^{(m)}$. The specific receiver relying on the weight matrices of the MMSE, ZF and IC MUDs are described in Section 2.3.2.1.2.

2.3.2.1.4 Optimum Power Sharing Between the SN and RN

The employment of an appropriate power sharing technique is proposed for apportioning the transmit power between the SN and RN. This will allow us to reduce the overall transmission power required in the TWR scheme. This is necessary, because the SR and the RD links require different received SNRs for achieving the same BER. The reason behind this is that the two-antenna virtual user at the SN and the RN constitutes a (2×2)-element MIMO scheme, which requires a lower SNR, i.e. a lower transmit power than the (2×1)-element RD link. Hence appropriately sharing the total transmit power between them allows us to reduce the overall power required. Naturally, in a practical system an appropriately designed agile SR power-control scheme is required for maintaining the optimum sharing of the transmit power between the SN and RN. We

consider a free-space path-loss model. The corresponding Reduced-Distance-Related-Pathloss-Reduction (RDRPR) [46, 47, 111] between MS_1 and the RN as well as between the RN and MS_2 are given by:

$$G_{s_1 r} = \left(\frac{d_{s_1 s_2}}{d_{s_1 r}}\right)^2, \tag{2.16}$$

and

$$G_{r s_2} = \left(\frac{d_{s_1 s_2}}{d_{r s_2}}\right)^2, \tag{2.17}$$

respectively, where d_{ab} denotes the geometrical distance between node a and node b. If the RN is located at the mid-point between MS_1 and MS_2, then we have $G_{s_1 r} = G_{r s_2} = 4$.

The average received Signal to Noise power Ratio (SNR) per-user per-receive antenna[2] at the receiver node b with respect to the transmitter node a can be computed as:

$$\begin{aligned} \gamma_R &= \frac{P_{T,a} E\{|G_{ab}|\}}{N_0} \cdot \frac{\sum_{b_i=1}^{N_b} \sum_{a_j=1}^{N_a} E\{|h_{b_i a_j}|^2\} E\{|x_{a_j}|^2\}}{N_b\, N_a} \\ &= \frac{P_{T,a} G_{ab}}{N_0}, \end{aligned} \tag{2.18}$$

where N_b and N_a are the number of antennas at node b and node a, respectively. Furthermore, x_{a_j} is the symbol transmitted from the jth antenna of node a, $h_{b_i a_j}$ is the channel coefficient from antenna a_j to antenna b_i, $P_{t,a}$ is the power transmitted from node a and the expected values are given by $\mathrm{E}\{|h_{b_i a_j}|^2\} = 1$ and $\mathrm{E}\{|x_{a_j}|^2\} = 1$. We define the term *transmit SNR*[3] as the ratio of the power transmitted from node a to the noise power encountered at the receiver of node b as:

$$\begin{aligned} \gamma_T &= \frac{P_{T,a} E\{|x_{a_j}|^2\}}{N_0} \\ &= \frac{P_{T,a}}{N_0}. \end{aligned} \tag{2.19}$$

Hence, the relationship between γ_T and γ_R can be shown to be:

$$\gamma_R = \gamma_T\, G_{ab}, \tag{2.20}$$

which is also given by

$$\mathrm{Y}_R = \mathrm{Y}_T + 10\log_{10}(G_{ab})\ [\mathrm{dB}], \tag{2.21}$$

where $\mathrm{Y}_R = 10\log_{10}(\gamma_R)$ and $\mathrm{Y}_T = 10\log_{10}(\gamma_T)$. Let us denote the transmit SNR of MS_1, MS_2 and the RN as γ_{T,s_1}, γ_{T,s_2} and $\gamma_{T,r}$, respectively. We jointly consider the two users as a single two-transmitter SN during the first TS and the RN is located at the mid-point between the two users.

[2] We introduced the terminology of per-user, per-receive antenna SNR for the sake of a fair comparison of the different scenarios considered and to emphasise the fact that these results may be applicable to other relaying scenarios.

[3] Although the concept of transmit SNR [111] is unconventional, because it relates the transmit power to the noise power at the receiver, which are at physically different locations, it is convenient for our discussions.

Hence, the power transmitted from both MSs is considered to be equal, i.e. $\gamma_{T,s} = \gamma_{T,s_1} = \gamma_{T,s_2}$. The average transmit SNR of the system can be computed as:

$$\bar{\gamma}_T = \frac{\gamma_{T,s} + \gamma_{T,r}}{2}, \tag{2.22}$$

$$= \frac{10^{\frac{\Upsilon_{T,s}}{10}} + 10^{\frac{\Upsilon_{T,r}}{10}}}{2}, \tag{2.23}$$

where we have $\Upsilon_{T,s} = 10\log_{10}(\gamma_{T,s})$ and $\Upsilon_{T,r} = 10\log_{10}(\gamma_{T,r})$. The proposed power sharing method is provided to minimize the overall transmit power, while ensuring that the RN achieve a BER of approximately 5×10^{-7} while the DN simultaneously achieves a BER of 10^{-6} at the lowest possible transmit SNR. More specifically, we first find the receive SNR required for the SR link, namely $\Upsilon_{R,s} = 10\log_{10}(\gamma_{R,s})$, and that of the RD link, namely $\Upsilon_{R,r} = 10\log_{10}(\gamma_{R,r})$, for achieving a BER of 5×10^{-7}. The difference between these receive SNRs is given by:

$$\begin{aligned} \Upsilon_{R,\Delta} &= \Upsilon_{R,r} - \Upsilon_{R,s}, \\ &= (\Upsilon_{T,r} + 10\log_{10}(G_{rs_2})) - (\Upsilon_{T,s} + 10\log_{10}(G_{s_1r})), \\ &= \Upsilon_{T,r} - \Upsilon_{T,s}\,[\text{dB}], \end{aligned} \tag{2.24}$$

where $\Upsilon_{R,\Delta} = 10\log_{10}(\gamma_{R,\Delta})$. Then in the non-decibel domain, the difference between these transmit SNRs is derived as:

$$\gamma_{R,\Delta} = \frac{\gamma_{T,r}}{\gamma_{T,s}}. \tag{2.25}$$

By referring to the Eq. (2.25), the $\gamma_{T,r}$ may be expressed as:

$$\gamma_{T,r} = \gamma_{R,\Delta}\gamma_{T,s}. \tag{2.26}$$

Then Eq. (2.22) may be rewritten as:

$$\bar{\gamma}_T = \frac{\gamma_{T,s} + \gamma_{T,r}}{2}, \tag{2.27}$$

$$= \frac{\gamma_{T,s} + \gamma_{R,\Delta}\gamma_{T,s}}{2},$$

$$= \frac{\gamma_{T,s}(1 + \gamma_{R,\Delta})}{2}$$

Thus, the transmit SNR at the SN is given by:

$$\gamma_{T,s} = \frac{2\bar{\gamma}_T}{1 + \gamma_{R,\Delta}}. \tag{2.28}$$

Similarly, by referring to Eq. (2.25), the $\gamma_{T,s}$ may be expressed as:

$$\gamma_{T,s} = \frac{\gamma_{T,r}}{\gamma_{R,\Delta}}. \tag{2.29}$$

Furthermore, Eq. (2.22) may be rewritten as:

$$\bar{\gamma}_T = \frac{\frac{\gamma_{T,r}}{\gamma_{R,\Delta}} + \gamma_{T,r}}{2}, \tag{2.30}$$

$$= \frac{\gamma_{T,r}(\frac{1}{\gamma_{R,\Delta}} + 1)}{2}.$$

By refereeing the Eq. (2.29) and Eq. (2.31), the transmit SNR at the RN can be formulated as:

$$\gamma_{T,r} = \frac{2\bar{\gamma}_T \gamma_{R,\Delta}}{1+\gamma_{R,\Delta}}. \quad (2.31)$$

Moreover, the overall system throughput η_s of our TWR scheme is given by:

$$\eta_s = \frac{LI_b}{N_1+N_2}, \quad (2.32)$$

where N_1 denotes the number of symbols received at the RN during the first TS, N_2 is the number of modulated symbols transmitted from the RN during the second TS, $L = 2$ denotes the number of users, while I_b is the number of information bits transmitted per user within a duration of $(N_1 + N_2)$.

2.3.2.2 Simulation Results

CM	TTCM
Modulation	QPSK
No. of iterations	4
Decoder	Approximate Log-MAP
Symbol per frame	1,200
No. of frames	10,000
Channel	Rayleigh fading channel
Pathloss	$G_{sr} = G_{rd} = 4$ (6.02dB)

Table 2.5: System parameters of proposed TTCM aided SDMA based TWR scheme.

An uncorrelated Rayleigh fading channel is considered and an outer iteration is defined as that when the SDMA detector and the TTCM decoder are activated once. As seen from Figure 2.15, the scheme employing ML MUD that invokes four outer iterations has the best BER performance and the ZF MUD has the worst BER performance in the SR link. There is an approximately 8.5 dB$-$3.9 dB=4.6 dB difference in terms of their received SNRs at a BER of 10^{-6}. Furthermore, after the fourth iteration the IC scheme outperforms the MMSE MUD. This is because the interfering signal introduced by the MMSE MUD is cancelled by the IC MUD. The performance of the ZF MUD cannot be further improved by having additional outer iterations, because the interfering signal has already been removed. In the first TS, the transmitted frame length is $N_1 = 1200$ symbols.

The performance of various TTCM-aided SDMA-based schemes employing ML MUD, when communicating over the RD link during the second TS is shown in Figure 2.16. When the concatenation method of Section 2.3.2.1 is employed, the total number of 4PSK modulated symbols transmitted from the RN is 2400. By contrast, when the modulo-two addition method of Section 2.3.2.1 is employed, we have 1200 symbols. However, due to the employment of two transmit antennas at

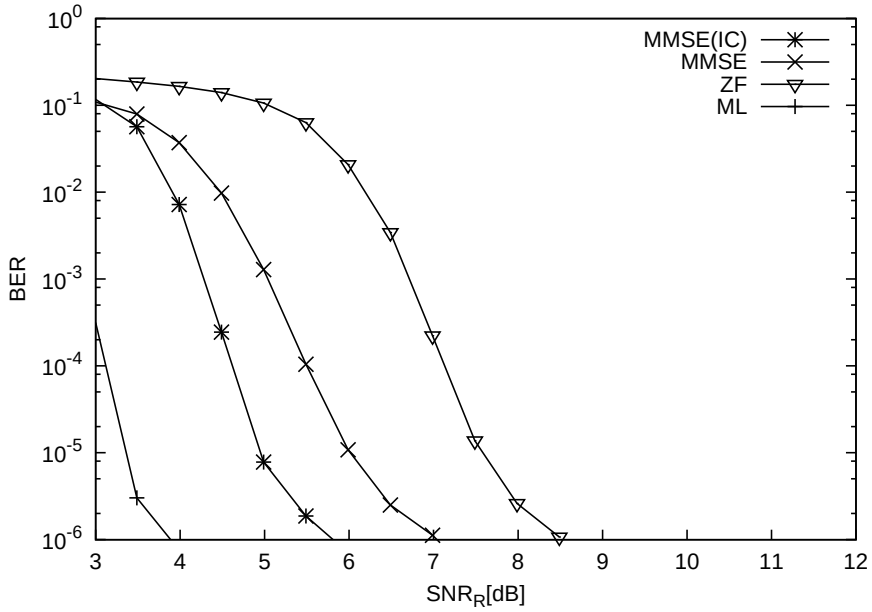

Figure 2.15: BER versus received SNR per-user per-receiver antenna performance of various 4PSK-TTCM-aided SDMA schemes employing ML, MMSE, IC and ZF MUDs in the SR link. The TTCM decoder employs 4 inner iterations and 4 outer iterations for exchanging extrinsic information with the SDMA detector. The corresponding parameters are shown in Table 2.5 and the frame length is $N_1 = 1200$.

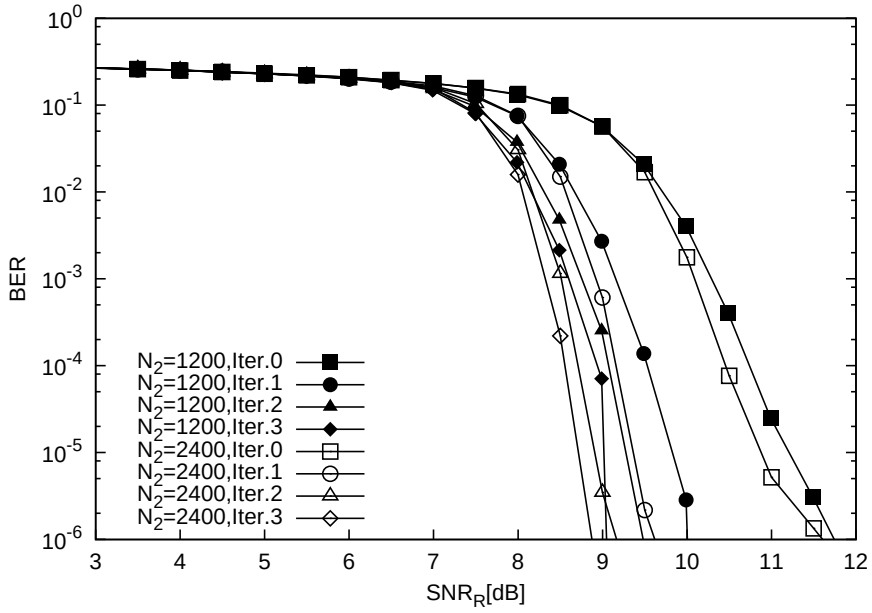

Figure 2.16: BER versus received SNR per-user per-receiver antenna performance of various 4PSK-TTCM-aided SDMA schemes employing ML MUD in the RD link. The TTCM decoder employs 4 inner iterations and 4 outer iterations for exchanging extrinsic information with the SDMA detector. The corresponding parameters are shown in Table 2.5 and the frame lengths considered are $N_2 = 1200$ and $N_2 = 2400$.

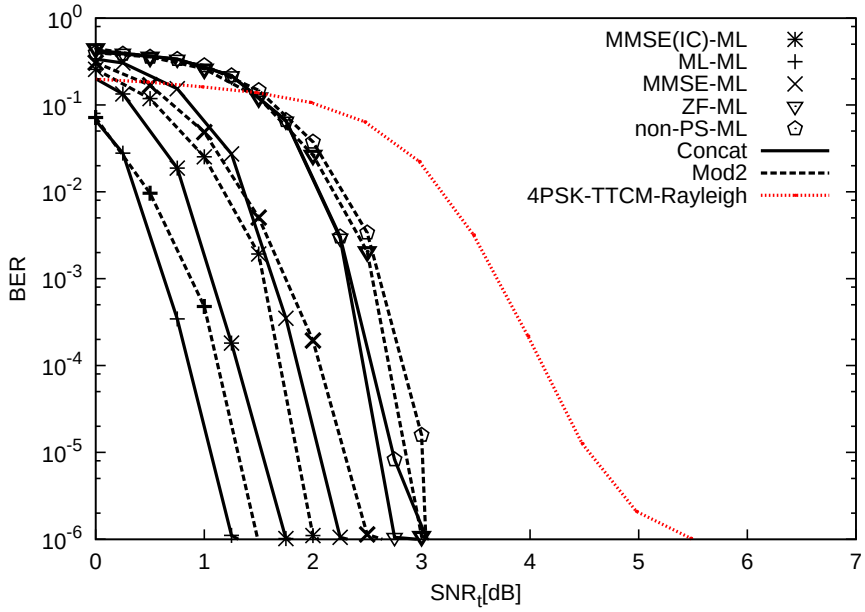

Figure 2.17: BER performance versus SNR$_t$ per user of various 4PSK-TTCM-aided SDMA-based TWR scheme. The notation 'MMSE-ML' is used to refer to a scheme employing MMSE MUD at the SR and then the ML MUD at the RD link. Similar meaning applies to the notations 'ML-ML', 'IC-ML' and 'ZF-ML'. The modulo-two addition method is represented by 'mod2' and the concatenation method is represented by 'concat'. Furthermore, all schemes employ the power sharing mechanism except those with the notation 'Non-PS'. The TTCM decoder employs 4 inner iterations and 4 outer iterations for exchanging extrinsic information with the SDMA detector. The 'TTCM-Rayleigh' scheme is our single-user benchmark which communicates over a single transmitter and a single receiver link. The parameters are shown in Table 2.5.

the RN, the total transmission period is given by $N_2 = 1200$ or $N_2 = 600$ symbols, depending on whether the concatenation or the modulo-two addition method is employed, respectively. As shown in Eq. (2.32), the overall system throughput of the scheme employing the concatenation method is $\eta_s = 1$ BPS. By contrast, that of the scheme using the modulo-two addition method is given by $\eta_s = 1.33$ BPS, because we have $I_b = 1200$ information bits transmitted per user. Based on Figure 2.15 and Figure 2.16, the differences between these received SNRs are shown in Table 2.6.

Figure 2.17 portrays the BER versus transmitted SNR per user performance of various TTCM-aided SDMA-based TWR schemes. We have also considered a single-user non-cooperative benchmark scheme denoted as 'TTCM-Rayleigh', where a single transmitter and a single receiver are employed. Its throughput is 1 BPS. At the same throughput, the TWR scheme employing the concatenation method, but operating without the power sharing mechanism, denoted as 'Concat:non-PS-ML', outperforms the 'TTCM-Rayleigh' benchmarker by approximately 5.5 dB$-$3 dB$=$ 2.5 dBs at a BER of 10^{-6}. When the power sharing mechanism is activated, a further 3 dB$-$1.2 dB$=$ 1.8 dBs

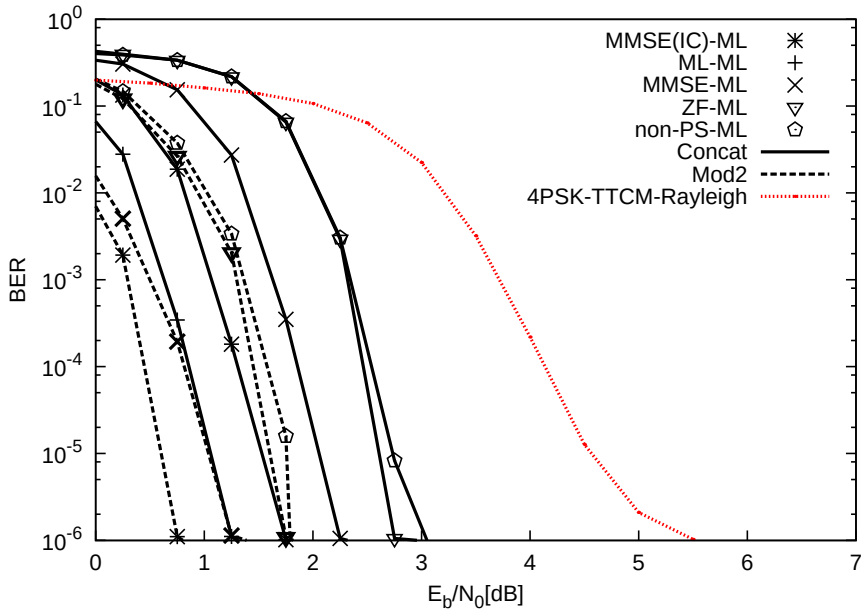

Figure 2.18: BER performance versus E_b/N_0 per user of various 4PSK-TTCM-aided SDMA-based TWR scheme. The notation 'MMSE-ML' is used to refer to a scheme employing MMSE MUD at the SR and then the ML MUD at the RD link. Similar meaning applies to the notations 'ML-ML', 'IC-ML' and 'ZF-ML'. The modulo-two addition method is represented by 'mod2' and the concatenation method is represented by 'concat'. Furthermore, all schemes employ the power sharing mechanism except those with the notation 'Non-PS'. The TTCM decoder employs 4 inner iterations and 4 outer iterations for exchanging extrinsic information with the SDMA detector. The 'TTCM-Rayleigh' scheme is our single-user benchmark which communicates over a single transmitter and a single receiver link. The parameters are shown in Table 2.5.

Methods ($Y_{R,\Delta}$)	Outer iteration	SNR difference, $Y_{R,\Delta}$			
		ML-ML	MMSE-ML	IC-ML	ZF-ML
Concatenation	Iteration 0	7.8dB	5.8dB	4.6dB	3.1dB
	Iteration 1	5.8dB	3.8dB	2.6dB	1.1dB
	Iteration 2	5.4dB	3.4dB	2.2dB	0.7dB
	Iteration 3	5.0dB	3.0dB	1.8dB	0.3dB
Modulo-two Addition	Iteration 0	7.9dB	5.9dB	4.7dB	3.3dB
	Iteration 1	6.2dB	4.2dB	3.0dB	2.5dB
	Iteration 2	5.6dB	3.6dB	2.4dB	0.9dB
	Iteration 3	5.3dB	3.3dB	2.1dB	0.6dB

Table 2.6: SNR_r differences between SN and RN $Y_{R,\Delta}$ in decibel. The results were extracted from Figure 2.15 and Figure 2.16.

SNR gain can be attained by the 'Concate:ML-ML' scheme over the 'Concat:non-PS-ML' scheme, as seen in Figure 2.17 at a BER of 10^{-6}. The IC based scheme outperforms the MMSE and ZF based MUDs, while as expected, the ML based scheme gives the best BER performance.

Note that the SNR per bit is defined in Eq. (2.3). Figure 2.18 shows the BER versus transmit E_b/N_0 per user performance of various TTCM-aided SDMA-based TWR schemes, which is useful for comparing the performance of the schemes employing the concatenation and the modulo-two addition methods, because they have different throughputs. The scheme employing modulo-two addition outperforms that employing the concatenation method by approximately 1 dBs at a BER of 10^{-6}, as seen by comparing the 'Mod2:ML-ML' and the 'Concate:ML-ML' curves in Figure 2.18, where both schemes employ the ML MUD and the power sharing mechanism is activated. Similar improvements can be observed in Figure 2.18 for the IC, MMSE and ZF based schemes, when the modulo-two addition method is employed instead of the concatenation method. As seen in Figure 2.18, the 'Mod2:ML-ML' scheme outperforms the 'TTCM-Rayleigh' benchmark scheme by approximately 5.5 dB$-$0.2 dB$=$ 5.3 dBs, which is a benefit of the proposed power- and bandwidth-efficient SDMA-based TWR scheme. The MMSE-detected SDMA-based TWR scheme offers a lower complexity at the cost of a modest 0.8 dB$-$0.2 dB$=$ 0.6 dB SNR loss in comparison to the ML-based scheme, as shown by the 'Mod2:ML-ML' and 'Mod2:IC-ML' curves in Figure 2.18 at a BER of 10^{-6}.

2.3.3 TTCM aided SDMA Based TWR Impaired with Error Estimation

We have investigated a TTCM aided SDMA based TWR scheme assuming perfect knowledge of the Channel State Information (CSI) at all RN and DNs, in Section 2.3.2. However perfect CSI estimation is not realistic in practice [115], especially in a mobile communication system having time-varying wireless channels. In this section, we will investigate the performance of the TTCM aided SDMA based TWR scheme, when the CSI estimation is impaired by estimation errors.

2.3.3.1 System Model

In Section 2.3.2.1.1, the received signal of an SDMA system supporting L users is defined in Eq. (2.4). In the case of imperfect channel knowledge, the estimate of the channel gain matrix $\tilde{H}$ is constructed by the channel gain matrix H modeled by independent zero-mean complex-valued Gaussian random variables and the channel error matrix $\tilde{N}$ that has a variance of $var(\tilde{N})$. The estimation of the channel gain matrix may be written as [116, 117]:

$$\tilde{H} \quad = \quad H + \tilde{N} \, . \tag{2.33}$$

The channel matrix H between the two users and the twin-antenna aided RN is defined in Eq. (2.5). The channel estimation error $\tilde{N}$ is assumed to be independent identical Gaussian distributed obeying the standard Gaussian distribution of zero mean. The degree of CSI estimation errors is gov-

erned by the Channel Estimation Factor (CEF), namely w (dB) defined by:

$$w = 10\log_{10}\frac{1}{\text{var}(\tilde{N})}\,[\text{dB}]\,. \tag{2.34}$$

Then the received signal model of an SDMA system impaired by imperfect channel estimation may be rewritten as:

$$\begin{aligned} Y &= \tilde{H}X + n \\ &= (H + \tilde{N})X + n\,. \end{aligned} \tag{2.35}$$

We employed the MMSE, ZF, IC and ML based MUDs in the SR link of our proposed system. However, only the most powerful ML MUD is used in the RD link, since there is only a single receive antenna at each DN, hence all the other MUDs would result in a high error-floor in this rank-deficient scenario. Moreover, the algorithms of these MUDs have been introduced in Section 2.3.2.1.2. In a realistic system, both pilot-aided channel estimation [118], as well as blind channel estimation [119, 120] and semi-blind channel estimation [121] may be employed. However, we emphasize that regardless of the estimation techniques employed, the estimation error is actually non-Gaussian, hence using a Gaussian model constitutes an approximation. The simulation results of our proposed scheme subjected to CSI estimation channel errors are discussed in Section 2.3.3.2.

2.3.3.2 Simulation Results

The simulation parameters of our proposed system is characterized in Table 2.7. Figure 2.19

Coded Modulation	TTCM
Modulation	4PSK
No. of iterations	4
Decoder	Approximate Log-MAP
Symbols per frame	1200
No. of frames	10000
Channel	Rayleigh fading channel
Pathloss	$G_{sr} = G_{rd} = 4$ (6.02dB)

Table 2.7: System parameters of our proposed scheme in imperfect channel when the CEF is $w = 15$ dB.

characterizes the BER versus SNR_r performance of the 4PSK-TTCM-aided SDMA scheme when employing the ML MUD in the SR link for transmission over the Rayleigh fading channel, assuming imperfect CSI at the receiver. The channel estimation error is governed by the CEF, w of Eq. (2.34), and the BER performance approaches to the benchmarker's performance having a

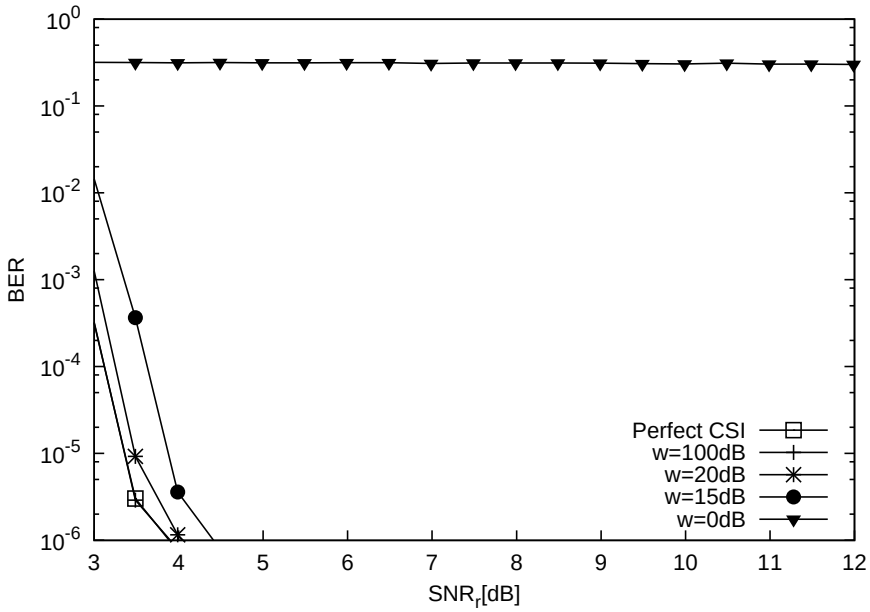

Figure 2.19: BER versus received SNR per-user per-receiver antenna performance of various 4PSK-TTCM-aided SDMA schemes employing ML MUD in the SR link having imperfect CSI governed by the ratio w. The TTCM decoder employs 4 inner iterations and 4 outer iterations. The parameters are refer to Table 2.7 and the frame length is $N_1 = 1200$.

perfect CSI, as w increases. The CEF of the benchmark with the perfect CSI is $w = \infty$. Observe in Figure 2.19 that we have considered four values of associated w for our proposed imperfect- based scheme, namely 100 dB, 20 dB, 15 dB and 0 dB. The scheme associated with $w = 0$ dB exhibits a high BER floor, since the channel estimation is inadequate for practical detection. Additionally, the BER performance governed by $w = 100$ dB overlaps with the ML MUD performance in perfect channel. We have investigated the BER performance of our proposed scheme both under perfect and imperfect channel estimation. We will use $w = 15$ dB for the remaining simulations in this section.

As seen from Figure 2.20, the proposed scheme that employs the ML MUD has the best BER performance and there is an approximately 9.8 dB$-$4.4 dB$=$ 5.4 dB SNR difference between the ML MUD and the ZF MUD at a BER of 10^{-6}. By comparing Figure 2.20 and Figure 2.15, it is clear that the BER performance of the 4PSK-TTCM-aided SDMA scheme associated with imperfect channel estimation has a worse performance compared to that of the perfect channel estimation scenario. Additionally, the BER performance of the ML MUD in the imperfect channel scenario exhibited a further 4.4 dB -3.9 dB $=$ 0.5 dB SNR loss over the ML MUD having a perfect channel estimation. The BER performance of the other three MUDs relying on the perfect channel estimation is shown in Figure 2.15. Observe from Figure 2.20, they have approximately 1 dB SNR loss at the BER of 10^{-6} in comparison to their counterparts having a perfect channel estimation of Figure 2.15. Figure 2.21 portrays the BER versus received SNR per-user per-receiver

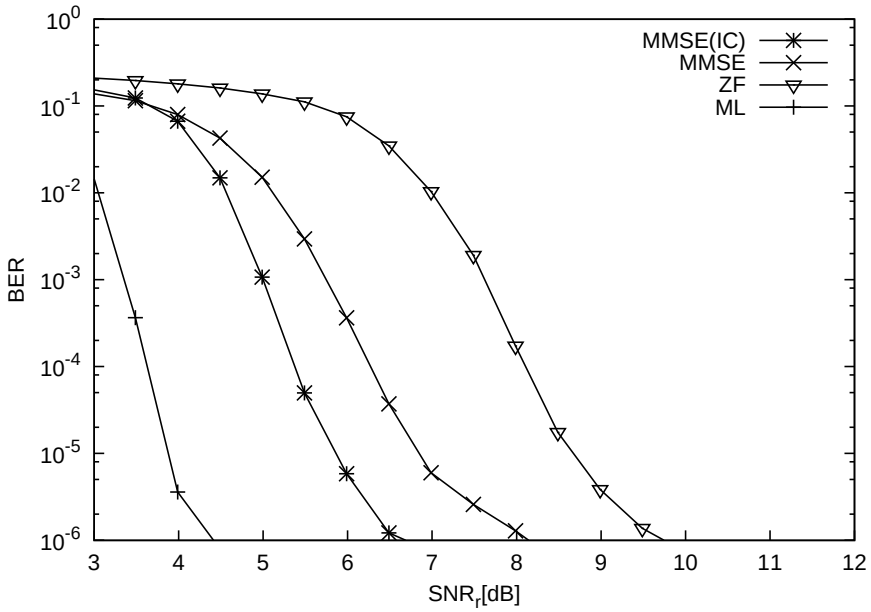

Figure 2.20: BER versus received SNR per-user per-receiver antenna performance of various 4PSK-TTCM-aided SDMA schemes employing ML, MMSE, IC and ZF MUDs in the SR link. The TTCM decoder employs 4 inner iterations and 4 outer iterations for exchanging extrinsic information with the SDMA detector in **imperfect channel while $w = 15$ dB**. The parameters are refer to Table 2.7 and the frame length is $N_1 = 1200$.

antenna performance of various 4PSK-TTCM-aided SDMA schemes employing the ML MUD in the RD link associated with a CSI estimation error of $w = 15$ dB. When the concatenation method of Section 2.3.2.1 is employed, the total number of 4PSK modulated symbols transmitted from the RN is $N_2 = 2400$. By contrast, when the modulo-two addition method of Section 2.3.2.1 is invoked, we have $N_2 = 1200$ symbols. Similar to Figure 2.16, the scheme employing the ML MUD in conjunction with the concatenation method that invokes four outer iterations has the best BER performance and the ZF MUD relying on the modulo-two addition method has the worst BER performance in the RD link at a BER of 10^{-6}. Furthermore, the IC MUD outperforms the MMSE MUD after the fourth iteration, since the interfering signal that cannot be mitigated by the MMSE MUD is successfully reduced by the IC MUD.

The BER versus transmitted SNR per user performance of various 4PSK-TTCM-aided SDMA-based TWR schemes associated with a realistic CSI estimation error is shown in Figure 2.22. The BER performance of the TWR schemes that employed the concatenation method (concat) are substantially better than that using the modulo-two (Mod2) method. More explicitly the 'Concat:ML-ML', outperforms the 'Mod2:ML-ML' by approximately 3.5 dB -3 dB $= 0.5$ dB at a BER of 10^{-6}. Observe in Figure 2.17, that the ZF MUD based scheme having a CSI estimation error is inferior to the scheme employing ZF MUD based on perfect channel estimation by approximately 4.9 dB -2.9 dB $= 2$ dB at a BER of 10^{-6}. As we expected, the performance of IC based scheme

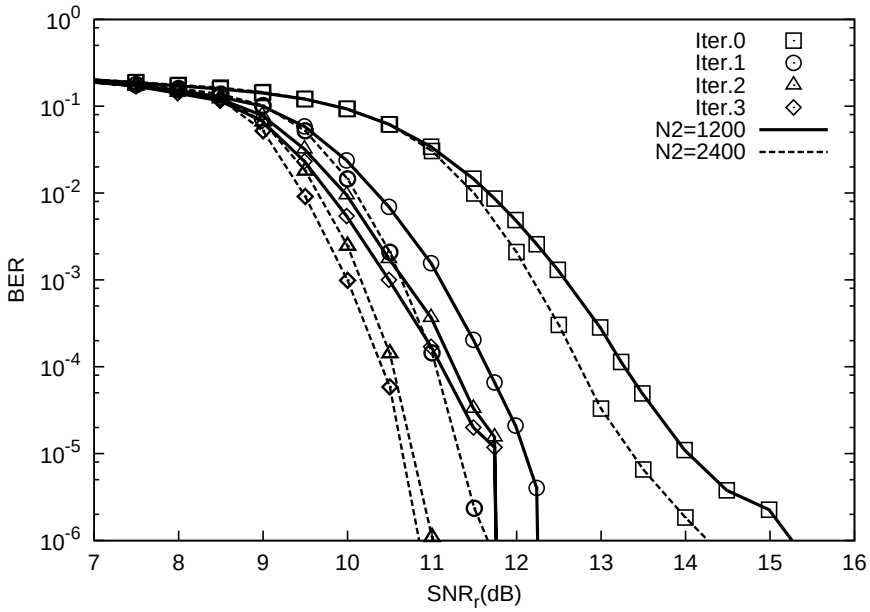

Figure 2.21: BER versus received SNR per-user per-receiver antenna performance of various 4PSK-TTCM-aided SDMA schemes employing ML MUD in the RD link in **imperfect channel having $w = 15$ dB**. The TTCM decoder employs 4 inner iterations and 4 outer iterations for exchanging extrinsic information with the SDMA detector. The parameters are refer to Table 2.7 and the frame lengths considered are $N_2 = 1200$ and $N_2 = 2400$.

Methods ($\Upsilon_{R,\Delta}$)	Outer iteration	SNR difference, $\Upsilon_{R,\Delta}$			
		ML-ML	MMSE-ML	IC-ML	ZF-ML
Concatenation	Iteration 0	9.7dB	6.0dB	7.3dB	4.2dB
	Iteration 1	7.1dB	3.4dB	4.5dB	1.6dB
	Iteration 2	6.5dB	2.8dB	4.1dB	1.0dB
	Iteration 3	6.3dB	2.6dB	3.9dB	0.8dB
Modulo-two	Iteration 0	10.7dB	7.0dB	8.3dB	5.2dB
	Iteration 1	7.8dB	4.1dB	5.4dB	2.3dB
Addition	Iteration 2	7.3dB	3.6dB	4.9dB	0.8dB
	Iteration 3	7.3dB	3.6dB	4.9dB	0.8dB

Table 2.8: System parameters and SNR_r differences between SN and RN, $\Upsilon_{R,\Delta}$ in decibel when the CEF is $w = 15$ dB. The results were extracted from Figure 2.20 and Figure 2.21.

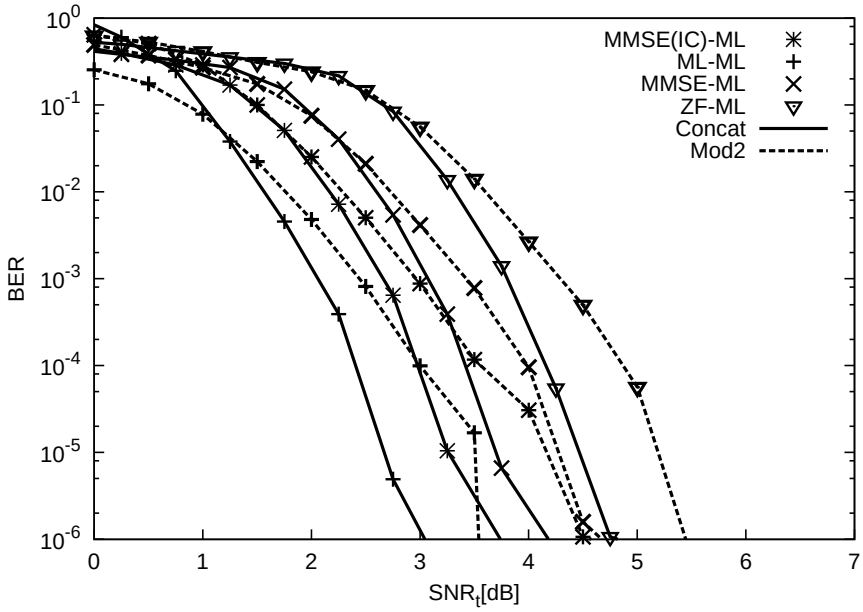

Figure 2.22: BER versus transmitted SNR per user performance of various 4PSK-TTCM-aided SDMA-based TWR schemes in **imperfect channel having $w = 15$ dB**. The notation 'MMSE-ML' is used to refer to a scheme employing MMSE MUD at the SR and then the ML MUD at the RD link. Similar meaning applies to the notations 'ML-ML', 'IC-ML' and 'ZF-ML'. The modulo-two addition method is represented by 'mod2' and the concatenation method is represented by 'concat'. Furthermore, all schemes employ the power sharing mechanism. The parameters are refer to Table 2.7.

outperforms the MMSE and ZF based MUDs. Figure 2.23 shows the BER versus E_b/N_0 per user performance of various 4PSK-TTCM-aided SDMA-based TWR schemes associated with a CSI estimation error. The schemes employing the Mod2 method outperform the concat method by approximately 0.8 dBs at a BER of 10^{-6}. Similar improvements can be obtained for the IC, MMSE and ZF MUDs based schemes, when the modulo-two addition method is employed.

2.3.4 Adaptive TTCM

As early as 1968, Hayes found that an efficient technique of mitigating the detrimental effects of channel fading is to adaptively adjust the modulation and/or the channel coding format as well as a range of other system parameters based on the near-instantaneous channel quality information perceived by the receiver, which is fed back to the transmitter with the aid of a feedback channel [122]. In 1996 Torrance and Hanzo [123] proposed a set of mode switching levels designed for achieving a high average BPS throughput, while maintaining a target average BER. Moreover, channel coding in conjunction with adaptive modulation in a narrow-band environment was characterized by Chua and Goldsmith in 1997 [124]. In an effort to provide a fair comparison of the various coded modulation schemes in 2001, Ng, Wong and Hanzo [125] have founded that TTCM was the best scheme at

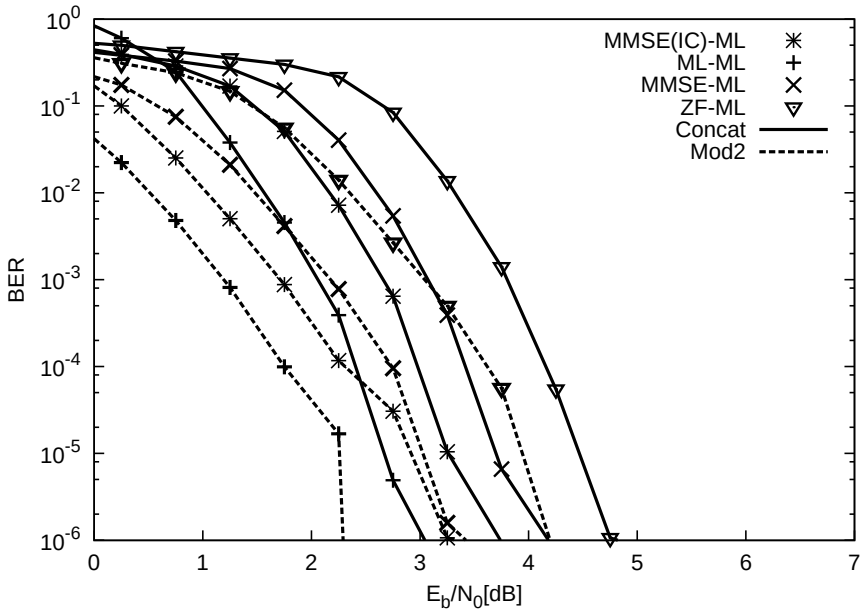

Figure 2.23: BER versus transmitted E_b/N_0 per user performance of various 4PSK-TTCM-aided SDMA-based TWR schemes. The notation 'MMSE-ML' is used to refer to a scheme employing MMSE MUD at the SR and then the ML MUD at the RD link. Similar meaning applies to the notations 'ML-ML', 'IC-ML' and 'ZF-ML'. The modulo-two addition method is represented by 'mod2' and the concatenation method is represented by 'concat'. Furthermore, all schemes employ the power sharing mechanism. The parameters are refer to Table 2.7.

a given decoding complexity among the TCM, TTCM, Bit-Interleaved Coded Modulation (BICM) and Iterative-Decoding assisted BICM (BICM-ID). The past research contributions on Adaptive Coded Modulation (ACM) emerging during 1968 to 2006 has been studied in [107, 126] as shown in Table 2.9. The milestone of the literature after 2007 are shown in Table. 2.10. Referring to [126], in order to efficiently react to the changes in channel quality, the following steps should be taken:

- *Channel quality estimation*: A reliable estimation of the channel transfer function for the next active transmit TS is necessary, in order to appropriately select the transmission parameters to be employed for the next transmission.
- *Choice of the appropriate parameters for the next transmission*: Based on the prediction of the channel conditions for the next TS, the transmitter has to select the appropriate modulation and channel coding modes.
- *Signalling and detection of the parameters employed*: The receiver has to be informed, as to which demodulator parameters to employ for the received packet.

Having introduced a range of various fixed-mode based TTCM schemes in Section 2.2. In this section, we will discuss the near-instantaneously Adaptive TTCM (ATTCM) scheme. The ATTCM

modes are controlled by the near-instantaneous channel conditions. More specifically, a more vulnerable, but higher-throughput TTCM mode, such as TTCM based 32QAM or 64QAM can be employed, when the channel conditions are good, while a lower-throughput but more robust TTCM mode is used, namely TTCM aided 4PSK, when the channel conditions are poor. More specifically, ATTCM is capable of maximizing the throughput, when the channel quality improves and vice versa.

2.3.4.1 System Structure

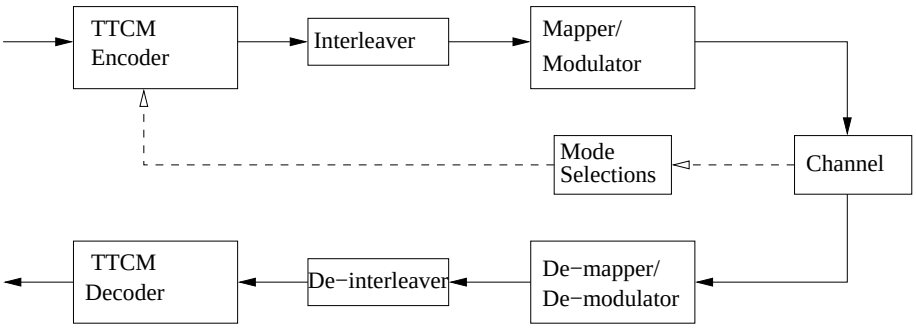

Figure 2.24: The schematic of ATTCM scheme.

The schematic of the near-instantaneous ATTCM arrangement is depicted in Figure 2.24. The transmitter extracts the ATTCM mode signalled back by the receiver employing the mode selection mechanism in order to adjust the ATTCM mode suitable for the prevalent channel [107]. The near-instantaneously adaptive scheme requires a reliable feedback link from the receiver to the transmitter. The effective throughput (or iBPS) range of the ATTCM encoder modes are given by:

- No transmission (NoTx): 0 iBPS;
- TTCM-QPSK(or 4PSK): 1 iBPS;
- TTCM-8PSK: 2 iBPS;
- TTCM-16QAM: 3 iBPS;
- TTCM-32QAM: 4 iBPS;
- TTCM-64QAM: 5 iBPS;

2.3.4.2 Mode-Switching Operation of ATTCM

The ATTCM mode switching thresholds Y =$[\gamma_0, \gamma_1, \gamma_2, \gamma_3, \gamma_4]$ are determined based on the required target BER or FER performance curves of each of the five TTCM schemes, as shown in

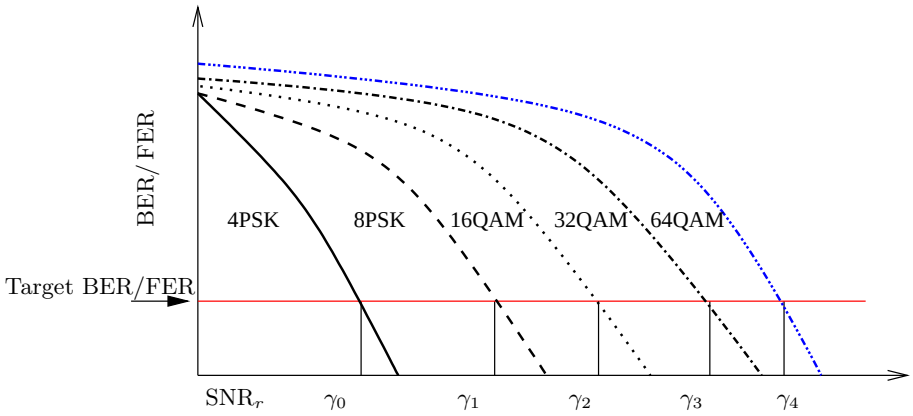

Figure 2.25: Mode selection according to a target BER or FER.

Figure 2.25. Based on the target BER or FER, the related thresholds can be obtained. Specifically, the ATTCM mode switching operation is based on the following algorithm:

$$\text{MODE} = \begin{cases} \gamma_R > \gamma_4, & \text{TTCM-64QAM;} \\ \gamma_3 < \gamma_R \leq \gamma_2, & \text{TTCM-32QAM;} \\ \gamma_2 < \gamma_R \leq \gamma_3, & \text{TTCM-16QAM;} \\ \gamma_1 < \gamma_R \leq \gamma_2, & \text{TTCM-8PSK;} \\ \gamma_0 < \gamma_R \leq \gamma_1, & \text{TTCM-4PSK;} \\ \gamma_R \leq \gamma_0, & \text{No-Tx;} \end{cases} \tag{2.36}$$

where γ_R is the SNR at the receiver. Hence, an appropriate TTCM modulation mode can be selected according to the instantaneous received SNR γ_R using Eq. (2.36).

2.3.4.3 Fading Channel Model

We considered a quasi-static Rayleigh fading channel, where the channel's path gain remains constant over a transmission block, but it is faded independently between each transmission interval. Explicitly, the complex-valued channel envelope is constituted by the combination of the channel's constant path gain and phase value.

As seen in Figure 2.6 from Section 2.3.1, the time-variant channel can be divided into two parts, namely the small-scale / fast-fading and the large scale shadow / slow-fading. Observe in Figure 2.26a the stylized quality variation of the "shadow-and-fast" Rayleigh fading channel and the stylized BPS throughput of our ACM system. When the channel gain incorporates both the slow- and fast- fading components, the adaptive transmission may adapt to both, provided that the channel gain fluctuates very slowly, albeit in most practical cases it only counteracts the shadow fading since the fast fading changes too quickly for an accurate measurement. The channel's quality is assumed be known at the transmitter. Let us assume that the symbol duration is limited to T_s. If

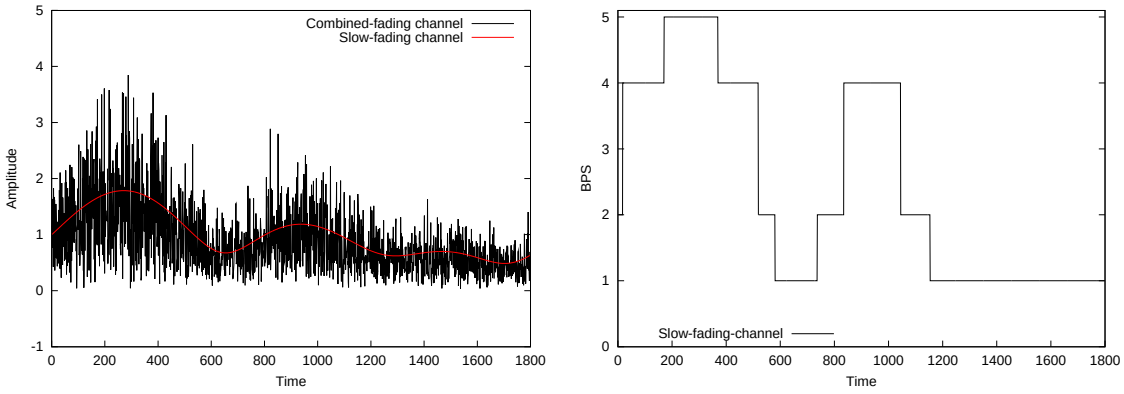

(a) Amplitude versus Time

(b) BPS versus Time

Figure 2.26: The envelope of the Rayleigh fading channels and the corresponding BPS versus time performance at a target BER of 10^{-5}. The ATTCM switching thresholds are based on Table 2.3, which are $\gamma_{ATTCM} = [4.9, 12.2, 16.1, 24.8]$.

the baud rate is $R_{baud} = \frac{1}{T_s}$, then the fading rate normalized to the data rate is given by:

$$f_d = \frac{F_d}{R_{baud}}, \tag{2.37}$$

where F_d is the Doppler frequency. When $f_d = 0.001 = \frac{1}{1000}$ for the shadow fading channel, the channel does not change over 1000 symbols. Since the fading is slow, we may neglect the change of the fading process over one symbol duration T_s. Hence, we assume that the complex fading envelop remains constant over a symbol period. In the following chapters, we have implemented the ATTCM scheme in different cooperative scenarios in order to achieve a conjugated system throughput.

The BER and iBPS performance of ATTCM based on four modulation modes, when communicating over quasi-static Rayleigh fading channels is shown in Figure 2.27, while the BER target is below 10^{-5}. The resultant BER performance is kept below the BER target, in order to minimize the potential error propagation. Moreover, the FER and iBPS performance of ATTCM recorded for transmission over quasi-static Rayleigh fading channel is shown in Figure 2.28. In Figure 2.28, the FER target is below 10^{-3}. Hence, the FER of the ATTCM based on four modulation schemes is below this target.

2.4 Chapter Conclusions

In this chapter, the principle of fixed-mode TTCM has been described in Section 2.2, while its performance was characterized in Section 2.3.2. Explicitly in Section 2.3.2, we first quantified the achievable BER performance of our TTCM-aided SDMA schemes, when the ZF, MMSE, IC and ML MUDs are considered in the SR and RD links, respectively. Then, we invoked a power shar-

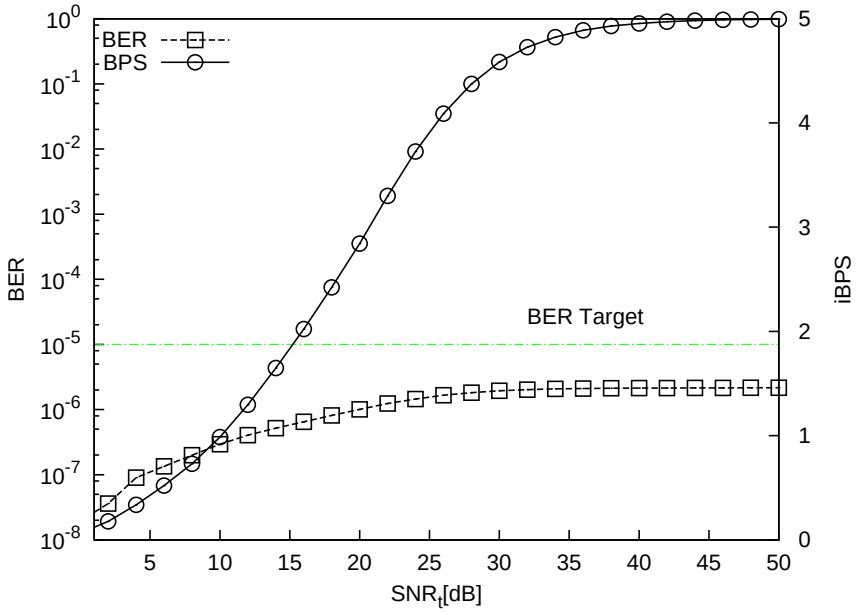

Figure 2.27: The BER and iBPS versus SNR$_t$ performance of 4PSK, 8PSK, 16QAM, and 64QAM for TTCM transmission over quasi-static Rayleigh fading channel using block size 12000 symbols. The related simulation parameters are detailed in Table 2.1. The target BER is below 10^{-5} and its corresponding received SNR are shown in Table 2.3.

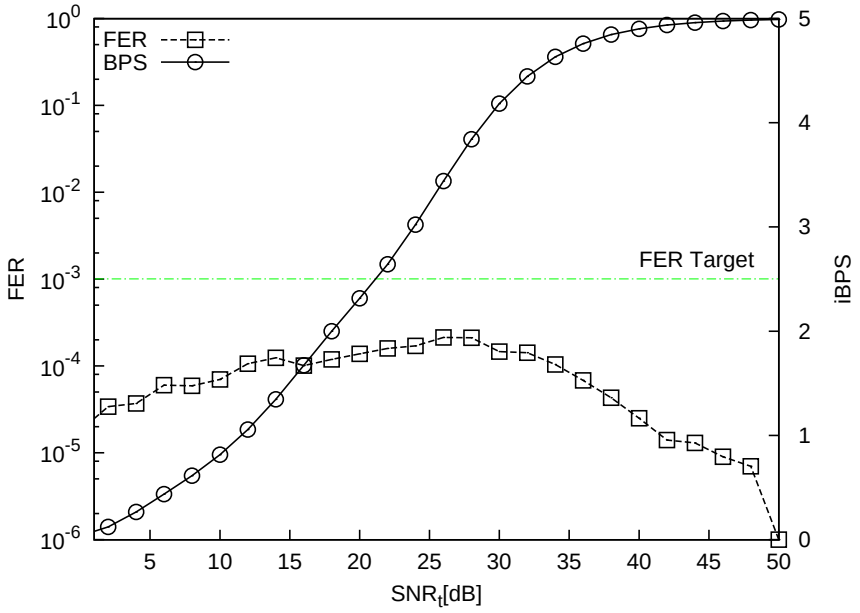

Figure 2.28: The FER and iBPS versus SNR$_t$ performance of 4PSK, 8PSK, 16QAM, and 64QAM for TTCM transmission over quasi-static Rayleigh fading channels using block size 12000 symbols. The related simulation parameters are detailed in Table 2.1. The target FER is below 10^{-3} and its corresponding received SNR are shown in Table 2.4.

Year	Author(s)	Contribution
1968	Hayes [103]	Envisioned an adaptive receiver and a feedback channel.
1972	Cavers [127]	Variable-rate transmission for Rayleigh fading channels.
1974	Hentinen [128]	Adaptive transmission schemes for fading channels.
1991	Massoumi *et al*. [129]	Adaptive trellis coded modulation for mobile communications.
1995	Otsuki *et al*. [130]	Adaptive square QAM constellations.
1996	Torrance *et al*. [131]	Optimization of switching levels for adaptive modulation in slow Rayleigh fading.
1997	Goldsmith *et al*. [132]	Variable-rate, variable-power MQAM for fading channels.
1998	Lim *et al*. [133]	Adaptive modulation/TDMA/TDD system using bi-directional multipath fading compensation.
1999	Alouini *et al*. [134] Wong *et al*. [135]	Closed-form solutions were obtained for the Rayleigh fading channel capacity under three adaptive policies. Upper-bound performance of a wide-band burst-by-burst adaptive modem.
2000	Duel-Hallen [136] Hole *et al*. [137] Wong *et al*. [138] Lau *et al*. [139]	Long-range channel quality prediction techniques. Adaptive multidimensional coded modulation over flat fading channels. Upper-bound performance of a wide-band adaptive modem. Adaptive bit interleaved TCM for Rayleigh fading channels.
2001	Choi *et al*. [140] Ng *et al*. [125]	Optimum mode-switching assisted adaptive modulation. Burst-by-burst adaptive decision feedback equalized TCM, TTCM, BICM and BICM-ID.
2003	Zhang *et al*. [141]	OFDM-based adaptive TCM schemes in both single- and multi-user environments.
2005	Zhou *et al*. [142]	Adaptive modulation aided MIMO systems both with perfect and imperfect channel state information.
2006	Duong *et al*. [143]	ACM with receive antenna diversity and imperfect channel knowledge both at the receiver and transmitter.

Table 2.9: Milestones of ACM (1968-2006) [107].

ing mechanism for minimizing the overall transmit power based on these single-link performances. Observe in Figure 2.17 that the power sharing aided scheme is capable of saving approximately 1.8 dB of SNR when compared to using no power sharing. In Figure 2.17 and Figure 2.18 we have also quantified the performance of the TTCM-aided SDMA-based TWR scheme, when either the concatenation or modulo-two addition methods of Section 2.3.2.1 are employed at the RN. As seen in Figure 2.18, the modulo-two addition based method is capable of providing about 1dB of SNR

Year	Author(s)	Contribution
2007	Caire [144]	Information theoretic foundations of ACM.
	Wang *et al*. [145]	Analyzing and optimizing ACM jointly with ARQ for QoS-guaranteed traffic.
	Svensson [146]	Introduction to adaptive QAM modulation schemes for known and predicted channels.
2008	Huang *et al*. [147]	Novel pilot-free adaptive modulation for wireless OFDM systems.
2009	Jiang *et al*. [148]	Optimal selection of channel sensing order in cognitive radio.
	Fantacci *et al*. [149]	Adaptive modulation and coding techniques for OFDMA systems.
2010	Djordjevic [150]	Adaptive modulation and coding for Free-Space Optical (FSO) channels.
2011	Jiang [151]	A singular-value-based adaptive modulation and cooperation scheme for virtual-MIMO systems.
	Piro *et al*. [152]	Simulating LTE cellular systems: an open-source framework.
2012	Li *et al*. [153]	Scalable video multicast with adaptive modulation and coding in broadband wireless data systems.
2013	Mastronarde [154]	Joint physical layer and system level power management for delay sensitive wireless communications.
2014	Yoon *et al*. [155]	Video multicast with joint resource allocation and adaptive modulation and coding in 4G networks.
2015	Wan *et al*. [156]	ACM is appealing for underwater acoustic communications to improve the system efficiency.

Table 2.10: Milestone of ACM (2007-2015).

gain. In Figure 2.18, we found that our proposed ML-detected SDMA-based TWR scheme is capable of outperforming the non-cooperative TTCM benchmark scheme by approximately 5.3 dBs at a BER of 10^{-6}. The MMSE detected scheme offers the best compromise in terms of the detection complexity imposed and the performance gain attained. Furthermore, in Section 2.3.3, 4PSK-TTCM-aided SDMA-based TWR scheme relied on specific imperfect channel estimation. Hence its BER and throughput are much worse than that of the perfect channel estimation scenario. Specifically, the comparison of our 4PSK-TTCM-aided SDMA-based TWR scheme recorded for both perfect and imperfect channels is shown in Table 2.11. Following the introduction of various fixed-mode based TTCM schemes, the adaptive modes of TTCM relying on all these fixed-mode schemes were studied in Section 2.3.4. These adaptive TTCM schemes will be extensively used throughout the following chapters.

Method	Modulation	System	Throughput(η)	MUD	SNR	E_b/N_0
Modulo-and two	4PSK	Perfect Channel	1.0 BPS	ML	1.45dB	0.2dB
				IC	2.0dB	0.8dB
				MMSE	2.5dB	1.2dB
				ZF	3.0dB	1.8dB
		Imperfect Channel	1.0 BPS	ML	3.5dB	2.3dB
				IC	4.5dB	3.2dB
				MMSE	4.65dB	3.4dB
				ZF	5.48dB	4.2dB

Table 2.11: Comparison of Figure 2.17, Figure 2.18, Figure 2.23 and Figure 2.22 at $BER = 10^{-6}$ with the same parameters.

Chapter 3

Cooperative Communication Between Cognitive and Primary Users

3.1 Introduction

In Chapter 1 and Chapter 2 we have reviewed the history of Cooperative Cognitive Radio (CCR) and ACM, respectively. Let us now investigate the principles and the corresponding implementation of ACM in relay aided CCR systems. Goldsmith *et. al.* [157], survey the fundamental capacity limits and the associated transmission techniques of Cognitive Radio (CR), which exploits all available information about the activity, the channels, the coding and the messages exchanged by the wireless network nodes that share the same radio spectrum. Moreover, the most common paradigms associated with CRs are the so-called underlay, overlay and interweave networks [157]. In the underlay paradigm, the Cognitive Users (CUs) communicate with the aid of the Primary Users (PUs) under the constraint that the interference imposed by the CUs on the PUs must not degrade the PUs' communication quality. In contrast to the underlay scheme, the CUs in the interwave paradigm can only transmit simultaneously with a PU in the event of a false spectral hole detection. Thus in effect, the CU's transmit power is limited by the sensing range of its spectral hole sensor, not by the interference experienced. Moreover, in the overlay paradigm, both the CU and PU communicate using the same frequency band in the same geographic space, assuming that the CUs assisted the transmissions of the PUs by invoking cooperative communication techniques, such as advanced coding and cognitive relaying techniques [157, 158]. Cooperative communication [159] is capable of supporting users by providing an improved integrity or throughput with the advent of user cooperation [160]. In this chapter, we have considered the two most popular collaborative protocols which are the Decode-and-Forward (DAF) and the Amplify-and-Forward (AAF) schemes [161]. Additionally, the cooperative communication aided CR systems may be categorized into three types as discussed in Chapter 1. We have studied the type in which the cooperation is between the PUs and CUs in this chapter, where the PUs have a higher priority than

the CUs, and the CUs may act as Relay nodes (RNs) for PUs [39, 40]. More specifically, the active cooperation [39] among the PUs and CUs would allow the PUs to transmit at a lower power and/or at a higher throughput, while at the same time enabling the CUs to communicate using the released bandwidth. Another interesting protocol involving simultaneous transmissions of the PUs and CUs has been proposed in [38] for maximizing the overall achievable rate. In this Chapter, we have proposed an active cooperation between the PUs and the CUs, which have the potential of leading to a transmission power reduction and transmission rate increase for both the PUs and the CUs. Alternatively, the required bandwidth of the PU may be reduced and the freed bandwidth may be leased to a group of CUs for their secondary communications. More explicitly, our cooperative protocol allows a CU to serve as a RN for relaying the signal of the first PU, which is a SN, to the second PU, which is a Destination Node (DN). This is commonly referred to as the overlay paradigm, and various papers have focused on this model, when appointing a single PU [23, 162]. In our approach, we aim for increasing the CU's own data rate by exploiting the bandwidth released by the PUs, as well as increasing the throughput of PUs by using one of these CUs as a RN. In our proposed One-Way Relaying (OWR) aided CCR system, we have considered multiple CUs and a pair of PUs as SN and DN. We have employed the relay selection technique of [17] for choosing the best CU to act as a RN in order to help the PU to successfully deliver its information. Moreover, we have also proposed a novel TWR aided CCR scheme, which has two PUs in the system. We have considered two protocols in this scenario. The first protocol is based on a Time Division Broadcast Channel (TDBC) [163], which relies on three time slots, while the second one is based on a Multiple-Access Broadcast Channel (MABC) [163], which requires only two time slots. Sophisticated coding and modulation schemes are designed for assisting an active cooperation based CR system.

In CR systems the link-quality varies across a wide range, which cannot be adjusted by power-control, because it is predominantly due to the fluctuating interference. Hence near-instantaneously adaptive coded modulation is proposed, which is capable of accommodating these differences. We have considered the idealistic adaptive schemes based on both the Continuous-input Continuous-output Memoryless Channel (CCMC) and on the Discrete-input Continuous-output Memoryless Channel (DCMC) [164]. More specifically, the CCMC based adaptive scheme assumes that idealistic capacity-achieving coding and modulation schemes are employed for communicating exactly at Shannon's capacity. By contrast, the DCMC based adaptive scheme assumes that an idealistic capacity-achieving code is employed for aiding the PSK/QAM modulation schemes considered, for the sake of operating right at the modulation-dependent DCMC capacity. Furthermore, we also considered a practical adaptive scheme based on power- and bandwidth-efficient TTCM [165], which is a joint coding and modulation scheme that has a structure similar to binary turbo codes. Additionally, the TTCM schemes [95] were designed based on the best component Trellis Coded Modulation [99] components using the so-called 'punctured' minimal distance criterion for communicating over the AWGN channel and has been introduced in Chapter 2. The transmission

rate/throughput (or (Information Bit Per Symbol)(iBPS)) of our system is adapted according to the instantaneous channel conditions. A higher-throughput TTCM scheme is employed when the channel conditions are good, while a lower-throughput TTCM scheme or no transmission is used, when the channel conditions are poor.

3.2 System Design of Our Idealistic CCR Scheme

In this section, we adopt the CCR philosophy of [39, 40] relying on the cooperation between a PU/SN [1] and a CU/RN for conveying the source message to another PU/ DN. To facilitate efficient

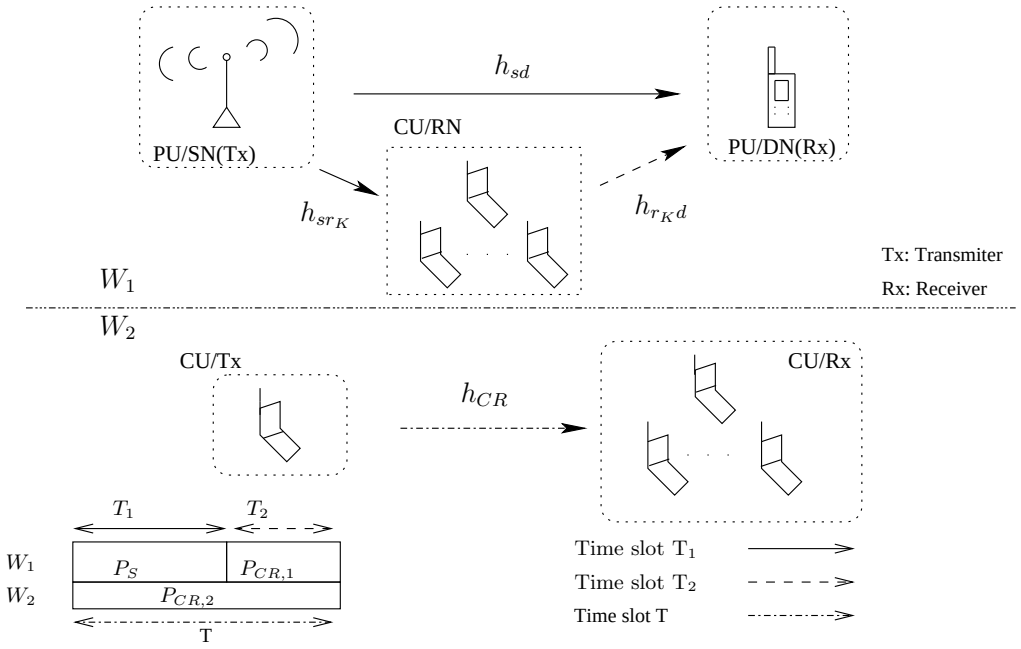

Figure 3.1: The PU's and CU's spectrum-access model. The total time slot duration is $T = T_1 + T_2$ and the bandwidth is $W_0 = W_1 + W_2$

spectrum sharing between the PU and CUs, we consider configuring and sharing the frequency bands of W_1 and W_2, as shown in Figure 3.1. Observe in Figure 3.1 that the CUs act as the RNs and assist the PU/SN in transmitting its signal in one of the frequency bands, namely in W_1. In the other frequency band, namely W_2, the PU/SN remains silent and the other CUs transmit their own signals by using the entire time slot T. Specifically, Figure 3.2 illustrates the bandwidth, time period and power allocation for the PU and CUs, where T and W_0 are the original time period and bandwidth allocated for the PU/SN to transmit its source message to the PU/DN. When the PU/SN is assisted by a CU/RN, the PU/SN only has to utilize a fraction of T and W_0 in order to convey the source message to the PU/DN. More specifically, the PU/SN and CU/RN will share the bandwidth W_1 to convey the source message to the PU/DN, while the other CUs may use the remaining bandwidth of ($W_2 = W_0 - W_1$) for their own communications. In other words, a

[1] We represent the PU acting as the source node as PU/SN. Similarly, CU/RN denotes the CU acting as a relay node, while PU/DN denotes the PU acting as the destination node.

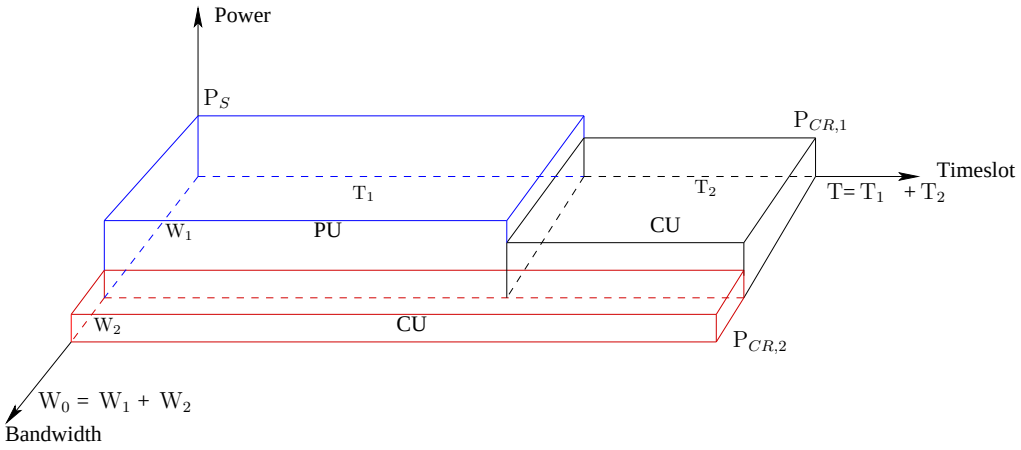

Figure 3.2: The bandwidth, time period and power allocation for the PU and CU, which obey the protocols of Figure 3.1. The total time slot duration is $T = T_1 + T_2$ and the total bandwidth is $W_0 = W_1 + W_2$.

CU/RN assists in saving some of the transmission power of the PU/SN due to the reduction of the transmission period from T to T_1. In return, the PU/SN would release the bandwidth W_2 to other CUs. More specifically, let us assume that the transmission power per unit frequency emanating from the PU/SN is P_S watts/Hz and the target transmission rate is P_{PU} bits/s. The PU/SN transmits using the power of P_S during T_1, while the CU/RN forwards the source message using the power of $P_{CR,1}$ during T_2 and the second CU can broadcast its message to other CUs using the power of $P_{CR,2}$ during the entire time period T.

During the first time slot T_1, the PU/SN broadcasts the source message x to both the CU/RN and the PU/DN. The signal received at the PU/DN via the SD[2] link is given by:

$$y_{sd} = \sqrt{P_S} h_{sd} x + n_{sd} \,, \tag{3.1}$$

and the signal received at the CU/RN via SR link is:

$$y_{sr} = \sqrt{P_S} h_{sr} x + n_{sr} \,, \tag{3.2}$$

where n_{sd} and n_{sr} are the AWGN processes having an average single-sided noise power per unit frequency of $N_0 = 4.0 \times 10^{-21}$ watts/Hz [39] in the SD and SR links, respectively. In this section, we have adopted the AAF model of [39] and additionally we extended it to our DAF model. Hence our CU/RN is capable of carrying out either the AAF or the DAF operation.

During the second time slot T_2 the CU/RN would forward the source message to the PU/DN using the transmission power of $P_{CR,1}$ watts/Hz. When considering the DAF protocol, provided that the RN is capable of decoding the transmitted symbol correctly, it forwards the decoded symbol with a power $P_{CR,1}$ to the DN. Otherwise the RN remains idle. The signal received by the PU/DN

[2]The SD link is represented by the link between the PU/SN and the PU/DN. The SR link represents the communication link between the PU/SN and the CU/RN. Additionally, the communication link between the CU/RN and the PU/DN is referred to as the RD link.

via the Relay-to-Destination (RD) link may be formulated as:

$$y_{rd}^{DAF} = \sqrt{P_{CR,1}}h_{rd}x + n_{rd} . \quad (3.3)$$

Similarly, when considering the AAF cooperation protocol, the CU/RN amplifies the received signal and forwards it to the PU/DN at a transmit power of $P_{CR,1}$. The signal received by the PU/DN via the RD link may be expressed as:

$$y_{rd}^{AAF} = \omega_A \sqrt{P_{CR,1}}h_{rd}y_{sr} + n_{rd} , \quad (3.4)$$

where $\omega_A = \frac{1}{\sqrt{P_S|h_{sr}|^2+N_0}}$ [13] is the amplification factor. Then the signal received by the PU/DN under the AAF protocol via the RD link may be rewritten as

$$\begin{aligned} y_{rd}^{AAF} &= \frac{\sqrt{P_{CR,1}}h_{rd}y_{sr}}{\sqrt{P_S|h_{sr}|^2+N_0}} + n_{rd} , \\ &= \frac{\sqrt{P_{CR,1}P_S}h_{rd}h_{sr}}{\sqrt{P_S|h_{sr}|^2+N_0}}x + \frac{\sqrt{P_{CR,1}}h_{rd}}{\sqrt{P_S|h_{sr}|^2+N_0}}n_{sr} + n_{rd} . \end{aligned} \quad (3.5)$$

The channel gains h_{sd}, h_{sr} and h_{rd} are assumed to be independent complex Gaussian random variables with zero mean and variances of σ_{sd}^2, σ_{sr}^2 and σ_{rd}^2, respectively. The channel variance is [13, 166]: $\sigma_{ab} = \left(\frac{\lambda}{4d_{ab}\pi}\right)^{\alpha} = \left(\frac{c}{4d_{ab}f_c\pi}\right)^{\alpha}$. Where d_{ab} denotes the geometrical distance between node a and node b, the wavelength is $\lambda = \frac{c}{f_c}$, where c is the speed of light and we consider a carrier frequency of f_c =350 MHz. Furthermore we consider an outdoor environment, where the path-loss exponent [167] is given by $\alpha = 3$.

In our scheme, the PU/SN transmits during T_1, while the CU/RN transmits during T_2. Both the PU/SN and CU/RN utilize the bandwidth W_1. When the AAF protocol is employed based on Shannon's capacity theorem, the CCMC capacity of the cooperative relay channel over the bandwidth of W_1 Hz is given by:

$$C_{PU}^{AAF} = \frac{W_1}{2}\log_2\left[1 + \frac{P_S|h_{sd}|^2}{N_0} + f_{CR}\right] , \quad (3.6)$$

where we have [pg. 122] [13]: $f_{CR} = \frac{P_S P_{CR,1}|h_{sr}|^2|h_{rd}|^2}{(P_S|h_{sr}|^2+P_{CR,1}|h_{rd}|^2+N_0)N_0}$. When we consider the DAF protocol, the capacity of our system is limited by the capacity of either the SR link or that of the combined channel constituted by the SD and RD links which ever is lower. Then the CCMC capacity of DAF transmissions over W_1 Hz can be formulated as [pg. 126] [13]:

$$C_{PU}^{DAF} = \frac{W_1}{2}\min\left[\log_2(1 + \frac{P_S|h_{sd}|^2}{N_0} + \frac{P_{CR,1}|h_{rd}|^2}{N_0}), \log_2(1 + \frac{P_S|h_{sr}|^2}{N_0})\right] , \quad (3.7)$$

The factor $\frac{1}{2}$ in Eq. (3.6) and Eq. (3.7) indicates that the PU only utilizes the first time slot T_1 of Figure 3.1, which the CU uses the second time slot T_2 to transmit its signals. Without loss of generality, we assume $T_1 = T_2 = \frac{T}{2}$. Based on Eq. (3.6), the bandwidth required for achieving a transmission rate of $R_{PU} \leqslant C_{PU}^{AAF}$ may be formulated as:

$$W_1 \geqslant \frac{2R_{PU}}{\log_2\left[1 + \frac{P_S|h_{sd}|^2}{N_0} + \frac{P_S P_{CR,1}|h_{sr}|^2|h_{rd}|^2}{(P_S|h_{sr}|^2+P_{CR,1}|h_{rd}|^2+N_0)N_0}\right]} . \quad (3.8)$$

For the DAF protocol, the bandwidth requirement of W_1 can be expressed as:

$$W_1 \geqslant \frac{2R_{PU}}{\min\left[\log_2(1+\frac{P_S|h_{sd}|^2}{N_0}+\frac{P_{CR,1}|h_{rd}|^2}{N_0}), \log_2(1+\frac{P_S|h_{sr}|^2}{N_0})\right]} . \tag{3.9}$$

In the non-cooperative case, the CCMC capacity of the PU/SN is given by:

$$C^*_{PU} = W_0 \log_2\left[1+\frac{P_{PU}|h_{sd}|^2}{N_0}\right] . \tag{3.10}$$

For the following derivation, we use the C_{PU} to represent C^{DAF}_{PU} and C^{AAF}_{PU}.

It can be shown that the transmission power originally required for achieving $R_{PU} = C_{PU}$ is given by:

$$P_{PU} = \frac{N_0(2^{\frac{R_{PU}}{W_0}}-1)}{|h_{sd}|^2} . \tag{3.11}$$

As seen in Figure 3.1, a group of CUs is capable of communicating using the released bandwidth W_2 for the entire period of T, while a CU is helping the PU/SN as a RN. The received signal for CUs to transmit its own signal in the whole time slot T is given by:

$$y_{CR} = \sqrt{P_{CR,2}}h_{CR}x_{CR} + n_{CR} , \tag{3.12}$$

where h_{CR} denotes the channel between a CU's transmitter (CU/SN) and its destination (CU/DN) for its own transmission. The source message x_{CR} transmit from CU/SN to CU/DN and n_{CR} is the AWGN process. Then, the achievable transmission rate of the CUs is given by:

$$R_{CR} = W_2 \log_2\left[1+\frac{P_{CR,2}|h_{CR}|^2}{N_0}\right] , \tag{3.13}$$

If the total transmission power of CUs is limited to P_{CR}, then we have:

$$P_{CR} = \frac{1}{2}P_{CR,1}W_1 + P_{CR,2}W_2 . \tag{3.14}$$

In this way, the CUs can decide how to allocate their joint transmission power in order to maximize their own data rate. Let us define the ratio of transmission power allocated for helping the PU/SN to the total transmission power of the CUs over the bandwidth W_1 as:

$$\psi = \frac{\frac{1}{2}P_{CR,1}W_1}{P_{CR}} , \tag{3.15}$$

where ψ = [0 1]. Similarly, the ratio of the transmission power allocated to transmit the CUs' data to the total transmission power of the CUs, over the bandwidth W_2 can be defined as:

$$1-\psi = \frac{P_{CR,2}W_2}{P_{CR}}. \tag{3.16}$$

More specifically, the transmission power $P_{CR,1}$ at CU/RN may be determined from Eq. (3.8) and Eq. (3.15). On the other hand, the CU's own data rate using the released bandwidth $W_2 = W_0 - W_1$ may be derived as :

$$R_{CR} = (W_0 - W_1)\log_2\left[1+\frac{P_{CR}|h_{CR}|^2(1-\psi)}{(W_0-W_1)N_0}\right] , \tag{3.17}$$

which can be optimized with respect to ψ. Moreover, refer to Eq. (2.16) of Chapter 2, the Reduced-Distance-Related-Pathloss-Reduction (RDRPR) [168, 169] experienced in this system by the SD, SR and RD links with respect to the SD link as a benefit of its reduced distance based path-loss can be expressed as [168]:

$$G_{sd} = (\frac{d_{sd}}{d_{sd}})^3 \ , \ G_{sr} = (\frac{d_{sd}}{d_{sr}})^3 \ \text{ and } \ G_{rd} = (\frac{d_{sd}}{d_{rd}})^3 \tag{3.18}$$

respectively. Naturally, the RDRPR of the SD link with respect to itself is unity, i.e. we have $G_{sd} = 1$. Our quantitative results for the AAF and DAF aided CCR scheme will be discussed in Section 3.2.1.

3.2.1 Simulation Results

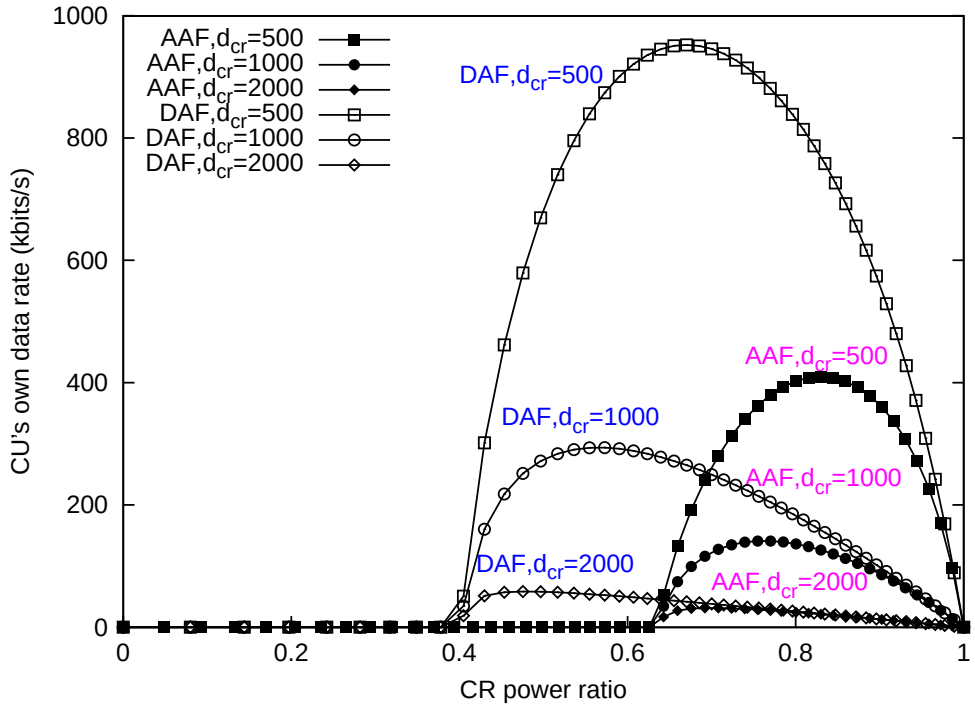

Figure 3.3: The CU's own data rate based on DAF and AAF protocols. The corresponding RDRPR factors are given by $G_{sd} = 1$, $G_{sr} = 8$ ($d_{sr} = \frac{d_{sd}}{2}$) and $G_{rd} = 1$ ($d_{rd} = d_{sd}$).

The relationship of the power ratio ψ and the data rate of the CU is shown in Figure 3.3 and Figure 3.4. Figure 3.3 illustrates the CU's own data rate with respect to the power ratio ψ, when the RDRPR factors are given by $G_{sd} = G_{rd} = 1$ and $G_{sr} = 8$. We assume that the total bandwidth is $W_0 = 1$ MHz and the target transmission rate of the PU/SN is $R_{PU} = 500$ Kbits/s. The total transmission power of the CU is $P_{CR} = 10$ dBm. In this system we assumed that the PU has maintained the same transmission power, which is $P_S = P_{PU}$ based on Eq. (3.11). Then, we plotted the data rate of the CU based on three different values of the distance d_{cr} between the CU and its own destination, namely for d_{cr} = 500 m, 1 km and 2 km. Finally, the optimum ratios of the relay power over the total power budget are given by 64.5%, 53% and 45% (with respect to

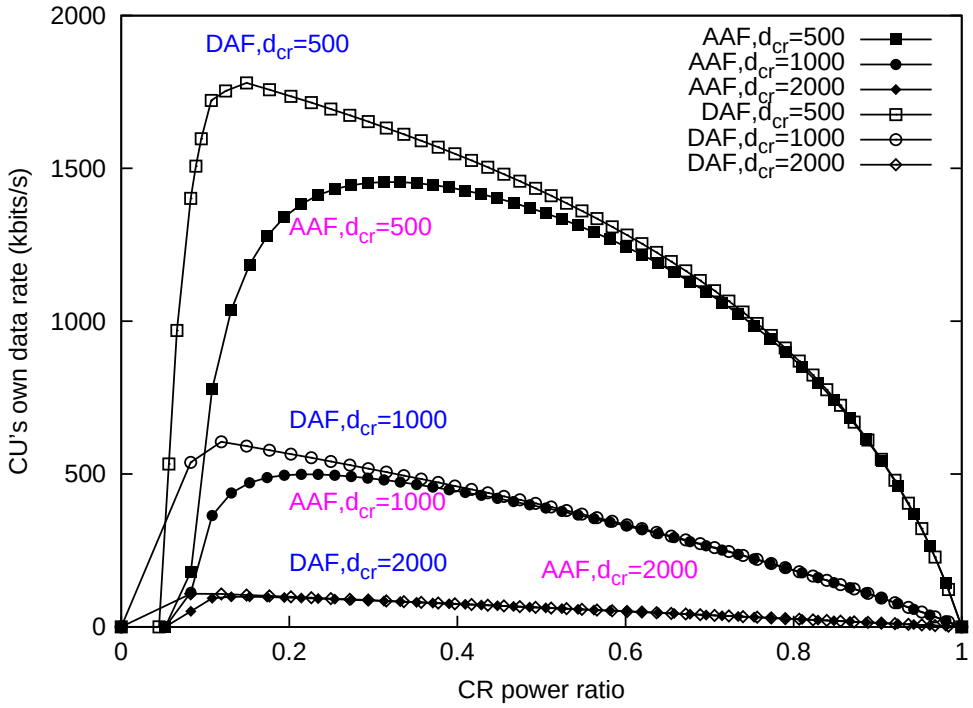

Figure 3.4: The CU's own data rate based on DAF and AAF protocols. The corresponding RDRPR factors are given by $G_{sd} = 1$, $G_{sr} = 8$ ($d_{sr} = \frac{d_{sd}}{2}$) and $G_{rd} = 8$ ($d_{rd} = \frac{d_{sd}}{2}$).

d_{cr}=500 m, 1 km and 2 km) when using the DAF protocol. Similarly, the optimum power ratios for the AAF protocol are given by 82%, 72% and 65%. As seen in Figure 3.3, a CU/RN has offered a proportion of its transmission power to help the PU/SN, while $0 \leqslant \psi \leqslant 0.4$. During this period, the CU's own data rate is identical to zero. Figure 3.4 shows the corresponding results when the RN is right in the middle of the PU/SN and PU/DN link, where the RDRPR factors are given by $G_{sd} = 1$ and $G_{sr} = G_{rd} = 8$. The optimum ratio of the relay power over the total power is 16%, 14% and 12% for d_{cr}=500 m, 1 km and 2 km, respectively, when using DAF detection. Moreover, the corresponding values for AAF detection are given by 33%, 20% and 12%. Observe in Figure 3.3 and Figure 3.4 that if the CU/RN is half-way between the SN and the DN, a CU/RN only has to dedicate a smaller proportion of its transmission power for aiding the PU/SN. Furthermore, as d_{cr} increases, the CU's own data rate drops due to its increased pathloss.

3.3 Fixed Mode Transmission

In this section, we investigate the achievable bandwidth reduction based on four fix-mode transmission schemes. More specifically, System A in Figure 3.5 is a non-cooperative system, while System B, System C and System D are relay aided CCR systems. We assume that both the SN and the DN are PUs and the RN is a CU. The passband bandwidth ζ of PSK/QAM modulation is assumed to be the same as the Baud-rate (or symbol rate) of R_s symbol/s, while the baseband bandwidth is given

by $R_s/2$ symbol/s, when an ideal lowpass filter is assumed. The bit rate of the system is given by:

$$R_b \quad = \quad \eta \times R_s \text{ (bit/s)} , \tag{3.19}$$

where η is the throughput in Bit Per Symbol (BPS). When considering a pathloss exponent of $\alpha = 3$, we have a RDRPR of $G = 2^\alpha = 8$, which is $\tilde{G} = 10\log_{10}(8) = 9$ dB when the RN is located at the mid-point between the SN and the DN. The received SNR (SNR_r) in decibel is given by:

$$SNR_r \quad = \quad SNR_t + \tilde{G} . \tag{3.20}$$

and the *transmit SNR*[3] is expressed as:

$$SNR_t \quad = \quad 10\log_{10}(\frac{P_t}{N_0}) , \tag{3.21}$$

where P_t is the transmit power and N_0 is the single-sided noise power. We assume that a BER of 10^{-5} or less is required at the DN, where received SNRs of 9dBs and 18dBs are necessitated at the DN, when TTCM-8PSK and TTCM-64QAM are employed, respectively. The SD link is assumed to be of low quality and hence it is considered to be unavailable in this example.

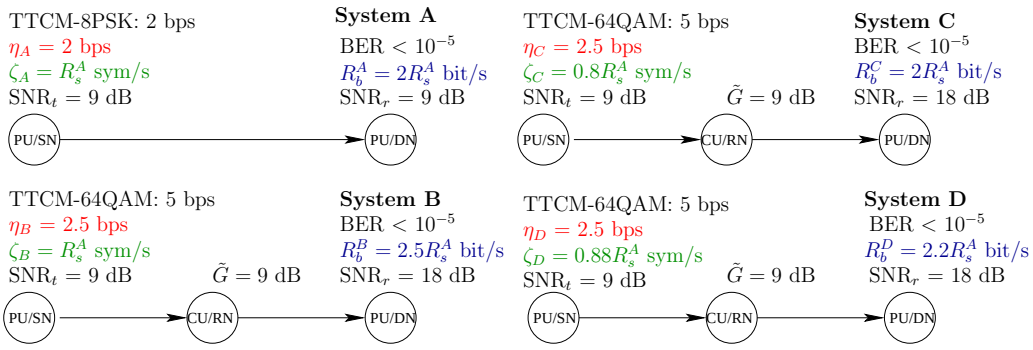

Figure 3.5: Comparison of a non-cooperative scheme and of three relay-assisted DAF-CR schemes, where the target SNR_t is 9dB and the target BER is below 10^{-5}. Additionally, the relay-assisted schemes were rely on the protocols of Figure 3.1 where the CU helps the PU to transmit its information.

As seen from Fig. 3.5, the PU/SN of System B is capable of increasing its throughput to $\eta_B = 2.5$ BPS from the $\eta_A = 2$ BPS value of System A, when using the same bandwidth of $\zeta = R_s$. Their bit rate rate is $\frac{R_b^A}{R_b^B} = \frac{2R_s^A}{2.5R_s^B}$ upon assuming that System A and System B have the same symbol rate of $R_s^A = R_s^B$, while the relationship of their bit rate is given by:

$$\begin{aligned} R_b^B \quad &= \quad \frac{\eta_B}{\eta_A} R_b^A , \\ &= \quad 1.25 R_b^A . \end{aligned} \tag{3.22}$$

Thus, System B has a 25% higher bit rate than System A within the same bandwidth. Then the relationship between the bit rate of System B, R_b^B and symbol rate of System A, R_s^A is given by:

$$R_b^B = 1.25R_b^A = 1.25 \times 2R_s^A = 2.5R_s^A .$$

[3]The concept of transmit SNR [169] is unconventional, as it relates quantities to each other at two physically different locations, namely the transmit power to the noise power at the receiver, which are at physically different locations.

By contrast, both System A and System C have the same bit rate of $R_b^A = R_b^C$, while the relationship of their symbol rates is given by:

$$\begin{aligned} R_s^C &= \frac{\eta_A R_s^A}{\eta_C}, \\ &= 0.8 R_s^A . \end{aligned} \tag{3.23}$$

Hence, System C is capable of providing the same bit rate using only 80% of the original bandwidth. This is achieved as a benefit of its lower Baud-rate of $\frac{\eta_A}{\eta_C} R_s$, where $\frac{\eta_A}{\eta_C} = \frac{2}{2.5} = 0.8$ is the throughput ratio of System A to System C. Then the relationship between the bit rate of System C and the symbol rate of System A is $R_b^C = 2R_S^A$.

More specifically, the bandwidth-reduction factor is given by:

$$B_s = 1 - \frac{\eta_A}{\eta_C} . \tag{3.24}$$

Therefore, a CU assisting the PU's transmission is capable of saving 20% ($1 - 0.8 = 0.2 = 20\%$) of the PU's bandwidth. Thus, this reduced bandwidth can then be shared among other CUs. If we create a System D in a practical approache where the bit rate of the PU is lower than that of System B, but higher than that of System A, then we have $R_b^D = 1.1 R_b^A$. By referring to Figure 3.5, we have $\eta_A = 2.0$ BPS and $\eta_D = 2.5$ BPS. Furthermore, we have $R_b^D = 1.1\eta_A \times R_s^A = 1.1 \times 2 \times R_s^A = 2.2 \times R_s^A$. Based on Eq. (3.23), we have $R_s^D = \frac{\eta_A R_s^A}{\eta_D} = \frac{2.2}{2.5} R_s^A = 0.88 R_s^A$. Then the bandwidth-reduction factor becomes $B_s = 1 - \frac{\eta_A}{\eta_D} = 1 - 0.88 = 0.12$. In this situation, System D is capable of reducing the original bandwidth by 12% for the CU's benefit, while the PU enjoys an additional 0.5 BPS throughput increment. The comparisons of these four systems are shown in a nutshell in Table 3.1.

Fixed model type	System A	System B	System C	System D
Bit-per-symbol η	η_A = 2.0 BPS	η_B = 2.5 BPS	η_C = 2.5 BPS	η_D = 2.5 BPS
Bit rate(bit/s)	R_b^A	$R_b^B = 1.25 R_b^A$	$R_b^C = R_b^A$	$R_b^D = 1.1 R_b^A$
Symbol rate(sym/s)	R_s^A	$R_s^B = R_S^A$	$R_s^C = 0.8 R_S^A$	$R_s^D = 0.88 R_S^A$
Bit rate / R_s^A	$\frac{R_b^A}{R_s^A} = 2.0$	$\frac{R_b^B}{R_s^A} = 2.5$	$\frac{R_b^C}{R_s^A} = 2.0$	$\frac{R_b^D}{R_s^A} = 2.2$
Bandwidth-reduction(B_s)	$1 - \frac{\eta_A}{\eta_A} = 0$ (0%)	$B_s^B = B_s^A$ (0%)	$1 - \frac{\eta_A}{\eta_C} = 0.20$ (20%)	$1 - \frac{\eta_A}{\eta_D} = 0.12$ (12%)

Table 3.1: The parameters of four fixed-mode CCR schemes.

3.3.1 Simulation Results

Although the Systems B, C and D introduced in Section 3.3 are all relay-aided CCR schemes, we have had different design objectives for their bit rate and symbol rate. Hence, they also illustrate the different benefits of the CCR networks.

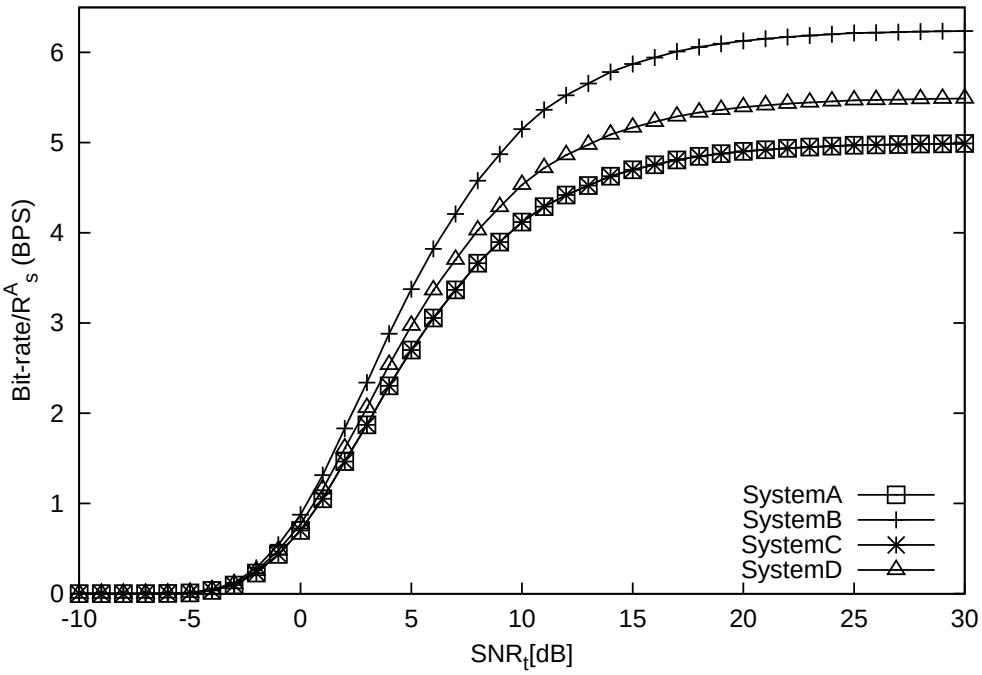

Figure 3.6: The SNR_t vs Bit rate/R_S^A performance of the ATTCM aided SystemA, SystemB, SystemC and SystemD. The corresponding switching thresholds are refer to Table 3.2.

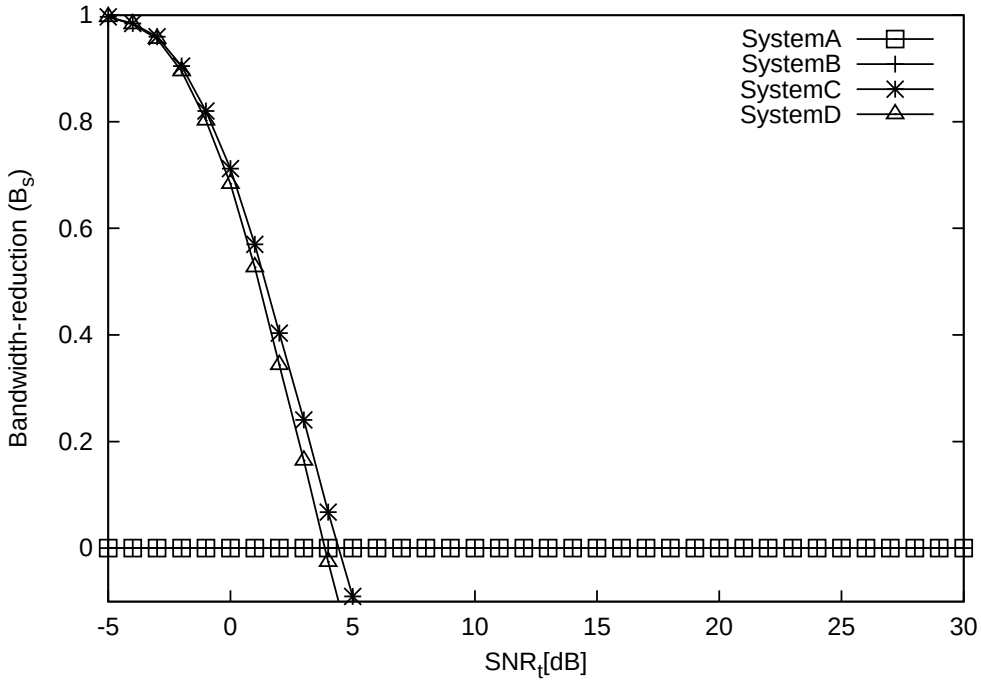

Figure 3.7: The SNR_t vs Bandwidth-reduction (B_s) performance of ATTCM aided SystemA, SystemB, SystemC and SystemD. The corresponding switching thresholds are refer to Table 3.2.

Let us now refer to Figure 3.6 and Figure 3.7, where we consider ATTCM instead of fixed-mode 8PSK and 64QAM. The system labelled as ATTCM-SystemA is the classic non-cooperative scheme, while ATTCM-SystemB, ATTCM-SystemC and ATTCM-SystemD are all relay-aided CCR schemes. As seen in Figure 3.6, the ATTCM-SystemB achieves the highest bit rate but uses all available bandwidth, i.e. no bandwidth reduction, as seen in Figure 3.7. By contrast, ATTCM-SystemC achieves the highest bandwidth reduction as observed in Figure 3.7, while maintaining the same bit rate as ATTCM-SystemA. Furthermore, ATTCM-SystemD achieved both a practical bit rate improvement as well as some bandwidth reductions.

3.4 Adaptive Mode Transmission

We have shown in Section 3.3 that it is both possible and practical for the PU to release the available bandwidth for supporting the CU's own transmission in exchange for an increased transmission throughput as in the ATTCM-SystemD discussed in Table 3.1. In this section, we proposed both one-way and two-way relaying schemes for CCR applications.

3.4.1 The ATTCM Algorithm

In our proposed system, we will make use of this power- and bandwidth-efficient TTCM scheme which has been introduced in Section 2.2. Employing TTCM has the advantage that the system's effective throughput can be increased upon increasing the code rate, when the channel-quality improves. Additionally, both the BER and FER performance of the system may be improved when TTCM is used [96]. Recently, various TTCM schemes were designed in [97] with the aid of the Extrinsic Information Transfer (EXIT) charts [100, 101] and union bounds for the sake of approaching the capacity of the Rayleigh fading channel. The TTCM encoder comprises two identical parallel-concatenated TCM encoders [99] linked by a symbol interleaver. The first TCM encoder directly processes the original input bit sequence, while the second TCM encoder manipulates the interleaved version of the input bit sequence. Then the bit-to-symbol mapper maps the input bits to complex-valued symbols using the SP-based labelling method [96]. The structure of the TTCM decoder is similar to that of binary turbo codes, but each decoder alternately processes its corresponding encoder's channel-impaired output symbol, and then the other encoder's channel-impaired output symbol [pg.764] [96]. More details on the TTCM principles may be found in [96].

We have employed an ATTCM scheme for protecting the SR and the RD links, where the effective throughput range is given by iBPS$=\{0,1,2,3,5\}$ BPS when no transmission, QPSK, 8PSK, 16QAM and 64QAM are considered, respectively. Moreover, the ATTCM mode switching thresholds $\Upsilon=[\gamma_0,\gamma_1,\gamma_2,\gamma_3]$ are determined based on the BER performance curves of each of the four TTCM schemes. Hence, in this chapter, the switching thresholds are based on the BER performance of a TTCM scheme communicating over an AWGN channel, as shown in Figure 3.8

and also over Rayleigh fading channels by observing in Figure 3.9. Specifically, referring to

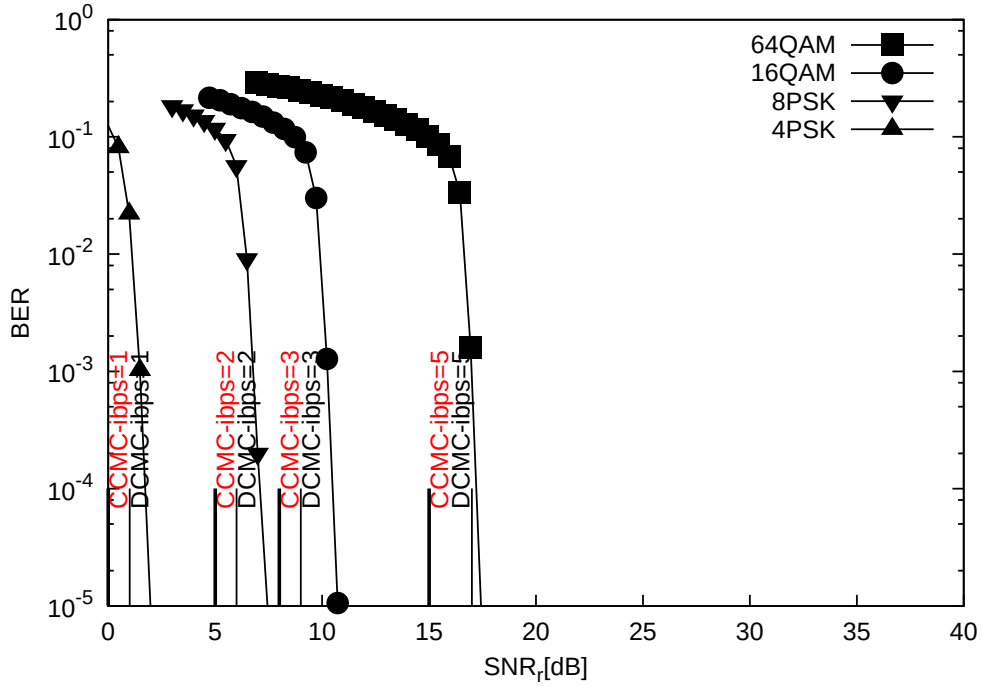

Figure 3.8: The BER versus SNR$_r$ performance of TTCM using a frame length of 1200 symbols, when communicating over AWGN channels. Four TTCM iterations were invoked. The parameters are shown in Table 2.1.

Section 2.3.4 we consider the five TTCM modes and the ATTCM mode switching operation based on the following algorithm:

$$\text{MODE} = \begin{cases} \gamma_R > \gamma_3, & \text{TTCM-64QAM, iBPS=5 BPS;} \\ \gamma_2 < \gamma_R \leq \gamma_3, & \text{TTCM-16QAM, iBPS=3 BPS;} \\ \gamma_1 < \gamma_R \leq \gamma_2, & \text{TTCM-8PSK, iBPS=2 BPS;} \\ \gamma_0 < \gamma_R \leq \gamma_1, & \text{TTCM-4PSK, iBPS=1 BPS;} \\ \gamma_R \leq \gamma_0, & \text{No-Tx, iBPS=0 BPS;} \end{cases} \tag{3.25}$$

The ATTCM based switching thresholds, namely Υ_{ATTCM} are shown in Table 3.2, where we specifically chose the switching thresholds for ensuring that the average BER at the RN is lower than 10^{-5}.

3.4.1.1 The CCMC and DCMC Capacity

Shannon quantified the capacity of a SISO AWGN channel in 1948 [103]. Followed by Shannon's work, there was a race by various researchers to design practical coding schemes that can approach the channel capacity. Shannon's capacity bound or the CCMC capacity over AWGN channel can be written as:

$$C_{CCMC}^{AWGN} = WT \log_2(1+\gamma) \text{ [BPS]}, \tag{3.26}$$

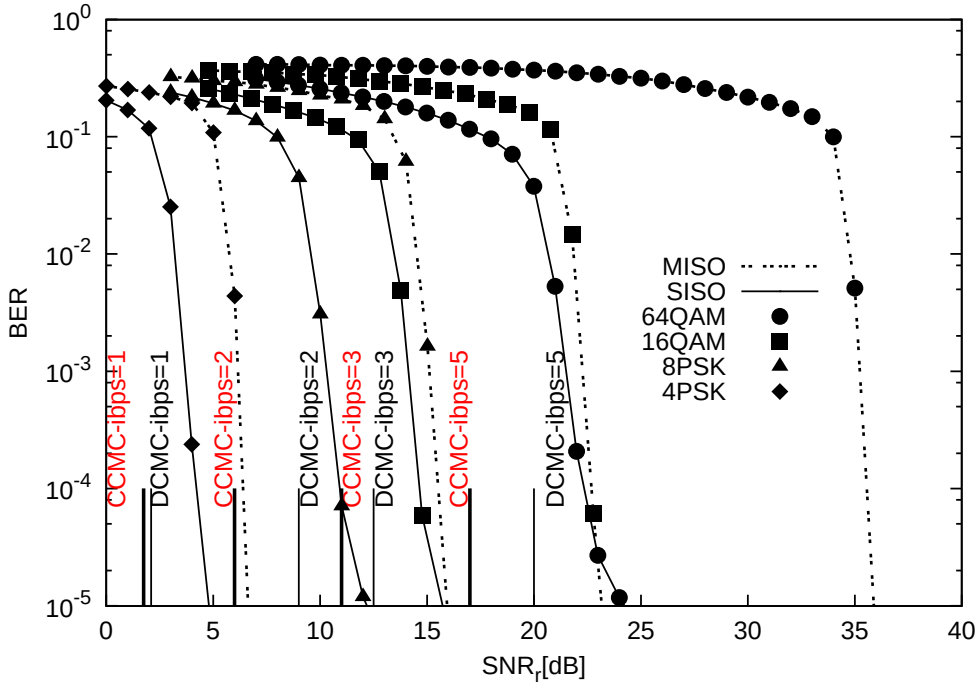

Figure 3.9: The BER versus SNR_r performance of TTCM aided Multiple-Input-Single-Output (MISO) system and TTCM aided Single-Input-Single-Output (SISO) system. A frame length of 1200 symbols was employed when communicating over uncorrected Rayleigh channels. Four TTCM iterations and four outer iterations with the MISO detector is used in MISO system. The parameters are shown in Figure 2.1.

where W is the bandwidth assuming an ideal low-pass filtering, T is the time interval and γ is the channel SNR. The Discrete Memoryless Channel (DMC) [170] is a channel model where the input and output symbols are discrete sets and the channel is memoryless [170]. DCMC is a relative of the DMC, where the input of the channel is from a discrete set of M-ary values:

$$x \in \{x^{(m)}\},\ (i = 0, 1, \cdots, M-1)\ , \tag{3.27}$$

with M denoting the constellation size. Additionally, the channel's output has continuous values, which are given by:

$$y \in [-\infty, \infty]\ . \tag{3.28}$$

If the M-ary symbols are equiprobable distributed, the probability of transmitting $x^{(m)}$ is given by:

$$\mathrm{P}(x^{(m)}) \quad = \quad \frac{1}{M},\ (m = 0, \cdots, M-1)\ . \tag{3.29}$$

The probability density function (pdf) of receiving y given that $x^{(n)}$ is transmitted may be expressed as [171]:

$$p(y|x^{(n)}) \quad = \quad \frac{1}{\pi N_0} \exp\left(\frac{-|y - x^{(n)}|^2}{N_0}\right)\ . \tag{3.30}$$

where we have

$$p(y) \quad = \quad p(y|x^{(n)}) \cdot \mathtt{P}(x^{(n)}) \, . \tag{3.31}$$

More specifically, the mutual information of receiving y when $x^{(n)}$ is transmitted is given by $\log_2[p(y|x^{(n)})/p(y)]$, hence the capacity of the DCMC formulated for the transmission of M-ary signals is [170, 171]:

$$\begin{aligned} C_{DCMC} &= \max_{\mathtt{P}(x^{(n)})} I(X;Y) \\ &= \max_{\mathtt{P}(x^{(n)})} \sum_{m=0}^{M-1} \int_{-\infty}^{\infty} p(y|x^{(m)}) \mathtt{P}(x^{(m)}) \log_2 \left[\frac{p(y|x^{(m)})}{\sum_{n=0}^{M-1} p(y)} \right] dy \, , \end{aligned} \tag{3.32}$$

where $I(X;Y)$ denotes the average mutual information of receiving the output Y due to the input X and $p(y)$ is defined in Eq. (3.31). Hence the capacity of the DCMC recorded for transmission over an AWGN channel can be formulated as [99]:

$$C_{DCMC}^{AWGN} = \log_2(M) - \frac{1}{M} \sum_{m=0}^{M-1} E \left[\log_2 \sum_{n=0}^{M-1} \exp\left(\frac{-|(x^{(m)} - x^{(n)}) + n|^2 + |n|^2}{N_0}\right) \right] \quad , \tag{3.33}$$

where n is the AWGN having a variance of $\frac{N_0}{2}$ per dimension at the receiver.

Moreover, the complex-valued Rayleigh fading coefficient is defined as:

$$h \quad = \quad h_i + h_q \cdot j \, , \tag{3.34}$$

where $j = \sqrt{-1}$, while h_i and h_q are the in-phase and quadrature-phase coefficients, respectively. Specifically, they are zero-mean independent identically distributed Gaussian random variables when considering an uncorrelated Rayleigh fading channel. The CCMC capacity of a Rayleigh fading channel may be expressed as [164]:

$$C_{CCMC}^{Ray} \quad = \quad E\left[WT \log_2(1 + h\gamma)\right] \ \ [\text{BPS}] \, . \tag{3.35}$$

Furthermore, the DCMC capacity of a Rayleigh fading channel can be formulated as [170]:

$$C_{DCMC}^{Ray} = \log_2(M) - \frac{1}{M} \sum_{n=0}^{M-1} E \left[\log_2 \sum_{m=0}^{M-1} \exp\left(\frac{-|h(x^{(m)} - x^{(n)}) + n|^2 + |n|^2}{N_0} \right) \right] \, , \tag{3.36}$$

where the index n is different from the index m.

Figure 3.10 presents the capacity versus SNR_t performance of the CCMC and DCMC schemes for transmission over AWGN channels. In Figure 3.10, we have compared the DCMC capacity for 4PSK, 8PSK, 16QAM and 64QAM schemes to the ideal CCMC capacity. Specifically, the asymptotic DCMC capacity is 2 BPS for 4PSK, 3 BPS for 8PSK, 4 BPS for 16QAM and 6 BPS for 64QAM. In our ATTCM scheme, we activated the appropriate modulation mode according to the corresponding channel SNR. Figure 3.11 shows the CCMC and DCMC capacity curves based on the uncorrelated Rayleigh fading channel. We note that Shannon's CCMC capacity is only restricted by the SNR and the bandwidth. The switching thresholds of the corresponding CCMC and DCMC schemes at a target BER below 10^{-5} are shown in Table 3.2. Observe from Table 3.2 that the SNR required for transmission over an uncorrelated Rayleigh fading channel is higher than that for an AWGN channel.

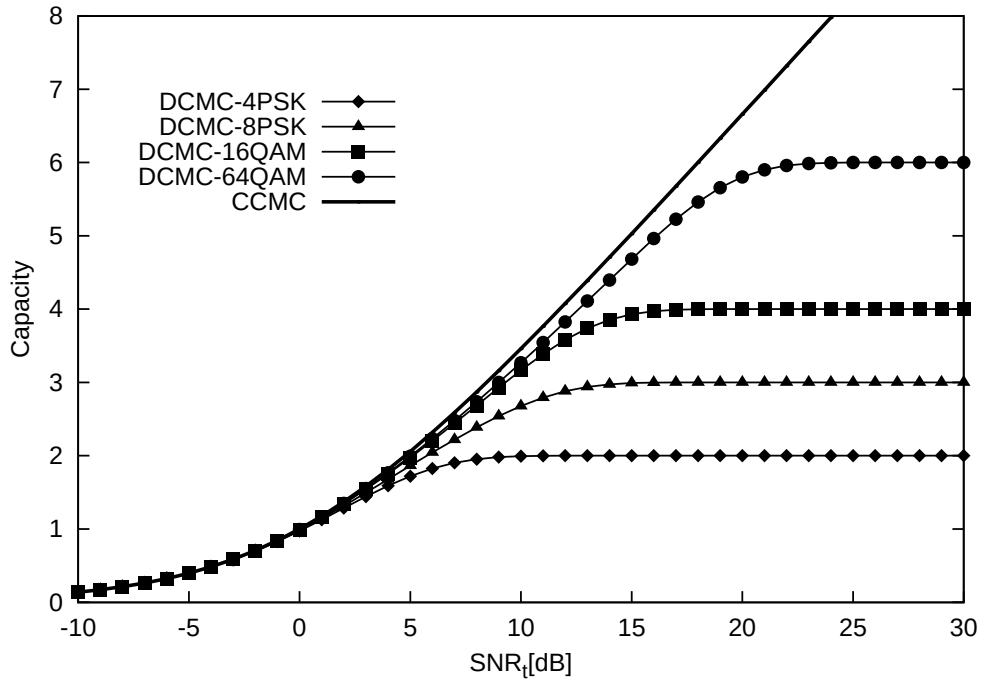

Figure 3.10: The CCMC and DCMC capacity curves based on AWGN channels.

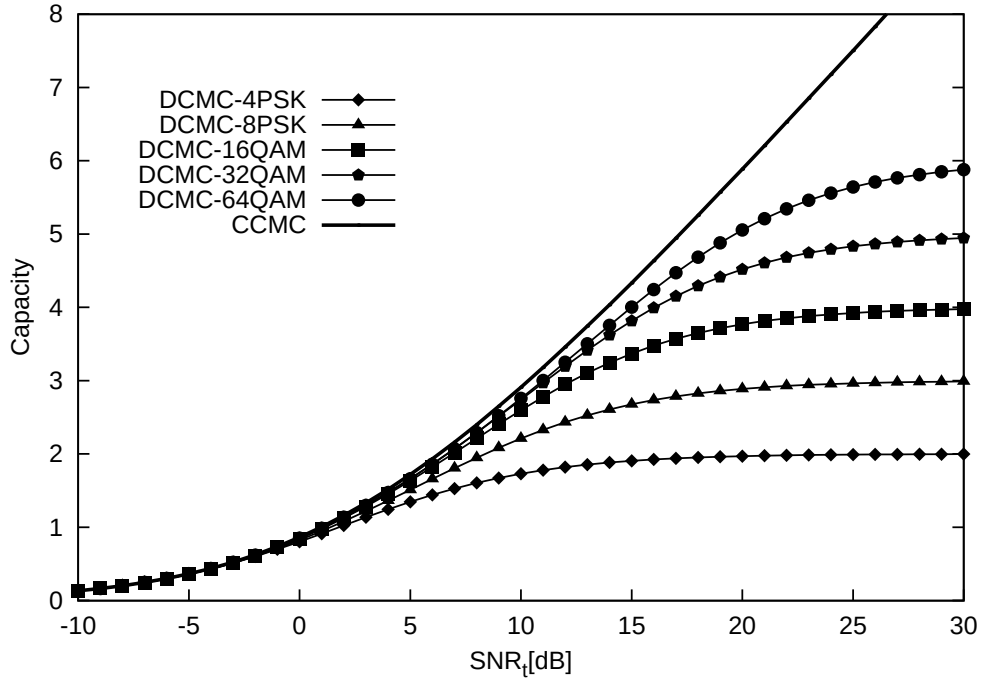

Figure 3.11: The CCMC and DCMC capacity based on uncorrelated Rayleigh fading channels.

Channel	Y[dB] at BER= 10^{-5}						
	AWGN			Uncorrelated Rayleigh			
Coding/ Modulation	ATTCM	DCMC	CCMC	ATTCM	DCMC	CCMC	iBPS
4PSK	1.8	1	0	4.8	2	1.75	1
8PSK	7.2	6	5	12	8	6	2
16QAM	10.7	9	8	16	12.5	11	3
64QAM	17.1	17	15	24	20	17	5

Table 3.2: The SNR thresholds of TTCM, DCMC and CCMC schemes, when communicating over AWGN and uncorrelated Rayleigh fading channels. The values are tabulated based on Figure 3.8 and Figure 3.9.

3.4.2 One-Way Relaying Aided CCR Scheme

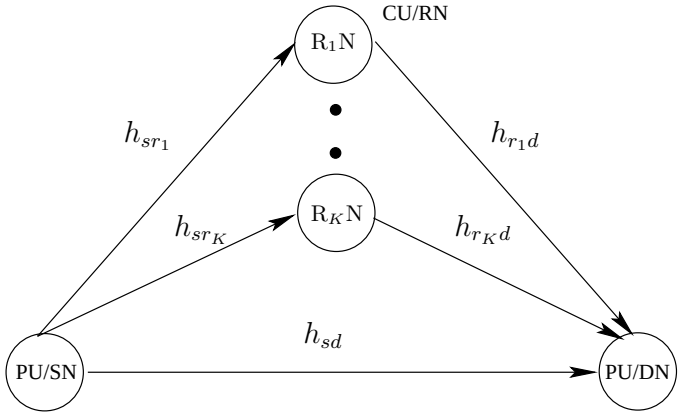

Figure 3.12: The schematic of a two-hop relay-aided system, which constitute an extension of Figure 3.1 relying on multiple CUs. The quasi-static Rayleigh fading channel between node *a* and node *b* is denoted as h_{ab}.

As shown in Figure 3.1, we consider a single SN, K RNs, and a single DN. All relays operate in the half-duplex DAF mode and it is assumed that each relay only knows its own channel, but the DN receiver knows all channel value with the aid of training. In addition, the benefit of the direct SD link is also considered. The signal received by node b from node a is given by:

$$y_{ab} = \sqrt{G_{ab}}\sqrt{P_{ab}}h_{ab}x + n\,, \tag{3.37}$$

where G_{ab} denotes the RDRPR experienced by the link between node a and node b, while h_{ab} represents the symmetric quasi-static Rayleigh fading channel gain of the ab link and we assume that all channel gains are independent of each other. The quasi-static Rayleigh fading channels between the SN and the RNs are denoted as $\{h_{sr_k}\}_{k=1}^{K}$, while those between the RNs and the DN are represented by $\{h_{r_kd}\}_{k=1}^{K}$. The power term P_{ab} is normalized to unity. We use the notation γ_{ab}

to refer to the instantaneous receive SNR of the link between node a and node b, so that

$$\gamma_{ab} = \frac{G_{ab}|h_{ab}|^2}{N_0}. \tag{3.38}$$

In our proposed system we have considered perfect channel estimation. In the non-cooperative scheme of System A, $|h_{sd}|^2$ is used for computing the SNR$_r$. Additionally, all cognitive relays are located near the center of the system, hence we have $G_{sr} = G_{rd} = 8$. We have considered a SISO [172] system for both the SR and RD link in our OWR system, where each node has one antenna, and employed ML MUD. The ML MUD provides the best possible performance at the cost of the highest complexity, which is a non-linear detector, and it is optimal in terms of minimizing the symbol error probability, when all possible vectors are equally likely [113]. As we discussed in Section 3.4.1, each of our communication links is assisted by the ATTCM scheme, as shown in Figure 3.13.

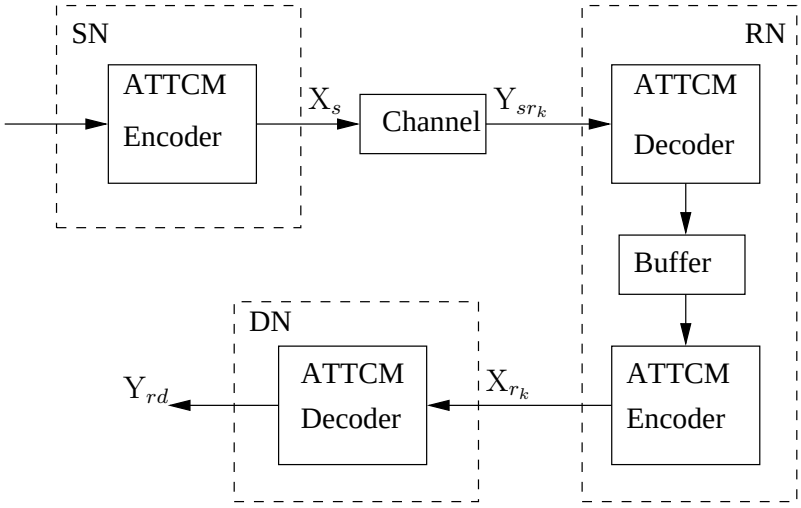

Figure 3.13: The block diagram of the ATTCM assisted one-way relaying aided CCR scheme obeying Figure 3.12.

Among the K available relays only the specific relay that provides the highest instantaneous SNR, which is given by Eq. (3.38), is selected for forwarding the signal transmitted from the SN to the DN. We have considered two methods to choose the best relay. The first one is the conventional max-min technique [173], while the second one is the max-sum technique [174] that maximizes the instantaneous sum rate.

3.4.2.1 Max-Min Relay Selection Technique

The capacity of this two-hop scheme is limited by the particular hop that has the minimum SNR, namely $\{\min[|\gamma_{sr_i}|^2, |\gamma_{r_id}|^2]\}$, which may also be deemed to be the "bottleneck" [17]. We have $(K+1)$ links spanning from the SN to the DN supported by K RNs as well as the SD link, as seen in Figure 3.12. The *max-min* relay selection technique is based on maximizing the transmission rate by selecting the particular RN, whose lower-quality hop is the best amongst the pair of links of

the k RNs [17, 173]:

$$k = \arg\max_{i} \{\min[\gamma_{sr_i}, \gamma_{r_i d}]\} . \quad (3.39)$$

Under this policy, the best RN imposes the most restrictive "bottleneck" among the RNs. When employing the max-min relay selection technique, the size of the buffer at each RN equals to one frame length.

3.4.2.2 Max-Sum relay selection technique

In contrast to the max-min RN selection, in the max-sum technique there are $(K+1)$ links spanning from the SN to the DN, as shown in Figure 3.12. We only choose one of the K RNs to assist the PU/SN. We denote the squared sum of the SR and RD channels via the kth RN as: $\{|\gamma_{sr_k}|^2 + |\gamma_{r_k d}|^2\}$. The specific RN that exhibits the maximum value of the sum-rate from the entire set of the K RNs is selected for relaying. The max-sum relay selection technique focuses on the sum-rate and selects the specific relay that maximizes the instantaneous sum rate, directly which depends on the sum rate of the SNRs $(\gamma_{sr_i} + \gamma_{r_i d})$ defined as [174]:

$$k = \arg\max_{i} [\gamma_{sr_i} + \gamma_{r_i d}] . \quad (3.40)$$

However, when consider the max-sum relay selection technique, we assume that the buffer at each RN will never be empty nor would it overflow.

The comparison of these Max-Min and Max-sum methods is shown in Figure 3.14. Referring to Figure 3.14, we compared the corresponding iBPS versus SNR_t of the ATTCM-SystemC-CR scheme by employing the max-min and max-sum relay selection techniques. Their average throughputs are identical, when the number of RNs is one. In Figure 3.14, the curves of employing the max-min relay selection and the max-sum relay selection overlapped at $SNR_t = -7$ dB for $K = 10$ and at $SNR_t = -6$ dB for $K = 4$.

3.4.2.3 Simulation Results

In this section, we would study the performance of a practical OWR aided CCR scheme. Additionally, we have considered two scenarios for obtaining the switching thresholds. More specifically, 'Scenario 1' is based on the AWGN channel, while 'Scenario 2' is on the uncorrelated Rayleigh fading channel. In both scenarios, we have employed the max-sum relay selection technique and the min-max relay selection technique for selecting the best relay.

3.4.2.3.1 Scenario 1: The Switching Thresholds Are Based On AWGN Channel

For convenience, the ATTCM-based OWR aided in CCR scheme is denoted as ATTCM-OWR. Similarly, the notations CCMC-OWR and DCMC-OWR denote the OWR aided CCR schemes that

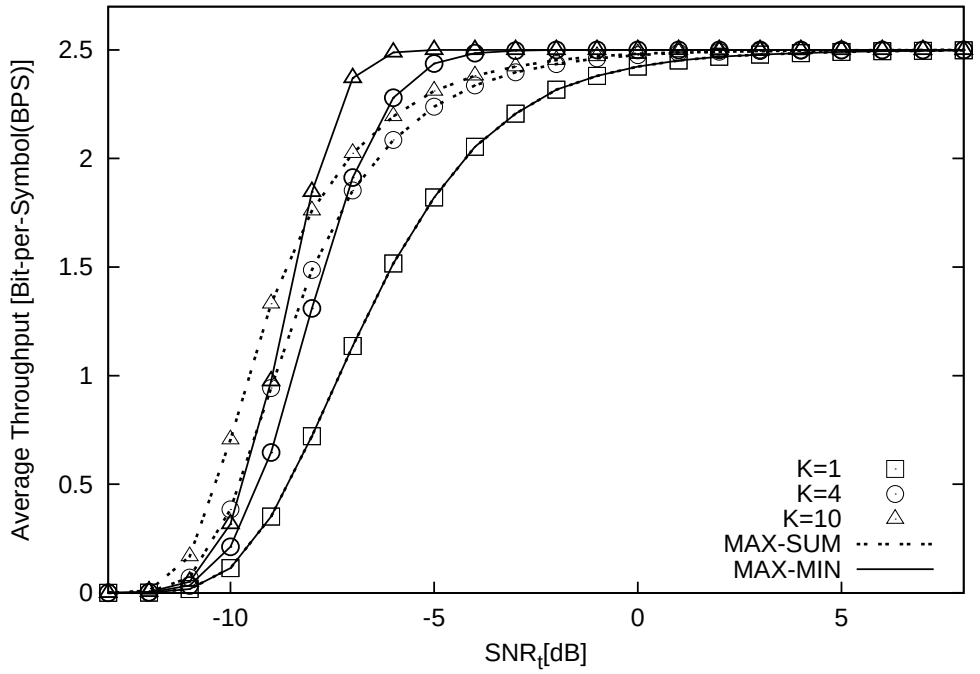

Figure 3.14: The iBPS throughput versus SNR_t of the ATTCM-SystemC-CR scheme communicating over quasi-static Rayleigh fading channels. A BER below 10^{-5} is maintained and $G_{sr} = G_{rd} = 8$. The "Max-Min" and "Max-Sum" techniques are employed, which are described in Section 3.4.2.1 and Section 3.4.2.2, respectively. The corresponding switching thresholds are based on the uncorrelated Rayleigh fading channel. **The number of RNs is $K = 1$, $K = 4$ and $K = 10$.** The corresponding switching thresholds are refer to Table 3.2.

are based on the CCMC and DCMC capacities, respectively as described in Section 3.4.1.1. We use η_A to denote the throughput of System A and η_C to represent the average throughput of System C in Table 3.1. Figure 3.15 shows the iBPS value versus SNR_t of the ATTCM-OWR, CCMC-OWR and DCMC-OWR schemes employing the max-sum relay selection technique of Section 3.4.2.2. As seen from Figure 3.15, the η_A value of the three schemes became saturated at 5 BPS, for $SNR_t \geq$ 30 dB. In general, the CCMC-OWR represents the upper bound, because the CCMC capacity is the highest. The intersection point of the η_A and η_C curves for the ATTCM-OWR scheme is at $SNR_t = 14$ dB, while those for the CCMC-OWR and DCMC-OWR modes are at 11 dB and 12 dB, respectively. When we have $\eta_C < \eta_A$ beyond the intersection point, cooperation is no longer beneficial. Hence, our cognitive system will employ System A for $\eta_A > \eta_C$. Observe from Figure 3.15 that when the number of RNs is increased to $K = 4$, the η_C^{CCMC} curve converges to the asymptotic value of 2.5 BPS for $SNR_r \geq 13$ dB, which is $18 - 13 = 5$ dBs earlier than that of employing a single RN. This is because when the number of RNs is increased, we have a higher chance of selecting a better RN for assisting the PU/SN. In contrast to Figure 3.15, Figure 3.16 used the max-min relay selection technique of section 3.4.2.1. The η_C^{ATTCM} curve of Figure 3.16 converges to 2.5 BPS for $SNR_r = 6$ dB and $K = 4$. Additionally, the η_C^{ATTCM} curve converges

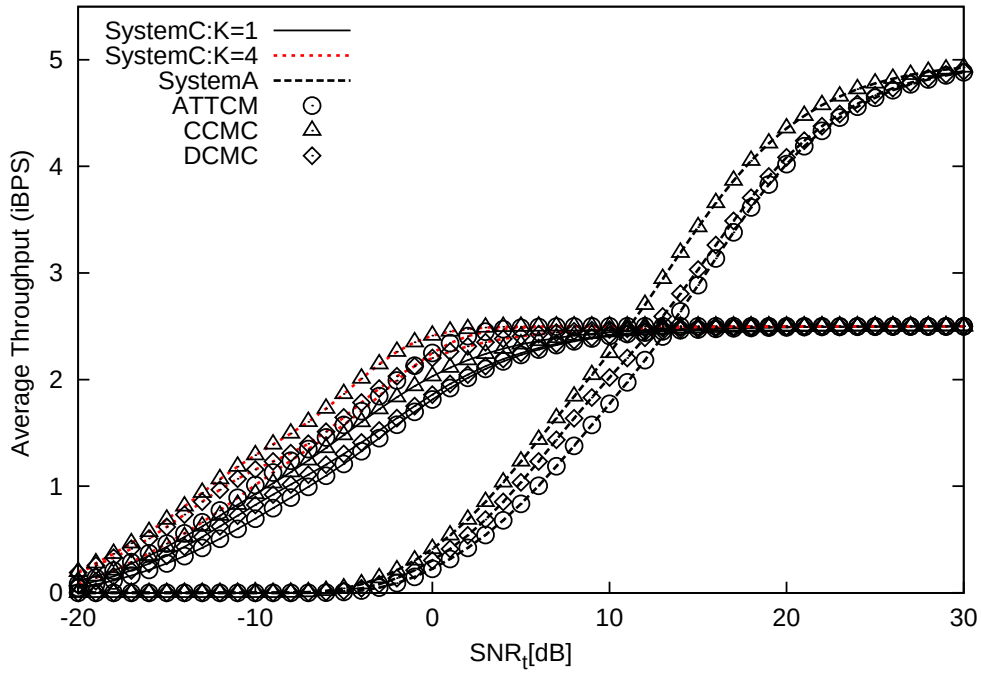

Figure 3.15: The iBPS throughput versus SNR_t of the OWR-aided ATTCM, as well as the perfect CCMC and DCMC schemes in our CCR system communicating over quasi-static Rayleigh fading channels by employing the **max-sum relay selection** technique. A BER below 10^{-5} is maintained under **Scenario 1** and $G_{sr} = G_{rd} = 8$. The "SystemC" label refers to System C in Section 3.3, while the "SystemA" label refers to the non-cooperation System A in Section 3.3. The number of RNs is $K = 1$ and $K = 4$. The corresponding switching thresholds are refer to Table 3.2.

to 2.5 BPS for $SNR_r \geq 16$ dB, which is 10 dB higher than that of employing the max-min relay selection method.

Figure 3.17 illustrates the attainable bandwidth-reduction (B_s) versus SNR_t for the ATTCM-OWR, CCMC-OWR and DCMC-OWR schemes employing the max-min relay selection technique of section 3.4.2.1, when the number of RNs is given by one and four. We have employed the max-min relay selection technique, since it does not require an ideal buffer used by the max-sum relay selection method. As seen from Figure 3.17, the attainable bandwidth-reduction B_s is slightly higher, when the number of RNs is increased to four. It is also interesting to observe that the ATTCM-OWR scheme is capable of reducing the bandwidth more substantially compared to the idealistic DCMC-OWR and CCMC-OWR schemes. Furthermore, as the SNR increases, the bandwidth-reduction factor also reduces. This is because when the SNR is high, the quality of the SD link is sufficiently high for a fixed transmission throughput of $\eta_A = 5$ BPS. The inclusion of a RN at high SNRs would double the transmission period, without actually increasing the transmission throughput. Hence, we are only interested in the operational region of $B_s > 0$. Note furthermore from Figure 3.16 that at an SNR of 5 dB, the ATTCM-CR-SystemA scheme can only achieves a throughput of 0.83 BPS. However, with the aid of the best RN selected from four cooperating CUs,

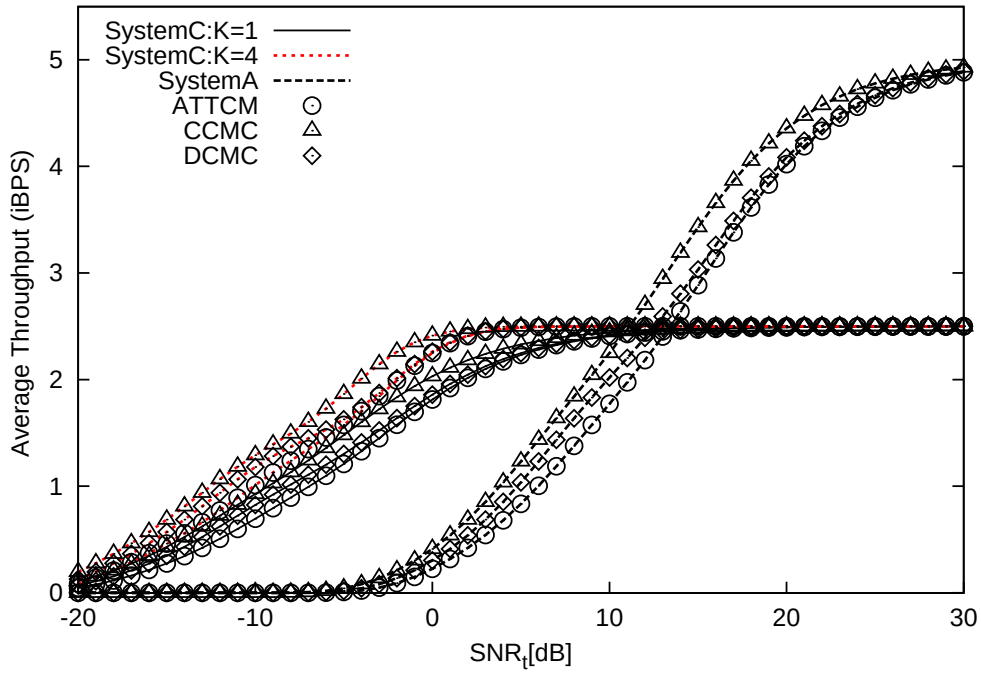

Figure 3.16: The iBPS throughput versus SNR_t of OWR-aided the ATTCM, as well as the perfect CCMC and DCMC schemes in CCR system communicating over quasi-static Rayleigh fading channels by employing the **max-min relay selection** technique. A BER below 10^{-5} is maintained under **Scenario 1** and $G_{sr} = G_{rd} = 8$. The label "SystemC" refers System C in Section 3.3, while "SystemA" refers to the non-cooperation System A in Section 3.3. The number of RNs is $K = 1$ and $K = 4$. The corresponding switching thresholds are refer to Table 3.2.

the ATTCM-SystemC would enable the PU to transmit at a throughput of 2.47 BPS. This may also be translated into a maximum bandwidth reduction of $(1 - \frac{0.83}{2.47}) = 0.67 = 67$ %.

3.4.2.3.2 Scenario 2: The Switching Thresholds Are Based On Rayleigh fading Channel

Figure 3.18 and Figure 3.19 show the corresponding iBPS throughput versus SNR_t of the OWR-aided ATTCM, as well as the perfect CCMC and DCMC-achieving schemes and the corresponding thresholds are based on the Rayleigh fading channel, as shown in Table 3.2. As seen from Figure 3.18 and Figure 3.19, the curves recorded for the CCMC-achieving scheme are always the best. In general, the CCMC-SystemA and CCMC-SystemC arrangements represent the upper bound. For $SNR_t > 38$ dB, the iBPS value of the three schemes became saturated at 5 BPS. As seen in Figure 3.18, the max-sum relay selection technique has been employed. The intersection point of the ATTCM-SystemC and ATTCM-SystemA schemes of Figure 3.18 is at $SNR_t = 19$ dB, while those of the CCMC-SystemC and CCMC-SystemA modes is at 13 dB and that of the DCMC mode is at 15 dB. Naturally, at their intersection point, the throughput of System A and System C is identical. The throughput of the 'CCMC mode' is always better than that of the DCMC and

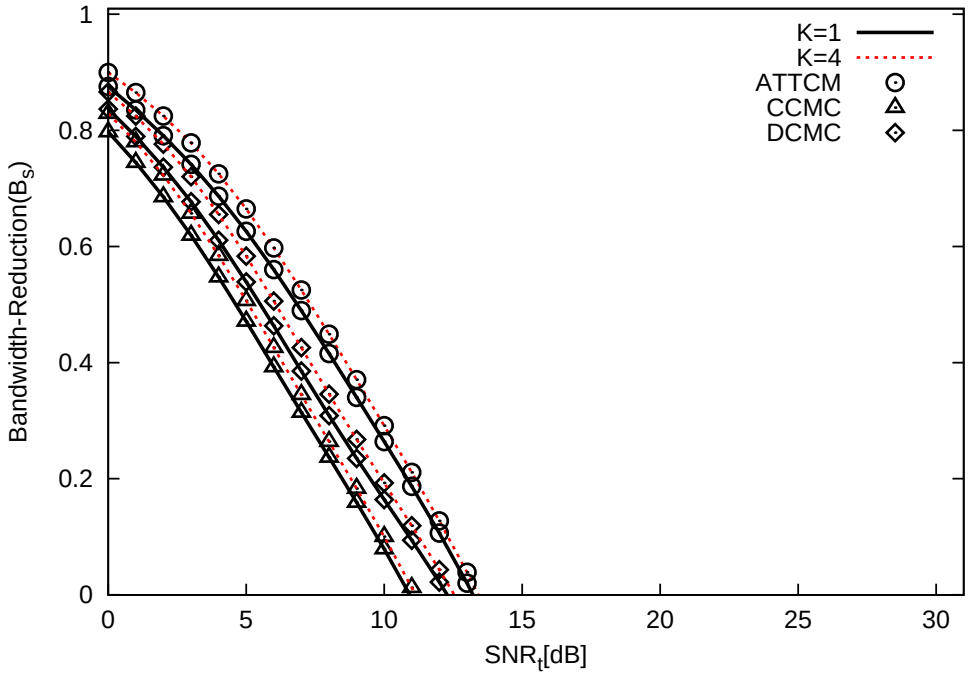

Figure 3.17: The attainable bandwidth-reduction value versus SNR_t of the OWR-aided ATTCM, CCMC and DCMC-achieving schemes communicating over quasi-static Rayleigh fading channels and employing the **max-min relay selection** technique. A BER of below 10^{-5} is maintained under **Scenario 1** and RDRPR is given by $G_{sr} = G_{rd} = 8$. The number of RNs is $K = 1$ and $K = 4$. The corresponding switching thresholds are refer to Table 3.2.

ATTCM schemes. Additionally, the throughput of all System C based schemes is higher than those based on System A before their intersection point. Cooperation is no longer beneficial beyond the intersection point owing to the extra time-slot required. Observe that when the number of RNs is increased to $K = 4$, the SystemC-related CCMC curve converge to the asymptotic value of 2.5 BPS for $SNR_t \geq 5$ dB, which is 5 dBs earlier than their counterparts having $K = 1$. In Figure 3.19, we have employed the max-min relay selection technique. The curve of the perfect CCMC aided SystemC converges to 2.5 BPS at $SNR_t \geq 2$ dB, when the number of RNs is $K = 4$. Hence, when employing the max-min relay selection technique, the SystemC-based schemes will converge to the asymptotic BPS faster than that employing the max-sum relay selection technique. Figure 3.20 portrays the performance of the corresponding iBPS value versus SNR_t of the ATTCM, as well as the perfect CCMC and DCMC-achieving OWR in our CCR schemes communicating over quasi-static Rayleigh fading channels, in comparison to that of Shannon's capacity bound. We will refer to the perfect CCMC capacity based curves as the upper bound. However, the DCMC capacity is more pertinent in the context of designing realistic schemes based on actual modulation and coding schemes. As expected, when we have a RDRPR of $G_{sr} = G_{rd} = 8$, the iBPS performance is improved compared to that of $G_{sr} = G_{rd} = 1$. There are two transmission links in our OWR scheme, namely the SR link and the RD link. Based on our ATTCM mode switching

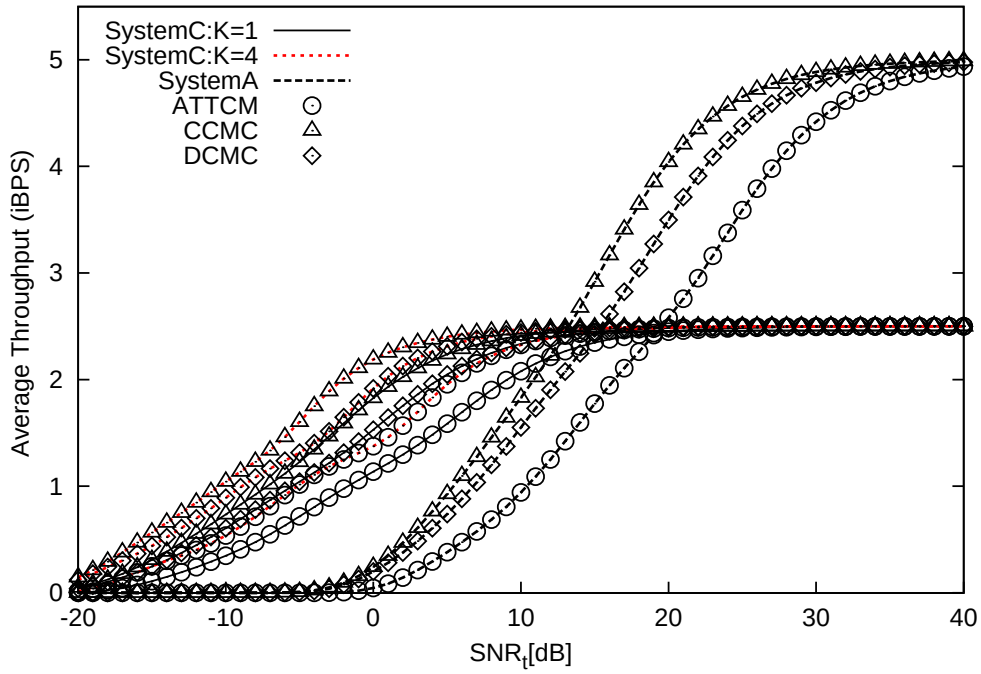

Figure 3.18: The iBPS throughput versus SNR_t of the OWR-aided ATTCM, as well as the perfect CCMC and DCMC-achieving CCR schemes communicating over quasi-static Rayleigh fading channels by employing the **max-sum relay selection** technique. A BER below 10^{-5} is maintained under **Scenario 2** and $G_{sr} = G_{rd} = 8$. The label "SystemC" is represents the relay aided system of Section 3.3, while "SystemA" refers to the non-cooperative System A of Section 3.3. The number of RNs is $K = 1$ and $K = 4$. The corresponding switching thresholds are refer to Table 3.2.

thresholds, the system will activate the 64QAM mode for $\gamma_R > \gamma_3$. If both the SR and RD links have achieved their best performance associated with 64QAM, then the throughput of these two links becomes 5 BPS. However, we have two time-slots in our CCR scheme, where both SN and RN transmitted the same amount of information. Thus, our overall system throughput becomes $\eta_{SRD}^{one-way} = \frac{iBPS_{SR}+iBPS_{RD}}{2\times Timeslot} = \frac{5+5}{2\times 2} = 2.5$ BPS in the high-SNR region.

3.4.3 Two-Way Relaying Aided CCR Scheme

Having studied the ATTCM aided OWR assisted CCR scheme in Section 3.4.2, we will now consider how the OWR system may be extended to a TWR assisted CCR system, where the two PUs act as the SNs and the DNs for each other. The schematic of the MABC-TWR scheme is shown in Figure 3.21, which consists of two source nodes: Source Node 1 (SN_1) and Source Node 2 (SN_2), K number of RN and two destination nodes: Destination Node 1 (DN_1) and Destination Node 2 (DN_2). During the first cooperative transmission period, both PUs transmit their signals simultaneously from their SNs, namely PU/SN_1 and PU/SN_2, to the CU/RN.

We have considered two protocols in our proposed scheme namely the TDBC and MABC.

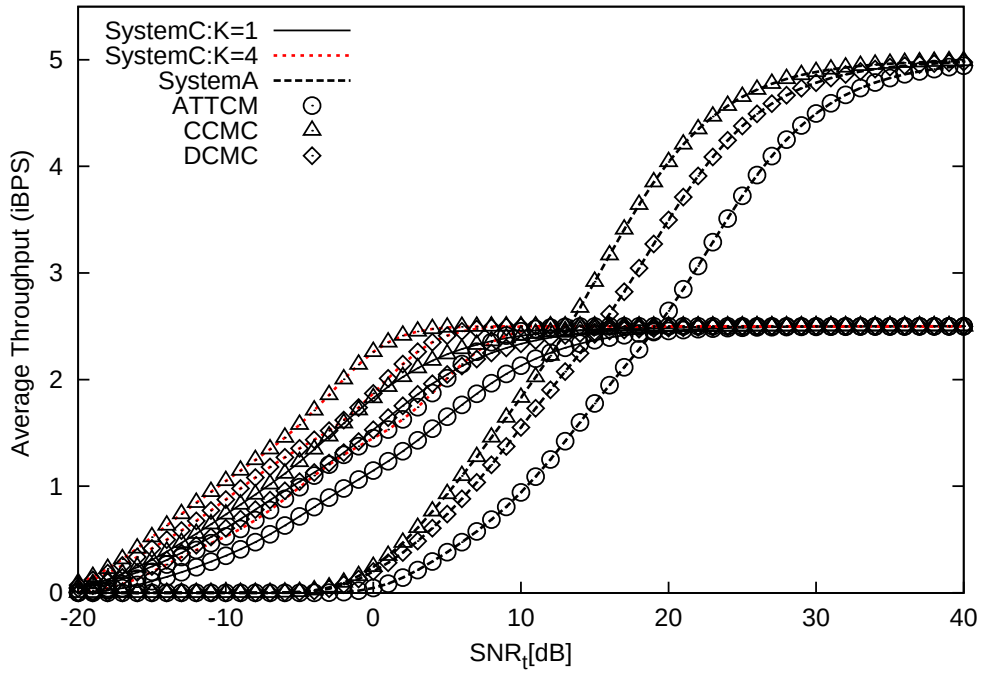

Figure 3.19: The iBPS throughput versus SNR_t of the OWR-aided ATTCM, as well as the perfect CCMC and DCMC-achieving CCR schemes communicating over quasi-static Rayleigh fading channels by employing the **max-min relay selection** technique. A BER below 10^{-5} is maintained under **Scenario 2** and $G_{sr} = G_{rd} = 8$. The label "SystemC" represents relay aided system of Section 3.3, while "SystemA" label refers to the non-cooperative System A of Section 3.3. The number of RN is $K = 1$ and $K = 4$. The corresponding switching thresholds are refer to Table 3.2.

In the TDBC protocol shown in Figure 3.21, there is no interference hence the corresponding complexity at the RN is kept low. Three time slots are used for two data flows, which are $s_1 \rightarrow r$, $s_2 \rightarrow r$, and $s_1 \leftarrow r \rightarrow s_2$, where s_1 and s_2 denote the two primary sources, while r denotes the CU which acts as a RN. By contrast, the MABC protocol requires two time slots for transmitting two data flows, which are $s_1 \rightarrow r \leftarrow s_2$ and $s_1 \leftarrow r \rightarrow s_2$. Since the sources transmit their information simultaneously, the MABC system suffers from self-interference. In our work, we have invoked an advanced MUD technique at the RN in order to decode both information streams of the SNs and to cancel the self-interference. Explicitly, in the MABC protocol, two signals were transmitted simultaneously from the two PU/SNs, where each PU has a single antenna. Additionally, we have used the powerful maximum likelihood MUD for detecting the two source signals using a single-antenna aided CU/RN, which constitutes a (2×1)-element MISO [172] system for the SR links. This powerful MUD was required for eliminating avalanche-like error propagation at the RNs. However, opted for (1×1)-element SISO system for the RD link, where each DN employs a single antenna for detecting its wanted signal arriving from the RN. By contrast, in the TDBC protocol, we have a (1×1)-element SISO system in the two SR links and a single RD link, because the two SNs use two separate time periods for transmitting their information to the RN, respectively.

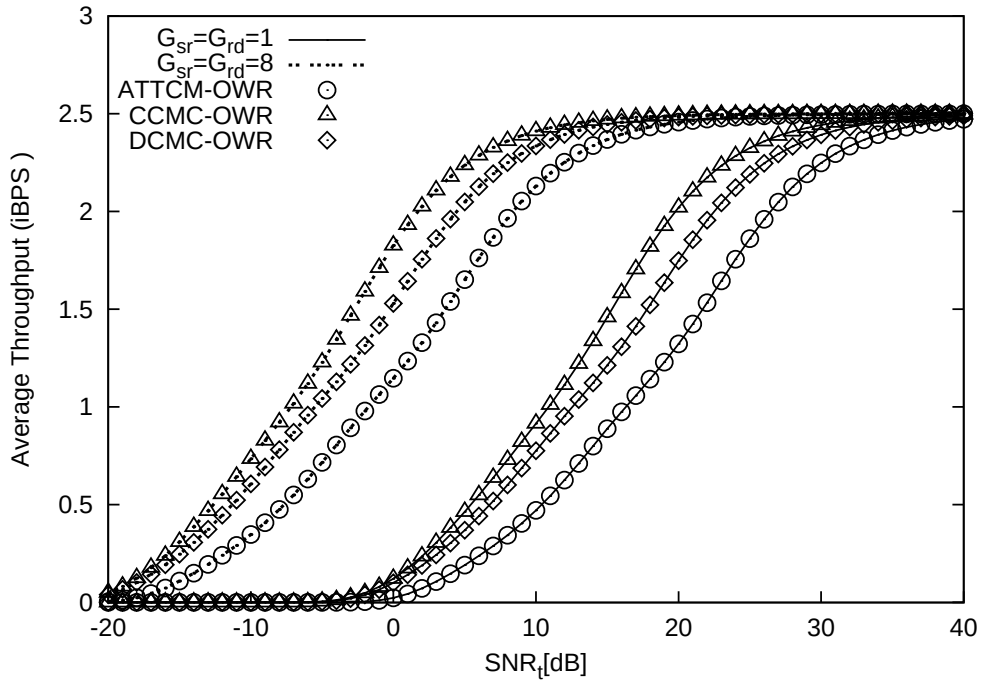

Figure 3.20: The iBPS throughput versus SNR_t of the OWR-aided ATTCM, as well as the perfect CCMC and DCMC-achieving CCR schemes communicating over quasi-static Rayleigh fading channels compared to the CCMC capacity of the Rayleigh channel. The "Shannon-Capacity-Ray" label refers to the CCMC capacity in Rayleigh channel. The number of relays is $K = 1$. The label "OWR" represents the one-way relay system. **The corresponding RDRPR are $G_{sr} = G_{rd} = 8$ and $G_{sr} = G_{rd} = 1$.** The corresponding switching thresholds are refer to Table 3.2.

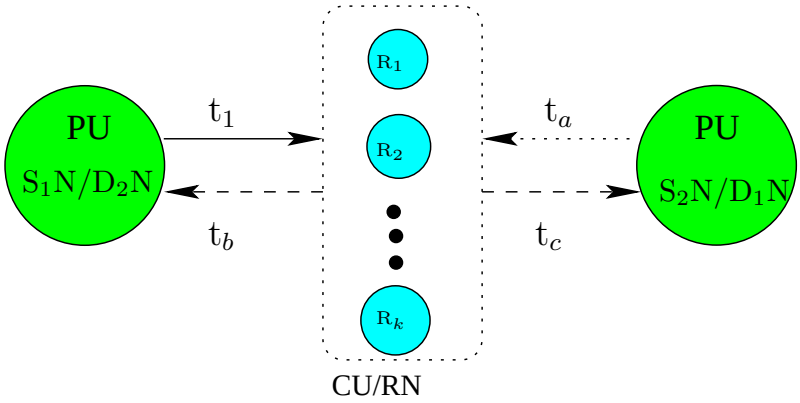

Figure 3.21: The schematic of a TWR-CR system, including two PUs and K CUs. For MABC, $t_a = t_1$ and $t_b = t_c = t_2$, where t_1 is the first transmission period and t_2 is the second transmission period. For TDBC, $t_a = t_2$ and $t_b = t_c = t_3$, where t_3 is the third transmission period. This is a transformation of Figure 3.1, where the PUs are acting as SNs as well as DNs.

We have opted for appointing the best relay has the set of available K RNs that experience identically and independently distributed (i.i.d) fading. Then the selected best RN decodes and forwards the received signals to the intended destinations, namely to the PU/DN$_1$ and PU/DN$_2$, respectively, during the second cooperative transmission period. Hence, the overall system throughput becomes higher than that of a OWR scheme, which requires two time slots for transmitting a single user's information. Again, each of the communication links is assisted by our ATTCM scheme. By referring to Eq. (3.37), the signal transmitted from the SNs to the kth RN in our MABC TWR system is given by:

$$y_{sr_k} = \sqrt{G_{sr_k}}\sqrt{P_{sr_k}}h_{sr_k}X + n\,, \tag{3.41}$$

where X is a vector hosting both SNs' signal. We can view the two SNs as a combined two-antenna assisted SN, where Eq. (3.41) is a (2×1)-element MISO system. Furthermore, the signal received by the DNs from the RNs is given by:

$$y_{r_kd} = \sqrt{G_{r_kd}}\sqrt{P_{r_kd}}h_{r_kd}x + n\,, \tag{3.42}$$

where the RDRPR experienced by each link is defined as:

$$G_{SR_1} = G_{SR_2} = G_{RD_1} = G_{RD_2} = 2^3 = 8 \tag{3.43}$$

in our TWR aided proposed CCR system, since the RN is located midway between the SN and the DN. Additionally, the channel gains $h_{S_1R_k}$, $h_{S_2R_k}$, $h_{R_kD_1}$ and $h_{R_kD_2}$ are independent of each other, each of which is represented by a quasi-static Rayleigh fading channel. The Gaussian noise vector n has a zero mean and a noise variance of $N_0/2$ per dimension. By contrast, the SNR at the kth SR link is computed as:

$$\gamma_{(r,sr_k)} = \frac{G_{sr_k}|h_{sr_k}|^2}{N_0}\,. \tag{3.44}$$

Similarly, the SNR at the RD receiver is given by:

$$\gamma_{(r,r_kd)} = \frac{G_{r_kd}|h_{r_kd}|^2}{N_0}\,. \tag{3.45}$$

Again, we considered the max-min relay selection technique of Section 3.4.2.1 as defined in Eq. (3.39) for selecting the best RN in our proposed TWR-CR scheme.

Additionally, as seen from Figure 3.9, we have chosen the ATTCM-MABC and ATTCM-TDBC schemes' switching thresholds for ensuring that the BER at the RN became lower than 10^{-5}. The reason why we have chosen the BER at the RN to be lower than 10^{-5} for the MABC protocol is because the error floor emerging at BER$< 10^{-5}$ can be removed by using a long outer block code, such as a Reed Solomon code. The performance of the TDBC and the MABC aided schemes is characterized in Section 3.4.3.1.

Channel	Uncorrelated Rayleigh			iBPS
	Y[dB] at BER= 10^{-5}			
Coding	ATTCM			
Protocol/ Modulation	MABC-SR, $Y_{ATTCM}^{(MABC,SR)}$	MABC-RD, $Y_{ATTCM}^{(MABC,RD)}$	TDBC, Y_{ATTCM}^{TDBC}	
4PSK	6.5	4.8	4.8	1
8PSK	15.5	12	12	2
16QAM	22	16	16	3
64QAM	35.8	24	24	5

Table 3.3: SNR threshold values of the ATTCM-TDBC and ATTCM-MABC schemes communicating over uncorrelated Rayleigh fading channels. The values are tabulated from Figure 3.9.

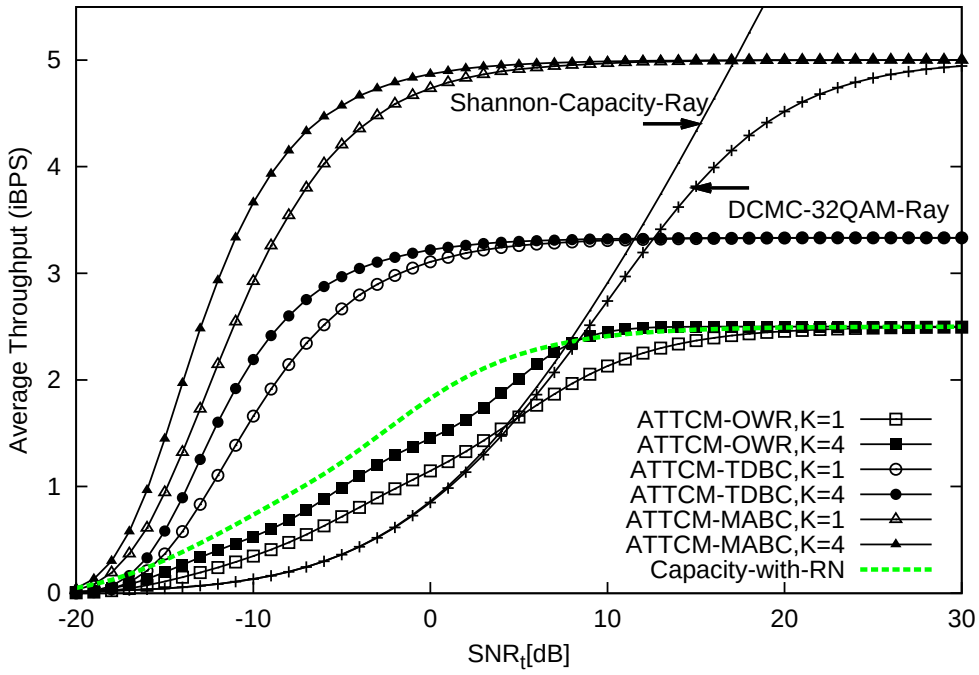

Figure 3.22: The iBPS throughput versus SNR_t of the OWR and TWR-aide ATTCM schemes in our CCR system communicating over quasi-static Rayleigh fading channels by employing the **min-max relay selection technique**. The "DCMC-32QAM-Ray" label refers to the DCMC capacity of 32QAM in a Rayleigh channel, while the "Shannon-Capacity-Ray" refers to the CCMC capacity in a Rayleigh channel. A BER below 10^{-5} is maintained under **Scenario 2** and $G_{sr} = G_{rd} = 8$. The corresponding switching thresholds are refer to Table 3.3.

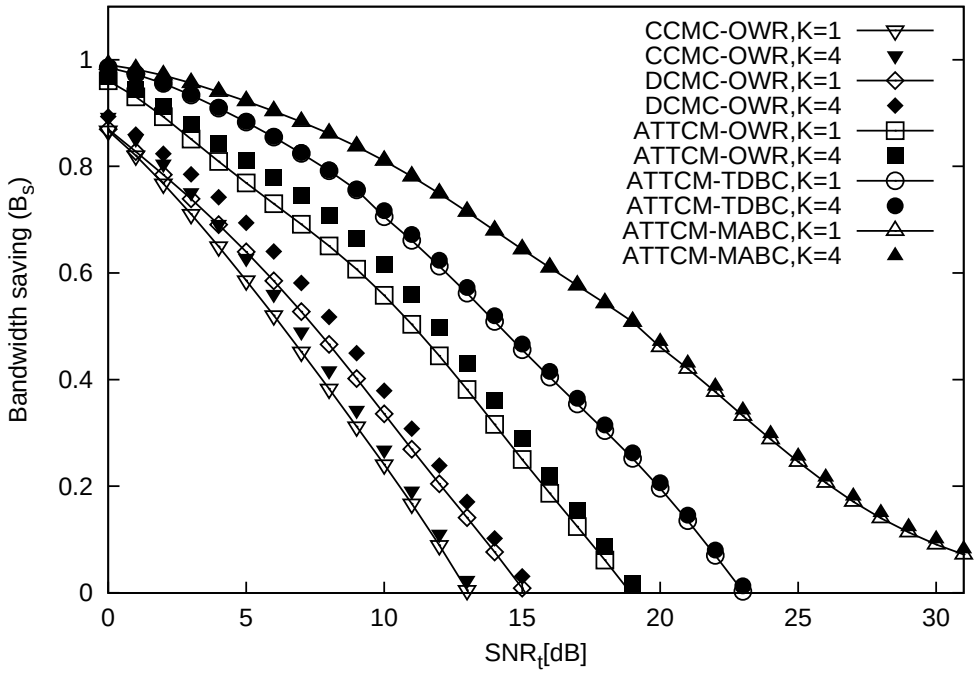

Figure 3.23: Bandwidth reduction B_s versus SNR_t for the OWR and TWR-aided ATTCM schemes in our CCR system communicating over flat Rayleigh fading channels and maintaining a BER below 10^{-5}. The number of frames simulated was 10^6. $G_{sr} = G_{rd} = 8$, **The number of RNs in these schemes is** $K = 1$ **and** $K = 4$. The corresponding switching thresholds are refer to Table 3.3.

3.4.3.1 Simulation Results

As seen in Figure 3.22, both our proposed ATTCM aided MABC and TDBC TWR system have a higher throughput than the proposed OWR system, when we consider the same number of RNs in the OWR system. In the MABC TWR system, the iBPS value became saturated at 5 BPS for $\text{SNR}_t \geqslant 11$ dB. The two SNs send their information simultaneously to a RN and then the RN broadcasts the combined information to the two DNs. The system throughput of the MABC TWR system is $\eta_{SRD}^{MABC} = \frac{iBPS_{S_1R}+iBPS_{S_2R}+iBPS_{R_1D}+iBPS_{R_2D}}{2\times Timeslot}$. When the MABC system has encountered the best possible channel conditions, the throughput became $\eta_{SRD}^{MABC} = \frac{5+5+5+5}{2\times 2} = 5$ BPS. Therefore, the asymptotic throughput of our proposed MABC TWR system ($\eta_{SRD}^{two-way}$) is twice that of the OWR scheme ($\eta_{SRD}^{one-way}$). By contrast, the iBPS value of the TDBC TWR system became saturated at 3.3 BPS for $\text{SNR}_t \geqslant 12$ dB. The TDBC-TWR system required three time slots, hence its η_{SRD} value is lower than that of the MABC scheme beyond $SNR_t = 1$ dB. The throughput of the TDBC TWR system is $\eta_{SRD}^{TDBC} = \frac{5+5+5+5}{2\times 3} = 3.3$ BPS, when each link has achieved its best condition. Moreover, its asymptotic throughput is 0.8 BPS higher than the throughput of the OWR system. Figure 3.22 shows the corresponding iBPS versus SNR_t performance of our proposed TWR system in comparison to the CCMC and DCMC capacity. Additionally, the curve of the MABC scheme are overlapped with the DCMC capacity for 32QAM at $SNR_t \geqslant 30$ dB.

Figure 3.23 illustrates the attainable bandwidth-reduction (B_s) versus SNR_t for the ATTCM, the CCMC and the DCMC aided OWR as well as for the ATTCM-aided TWR schemes. As seen from Figure 3.23, the attainable bandwidth-reduction B_s is slightly higher for the OWR scheme, when the number of RNs is increased from $K = 1$ to $K = 4$. It is also interesting to observe that the practical ATTCM scheme is capable of reducing the bandwidth more substantially compared to the idealistic DCMC and CCMC schemes. Furthermore, as the SNR increases, the bandwidth-reduction factor also reduces. This is because when the SNR is high, the quality of the SD link is sufficiently high for a fixed transmission throughput of 5 BPS. The inclusion of a RN at high SNRs would only double the transmission period, without actually increasing the transmission throughput. Hence, we are only interested in the operational region, while we have $B_s > 0$. Note furthermore from Figure 3.19 that at an SNR of 5 dB, the ATTCM-SystemA scheme can only achieve a throughput of 0.38 BPS. However, with the aid of the best RN selected from four cooperating CUs, the ATTCM-SystemC would enable the PU to transmit at a throughput of 2.0 BPS. This may also be translated into a maximum achievable bandwidth reduction of $(1 - \frac{0.38}{2.0}) = 0.81 = 81$ %. Figure 3.23 also illustrates the attainable bandwidth-reduction (B_s) versus SNR_t for the ATTCM aided MABC and TDBC TWR system. Since we are only interested in the operational region of $B_s > 0$, for $SNR_t > 15$ dB, the proposed schemes relying on OWR are no longer beneficial for the range of $B_s < 0$. The proposed TWR scheme can use the entire bandwidth, since the bandwidth-reduction of the TWR scheme is always higher than zero. Observe from Figure 3.19 that at an SNR_t of 5 dB, the ATTCM-SystemA scheme achieves a throughput of 0.38 BPS. However, as seen in Figure 3.23, the ATTCM-SystemC regime relying on TDMC TWR would enable the PU to transmit at a throughput of 3.2 BPS. Similarly, the ATTCM-SystemC relying on MABC TWR would enable the PU to transmit at a throughput of 3.9 BPS. This may be translated into a bandwidth reduction of $(1 - \frac{0.38}{3.2}) = 0.88 = 88\%$ for the TDBC scheme. In addition, it will lead to a bandwidth reduction of $(1 - \frac{0.38}{4.7}) = 0.92 = 92\%$ for the MABC scheme. Furthermore, the bandwidth reduction can be increased by $88 - 81 = 7\%$ upon employing the TDBC scheme compared to the OWR scheme. Additionally, $92 - 81 = 11\%$ bandwidth reduction can be attained by employing the MABC scheme in comparison to the OWR system. Moreover, at a given SNR, the TWR-CR system always attains a higher B_s value, than the corresponding OWR system.

3.4.4 A Simple Test For Verification

In this section, we have carried out a simple test for verifying the accuracy of our simulation results. In Figure 3.24, we compared the curve based on the CCMC capacity of the Rayleigh fading channel, as shown in Figure 3.11 and our simulation curve of the non-cooperative scheme, which is based on the CCMC thresholds of Table 3.11. More specifically, based on the CCMC capacity curve, we find the corresponding SNR values at $iBPS = \{0, 1, 2, 3, 4, 5\}$ as the switching thresholds. Observe from Figure 3.24, that the distance between the curve of the CCMC aided non-cooperative scheme (SystemA) and Shannon's channel capacity, is denoted as d_{TS}. We expect these to overlap, when we

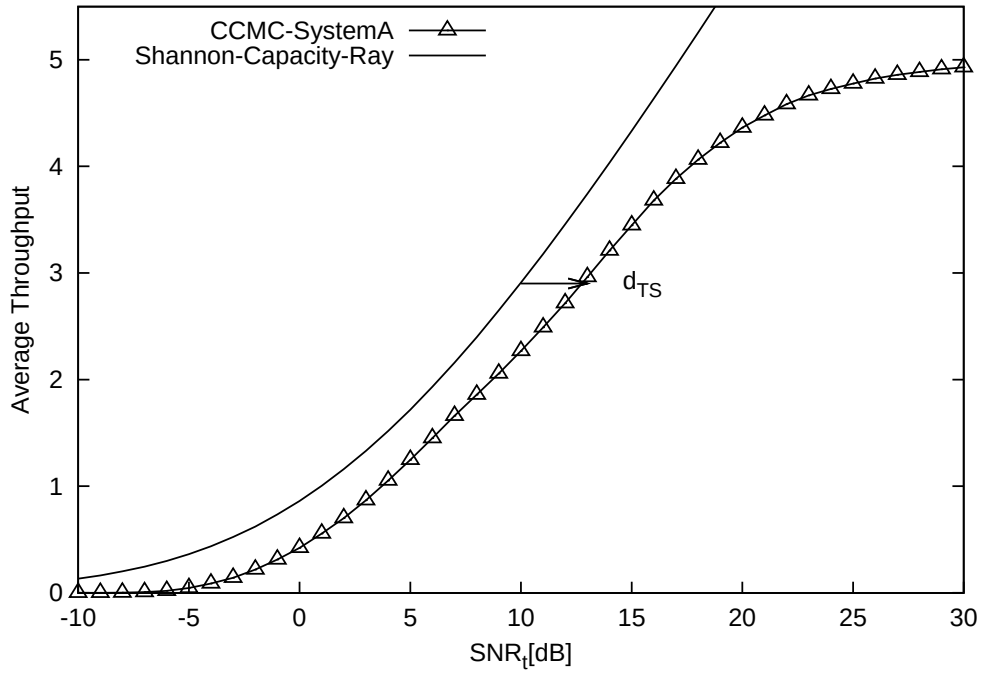

Figure 3.24: The BPS throughout versus SNR_t of the CCMC aided System A of Section 3.3 communicating over quasi-static Rayleigh fading channels and Shannon's capacity in a Rayleigh channel. The "Shannon-Capacity-Ray" label refers to Shannon's CCMC channel capacity based on a Rayleigh channel. A BER below 10^{-5} is maintained under **Scenario 2** and $G_{sr} = G_{rd} = 1$.

have more switching levels, since our switching thresholds of the CCMC-SystemA scheme were derived from Shannon's channel capacity of the Rayleigh fading channel, as shown in Figure 3.11. The CCMC-SystemA characterized in Figure 3.24 has 6 different BPS levels within a BPS range of $\{0, \cdots, 5\}$, with a step size of 1 bit. We can increase the number of BPS levels by reducing the step size to $B_{step} = \{0.5, 0.2, 0.1, 0.01\}$ while fixing the BPS range to $\{0, \cdots, 5\}$. As seen in Figure 3.25, when B_{step} is reduced, the corresponding CCMC-SystemA performance approaches the capacity curve. Hence, we have verified that our adaptive schemes studied in this chapter obey the channel capacity limit.

3.5 Chapter Conclusions

In this chapter, we have studied both the DAF and AAF assisted CCR schemes and quantified the optimum power ratio required for achieving the best transmission throughput for the CU. We proposed a practical ATTCM aided OWR-CCR scheme, where adaptive coding and modulation were invoked according to the near-instantaneous channel conditions. We found that the proposed OWR-CR scheme enables the PU to transmit at an improved transmission rate for a given SNR, while releasing a significant amount of bandwidth for exploitation by the CUs, despite operating

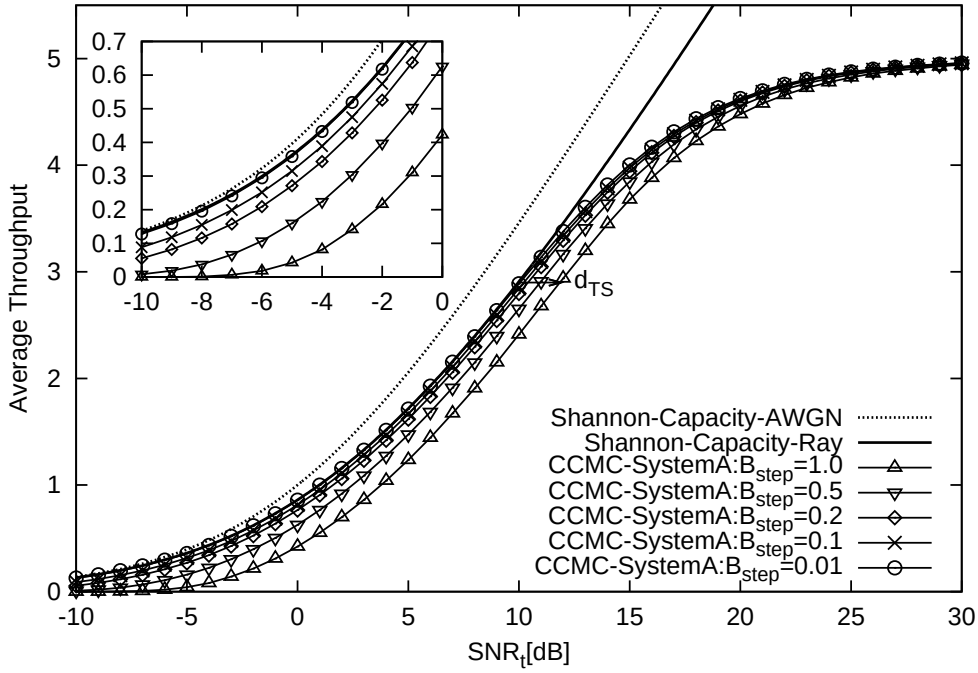

Figure 3.25: The BPS throughput versus SNR_t of the perfect CCMC aided System A communicating over quasi-static Rayleigh fading channels associated with different step sizes. A BER below 10^{-5} is maintained under **Scenario 2** and $G_{sr} = G_{rd} = 1$.

at a reduced SNR. In the process of implementing the OWR-CR scheme, we have compared two relay selection techniques, namely the max-min and max-sum techniques of Section 3.4.2. Both methods are capable of choosing the best relay for relaying the information transmitted from the RNs to the DN. More specifically, we found that the max-min relay selection technique is more practical to use, since it does not require an idealistic buffer that will never be empty nor overflow, which was needed by the max-sum method. Additionally, we have considered two scenarios, 'Scenario 1' and 'Scenario 2', of Section 3.4.2.3.1 and Section 3.4.2.3.2. Furthermore, both the DCMC and CCMC capacity were employed in our proposed OWR-CR scheme as the benchmark schemes. Then a practical TTCM scheme was investigated and benchmarked against these idealistic adaptive schemes. In Table 3.4, we compared the corresponding SNR value with respect

Thresholds	Scenario 1: AWGN channel			Scenario 2: Rayleigh fading channel		
SystemC	CCMC	DCMC	ATTCM	CCMC	DCMC	ATTCM
Max-sum relay selection	13 dB	15 dB	16 dB	15 dB	18 dB	22 dB
Max-min relay selection	4 dB	6 dB	7 dB	6 dB	9 dB	13 dB

Table 3.4: The SNR, where the corresponding iBPS of SystemC converges to 2.5 BPS, where the number of RN is $K = 4$. The thresholds are based on Table 3.2. This table is extracted from Figure 3.15, Figure 3.16, Figure 3.18 and Figure 3.19.

to the average throughput of SystemC that saturated at 2.5 BPS. Specifically, the schemes that employed the max-min relay selection technique require a reduced SNR for converging to the final 2.5 BPS limit. Moreover, in order to maximize the CU's own data rate and to improve the exploitation of the bandwidth released by the PUs, we also proposed a TWR-CR scheme by employing the MABC and TDBC protocols using the max-min relay selection technique of Section 3.4.2.1. The simulation results demonstrated that the TWR-CR scheme is capable of achieving a higher bandwidth reduction than the OWR-CR scheme, while improving the system's average throughput. The bandwidth reduction attained by the proposed TWR-CR scheme is more than 80% of the PU's bandwidth. The comparisons of bandwidth reduction based on our OWR-CR and TWR-CR schemes are shown in Table 3.5. Specifically, $92 - 81 = 11\%$ additional bandwidth reduction can be attained by employing the MABC scheme in comparison to the OWR-CR system, when using the same thresholds. Furthermore, we have carried out a simple test in Section 3.4.4 to verify the validity of our simulation results.

ATTCM-CR scheme	η_A	η_C	Bandwidth Reduction (B_s)
OWR-Scenario 1	0.83 BPS	2.47 BPS	67%
OWR-Scenario 2	0.38 BPS	2.0 BPS	81%
TDBC-Scenario 2	0.38 BPS	3.2 BPS	88%
MABC-Scenario 2	0.38 BPS	4.7 BPS	92%

Table 3.5: The bandwidth reduction value of the ATTCM-CR scheme at $SNR_t = 5$ dB, which was extracted from Figure 3.17 and Figure 3.23. The SNR thresholds of the "OWR-AWGN" scheme are derived from the TTCM aided AWGN channel, which has been discussed in Section 3.4.2.3.1. The label of "Rayleigh" indicates that the thresholds are derived from the TTCM aided Rayleigh fading channel, which has been described in Section 3.4.2.3.2 and Section 3.4.3.

In the next chapter, we will consider the overlay CCR scheme and use a dynamical network coding technique for exploiting the available bandwidth of the PUs.

Chapter 4

Adaptive Dynamic Network Coding in Cooperative Cognitive Radio networks

4.1 Introduction

In Chapter 3, we have employed both One Way Relay (OWR) and Two Way Relay (TWR) aided cooperative systems. In this chapter, we employ the Multiple Access Relay Channel (MARC) concept in our Cooperative Cognitive Radio (CCR) system for Uplink (UL) communication supporting multiple Primary Users (PUs) and a common Base Station (BS). The source information is transmitted from the PUs to the BS with the aid of multiple Cognitive Users (CUs), which act as the Relay Nodes (RNs). Moreover, we investigated the Network Coding (NC) technique, which was originally proposed by Ahlswede, Cai, Li and Yeung in 2000 [175]. The NC technique is capable of beneficially increasing the network capacity by invoking coding at the various nodes in a network, instead of simply supporting routing functions. According to Yeung's paper [176]: "NC has propagated to various fields in engineering in the past decade, including wireless communications, channel coding, computer networks, switching theory, cryptography, computer networks, data storage and computer science." Moreover, NC has been shown to be capable of increasing the achievable throughput, robustness and security, while minimising both the amount of dissipated energy and the delay of packets travelling through the network [175, 177]. The benefits of NC aided cooperative systems were studied in [178–180] with the most important one being the reduction of the redundant information [180].

More specifically, we mainly focus our attention on the family of Dynamic Network Codes (DNCs), which were proposed by Ming in [181], where each user broadcasts its own information frame both to the BS as well as to the other users during the first transmission period. After this phase, each user transmits a non-binary linear combination of its own frame and of the other users' information frames, to the BS [181]. The family of Generalized Dynamic Network Codes (GDNC) [182, 183]

constitutes an generalized extension of DNCs. In contrast to [181], the GDNC of [183] allows each user to broadcast several information frames during the broadcast phase via orthogonal channels [183], as well as to transmit several non-binary linear combinations, as parity frames during the cooperative phase via orthogonal channels. The design of network codes for multi-user, multi-relay scenarios has been investigated in [184, 185], where the users transmit their independent information to the BS with the aid of the RNs. In line with the system model proposed in [184], we assume that the CUs act as the RNs to help the PUs in transmitting their information to the BS. More specifically, in our proposed scheme, the CUs are capable of relaying the PU's message, while superimposing their own messages at the same time. This leads both to an increased overall throughput and to the reduction of the required transmission period of both the PUs and the CUs, thereby creating additional time-slots (TSs) for supporting additional users. The milestones of DNC related research are shown in Table 4.1. In order to increase the average transmission rate of GDNC without reducing its diversity order, an Adaptive Dynamic Network Code (ADNC) design was proposed in [182] based on the GDNC. In the ADNC scheme, the CUs only deliver their information to the BS, if the BS failed to recover the source message from the PUs. In our system model, we consider cooperation between the PUs and CUs, where CUs act as NC-aided RNs for conveying the information transmitted from the PUs. More explicitly, the principle of NC schemes presented in [181–184] is incorporated into an active cooperation based overlay network [157] conceived for a CR system, where the interference imposed on the PUs may be offset by using part of the CU's power to relay the PU's information.

Hence on this chapter an active cooperation based DNC scheme is proposed for overlay-based CCR schemes, in order to lease the PU's bandwidth to the group of CUs for their secondary communication. Moreover, a bandwidth-efficient Adaptive Trellis Turbo Coded Modulation (ATTCM) arrangement was introduced in Chapter 2, which is also employed in our proposed scheme for achieving a substantial performance improvement. The transmission rate/throughput of the system is adapted according to the near-instantaneous channel conditions, where a higher-throughput but vulnerable TTCM scheme is employed, when the channel conditions are good, while a lower-throughput but robust TTCM scheme or no transmission is used, when the near-instantaneous channel conditions are poor. Specifically, our ATTCM scheme is designed by considering the effects of both quasi-static Rayleigh fading as well as of uncorrelated Rayleigh fading. We have conceived an ADNC technique for our CCR system, where the CUs adaptively deliver their parity frames to the BS, depending on the success/failure of the PU's transmissions. Explicitly, the network encoder is activated in its adaptive mode for supporting the CUs depending on the Boolean value of the feedback flags generated based on the success/failure of the ATTCM decoder and of the network decoder, which is evaluated and fed back by the BS. During each broadcast session, all PUs transmit their information using the same fixed TTCM mode, which corresponds to that determined by the specific direct link having the lowest quality. Then in the cooperative phase, the "best" CU would support all the uplink transmissions towards the BS with the aid of its highest-throughput

Year	Author(s)	Contribution
2000	Ahlswede *et al*. [175]	Originally proposed the network concept for increasing the throughput of a network by invoking a simple coding scheme.
2003	Li *et al*. [186]	Linear network coding: a new strategy for information transmission in networks.
	Koetter [187]	An algebraic approach to network coding.
2005	Dougherty *et al*. [188]	Insufficiency of linear coding in network information flow.
2007	Popovski [189]	Physical network coding in two-way wireless relay channels.
2008	Katti *et al*. [190]	Practical wireless network coding.
	Koetter *et al*. [191]	Coding for errors and erasures in random network coding.
2009	Rong *et al*. [192]	Coding schemes for energy efficient multi-source cooperation aided Uplink transmission
	Dong *et al*. [193]	Wireless broadcast using network coding
2010	Ming [181]	Multiple-user cooperative communications based on linear network coding.
2011	Li *et al*. [177]	Linear network coding: theory and algorithms.
	Rebelatto *et al*. [182]	Adaptive distributed network-channel coding
	Nguyen *et al*. [194]	Performance bounds of network coding aided cooperative multiuser systems.
2012	Ming [184]	Design of network codes for multiple-user multiple-relay wireless networks.
	Rebelatto *et al*. [183]	Multiuser cooperative diversity through network coding based on classical coding theory.
2013	Nguyen *et al*. [195]	Irregular convolution and unity-rate coded network-coding for cooperative multi-user communications.
	Li *et al*. [185]	Generalized adaptive network coding aided successive relaying for noncoherent cooperation.
2014	Keshavarz [196]	Bounds on the benefit of network coding for wireless multicast and unicast.
2015	Chun *et al*. [197]	An adaptive network coding scheme for spectrum sharing in cognitive radio networks.

Table 4.1: Milestone of Dynamic Network Coding (2003-2015).

ATTCM mode. The received SNRs at the CUs and the BS may be used for determining the maximum throughput of each transmission link. Finally, our novel system is capable of simultaneously exploiting the advantages of ATTCM and ADNC for further improving the system performance.

4.2 System Model

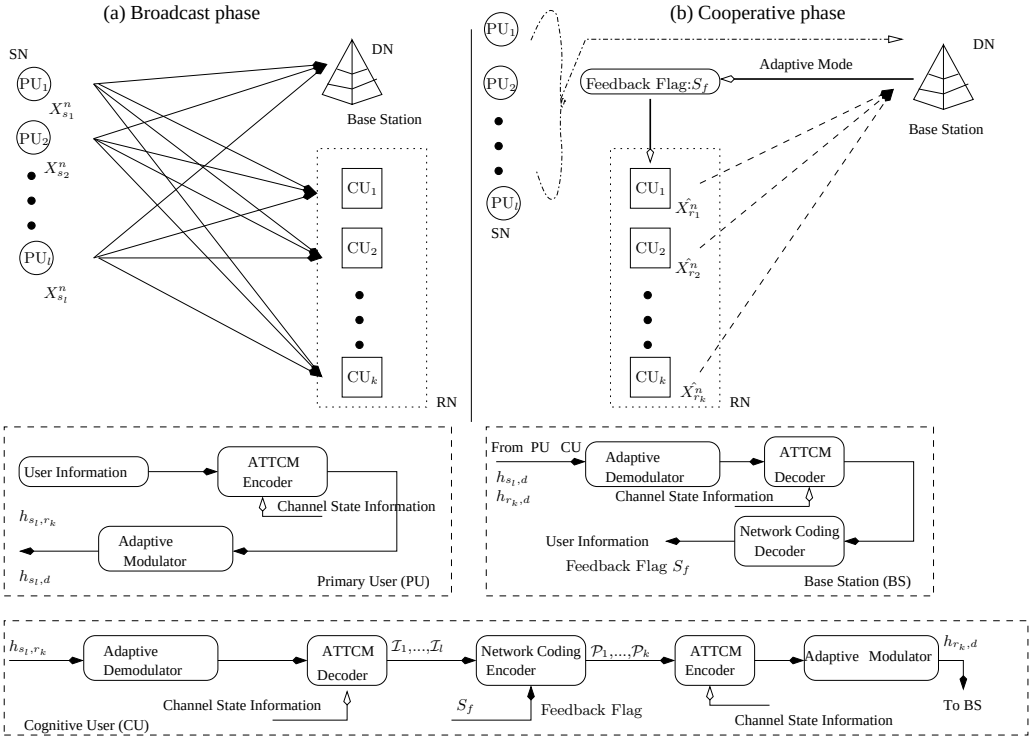

Figure 4.1: The architecture of the ATTCM aided DNC in the proposed CCR scheme, which obeys Figure 3.1, but additionally incorporate by adding the ATTCM and network coding components.

In our proposed system portrayed in Figure 4.1, we consider the transmission of the ADNC-CCR network. ATTCM is advocated for judiciously selecting a suitable modulation mode according to the near-instantaneous channel condition experienced in each transmission link, which would lead to the reduction of the PU's transmission power and/or to the increase of the overall system throughput, hence simultaneously saving bandwidth for the CUs. We assume that each PU has a direct transmission link to the BS, as seen in Figure 4.1. Additionally, we consider L PUs, where each PU broadcasts its information to a single BS and to K CUs during the broadcast phase. The BS then decodes the source information received from the PUs. Accordingly, the CUs encode the received information frames for constructing the corresponding parity frames, which are then transmitted to the BS during the cooperative phase. Hence the BSs receive the information frames from the PUs and also the parity frames from the CUs. We denote the network coded codewords transmitted by the kth CU/RN as $\{\overleftrightarrow{\hat{X}}^n_{r_k}\}_{k=1}^K$. The specific calculation of $\{\overleftrightarrow{\hat{X}}^n_{r_k}\}_{k=1}^K$ will be detailed in Section 4.2.2.

During the "(a) broadcast phase" seen in Figure 4.1, the lth PU/SN broadcasts its information frame $X_{s_l}^n$ within the nth frame to both the CUs/RNs and to the BS. The signal received at the BS via the Source-to-Destination (SD) link is given by:

$$y_{s_l d}^n = \sqrt{G_{s_l d}}\sqrt{P_S} h_{s_l d} X_{s_l}^n + n \,, \tag{4.1}$$

while that received at the k CU/RN via the Source-to-Relay (SR) link is:

$$y_{s_l r_k}^n = \sqrt{G_{s_l r_k}}\sqrt{P_S} h_{s_l r_k} X_{s_l}^n + n \,, \tag{4.2}$$

where P_S is the transmission power per unit frequency emanating from the PU/SN and $n \in N$, where N is the total number of frames. The $(N \times L)$ PUs simultaneously broadcast $(N \times L)$ information frames during the time duration T_1. Since a network-coding aided DAF protocol is employed at each CU/RN, the kth RNs forward the decoded-and-reencoded information frame $\hat{X}_{r_k}^n$ during the nth frame to the BS. Then, during the "(b) cooperative phase" of Figure 4.1, the signal received at the BS via the relay-to-destination (RD) link can be formulated as:

$$y_{r_k d}^n = \sqrt{G_{r_k d}}\sqrt{P_{CU}} h_{r_k d} \hat{X}_{r_k}^n + n \,, \tag{4.3}$$

where the CU/RN forwards the source information frame using the power P_{CU}. Similar to the broadcast phase, the overall transmissions during the cooperative phase are within the time duration of T_2. In our proposed system, the CUs act as the RNs, where the RNs are located half way between the PUs and BS. Accordingly, the Reduced-Distance-Related-Pathloss-Reduction (RDRPR) [168, 169] experienced by the SR link is given by:

$$G_{sr} = \left(\frac{d_{sd}}{d_{sr}}\right)^{\alpha} , \tag{4.4}$$

where α is the path-loss exponent [167]. Similarly, the RDRPR of the RD link with respect to the SD link is given by:

$$G_{rd} = \left(\frac{d_{sd}}{d_{rd}}\right)^{\alpha} . \tag{4.5}$$

Naturally, the RDRPR of the SD link with respect to itself is unity, i.e. we have $G_{s_l d} = 1$. We consider an outdoor environment [167], where $\alpha = 3$. Note that the same RDRPR is exploited by all the SR and RD links in our system. Thus, we have $G_{s_l r_k} = G_{r_k d} = 2^3 = 8$. Moreover, we consider a single non-dispersive transmission path for the SD, SR and RD links of our novel ATTCM-ADNC-CCR scheme. Each of the channels in Eq. (4.1), Eq. (4.2) and Eq. (4.3) is comprised of two components, which may be expressed as:

$$h = h_s \cdot h_f \,, \tag{4.6}$$

where the slow fading (or quasi static fading) coefficient h_s is constant for all symbols within a transmit frame. By contrast, the fast-fading (small-scale Rayleigh fading) coefficient h_f varies on a

symbol by symbol basis, which will be described in Section 4.2.1. According to Eq. (4.1), Eq. (4.2) and Eq. (4.3), the average received SNR at node b per frame is given by:

$$\begin{aligned} \gamma_R &= \frac{G_{ab}E[|x|^2]E[|h_f^2|]E[|h_s^2|]}{N_0}, \\ &= \frac{G_{ab}|h_{ab}|^2}{N_0}, \end{aligned} \tag{4.7}$$

where we have $E[|x|^2] = 1$ and $E[|h_f^2|] = 1$ for uncorrelated Rayleigh fading channels, which varies on a symbol by symbol basis, as discussed in Section 4.2.1 and we have $E[|h_s^2|] = |h_s|^2 = h_{ab}^2$. Then we determine the received SNRs of the $[l(k+1)+k]$th communication links by referring to Figure 4.1, which are $[\gamma_{s_l d}, \gamma_{s_l r_k}, \gamma_{r_k d}]$.

4.2.1 Adaptive TTCM

As described in Section 2.3.4, employing ATTCM has the advantage that the system's effective throughput can be increased upon increasing the code rate and constellation size, when the channel-quality improves, without any bandwidth expansion. Furthermore, the BER and FER performance of the system may also be improved or maintained to be under a certain threshold [96]. In Figure 4.1, both the PUs and CUs have employed ATTCM encoders, where the TTCM encoder comprises a pair of identical parallel-concatenated TCM encoders [99] linked by a symbol interleaver. The first TCM encoder directly processes the original input bit sequence, while the second one encodes the interleaved or scrambled version of the input bit sequence. Then the bit-to-symbol mapper maps the input bits to complex-valued ATTCM symbols using the classic Set Partition based labelling method [96]. Additionally, the BS decodes the information delivered from the PUs and CUs by the ATTCM decoder. The structure of the TTCM decoder is similar to that of binary turbo codes, where each decoder alternately processes its corresponding encoder's channel-impaired output symbol, and then the other encoder's channel-impaired output symbol [96][pg.764]. As shown in Figure 4.1, we invoked a near-instantaneously adaptive TTCM scheme for protecting the SR and the RD links, where the effective throughput range is given by $R_{tran} = \{0, 1, 2, 3, 4, 5\}$ BPS when no transmission, QPSK, 8PSK, 16QAM, 32QAM and 64QAM are considered, respectively. The selection of the modulation mode for each link is dependent on its channel condition. Therefore, the adaptive modulator/demodulator shown in Figure 4.1 is influenced by the channel quality of the transmission link.

Moreover, the mode switching thresholds $\Upsilon = [\gamma_0, \gamma_1, \gamma_2, \gamma_3, \gamma_4]$ were determined based on the FER performance curves of each of the five TTCM schemes when communicating over a Rayleigh fading channel, which is shown in Figure 4.2. Specifically, both the ATTCM mode switching

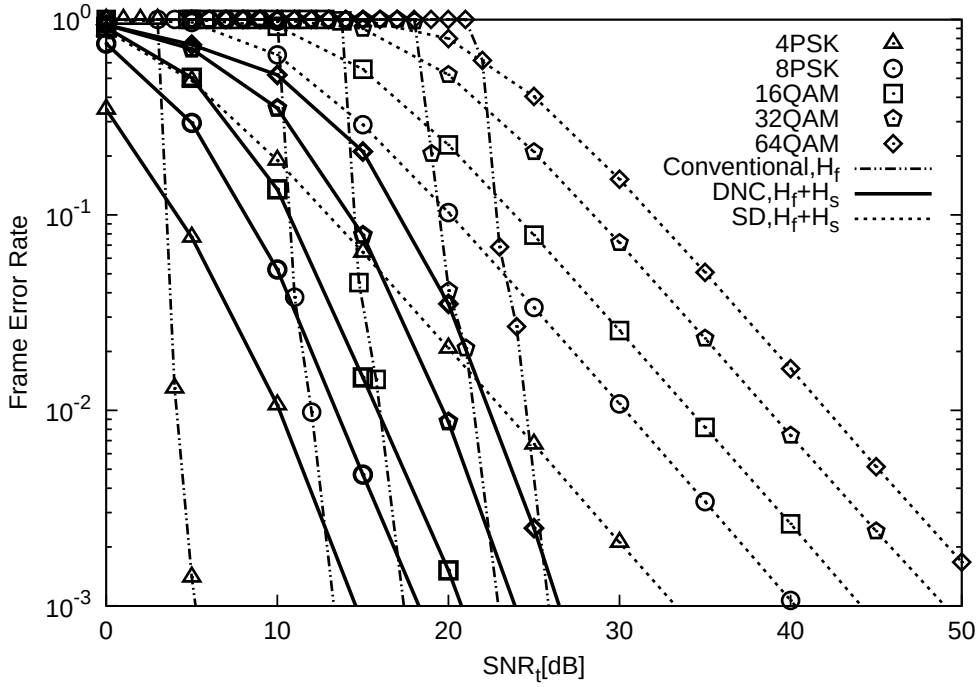

Figure 4.2: The FER performance versus SNR_t of TTCM for five fixed modulation modes. "Conventional" represents the FER performance of TTCM using a frame length of 12,000 symbols, when communicating over Rayleigh fading channels. Four TTCM iterations were invoked. "DNC" and "SD" denote the FER performance of TTCM-DNC and of the TTCM aided non-cooperative scheme for five fixed modulation modes using 10^6 frames, when communicating over the combined uncorrelated Rayleigh fading and quasi-static fading channels. The parameters are refer to Table 2.1.

operation and the transmission rate of the modes are based on the following algorithm:

$$\text{MODE} = \begin{cases} \gamma_4 \leq \gamma_R, & \text{TTCM-64QAM, } C^*\text{=5 BPS;} \\ \gamma_3 \leq \gamma_R < \gamma_4, & \text{TTCM-32QAM, } C^*\text{=4 BPS;} \\ \gamma_2 \leq \gamma_R < \gamma_3, & \text{TTCM-16QAM, } C^*\text{=3 BPS;} \\ \gamma_1 \leq \gamma_R < \gamma_2, & \text{TTCM-8PSK, } C^*\text{=2 BPS;} \\ \gamma_0 \leq \gamma_R < \gamma_1, & \text{TTCM-4PSK, } C^*\text{=1 BPS;} \end{cases} \tag{4.8}$$

where C^* is the effective throughput in terms of the number of . Furthermore, we have considered two cases, when we have $\gamma_R < \gamma_0$ for the ATTCM mode switching operation. In the first case (case 1), no transmission is invoked in order to save energy when $\gamma_R < \gamma_0$. By contrast, the second case (case 2) invokes the 4PSK modulation mode when $\gamma_R < \gamma_0$. Thus the output C^* of these two cases may be expressed as:

$$C^*\left(\gamma_R < \gamma_0\right) = \begin{cases} 0, & \text{case 1: No transmission;} \\ 1, & \text{case 2: TTCM-4PSK;} \end{cases} \tag{4.9}$$

As seen from Figure 4.2, we chose the switching thresholds carefully to ensure that the FER at the RN is lower than 10^{-3}, in order to minimize the potential error propagation from the CUs to the BS, then the thresholds are given in Table 4.2.

Channel	Uncorrelated Rayleigh	
Thresholds	Y[dB] at FER= 10^{-3}	
Coding/ Modulation	ATTCM	iBPS
4PSK	5.22	1 BPS
8PSK	12.25	2 BPS
16QAM	16.10	3 BPS
32QAM	21.15	4 BPS
64QAM	24.49	5 BPS

Table 4.2: The SNR thresholds of TTCM scheme when communicating over uncorrelated Rayleigh fading channels. The values are tabulated based on Figure 4.2.

4.2.2 Fixed Mode Network Coding Scheme

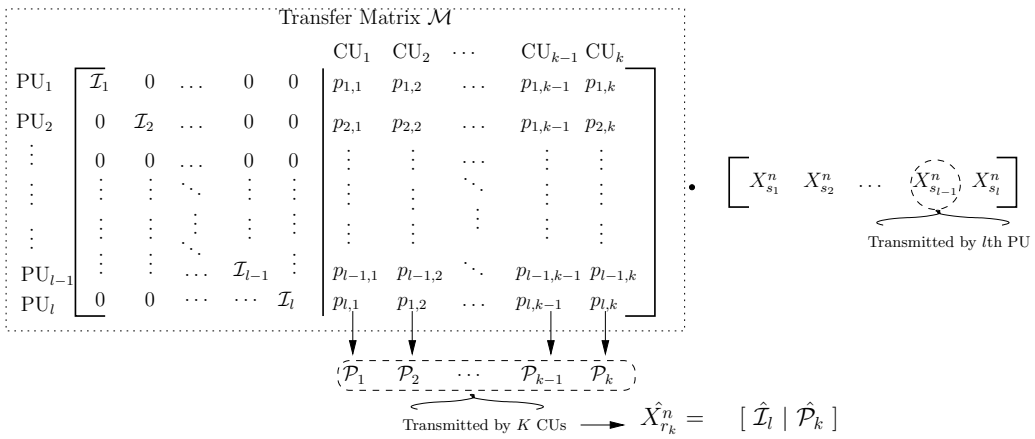

Figure 4.3: Illustration of the transfer matrix and the network encoding process engaged in the DNC-CCR scheme.

This section is devoted to detailing the encoding/decoding process of the network coding technique. Figure 4.1 shows how the CUs would successfully deliver the decoded information frames by employing the network encoding technique at the BS. The output codewords of the CUs are denoted as: $\{\overleftrightarrow{\hat{X}^n_{r_k}}\}_{k=1}^{K}$, while those of the kth CU during the nth frame may be expressed as:

$$\hat{X}^n_{r_k} = \mathcal{M} \cdot X^n_{s_l} = [\hat{\mathcal{I}}_l \mid \hat{\mathcal{P}}_k] \,, \tag{4.10}$$

where $X^n_{s_l}$ is the information frame transmitted from the lth PU within the nth frame to both the CUs and to the BS. Additionally, the transfer matrix $\mathcal{M}$ defined in [198] describes the corresponding

network codes invoked for our DNC-CCR scheme. As seen in Figure 4.3, the transfer matrix $\mathcal{M}$ is comprised of two components, since we have $\mathcal{M} = [\mathcal{I}_l|\mathcal{P}_k]$, where the identity matrix $\{\mathcal{I}\}_l$ ($l \in L$), represents the sequences transmitted from the PUs during the broadcast phase, while the parity matrix $\{\mathcal{P}\}_{l\times k}$ ($k \in K$) represents to the CUs' transmissions during the cooperative phase. Therefore, the corresponding entry $\mathcal{I}_l$ in Figure 4.3 represents the successful/unsuccessful reception of the information frame recovered at the BS during the broadcast phase, which obeys the following rule:

$$\mathcal{I}_l = \begin{cases} 0, & \text{If } X_{s_1}^n \text{ is not recovered successfully;} \\ 1, & \text{If } X_{s_1}^n \text{ is recovered successful;} \end{cases} \tag{4.11}$$

We note that the coefficient $p_{l,k}$ shown in Figure 4.3 is gleaned from the transfer matrix of a linear block code defined over the Galois field $GF(|q|)$, where $|q|$ is the alphabet size ($q = 2^b$), and b is an integer higher than zero [182,184]. The transfer matrix constructed over the $GF(|q|)$ is provided by the software application SAGE [199]. As shown in Figure 4.3, the variable $p_{l,k}$ represents the specific transmission state, during which the information frame is transmitted from PU_l to CU_k as detailed below:

$$p_{l,k} = \begin{cases} 0, & \text{unsuccessful;} \\ 1, & \text{successful;} \end{cases} \tag{4.12}$$

The network encoding process is represented by Eq (4.10), where we construct the parity frames $\hat{\mathcal{P}}_k = [P_1, P_2, \ldots, P_{k-1}, P_k]$ from the K CUs. Additionally, the parity frame transmitted by the kth CU is given by:

$$\mathcal{P}_k \;=\; \mathcal{I}_1 p_{1,k} \oplus \mathcal{I}_2 p_{2,k} \oplus \cdots \oplus \mathcal{I}_l p_{l,k}\,. \tag{4.13}$$

As an illustration, we present a specific example associated with $L = 2$ PUs and $K = 2$ CUs, where we have orthogonal channels among the pairs of PUs and CUs, as shown in Figure 4.4. We

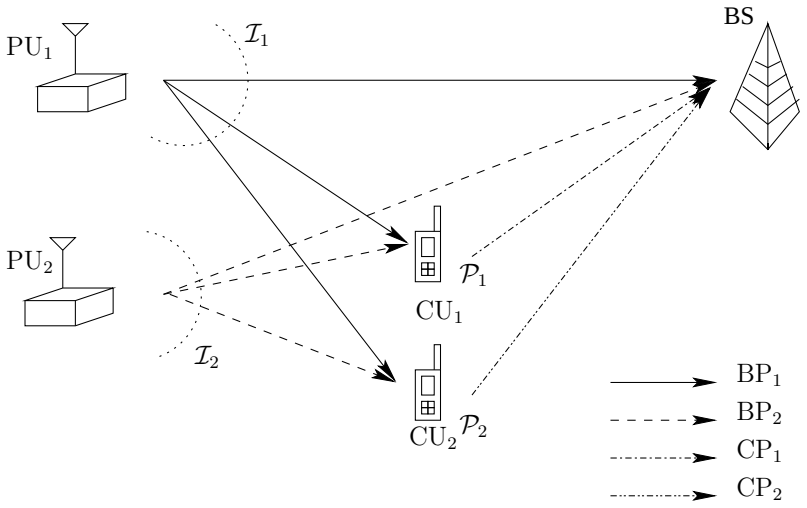

Figure 4.4: The schematic of DNC-CCR scheme based $M_{2\times 4}$ matrix. Two PUs intended to transmit their source messages $\mathcal{I}_1$ and $\mathcal{I}_2$, respectively.

assumed that each PU broadcasts $m_1 = 1$ information frame and then each CU transmits $m_2 = 1$

parity frame composed of the non-binary linear combinations of its information frames defined over $GF(|q|)$ to the BS. Then there are $(m_1 \times L + m_2 \times K) = 4$ phases during a transmission session, including the pair of broadcast phases BP_1 and BP_2 as well as the pair of cooperative phases CP_1 and CP_2. The coding arrangement of this specific example can be summarized as follows:

$$(BP_1) : PU_1 \xrightarrow[(=0/1)]{\mathcal{I}_1} CU_1,\ PU_1 \xrightarrow[(=0/1)]{\mathcal{I}_1} CU_2,\ PU_1 \xrightarrow[(=0/1)]{\mathcal{I}_1} BS\,; \tag{4.14}$$

$$(BP_2) : PU_2 \xrightarrow[(=0/1)]{\mathcal{I}_2} CU_1,\ PU_2 \xrightarrow[(=0/1)]{\mathcal{I}_2} CU_2,\ PU_2 \xrightarrow[(=0/1)]{\mathcal{I}_2} BS\,; \tag{4.15}$$

$$(CP_1) : CU_1 \xrightarrow[(=0/1)]{\overbrace{\mathcal{M}_{2\times4}(1,3)\cdot\mathcal{I}_1}^{\mathrm{PU_1 \to CU_1}} \oplus \overbrace{\mathcal{M}_{2\times4}(2,3)\cdot\mathcal{I}_2}^{\mathrm{PU_2 \to CU_1}}} BS\,; \tag{4.16}$$

$$(CP_2) : CU_2 \xrightarrow[(=0/1)]{\overbrace{\mathcal{M}_{2\times4}(1,4)\cdot\mathcal{I}_1}^{\mathrm{PU_1 \to CU_2}} \oplus \overbrace{\mathcal{M}_{2\times4}(2,4)\cdot\mathcal{I}_2}^{\mathrm{PU_2 \to CU_2}}} BS\,. \tag{4.17}$$

Note that the arrow '$\rightarrow$' represents the transmission direction. The notation $0/1$ below the right arrow of Eq. (4.17) indicates whether the transmission was successful or not, where $\mathcal{I}_l$ is defined in Eq. (4.11), which $p_{l,k}$ in Eq. (4.12). The notation '$\oplus$' represents the non-binary linear combination of the information frames. The corresponding transfer matrix $M_{2\times4}$ of [181, 198] constructed for our specific system of Figure 4.4 is defined as:

$$\mathcal{M}_{2\times4} = \left[\begin{array}{cc|cc} 1 & 0 & 1 & 1 \\ 0 & 1 & 1 & 2 \end{array}\right]. \tag{4.18}$$

Observe by referring to Eq. (4.13) that the parity frame is transmitted from CU_1 to the BS during CP_1 may be expressed as:

$$\mathcal{P}_1 = \mathcal{M}_{2\times4}(1,3)\mathcal{I}_1 \oplus \mathcal{M}_{2\times4}(2,3)\mathcal{I}_2 = \mathcal{I}_1 \oplus \mathcal{I}_2\,. \tag{4.19}$$

Then the parity frame $\mathcal{P}_2$ of from CU_2 during CP_2 becomes:

$$\mathcal{P}_2 = \mathcal{M}_{2\times4}(1,4)\mathcal{I}_1 \oplus \mathcal{M}_{2\times4}(2,4)\mathcal{I}_2 = \mathcal{I}_1 \oplus 2\mathcal{I}_2\,, \tag{4.20}$$

where $\mathcal{M}_{2\times4}(i,j)$ represents row i and column j of the corresponding transfer matrix $\mathcal{M}$, with $i \in [1,2]$ and $j \in [1,2,3,4]$.

We also define the modified transfer matrix $\mathcal{M}'_{2\times4}$ with respect to the original transfer matrix $\mathcal{M}_{2\times4}$, which takes into account the success/failure of each transmission during a specific transmission session. If all the transmitted frames are successfully decoded, the modified transfer matrix is defined as $\mathcal{M}'_{2\times4}(i,j) = \mathcal{M}_{2\times4}(i,j)$.

In order to highlight our generic design principles, the $\mathcal{M}_{4\times8}$-based system is considered here for a more detailed description. This schematic of the DNC-CCR scheme based on the $\mathcal{M}_{4\times8}$ matrix is shown in Figure 4.5, where there are four BPs and four CPs. Additionally, the coding

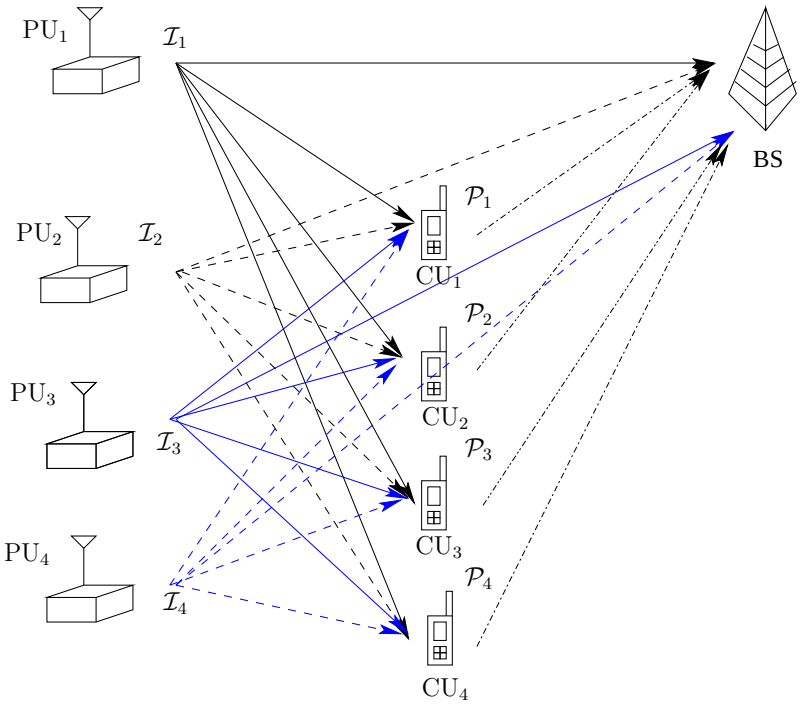

Figure 4.5: The schematic of DNC-CCR scheme based on a $\mathcal{M}_{4\times 8}$ matrix. Four PUs intend to transmit their source messages $\mathcal{I}_1$, $\mathcal{I}_2$, $\mathcal{I}_3$ and $\mathcal{I}_4$, respectively.

arrangement of our proposed system based on the $\mathcal{M}_{4\times 8}$ matrix can be summarized as follows:

$$(BP_1): PU_1 \xrightarrow[(=0/1)]{\mathcal{I}_1} CU_1/CU_2/CU_3/CU_4,\ PU_1 \xrightarrow[(=0/1)]{\mathcal{I}_1} BS\ ; \quad (4.21)$$

$$(BP_2): PU_2 \xrightarrow[(=0/1)]{\mathcal{I}_2} CU_1/CU_2/CU_3/CU_4,\ PU_2 \xrightarrow[(=0/1)]{\mathcal{I}_2} BS\ ; \quad (4.22)$$

$$(BP_3): PU_3 \xrightarrow[(=0/1)]{\mathcal{I}_3} CU_1/CU_2/CU_3/CU_4,\ PU_3 \xrightarrow[(=0/1)]{\mathcal{I}_3} BS\ ; \quad (4.23)$$

$$(BP_4): PU_4 \xrightarrow[(=0/1)]{\mathcal{I}_4} CU_1/CU_2/CU_3/CU_4,\ PU_4 \xrightarrow[(=0/1)]{\mathcal{I}_4} BS\ ; \quad (4.24)$$

$$(CP_1): CU_1 \xrightarrow[(=0/1)]{\overbrace{\mathcal{M}_{4\times 8}(1,5)\cdot\mathcal{I}_1}^{PU_1\to CU_1}\oplus\overbrace{\mathcal{M}_{2\times 4}(2,5)\cdot\mathcal{I}_2}^{PU_2\to CU_1}\oplus\overbrace{\mathcal{M}_{2\times 4}(3,5)\cdot\mathcal{I}_3}^{PU_3\to CU_1}\oplus\overbrace{\mathcal{M}_{2\times 4}(4,5)\cdot\mathcal{I}_4}^{PU_4\to CU_1}} BS\ ; \quad (4.25)$$

$$(CP_2): CU_2 \xrightarrow[(=0/1)]{\overbrace{\mathcal{M}_{4\times 8}(1,6)\cdot\mathcal{I}_1}^{PU_1\to CU_2}\oplus\overbrace{\mathcal{M}_{2\times 4}(2,6)\cdot\mathcal{I}_2}^{PU_2\to CU_2}\oplus\overbrace{\mathcal{M}_{2\times 4}(3,6)\cdot\mathcal{I}_3}^{PU_3\to CU_2}\oplus\overbrace{\mathcal{M}_{2\times 4}(4,6)\cdot\mathcal{I}_4}^{PU_4\to CU_2}} BS\ ; \quad (4.26)$$

$$(CP_3): CU_1 \xrightarrow[(=0/1)]{\overbrace{\mathcal{M}_{4\times 8}(1,7)\cdot\mathcal{I}_1}^{PU_1\to CU_3}\oplus\overbrace{\mathcal{M}_{2\times 4}(2,7)\cdot\mathcal{I}_2}^{PU_2\to CU_3}\oplus\overbrace{\mathcal{M}_{2\times 4}(3,7)\cdot\mathcal{I}_3}^{PU_3\to CU_3}\oplus\overbrace{\mathcal{M}_{2\times 4}(4,7)\cdot\mathcal{I}_4}^{PU_4\to CU_3}} BS\ ; \quad (4.27)$$

$$(CP_4): CU_2 \xrightarrow[(=0/1)]{\overbrace{\mathcal{M}_{4\times 8}(1,8)\cdot\mathcal{I}_1}^{PU_1\to CU_4}\oplus\overbrace{\mathcal{M}_{2\times 4}(2,8)\cdot\mathcal{I}_2}^{PU_2\to CU_4}\oplus\overbrace{\mathcal{M}_{2\times 4}(3,8)\cdot\mathcal{I}_3}^{PU_3\to CU_4}\oplus\overbrace{\mathcal{M}_{2\times 4}(4,8)\cdot\mathcal{I}_4}^{PU_4\to CU_4}} BS\ , \quad (4.28)$$

where $\mathcal{M}_{4\times 8}(i,j)$ represents the ith row and jth column of the corresponding transfer matrix $\mathcal{M}$, with $i \in [1,2,3,4]$ and $j \in [1,2,3,4,5,6,7,8]$. The corresponding transfer matrix $\mathcal{M}_{4\times 8}$ is

provided by [182, 183]:

$$\mathcal{M}_{4\times 8} = \left[\begin{array}{cccc|cccc} 1 & 0 & 0 & 0 & 3 & 7 & 3 & 6 \\ 0 & 1 & 0 & 0 & 5 & 7 & 7 & 4 \\ 0 & 0 & 1 & 0 & 2 & 4 & 6 & 1 \\ 0 & 0 & 0 & 1 & 5 & 5 & 3 & 2 \end{array}\right] . \tag{4.29}$$

Referring to Eq. (4.13) the parity frame transmitted from CU_1 to the BS during CP_1 may be expressed as:

$$\begin{aligned} \mathcal{P}_1 &= \mathcal{M}_{4\times 8}(1,5)\mathcal{I}_1 \oplus \mathcal{M}_{4\times 8}(2,5)\mathcal{I}_2 \oplus \mathcal{M}_{4\times 8}(3,5)\mathcal{I}_3 \oplus \mathcal{M}_{4\times 8}(4,5)\mathcal{I}_4 , \\ &= 3\mathcal{I}_1 \oplus 5\mathcal{I}_2 \oplus 2\mathcal{I}_3 \oplus 5\mathcal{I}_4 . \end{aligned} \tag{4.30}$$

Then the parity frame $\mathcal{P}_2$ transmitted from CU_2 during CP_2 becomes:

$$\begin{aligned} \mathcal{P}_2 &= \mathcal{M}_{4\times 8}(1,6)\mathcal{I}_1 \oplus \mathcal{M}_{4\times 8}(2,6)\mathcal{I}_2 \oplus \mathcal{M}_{4\times 8}(3,6)\mathcal{I}_3 \oplus \mathcal{M}_{4\times 8}(4,6)\mathcal{I}_4 , \\ &= 7\mathcal{I}_1 \oplus 7\mathcal{I}_2 \oplus 4\mathcal{I}_3 \oplus 5\mathcal{I}_4 , \end{aligned} \tag{4.31}$$

while the parity frame $\mathcal{P}_3$ transmitted during CP_3 may be expressed as:

$$\begin{aligned} \mathcal{P}_3 &= \mathcal{M}_{4\times 8}(1,7)\mathcal{I}_1 \oplus \mathcal{M}_{4\times 8}(2,7)\mathcal{I}_2 \oplus \mathcal{M}_{4\times 8}(3,7)\mathcal{I}_3 \oplus \mathcal{M}_{4\times 8}(4,7)\mathcal{I}_4 , \\ &= 3\mathcal{I}_1 \oplus 7\mathcal{I}_2 \oplus 6\mathcal{I}_3 \oplus 3\mathcal{I}_4 . \end{aligned} \tag{4.32}$$

The last parity frame $\mathcal{P}_4$ transmitted from CU_4 becomes:

$$\begin{aligned} \mathcal{P}_4 &= \mathcal{M}_{4\times 8}(1,8)\mathcal{I}_1 \oplus \mathcal{M}_{4\times 8}(2,8)\mathcal{I}_2 \oplus \mathcal{M}_{4\times 8}(3,8)\mathcal{I}_3 \oplus \mathcal{M}_{4\times 8}(4,8)\mathcal{I}_4 , \\ &= 6\mathcal{I}_1 \oplus 4\mathcal{I}_2 \oplus \mathcal{I}_3 \oplus 2\mathcal{I}_4 . \end{aligned} \tag{4.33}$$

Moreover, the modified transfer matrix $\mathcal{M}'$ of the actual communication is given by $\mathcal{M}'_{4\times 8}(i,j) = \mathcal{M}_{4\times 8}(i,j)$, provided that all transmitted frames are successfully decoded by the BS. In order to detect the information frames of the PUs, the BS has to be aware of how each parity frame was constructed at the CUs. Hence the modified transfer matrix $\mathcal{M}'_{i\times j}$ is assumed to be known at the BS. As shown in Figure 4.1, $(K \times m_2)$ parity frames are transmitted by the K CUs, which contain the non-binary linear combinations of its own information frames along with the successfully decoded information frames received from the L PUs. Let us denote the actual output codeword of the CUs as $\hat{X}'_{r_k{}^n}$ corresponding to the modified matrix $\mathcal{M}'_{i\times j}$. Hence $\hat{X}'_{r_k{}^n}$ contains all zeros, when the BS failed to successfully recover the $(L \times m_1)$ information frames or failed to receive the $(K \times m_2)$ parity frames, otherwise we have $\hat{X}'_{r_k{}^n} = \hat{X}_{r_k{}^n}$.

4.2.3 Adaptive Mode of Network Coding

In our scheme, we assume that the network-coding decoder at the BS is capable of sending back a feedback flag to the network encoders at the CU/RNs, as shown in Figure 4.1. The transmission of the parity frames from the CUs is controlled by this feedback flag. Additionally, we conceive and analyze an efficient ADNC scheme using two methods, namely M1 and M2 associated with different amount of feedback requirements.

4.2.3.1 ADNC-M1

By referring to [182], the ADNC-M1 adaptively adjusts the number of frames transmitted from the CUs for each transmission session. The BS feeds back a single bit, S_f, following the reception of a set of $(L \times m_1)$ information frames from the L PUs. If the CU/RNs received $S_f = 0$, this implies that the BS has failed to correctly decode the information frames received from all the PU/SNs and hence the CU/RNs have to transmit $(K \times m_2)$ parity frames to the BS. Otherwise, if the BS successfully decoded the PU's information, the value of the feedback flag is set to $S_f = 1$. Let us denote the number of CUs invoked in an actual transmission by employing the ADNC technique during the cooperative phase as $K^{'}$. The actual number of information frames, $K^{'}m_2$, transmitted from the K CUs by the ADNC-M1 technique obeys the following rules:

$$K^{'}m_2 = \begin{cases} 0, & S_f\text{=1;} \\ Km_2, & S_f\text{=0;} \end{cases}$$

where m_2 denotes the number of information frame transmitted per CU.

4.2.3.2 ADNC-M2

In contrast to ADNC-M1, in the scheme we assume that the BS feeds back L bits associated with the L PUs, namely S_{f_l}, to the CUs. Additionally, if the CUs received $\sum_{l=1}^{L}(S_{f_l}) = 0$, this implies that the BS has failed to correctly decode all the information packets received from the PUs and hence the CUs have to transmit the same number of parity frames to the BS. Otherwise, the CUs do not have to transmit, provided that we have $\sum_{l=1}^{L}(S_{f_l}) = 1$, which indicates that the BS has indeed succeeded in flawlessly decoding all PUs' frames. Moreover, if most of the PUs' information frames are successfully received by the BS, except for the failed detection of ϑ PUs, then the CU may only have to transmit ϑm_2 number of parity frames to the BS. Hence the number of parity frames required can be calculated by counting the specific number of the feedback flags indicating successful reception by the BS. More specifically, if the BS successfully received some of the information frames from the PUs, it will send a feedback flag to CUs, which will hence retransmit the failed information frames to the BS. Hence the adaptive configuration of the actual number of $K^{'}$ CUs' information frames obeys the following rules:

$$K^{'}m_2 = \begin{cases} 0, & \sum_{l}^{L}(S_{f_l})\text{=1;} \\ Km_2, & \sum_{l}^{L}(S_{f_1})\text{=0;} \\ \vartheta m_2, & \text{Otherwise;} \end{cases}$$

where ϑ denotes the number of CUs that have to relay the PU's information to the BS, $\vartheta \in L$. For example, the value of ϑ in our $\mathcal{M}_{2\times4}$-based scheme is 1, which implies that the BS failed to successfully decode a single PU's transmission. Additionally, in an $\mathcal{M}_{N_r\times N_c}$-based scheme, the value of ϑ is given by $(K - i)$. The CUs would relay the required ϑ parity frames to the BS during

the cooperative phase. In our system, the BS feeds back a small amount of information to the CUs, which may imposes an overhead. As a benefit, the CUs assist the PUs for the sake of avoiding the re-transmission of the PUs' information. The system's achievable performance will be discussed in Section 4.4.

4.3 System Design

In this section, the design guidelines of our proposed system will be discussed first. Then the transmission rates of both ADNC-M1 and ADNC-M2 are analysed. Based on our investigations of both the network coding rate and the diversity order of our ADNC-M1 and ADNC-M2 schemes, we decide upon our final recommended prototype system.

4.3.1 Adaptive TTCM transmission scenario

All transmission links shown in Figure 4.1 have employed the ATTCM scheme detailed in Eq. (4.8) and Eq. (4.9), where each link may employ different modulation modes during the entire transmission period. Under the DNC policy of Section 4.2.2, the PUs (or SNs) transmit at the same rate. We consider the "worst" PU, whose link towards both the CUs and the BS has the lowest SNR, which forces some of the PUs which actually experience a high SNR to transmit at a rate lower than their own affordable rate. This allows the CU to perform bit-by-bit combination of the decoded information. Thus, the lowest-rate, but most resilient modulation modes are activated for all the L SD and L SR links, which also affects the $(L \times K)$ SR links. The rate achievable at the SNs of our proposed scheme during the broadcast phases can be written as:

$$R_{Tx}^{PU_l} = \min\{C_{s_l d}^*, C_{s_l r_k}^*\}, \ l \in L, k \in K. \tag{4.34}$$

As for the K RD links, each link obeys the adaptive modulation mode selection rule of Eq. (4.8) and Eq. (4.9). Additionally, the achievable rate of the CU/RN to BS link during the cooperative phases is given by:

$$R_{Tx}^{CU_k} = \max\{C_{r_k d}^*\}, \ k \in K, \tag{4.35}$$

where the values of $C_{s_l d}^*$, $C_{s_l r_k}^*$ and $C_{r_k d}^*$ can be obtained from Eq. (4.8), depending on the instantaneous channel conditions. Our proposed scenario achieves a FER lower than the 10^{-3} target at the RN, in order to minimize the potential error propagation from the CUs to the BS. The strategy defined in Eq. (4.34) during the broadcast phase and Eq. (4.35) are not the only scenario we have investigated. We have also tested three other scenarios, which are listed in Table 4.3. More specifically, the corresponding FER and average throughput performances are shown in Figure 4.6.

By observing Figure 4.6, the Max-Max and Max-Min scenarios suffer from a higher FER than our 10^{-3} target, which leads to an excessive probability of errors at the CUs, although they may

Scenarios	Broadcast Phase: $R_{Tx}^{PU_l}$	Cooperative Phase: $R_{Tx}^{CU_k}$
Scenario 1: Min-Max	$\min\{C^*_{s_l d}, C^*_{s_l r_k}\}$	$\max\{C^*_{r_k d}\}$
Scenario 2: Min-Min	$\min\{C^*_{s_l d}, C^*_{s_l r_k}\}$	$\min\{C^*_{r_k d}\}$
Scenario 3: Max-Max	$\max\{C^*_{s_l d}, C^*_{s_l r_k}\}$	$\max\{C^*_{r_k d}\}$
Scenario 4: Max-Min	$\max\{C^*_{s_l d}, C^*_{s_l r_k}\}$	$\min\{C^*_{r_k d}\}$

Table 4.3: Compare four different scenarios

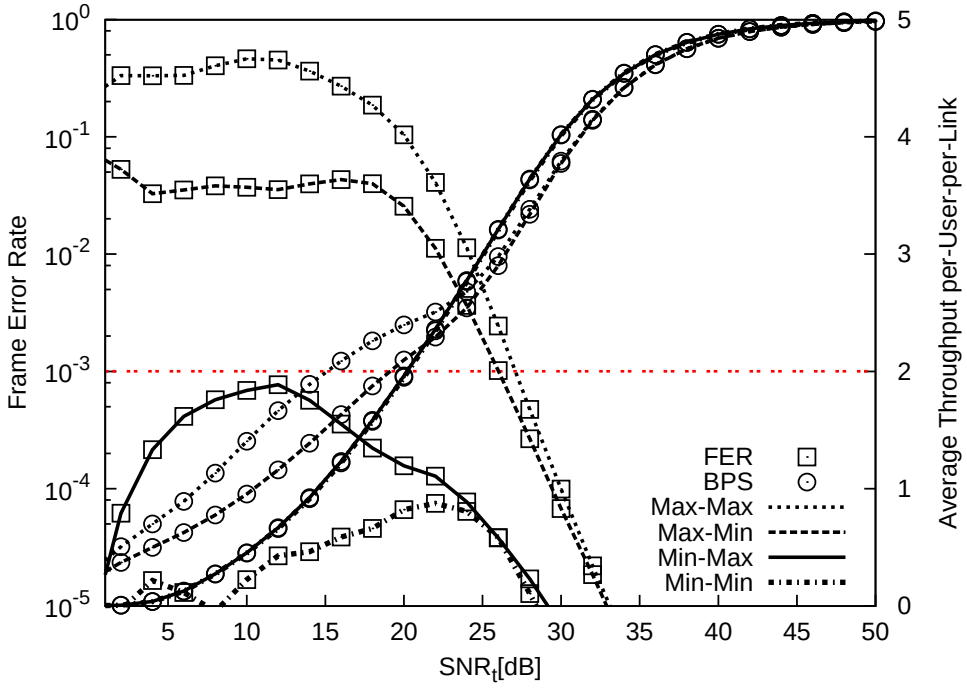

Figure 4.6: The FER and average throughput per user per link versus SNR_t of the proposed ATTCM-aided ADNC scheme based on the $\mathcal{M}_{4\times 8}$ matrix ADNC-M1 of Section 4.2.3.1. The corresponding switching thresholds are refer to Table 4.2.

achieve a higher throughput at $SNR_t < 23$ dB. By contrast, the Min-Max and Min-Min scenarios satisfy our FER target, which could minimize the potential error propagation from the CUs to the BS. However, the average throughput of the Min-Min scenario is the worst among these four scenarios. Moreover, the average throughput of Min-Max regime became better for $SNR_t \geq 23$ dB, it even approaches that of the Max-Max scenario. Hence, we utilised the Min-Max scenario, because it gives a better trade-off in terms of the FER and average throughput. The Min-Max scenario is employed for the rest of our investigations in this chapter.

4.3.2 Analysis of Transmission Rate

In this section, we investigate the attainable transmission rate of our proposed schemes. We assume that we have N-frame sessions and the length of each TS in the frame is T. As discussed in

Section 4.2, this TS is split into two parts, yielding $T = T_1 + T_2$, where T_1 is used for the PU's transmission during the broadcast phase and T_2 is allocated for the CUs to relay the combined information of both the PU and CU during the cooperative phase. If the PU activates a higher-throughput modulation mode, then the SNR required by the PU will be high. As a benefit, this will shorten the PU's transmission duration of T_1. Consequently, this would grant a longer transmission period for the CUs. Thus, we increase T_2, when T_1 is reduced. Moreover, we assumed that the PU and CU have the same Baud rate (symbol rate) of $R_s^{PU} = R_s^{CU}$ symbol/s during the entire transmission period. Meanwhile, the number of bits transmitted by the PU and CU in a aingle transmission session are the same, namely $N_b^{PU} = N_b^{CU}$ bits. Then the number of bits transmitted during the broadcast phase is given by:

$$N_b^{PU} = L\, R_s^{PU}\, R_{Tx}^{PU_l}\, T_1\,, \tag{4.36}$$

while those during the cooperative phase is:

$$N_b^{CU} = K'\, R_s^{CU}\, R_{Tx}^{CU_k}\, T_2\,, \tag{4.37}$$

where K' was defined in Section 4.2.3.2.

4.3.2.1 Fixed-mode DNC scheme

In our proposed DNC-CCR scheme of Section 4.2.2, the TSs are shared by the PU and CU. We assumed that the amount of information to be transmitted by the PU and CU is identical, thus we have:

$$L\, R_s^{PU}\, R_{Tx}^{PU_l}\, T_1 = K'\, R_s^{CU}\, R_{Tx}^{CU_k}\, T_2\,. \tag{4.38}$$

Then, based on Eq. (4.38), the relationship between T_1 and T_2 is given by:

$$\frac{T_2}{T_1} \;=\; \frac{L\, R_s^{PU}\, R_{Tx}^{PU_l}}{K'\, R_s^{CU}\, R_{Tx}^{CU_k}}\,. \tag{4.39}$$

Since $T_2 = T - T_1$, based on Eq. (4.39), we have

$$T_1 \;=\; \frac{K'\, R_{Tx}^{CU_k}}{L\, R_{Tx}^{PU_l} + K'\, R_{Tx}^{CU_k}}\, T\,. \tag{4.40}$$

The average throughput of the entire system may be quantified by the ratio of the total number of transmitted information bits divided by the number of transmission TSs. This metric is similar to the concept of the overall rate defined in [185][Eq. (18)]. We also assume that our proposed system transmits its messages at the same rate during each N-frame session. Then the overall throughput per frame per user in our proposed DNC-CCR scheme is given by:

$$\eta_{DNC} \;=\; \frac{1}{N}\sum_{n=1}^{N}\frac{\sum_{l=1}^{L} R_{Tx}^{PU_l} T_1}{L\times T}\,, \tag{4.41}$$

$$\;=\; \frac{1}{N}\sum_{n=1}^{N}\frac{\sum_{l=1}^{L}\frac{K'\, R_{Tx}^{PU_l}\, R_{Tx}^{CU_k}}{L\, R_{Tx}^{PU_l}+K'\, R_{Tx}^{CU_k}}}{L}\,, \tag{4.42}$$

where again, N denotes the number of frames and L is the total number of PUs. In our $\mathcal{M}_{2\times4}$-based system, the number of frames transmitted from the PU is $L = 2$, while, the number of information frames transmitted is $L = 4$ for the $\mathcal{M}_{4\times8}$-based system.

4.3.2.2 Adaptive Mode DNC scheme

Let us now consider the achievable transmission rate of our proposed ADNC-CCR scheme. In contrast to the fixed-mode DNC of Section 4.3.2.1, in the ADNC scheme, if all the PUs transmit all their messages to the BS successfully, the CUs do not have to relay the source information to the BSs. By contrast, the CUs will relay the source information to the BS, if any of the transmissions from the PU to the BS failed. Thus we can obtain the time allocations between PUs and CUs as follows:

$$T_1 \begin{cases} = T,\ T_2 = 0; \text{ If the PU's transmission is successful.} \\ = \frac{K^{'}\ R_{Tx}^{CU_k}}{L\ R_{Tx}^{PU_l} + K^{'}\ R_{Tx}^{CU_k}}\ T,\ T_2 = T - T_1; \text{ Otherwise;} \end{cases}$$

where $K^{'}$ is different in the ADNC-M1 scheme of Section 4.2.3.1 and in the ADNC-M2 scheme of Section 4.2.3.2. Moreover, if the PU transmitted successfully to the BS, we can save the entire T_2 duration for the CU's communication. However, if the PU failed to successfully transmit its message to the BS, then the CU would relay the PU's message to the BS. If the transmit SNR of the PU is higher, the relaying period of the CU will be reduced and this allows the system to grant a longer transmit-duration for the CUs. By contrast, at a low SNR the opposite trend prevails. When the PU's transmission is successful, the average throughput of L PUs relying on our ADNC-CCR scheme is given by:

$$\begin{aligned} \eta_{ADNC} &= \frac{1}{N}\sum_{n=1}^{N}\frac{\sum_{l=1}^{L} R_{Tx}^{PU_l} T}{LT}, \\ &= \frac{1}{N}\sum_{n=1}^{N}\frac{\sum_{l=1}^{L} R_{Tx}^{PU_l}}{L}. \end{aligned} \tag{4.43}$$

If the PU's transmission failed, then the CU/RN will transmit the PU's information to the BS. The overall throughput takes into consideration both the PU's information and the CU's own information, where we have $\eta_{ADNC} = \eta_{DNC}$, when the PU's transmission failed, where η_{DNC} is detailed in Eq. (4.42). Hence, the overall throughput per frame per user of the proposed ADNC scheme is given by:

$$\eta_{ADNC} = \begin{cases} \frac{1}{N}\sum_{n=1}^{N}\frac{\sum_{l=1}^{L} R_{Tx}^{PU_l}}{L} & \text{PU's transmission was successful;} \\ \frac{1}{N}\sum_{n=1}^{N}\frac{\sum_{l=1}^{L} R_{Tx}^{PU_l} T_1}{L\times T} & \text{PU's transmission failed;} \end{cases}$$

where T_1 is defined in Eq. (4.40).

4.3.2.3 Direct Transmission

The overall transmission rate per frame per user of the non-cooperative scheme recorded for the whole TS duration T becomes:

$$\eta_{SD} = \frac{1}{N}\sum_{n=1}^{N}\frac{\sum_{l=1}^{L} R_{Tx}^{PU_l}}{L} . \tag{4.44}$$

Finally, we will compare the overall performance of these two systems in Section 4.4.

4.3.3 Diversity Order and Network Code Rate

The network coding rate R_{NC} characterising the multiplexing capability of the network coding scheme exemplified in Section 4.2.2 may be expressed as:

$$R_{NC} = \frac{\text{Total number transmitted information frames of PUs}}{\text{Total number of information frames of PUs and CUs}} . \tag{4.45}$$

By further considering the ADNC scheme detailed in Section 4.2.3, the network code rate of ADNC-M1 is given by:

$$R_{NC}^{ADNC-M1} = \begin{cases} \frac{Lm_1}{Lm_1}, & S_f\text{=1;} \\ \frac{Lm_1}{Lm_1+Km_2}, & S_f\text{=0;} \end{cases} \tag{4.46}$$

Moreover, the network coding rate of the ADNC-M2 scheme may be expressed as:

$$R_{NC}^{ADNC-M2} = \begin{cases} \frac{Lm_1}{Lm_1}, & \sum_l^L (S_{f_l})\text{=1;} \\ \frac{Lm_1}{Lm_1+Km_2}, & \sum_l^L (S_{f_l})\text{=0;} \\ \frac{Lm_1}{Lm_1+\vartheta m_2}, & \text{Otherwise;} \end{cases} \tag{4.47}$$

where the number of CUs is assumed to be the same as the number of PUs in our design. As shown in Eq. (4.46) and Eq. (4.47), the resultant network coding rate is: $R_{NC}^{ADNC} = \frac{Lm_1}{Lm_1} = 1$, while the value of Km_2 can be adaptively adjusted toward 0 in order to increase the achievable multiplexing gain.

Referring to Figure 4.1, the network encoders of the CUs generate the parity frames based on the information frames. The network decoders at the BS will decode the parity frames based on the modified matrix introduced in Section 4.2.2. Therefore, the $M_{2\times4}$-based scheme and the $M_{4\times8}$-based scheme are comparable, since they share the same parameter values of $R_{NC}^{ADNC} = \frac{Lm_1}{Lm_1+Km_2} = \frac{1}{2}$, while $S_f = 0$ or $\sum_l^L (S_{f_l}) = 0$ refer to Eq. (4.46) and Eq. (4.47), respectively.

Accordingly, the information rate R_{info} of our proposed system can be expressed as [183]:

$$R_{info} = R_{NC} \times \eta_{ADNC} , \tag{4.48}$$

which is near-instantaneously time-variant [126, 200], since it may be changed for each transmission session. Furthermore, the diversity order reflecting the degree of space diversity gain attained by employing our network coding aided system may be expressed as [201]:

$$D_{ADNC} = K^{'} + m_2 , \tag{4.49}$$

where the value of $K^{'}$ is $K^{'} \in [0,4]$ for the ADNC-M1 scheme and $K^{'} \in [0,1,2,3,4]$ for the ADNC-M2 scheme, when $\mathcal{M}_{4\times 8}$ is used. Additionally, the maximum and minimum value of $D_{ADNC-M1}$ is identical to that of $D_{ADNC-M2}$, but the diversity order $D_{ADNC-M1}$ is higher than in the scenario $D_{ADNC-M2}$, when the BS fails to recover the PU's information, since the value of $K^{'}$ in the $D_{ADNC-M2}$ scheme can be $[1,2,3]$. Figure 4.7 shows both the FER performance and the average per-user per-link throughput versus E_b/N_0 for our ATTCM aided ADNC assisted CCR system based on the $\mathcal{M}_{4\times 8}$ matrix. It can be seen in Figure 4.7 that the FER performance of ADNC-M1 is better than that of the ADNC-M2, since it has a higher diversity order in some situations, when their throughputs are comparable. In our CCR scheme, we aim for reducing the bandwidth

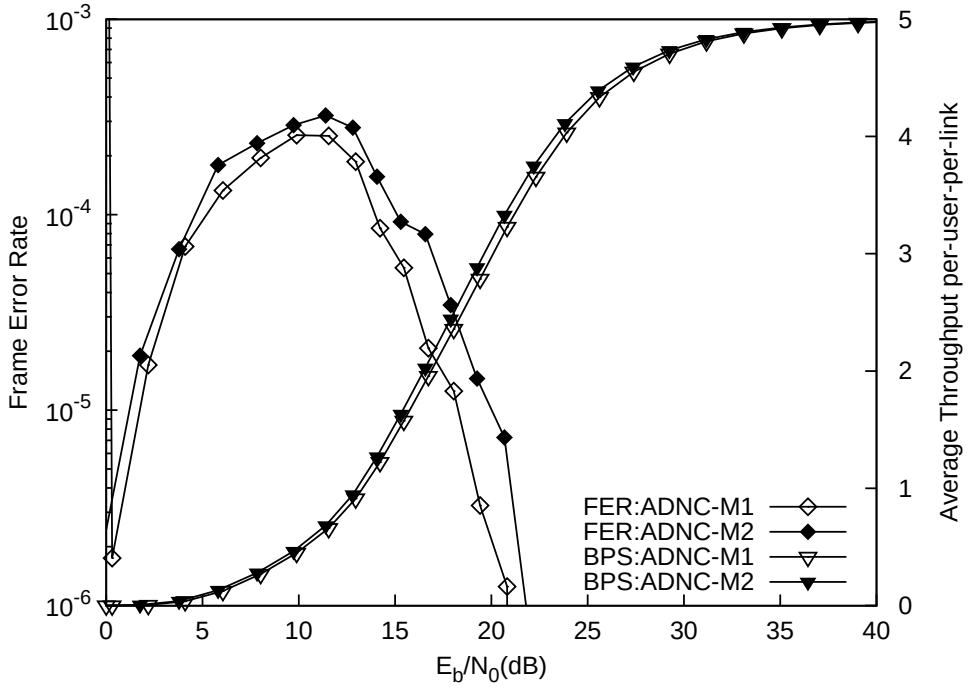

Figure 4.7: The FER performance and average throughput per user per link versus Eb/N_0 of the proposed ATTCM aided ADNC scheme based on the $\mathcal{M}_{4x8}$ matrix detailed in Section 4.3, as well as of ADNC-M1 for $K^{'} \in 0,4$, and ADNC-M2 for $K^{'} \in 0,1,2,3,4$. The corresponding switching thresholds are refer to Table 4.2.

requirement, while increasing the transmission rate of the PUs. We will employ ANDC-M2 in the investigations of Section 4.4 because it has a higher multiplexing gain.

4.4 Numerical Results and Discussions

Figure 4.2 shows the FER performance of the five individual non-adaptive TTCM modes of Eq. (4.8), when communicating over uncorrelated Rayleigh fading channels as well as the FER of TTCM-aided DNC and of the corresponding non-cooperative schemes, when transmitting over our com-

System	System 1	System 2
The output $C^*(\gamma_R < \gamma_0)$	case 1	case 2
Principle of ADNC	ADNC-M2	ADNC-M2
Channel	Rayleigh and Quasi static fading channel	Rayleigh and Quasi static fading channel
Number of frames N	10^6	10^6
Adaptive Coding	ATTCM	ATTCM
Modulation	Q-PSK, 8-PSK, 16-QAM, 32-QAM, 64-QAM	Q-PSK, 8-PSK, 16-QAM, 32-QAM, 64-QAM
FER bound	10^{-3}	10^{-3}
Transfer matrix of DNC	$\mathcal{M}_{2\times4}$, $\mathcal{M}_{4\times8}$	$\mathcal{M}_{2\times4}$, $\mathcal{M}_{4\times8}$
Number of PUs	$L = 2, 4$	$L = 2, 4$
Number of CUs	$K = 2, 4$	$K = 2, 4$
m_1 [frame]	1	1
m_2 [frame]	1	1
Pathloss exponent α	3	3

Table 4.4: The main parameters of our two systems, where System 1 includes a no transmission mode, while System 2 would invoke the TTCM-4PSK mode when the channel quality is poor.

bined[1] quasi-static (shadow) and Rayleigh (fast) fading channels. Figure 4.2 substantiates that the curves that consider only an uncorrelated Rayleigh fading channel always exhibit a better performance than the curves that characterise the combined quasi-static and Rayleigh fading scenarios. It is observed that the FER performance of our ATTCM aided DNC scheme is always better than that of the non-cooperative scheme, regardless of the specific modulation modes. Naturally, the 4PSK modulation mode has the best FER performance. It is shown in Figure 4.2 that the DNC-4PSK arrangement attains an approximately 20 dB gain in comparison to the SD-4PSK scheme at $FER = 10^{-3}$. As expected, the 64QAM mode has the worst FER performance, when viewing this comparison for an SNR-perspective, the DNC-64QAM scheme required an extra 12 dB power compared to both DNC-4PSK and to DNC-64QAM.

We define E_b/N_0 as the transmitted energy per bit to noise power spectral density ratio:

$$E_b/N_0 \text{ dB} \quad = \quad \gamma_t \text{ dB} - 10\log_{10}(R_{info}) \,, \tag{4.50}$$

where γ_t is the transmit SNR and R_{info} is the system's achievable throughput, which is defined in Eq. (4.48). Figure 4.8 shows the FER versus E_b/N_0 performance of the $\mathcal{M}_{2\times4}$ and $\mathcal{M}_{4\times8}$-based

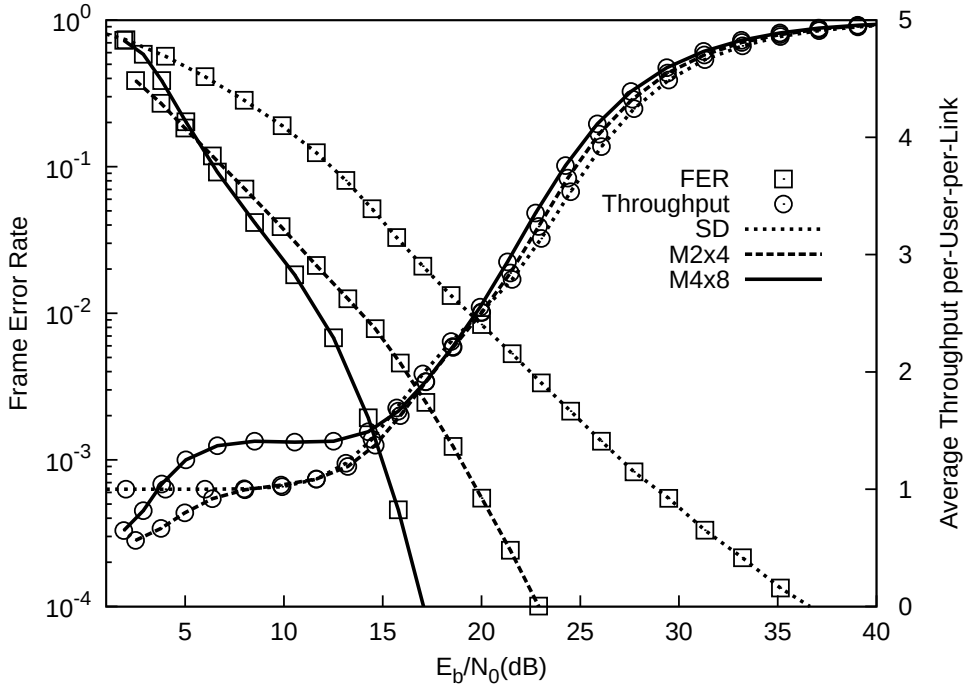

Figure 4.8: The FER performance and average throughput per user per link versus $Eb/N0_t$ of the proposed **System 2** of ATTCM aided ADNC scheme refer to Table 4.4. "M2x4" and "M4x8" represents the FER and average throughput of our ATTCM aided ADNC scheme activating one of five channel quality dependent modulation modes using 10^6 frames based on the matrix $\mathcal{M}_{2\times4}$ and $\mathcal{M}_{4\times8}$, respectively.

System 2 employing the ADNC arrangement, which represents the practical ATTCM transmission

[1]When the channel gain incorporates both the shadow- and fast-fading components, the adaptive transmission regime counteracts the shadow fading, but it is typically unable to accommodate the Rayleigh-fading.

scheme of Table 4.4, where System 1 includes a no transmission mode, while System 2 would invoke the TTCM-4PSK mode when the channel quality is poor, as introduced in Section 4.2.1. Its performance is benchmarked against that of the ATTCM aided non-cooperative communication scheme. As observed in Figure 4.8, the $\mathcal{M}_{4\times8}$-based scheme is capable of providing a significant E_b/N_0 performance improvement of 19 dB$-$15 dB$=$ 4 dB at $FER = 10^{-3}$ in comparison to the $\mathcal{M}_{2\times4}$-based scheme. In comparison to the non-cooperative schemes, our proposed $\mathcal{M}_{4\times8}$ and $\mathcal{M}_{2\times4}$-based ADNC arrangement has a better FER performance. More specifically, our $\mathcal{M}_{4\times8}$-based scheme attains an approximately 27 dB $-$15 dB$=$ 8 dB gain compared to its non-cooperative counterpart at FER=10^{-3}.

As we discussed in Section 4.3.2, the average throughput per user of the entire system can be summarized as:

$$\bar{\eta}_{ave} = \frac{\overbrace{LR_{tran}^{PU}T_{broadcast}}^{\text{Transmitted packet of PU}}}{\underbrace{LT_{broadcast}+KT_{cooperative}}_{\text{Required orthogonal channel}}} = \frac{LR_{tran}^{PU}}{L+K}. \tag{4.51}$$

Explicitly, Figure 4.8 illustrates the average throughput per-user per-link versus E_b/N_0 performance of the $\mathcal{M}_{2\times4}$ and $\mathcal{M}_{4\times8}$-based ATTCM-ADNC-CCR scheme, when we employed the five TTCM modes of Eq.(4.8) and used the case 2 scenario of Eq. (4.9). In contrast to the ADNC arrangement, at low SNRs the non-cooperative arrangement has a throughput of 1 iBPS. It is observed in Figure 4.8 that the throughput trends of these three schemes are similar and they approach 5 iBPS at $E_b/N_0 = 40$ dB. Therefore, the $\mathcal{M}_{4\times8}$-based scheme has the best FER performance at a comparable throughput. Figure 4.9a illustrates the mode selection probability of the 4PSK, 8PSK,

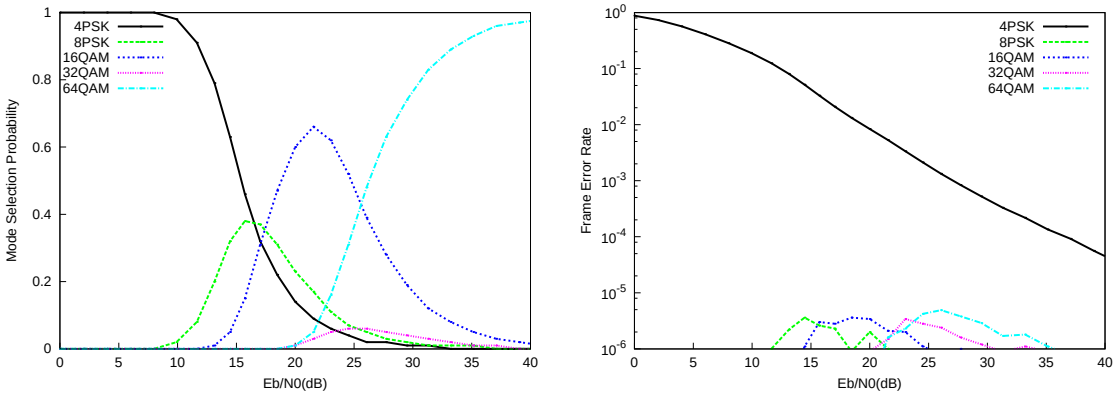

(a) Mode selection probability

(b) FER versus Eb/N_0

Figure 4.9: The FER performance and Mode selection Probability of each modulation mode versus $Eb/N0$ for the proposed **System 2** of Table 4.4 based on a **non-cooperative scheme**, which is obeyed Figure 4.12. The corresponding switching thresholds are refer to Table 4.2.

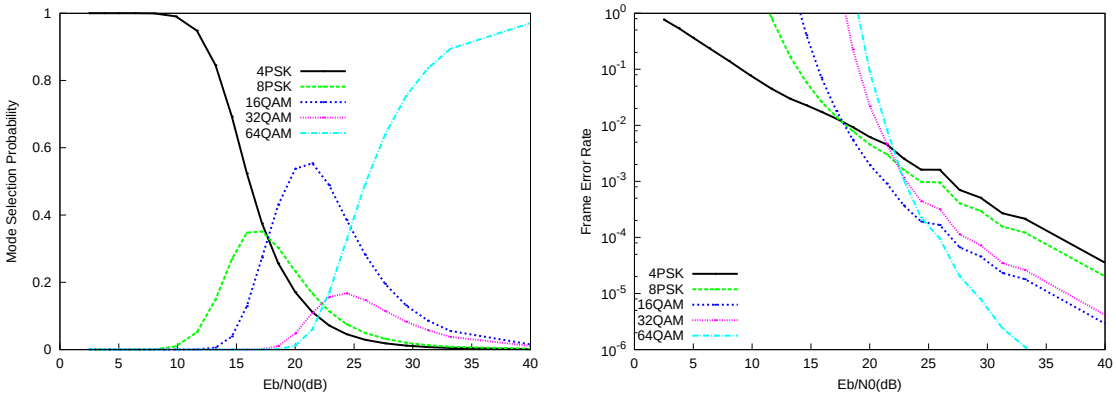

(a) Mode selection probability (b) FER versus Eb/N_0

Figure 4.10: The FER performance and Mode selection Probability of each modulation mode versus $Eb/N0$ for the proposed **System 2** of Table 4.4 based on $\mathcal{M}_{2\times4}$ **aided ADNC scheme**, which is obeyed Figure 4.12. The corresponding switching thresholds are refer to Table 4.2.

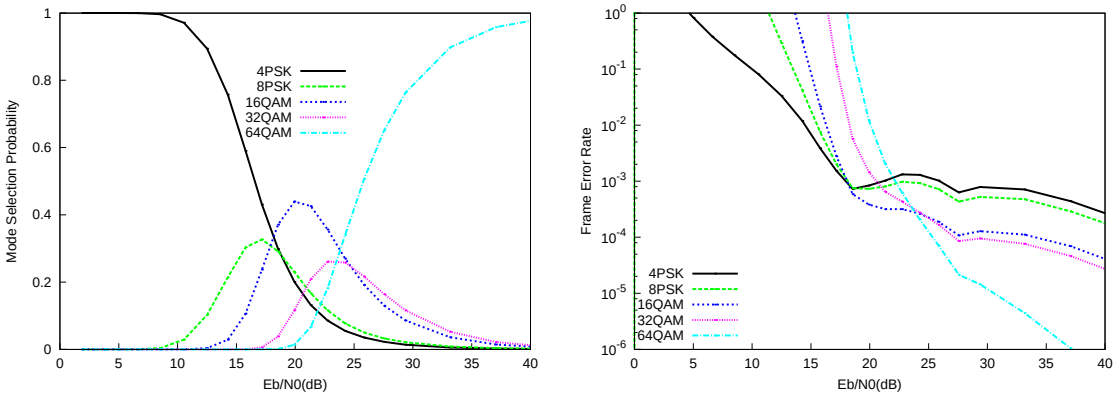

(a) Mode selection probability (b) FER versus Eb/N_0

Figure 4.11: The FER performance and Mode selection Probability of each modulation mode versus $Eb/N0$ for the proposed **System 2** of Table 4.4 based on $\mathcal{M}_{4\times8}$ **aided ADNC scheme**, which is obeyed Figure 4.12. The corresponding switching thresholds are refer to Table 4.2.

16QAM, 32QAM and 64QAM modes, when transmitting over our combined quasi-static (shadow) and Rayleigh (fast) fading channels for the non-cooperative scheme in the proposed System 2, as shown in Figure 4.8. Observe in Figure 4.9a that the 4PSK modulation mode is employed when the channel quality is poor, i.e. for $E_b/N_0 \leq 10$ dB, even when it is impossible to detect the 4PSK signals. Hence, the FER for the 4PSK mode is rather high. Additionally, the 16QAM modulation mode is the most frequently used one for 15dB$\leq E_b/N_0 \leq$ 30dB. When the channel quality is good enough, the 64QAM modulation mode will be employed. Figure 4.10a shows the mode selection probability of the five modulation modes in System 2 for the $\mathcal{M}_{2\times4}$ based ADNC scheme, as shown in Figure 4.8. By contrast, the mode selection probability of the five modulation modes in System 2 for the $\mathcal{M}_{4\times8}$ based ADNC are depicted in Figure 4.11a. Additionally, we have also considered the average FER performance of each modulation mode for the transmission period, which is given by:

$$FER_{ave} = \frac{\text{The number of erroneous frames of each mode}}{\text{Total number of coding session} \cdot N}. \quad (4.52)$$

In Figure 4.9b, Figure 4.10b and Figure 4.11b, we compare the FER performance of the five modulation modes of these three schemes in the context of System 2 to that of the ADNC performance shown in Figure 4.8. In our design, the FER target is below 10^{-3}. From Figure 4.9b, Figure 4.10b and Figure 4.11b, we find that the ADNC scheme maintained a FER under 10^{-3} using the five fixed modes. Having investigated both the FER and the throughput of System 2, we will discuss the relative performance of System 1, which employs a 'no transmission mode' in our proposed schemes. Figure 4.12 shows the FER versus SNR_t performance of our $\mathcal{M}_{2\times4}$ and $\mathcal{M}_{4\times8}$-based System 1 employing the ADNC arrangement, using the parameters shown in Table 4.4. In Figure 4.12, we compare the throughput of three schemes at a comparable FER. Explicitly, the non-cooperative scheme employed the BPSK, 8PSK, 16QAM of ATTCM transmission modes. The reason for considering three modulation modes for our non-cooperative scheme is because the FER performance of the non-cooperative benchmark scheme is somewhat poor. If a 32QAM modulation mode were to be used, the FER would become excessive. Similarly, we have only opted for four modulation modes for our ATTCM-ADNC-CCR $\mathcal{M}_{2\times4}$ matrix. Observe in Figure 4.12 that the FER recorded at the RN becomes lower than 10^{-3} both for the ADNC and for the non-cooperative scheme. The FER performance curves of the $\mathcal{M}_{2\times4}$ and of the $\mathcal{M}_{4\times8}$-based ATTCM-ADNC-CCR scheme and of the non-cooperative scheme crossed each other at $SNR_t = 10$ dB. Beyond that point, the FER performance of the ADNC scheme became better than that of the non-cooperative scheme, namely for SNR$_t > 11$ dB. Moreover, at FER=10^{-5} our proposed $\mathcal{M}_{4\times8}$-based scheme attains an 40 dB -26.5 dB$=$ 13.5 dB gain compared to the non-cooperative scheme.

As observed in Figure 4.12, our proposed $\mathcal{M}_{4\times8}$-based ADNC scheme has a better throughput than the non-cooperative scheme for $SNR_t > 25$ dB. Explicitly, we found in Figure 4.12 that the ADNC scheme achieved a throughput of 5.0 BPS, which is $5.0 - 3.0 = 2.0$ bits higher than that of the non-cooperative scheme at SNR$_t = 45$ dB. Observe furthermore in Figure 4.12 that the throughput of the $\mathcal{M}_{2\times4}$-based ADNC scheme is higher than that of the non-cooperative scheme

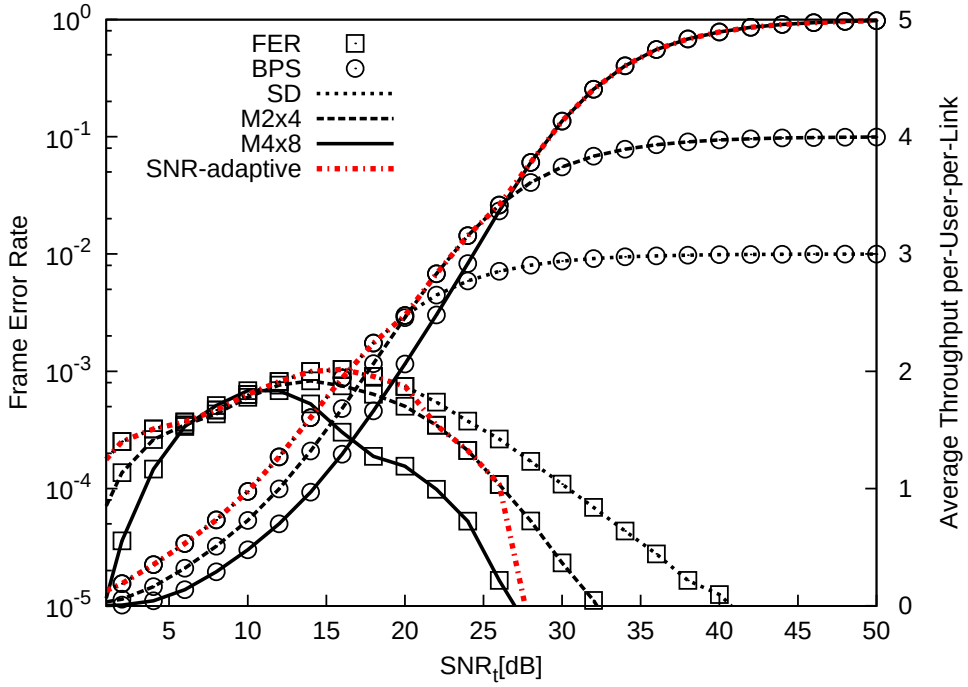

Figure 4.12: The FER performance and average throughput per user per link versus SNR$_t$ of the proposed **System 1** of ATTCM aided ADNC scheme refer to Table 4.4. "SD", "M2x4" and "M4x8" represents the FER and average throughput of our ATTCM aided non-cooperative scheme using one of three modulation modes and the ADNC scheme for four and five modulation modes based on matrix $\mathcal{M}_{2\times4}$ and $\mathcal{M}_{4\times8}$, respectively. "SNR-adaptive" ATTCM-ADNC-CCR scheme is represented that always activates the best scheme for the set of "SD", "M2x4" and "M4x8" based schemes in terms of the average throughput as a function of the SNR which has described in Section 4.4. The number of transmitted frames is 10^6. The corresponding switching thresholds are refer to Table 4.2.

for $SNR_t > 20$ dB. More specifically, the proposed $\mathcal{M}_{4\times8}$-based ADNC scheme requires four TSs, while the $\mathcal{M}_{2\times4}$-based scheme only requires two TSs, when the BS failed to flawlessly receive the source information from the SN, albeit these ADNC schemes failed to achieve a higher throughput for low SNR$_t$. Hence, it is better to activate a non-cooperative model at a low SNR, since its throughput per user per link is better. Then the "SNR-adaptive" ATTCM-ADNC-CCR system characterized in Figure 4.12 is the scheme that always activates the best scheme for the set of non-cooperative $\mathcal{M}_{2\times4}$- and $\mathcal{M}_{4\times8}$- based systems in terms of the average throughput as a function of the SNR. Note that at FER=10^{-4} the FER performance of the "SNR-adaptive" scheme is better than that of the $\mathcal{M}_{2\times4}$-based arrangement, but at FER=10^{-5} worse than that of the $\mathcal{M}_{4\times8}$ based scheme.

Figure 4.13a, Figure 4.14a and Figure 4.15a illustrate the mode selection probability of various modulation modes both for a non-cooperative scheme and for two ADNC schemes in the context of System 1. Explicitly, the FER and throughput are shown in Figure 4.12. As discussed before, we

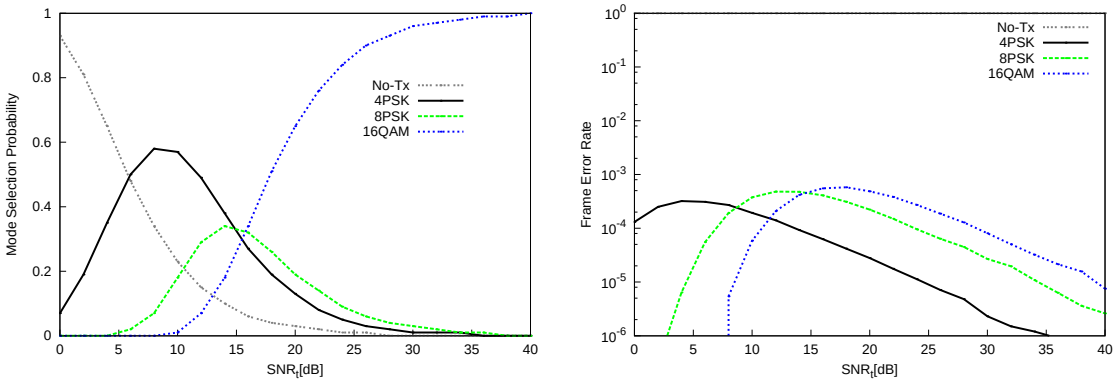

(a) Mode selection probability (b) FER versus SNR_t

Figure 4.13: The FER performance and Mode selection Probability of each modulation mode versus SNR_t for the proposed **System 1** of Table 4.4 based on a **non-cooperative scheme**, which is obeyed Figure 4.12. The corresponding switching thresholds are refer to Table 4.2.

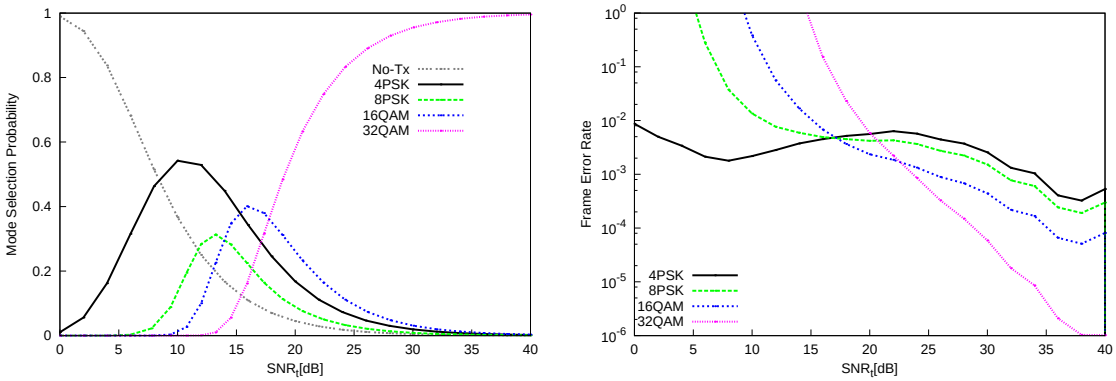

(a) Mode selection probability (b) FER versus SNR_t

Figure 4.14: The FER performance and Mode selection Probability of each modulation mode versus SNR_t for the proposed **System 1** of Table 4.4 based on $\mathcal{M}_{2\times4}$ **aided ADNC scheme**, which is obeyed Figure 4.12. The corresponding switching thresholds are refer to Table 4.2.

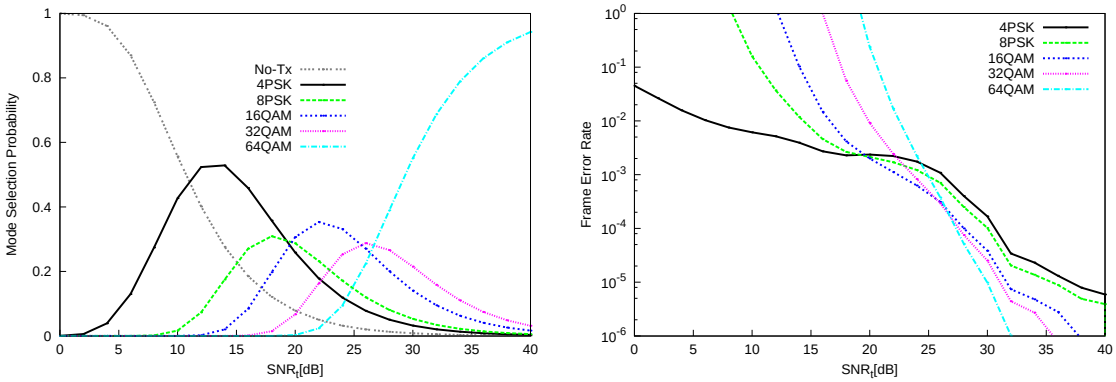

(a) Mode selection probability

(b) FER versus SNR_t

Figure 4.15: The FER performance and Mode selection Probability of each modulation mode versus SNR_t for the proposed **System 1** of Table 4.4 based on $\mathcal{M}_{4\times8}$ **aided ADNC scheme**, which is obeyed Figure 4.12. The corresponding switching thresholds are refer to Table 4.2.

have considered three modulation modes for our non-cooperative scheme, since the FER performance of the non-cooperative benchmark scheme is somewhat poor. For the same reason, we have only considered four modulation modes in our $\mathcal{M}_{2\times4}$ based ATTCM-ADNC-CCR based scheme. With reference to Figure 4.13, we can see that the 16QAM mode was used frequently, when the channel quality was good. By contrast, the 32QAM mode is the most commonly used one in System 1 for $\text{SNR}_t > 15$ dB as seen from Figure 4.14a. Moreover, the no-Tx mode is employed when the channel quality is poor, as demonstrated in Figure 4.13a, Figure 4.14a and Figure 4.15a. Furthermore, observe from Figure 4.13b, Figure 4.14b and Figure 4.15b, that the individual FER performance of these three schemes in the context of the System 1 is based on Eq. (4.52). In Figure 4.15b, the FER of 4PSK modulation mode is below 10^{-1}, for $0\text{ dB} < \text{SNR}_t < 10$ dB, because predominately the 4PSK modulation mode has been selected for $\text{SNR}_t < 10$ dB by referring to Figure 4.15a. The bandwidth-reduction factor (B_s) may be formulated as [202]:

$$B_s = 1 - \frac{\eta_{SD}}{\bar{\eta}_{ave}}, \tag{4.53}$$

where η_{SD} denotes the throughput of the non-cooperative system employing ATTCM, as defined in Eq. (4.44) and $\bar{\eta}_{ave}$ is defined in Eq. (4.51).

In Figure 4.16, we consider the attainable bandwidth reduction versus SNR_t for our ATTCM-ADNC-CCR system based on the $\mathcal{M}_{2\times4}$ and $\mathcal{M}_{4\times8}$ matrices of Table 4.4. It is observed in Figure 4.16 that the highest bandwidth reduction is achieved by the $\mathcal{M}_{4\times8}$-based ADNC scheme, which result in $B_s = 40$ % for $SNR_t \geq 42$ dB. Observe in Figure 4.12 that the corresponding maximum throughput of the ADNC scheme is $\eta_{ADNC} = 5$, while that of the non-cooperative scheme is $\eta_{SD} = 3$. Thus, based on Eq. (4.53), we arrive at $B_s = 1 - \frac{3}{5} = 0.4 = 40\%$. By referring to Figure 4.16, we observe that the $\mathcal{M}_{2\times4}$-based scheme may achieve $B_s = 25$ % at high

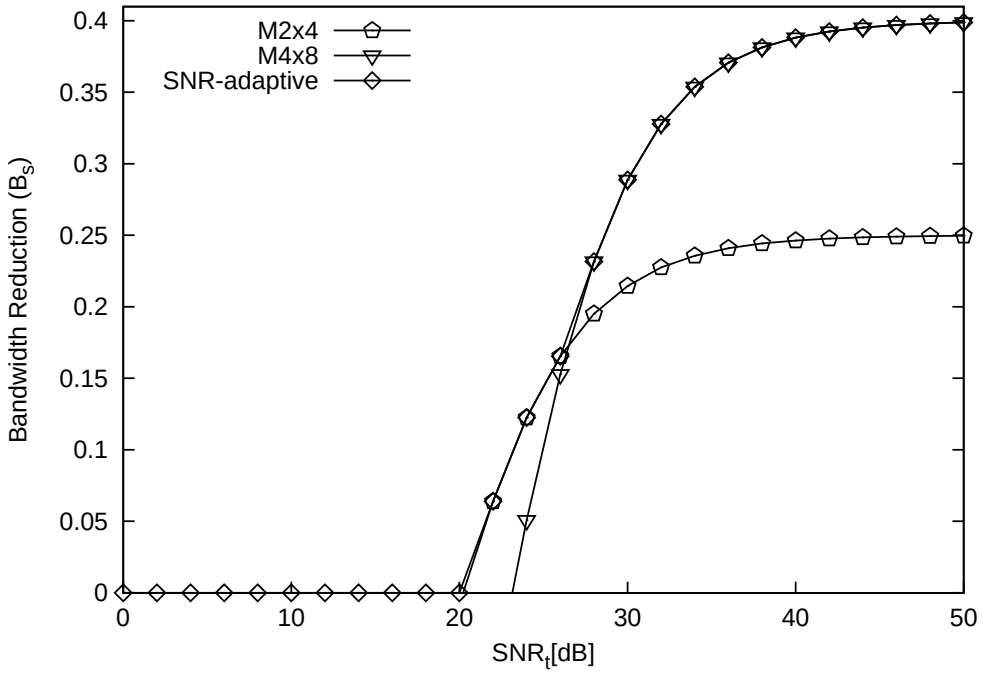

Figure 4.16: The bandwidth reduction B_s versus SNR_t of the proposed **System 1** of ATTCM aided ADNC scheme refer to Table. 4.4. "SD", "M2x4" and "M4x8" are denoted the FER and average throughput of ATTCM aided non-cooperative scheme using one of three modulation modes and the ADNC scheme for four and five modulation modes based on matrix $\mathcal{M}_{2\times4}$ and $\mathcal{M}_{4\times8}$, respectively. "SNR-adaptive" ATTCM-ADNC-CCR scheme is represented that always activates the best scheme for the set of "SD", "M2x4" and "M4x8" based schemes in terms of the average throughput as a function of the SNR which has described in Section 4.4.

SNRs, namely for $SNR_t \geq 42$ dB. Thus, the $\mathcal{M}_{4\times8}$-based ADNC scheme is capable of saving 40% $-25\%=$ 15% more bandwidth than the $\mathcal{M}_{2\times4}$-based ADNC scheme. Moreover, the performance of the "SNR-adaptive" ATTCM-ADNC-CCR scheme characterized in Figure 4.16 provides the highest bandwidth for the PU, regardless of the SNR. In our proposed ADNC-CCR schemes, the size of the DNC matrix and the number of frames transmitted per PU/CU would influence the number of supported PUs. More specifically, based on a $(N_r \times N_c)$-element DNC matrix $M_{N_r\times N_c}$, the number of PUs that can be supported over an N_r-frame periods is given by N_r/N_f, where N_f is the number of frames transmitted per PU during the N_r-frame period. Hence, the $\mathcal{M}_{4\times8}$-based DNC-CCR scheme is capable of supporting $L = \{1, 2, 4\}$ PUs, when we have $N_f = \{4, 2, 1\}$, respectively. We found that both the FER and the average throughput per user per link versus SNR_t performance would be similar, when supporting various number of PUs when using the same transfer matrix. Investigations based on a larger DNC matrix, such as the $\mathcal{M}_{6\times12}$ of [195], will be considered in our future work.

4.5 Chapter Conclusions

In this chapter, we have conceived an ATTCM-ADNC-CCR scheme, where both the ATTCM scheme and the ADNC technique were configured according to the near-instantaneous channel conditions. Additionally, we have considered an advanced method to feeding back the transmission state of the PUs from the BS to the CUs. More specifically, the BS would feed back a flag to the CUs concerning the success or failure of the transmission from each PU to the BS. By considering this method, we found that our proposed ATTCM-ADNC-CCR scheme enables the PU to transmit 2 BPS more information at a given SNR, which may be used for releasing up to 40% of the bandwidth for exploitation by the CUs. The overlay based CCR system of Chapter 3 only considered simple RNs without the capability of invoking the ADNC technique. By contrast, the network coding schemes investigated in this chapter were conceived for the CCR system, where the CUs were capable of transmitting the DNC-encoded information of both the PUs and CUs to the BS. Furthermore, in our proposed ATTCM-ADNC-CCR scheme, the ATTCM mode switching operation at the CUs/RNs was based on the corresponding FER performance of the TTCM scheme over a Rayleigh fading channel.

Chapter 5

Pragmatic Distributed Algorithm for Spectrum Access in Cooperative Cognitive Radio Networks

5.1 Introduction

In Chapter 3 and Chapter 4, we have investigated Cognitive radio (CR) schemes based on cooperation between Primary Users (PUs)s and Cognitive Users (CUs). In this chapter, we further extend our CR schemes to multiple PUs under two different scenarios. In the first scenario, all PUs will compete with each other, while in the second scenario, all PUs will cooperate with each other. More specifically, the PUs negotiate with the CUs concerning the specific amount of relaying and transmission time, which the CU will either accept or decline. Additionally, the CUs may serve as Relay Nodes (RNs) for relaying the signal received from the PUs to their destinations, only when both the PUs' and the CUs' minimum rate requirements are satisfied. This will reduce the required transmission power and/or increase the transmission rate of the PU. There are numerous contributions on spectrum access schemes and their impact on the throughput of the primary and cognitive networks [68, 81]. In this chapter, we also consider the overlay scheme associated with a Cognitive Radio (CR) network, which has been introduced in Section 1.3, where we require coordination or/and cooperation among the PUs and CUs. In CR networks, researchers tend to use three major utility functions: i) maximizing the utility of the PUs [98, 203], ii) maximizing the utility of the CUs [204–207], and iii) maximizing the total utility of both PUs and CUs [208–211]. The authors of [211] considered multiple PUs as well as CUs, where all PUs and CUs may be considered to be selfish, hence they may only be concerned about their own benefit, pursuing their own best strategies for maximizing their own rate or throughput.

In our work, we state a fairly general cooperative spectrum sharing problem, which is aimed at

maximizing the PUs' utility, and provide a solution in the form of a distributed algorithm that can be shown to be convergent but sub-optimal. In [98], a Conventional Distributed Algorithm (CDA) was proposed, which may be viewed as an evolution from the dynamic auction algorithms [212, 213], since it considers a resource-allocation [214] framework that facilitates a joint competitive strategy of the PUs and the CUs conceived for accessing the spectral resources. Moreover, the authors of [98] conceived a non-cooperative game, which employs the CDA for efficiently representing the interaction among the competing PUs, where each PU chooses its allocation independently of the others in order to improve its own performance. This is considered as our first scenario, where the PUs do not cooperate with each other. Explicitly, a spectral access strategy is designed for multiple PUs and CUs, where the PUs and CUs are carefully paired for ensuring that both the PUs' and the CUs' minimum sum-rate requirements are satisfied. Each paired CU assists in relaying its paired-PU's signal in exchange for a transmission opportunity using the PU's spectrum. However, the PUs under the CDA would sometimes compete among themselves for cooperating with the same relay, which may degrade both their utility and throughput. Moreover, in our design, a Pragmatic Distributed Algorithm (PDA) is proposed for supporting the efficient spectral access of multiple PUs and CUs in Cooperative Cognitive Radio networks. In contrast to the CDA, our proposed PDA, which may be classified as a repeated game [84, 215, 216], where all PUs are capable of cooperating with each other. This constitutes our second scenario where the PUs do not compete with each other. The PUs are motivated to form a grand coalition [217, 218] for achieving an increased expected PU rate by discouraging the PUs from competing with each other for the same CU's assistance. Furthermore, the concept of a penalty/punishment is introduced [215], which is imposed only for a carefully selected finite period for the sake of discouraging non-cooperation among PUs. Moreover, we show that the cooperative spectral access based on our PDA reaches an equilibrium, when it is repeated for a sufficiently long duration. These benefits are achieved, because the PUs are motivated to cooperate by the incentive of achieving a higher PU rate, whilst non-cooperation can be discouraged with the aid of a limited-duration punishment.

Furthermore, we invoke an attractive practical ATTCM scheme as discussed in Chapter 2, which appropriately adjusts the code rate and the modulation mode according to the near-instantaneous channel conditions. The transmission rate/throughput of our system is adapted according to the instantaneous channel conditions. A more vulnerable, but higher-throughput TTCM scheme is employed when the channel conditions are good, while a lower-throughput but more robust TTCM scheme is used, when the channel conditions are poor. Additionally, we have considered a pair of idealistic adaptive schemes based on both the capacity of CCMC and DCMC in our proposed CCR scheme as the upper bound. More specifically, the CCMC based adaptive scheme assumes that idealistic coding and modulation schemes are employed for communicating exactly at Shannon's capacity. By contrast, the DCMC based adaptive scheme assumes that an idealistic capacity-achieving code is employed for allowing the PSK/QAM modulation schemes considered to operate right at the modulation-dependent DCMC capacity. It was found that the joint design of coding,

modulation and user-cooperation may lead to significant mutual benefits for all the PUs and the CUs.

5.2 System Model

In our design, we consider an overlay CCR scheme supporting L_{PU} number of "PU transmitter (Pt) and PU receiver (Pr) pairs"[1], namely $\left(\{Pt_l\}_{l=1}^{L_{PU}}, \{Pr_l\}_{l=1}^{L_{PU}}\right)$, with the lth pair having a rate requirement of $R_{PU_l,req}$, and with each pair occupying a unique spectral band of a constant width. In our scheme, there are L_{CU} "CU transmitter (Ct) and CU receiver (Cr) pairs"[2], namely $\left(\{Ct_k\}_{k=1}^{L_{CU}}, \{Cr_k\}_{k=1}^{L_{CU}}\right)$ pairs, with the kth pair having a requirement of $R_{CU_k,req}$, and seeking to obtain access to a spectral band occupied by a (Pt, Pr) pair. We require that PUs and CUs share the spectrum, where the CU must suitably compensate the PU for being permitted to use the spectrum. Specifically, each Pt attempts to grant spectral access to a unique (Ct, Cr) pair in exchange for the Ct cooperatively relaying the Pt's data to the corresponding Pr. Four types of matching algorithms will be described in Section 5.5.1.

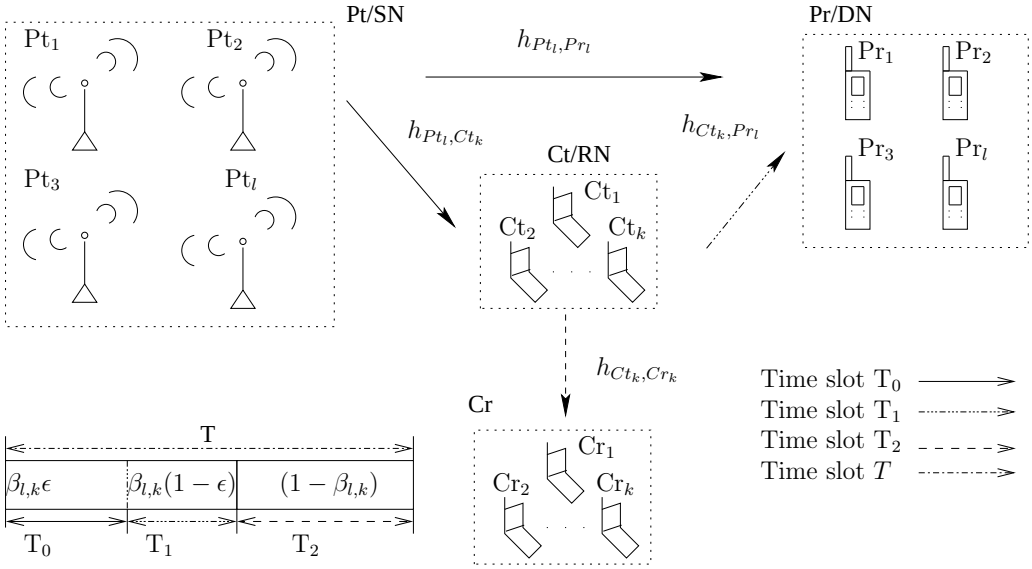

Figure 5.1: The spectrum-access model for primary user and cognitive user.

Figure 5.1 illustrates the time period allocation of the PUs and CUs, where T is the original time period allocated for the Pt to transmit its source message to the Pr. We will refer to $\{\beta_{l,k}\}_{l=1k=1}^{L_{PU}L_{CU}}$ as the time allocation fraction, where $0 < \beta_{l,k} < 1$. When the Pt is assisted by a Ct/RN, the Pt relies on a time-fraction of $\beta_{l,k}T$ to convey the source message to the Pr and Ct/RN. More specifically, the Pt simultaneously transmits its message to Pr and Ct/RN during the $T_0 = \beta_{l,k}T\epsilon_{l,k}$ time-period,

[1]The Pt-Pr pair constitutes the PU's transceiver. We represent the PU acting as the Source Node (SN) by Pt. Similarly, Pr denotes the PU which acts as the destination node PU.

[2]The Ct-Cr pair is the CU's transceiver. The notation Ct/RN represents the CU that acts as the relay node for helping the PU's transmission, while Ct denotes the CU that act as the SN to Cr, which denotes the destination node of a Ct.

where $0 < \epsilon_{l,k} < 1$. Additionally, the Ct/RN cooperatively relays the Pt's signal to Pr in the subsequent $T_1 = \beta_{l,k}(1-\epsilon_{l,k})T$ time-periods. Then the Pr applies maximum ratio combining for detecting the signal received from the Pt during the first T_0 time period, and the signal received from the Ct/RN in the subsequent T_1 time periods. After the PU has ceased its transmission, the system will allow the CUs to transmit their information to the other CUs by using the remaining time period of $T_2 = (1-\beta_{l,k})T$ for their own communications. In other words, a Ct/RN assists in saving some of the transmission powers of the Pt due to the reduction of the transmission period from T to (T_0+T_1). The Pt transmits during T_0, while the Ct/RN forwards the source message during T_1 and the Ct/SN can broadcast its message to other CUs during the time period T_2. Let us assume that the transmission power per unit frequency transmitted from the Pt is P_S watts/Hz and the target transmission rate is R_{PU} bits/s.

During the first Time-Slot (TS) T_0, the PU broadcasts the source message x to both the Pr and to the Ct/RN. We assume that our proposed scheme relies on a Time Division Multiple Access (TDMA) scheme, where PUs do not transmit simultaneously for the sake of avoiding any inter-user interference. The signal received at the Pr is given by:

$$y_{Pt_l,Pr_l} = \sqrt{P_S} h_{Pt_l,Pr_l} x + n_{Pt_l,Pr_l} \,, \tag{5.1}$$

and the signal received at the Ct/RN is:

$$y_{Pt_l,Ct_k} = \sqrt{P_S} h_{Pt_l,Ct_k} x + n_{Pt_l,Ct_k} \,. \tag{5.2}$$

During the second TS T_1 the Ct/RN would forward the source message to the Pr using the transmission power of P_{CR} watts/Hz. Similarly, the signal received by the Pr under the AAF protocol via the RD link may be expressed as:

$$y_{Ct_k,Pr_l} \;=\; \omega_A \sqrt{P_{CR}} h_{Ct_k,Pr_l} y_{Pt_l,Ct_k} + n_{Ct_k,Pr_l} \,, \tag{5.3}$$

where $\omega_A = \frac{1}{\sqrt{P_S |h_{Pt_l,Ct_k}|^2 + N_0}}$ [13] is the amplification factor, while n_{Pt_l,Pr_l}, n_{Pt_l,Ct_k} and n_{Ct_k,Pr_l} are the Gaussian noise vectors, which have a zero mean and a noise variance of $N_0/2$ per dimension. The channel gain terms h_{Pt_l,Pr_l}, h_{Pt_l,Ct_k} and h_{Ct_k,Pr_l} are assumed to be Rayleigh distributed, obeying the complex-valued Gaussian distribution of $\mathcal{CN}(0,1)$. In our system, the path loss is included in the channel gain term. In our scheme, both the Pt and the Ct/RN utilize the same bandwidth. The achievable instantaneous rate of the lth PU when employing the kth CU at a given $\beta_{l,k}$ may be represented as:

$$R_{l,k}^{PU}(\beta_{l,k}) \;=\; C_{PU_{l,k}} \beta_{l,k} \,. \tag{5.4}$$

where the capacity of PU $C_{PU_{l,k}}$ based on the Shannan theory is given by:

$$C_{PU_{l,k}} = \frac{T}{2} \log_2 \left[1 + \frac{\gamma_{PU} |h_{Pt_l,Pr_l}|^2}{d^{\alpha}_{Pt_l,Pr_l}} + f_{Pt,Ct,Pr} \right] \,, \tag{5.5}$$

where we have

$$f_{Pt,Ct,Pr} = \frac{\gamma_{PU}\gamma_{CU}|h_{Pt_l,Ct_k}|^2|h_{Ct_k,Pr_l}|^2}{\gamma_{PU}|h_{Pt_l,Ct_k}|^2 d^{\alpha}_{Ct_l,Pr_l} + \gamma_{CU}|h_{Ct_k,Pr_l}|^2 d^{\alpha}_{Pt_l,Ct_l} + d^{\alpha}_{Pt_l,Ct_l} d^{\alpha}_{Ct_l,Pr_l}} . \quad (5.6)$$

The factor $\frac{1}{2}$ in Eq. (5.5) is due to the time fraction $\epsilon_{l,k} = \frac{1}{2}$, when we have $T_0 = T_1$, where the Pt utilizes the first TS T_0 and the Ct/RN uses the second TS T_1 to transmit the PU's signals. If the $T_0 \neq T_1$, then the rate $R^{PU}_{l,k}$ at a given $\beta_{l,k}$ of the cooperative relay channel is given by:

$$R^{PU}_{l,k} = \beta_{l,k}\epsilon_{l,k} T \log_2 \left[1 + \frac{\gamma_{PU}|h_{Pt_l,Pr_l}|^2}{d^{\alpha}_{Pt_l,Pr_l}} + f_{Pt,Ct,Pr} \right] , \quad (5.7)$$

Note that the transmit SNR of the PU is $\gamma_{PU} = \frac{P_s}{N_0}$ and that of the CU is $\gamma_{CU} = \frac{P_{CR}}{N_0}$. Moreover, in the non-cooperative scenario, the achievable sum rate of the direct link between Pt_l and Pr_l is given by:

$$C^{*}_{PU} = T \log_2 \left[1 + \frac{\gamma_{PU}|h_{Pt_l,Pr_l}|^2}{d^{\alpha}_{Pt_l,Pr_l}} \right] , \quad (5.8)$$

while the minimum rate requirement of the PU is given by $R^{PU}_{l,req} = C^{*}_{PU}$.

The achievable transmission rate of the kth CU when assisting the lth PU at a given $\beta_{l,k}$ is formulated as:

$$R^{CU}_{l,k}(\beta_{l,k}) = (1-\beta_{l,k}) T \log_2 \left[1 + \gamma_{CU}|h^{(k)}_{Ct_k,Cr_k}|^2 \right] , \quad (5.9)$$

where the channel $h^{(k)}_{Ct_k,Cr_k}$ depends on the frequency band provided by Ct_k, while the pathloss is $\varrho = 1/d^{\alpha}_{ab}$ [13] and d_{ab} is the geometrical distance between node a and node b, while the path-loss exponent considered in our simulations is $\alpha = 4$. Moreover, we assume that Pt and Pr are located at the opposite sides of a square at a normalized distance of two, thus $d_{Pt_l,Pr_l} = 2.0$ as considered in [98] . Additionally, the Cts/RN and Crs are assumed to be randomly located within an internal square having an edge-length of one, hence we have ($0 < d_{Ct_k,Cr_k} < \sqrt{2}$). As shown in Figure 5.2, the distance between Pt and Ct/RN is defined as

$$d_{Pt_l,Ct_k} = \sqrt{|x_3 - x_1|^2 + |y_3 - y_1|^2} , \quad (5.10)$$

while the distance between Ct/RN and Pr is given by:

$$d_{Ct_k,Pr_l} = \sqrt{|x_2 - x_3|^2 + |y_2 - y_3|^2} , \quad (5.11)$$

where $x_1 = 0.0$, $x_2 = 2.0$ and $0 \leq y_2 = y_1 \leq 2$. Furthermore, we consider an outdoor environment, where the path-loss exponent is given by $\alpha = 4$ [167].

5.3 Formulation of the Optimization Problem

The achievable transmission rate of the PU given in Eq. (5.7) may be rewritten as:

$$R^{PU}_{l,k} = \beta_{l,k} C_{PU_{l,k}} , \quad (5.12)$$

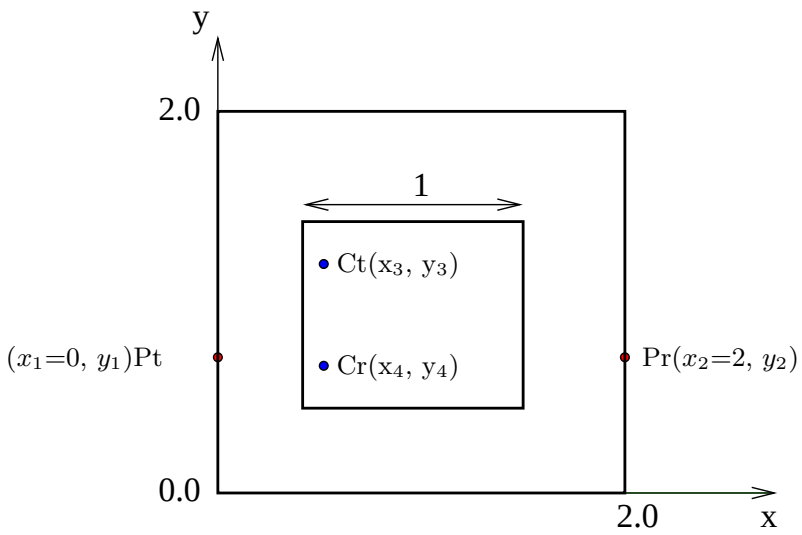

Figure 5.2: The system design of distance setting.

where $C_{PU_{l,k}}$ represents the PU's capacity by considering the cooperative relaying, which was defined in Eq. (5.5). Thus, the achievable transmission rate of the CU in Eq. (5.9) can be rewritten as:

$$R_{l,k}^{CU} = (1-\beta_{l,k})C_{CU_{l,k}}\,, \tag{5.13}$$

where $C_{CU_{l,k}}$ denotes the capacity between the transmitter Ct_k and the receiver Cr_k. Both PUs and CUs have their minimum rate requirements, thus in a valid cooperative relaying strategy, we must have:

$$\beta_{l,k}C_{PU_{l,k}} \geq R_{l,req}^{PU} \quad \text{and} \quad (1-\beta_{l,k})C_{CU_{l,k}} \geq R_{k,req}^{CU}\,. \tag{5.14}$$

Additionally, let us define a $(L_{PU} \times L_{CU})$-element matching matrix M, where the lth PU is matched to the kth CU, if their corresponding matching matrix entry is given by $m_{l,k} = 1$ and $m_{l,k} = 0$ otherwise. We also define a $(L_{PU} \times L_{CU})$-element time-slot allocation matrix T with elements $\beta_{l,k}$. In particular, the optimization problem of maximizing the matched sum rate can be formulated as [203, 208]:

$$\{M^{cen}, T^{cen}\} = \max_{M,T} \sum_{l=1}^{L_{PU}} \sum_{k=1}^{L_{CU}} m_{l,k} W(\beta_{l,k})\,, \tag{5.15}$$

$$\begin{aligned} s.t.\quad & (a) R_{l,k}^{PU}(\beta_{l,k}) \geq R_{l,req}^{PU}\,, \forall l \forall k \\ & (b) R_{l,k}^{CU}(\beta_{l,k}) \geq R_{k,req}^{CU}\,, \forall l \forall k \\ & (c) 0 \leq \beta_{l,k} \leq 1\,, \forall l \forall k \\ & (d) \sum_{l=1}^{L_{PU}} m_{l,k} \leq 1\,, \forall k \\ & (e) \sum_{k=1}^{L_{CU}} m_{l,k} \leq 1\,, \forall l\,. \end{aligned}$$

The conditions (a) and (b) are stipulated for ensuring that the minimum rate requirement of the PUs and CUs can be achieved. Condition (c) ensures that the TS allocation is limited to its bound. Finally, conditions (d) and (e) are imposed for ensuring that each PU(CU) will only be matched to one CU(PU). We assume that each transmitter-receiver pair has the knowledge of the number of PUs and CUs in the network. Without loss of generality, we also assume that the number of CUs is higher than the number of PUs. Moreover, the choice of the weight $W(\beta_{l,k})$ of Eq. (5.15) depends on the utility to be maximized.

- The optimization problem of considering matched PUs can be formulated as:

$$W_{PU}(\beta_{l,k}) \quad = \quad \beta_{l,k} C_{PU_{l,k}} \, . \tag{5.16}$$

- The optimization problem of considering matched CUs is given by:

$$W_{CU}(\beta_{l,k}) \quad = \quad (1-\beta_{l,k}) C_{CU_{l,k}} \, . \tag{5.17}$$

- The optimization problem of maximizing the total sum rate of matched PUs and CUs may be expressed as:

$$W_{total}(\beta_{l,k}) \quad = \quad \beta_{l,k} C_{PU_{l,k}} + (1-\beta_{l,k}) C_{CU_{l,k}} \, . \tag{5.18}$$

Note that, the cooperation between the PUs and CUs is facilitated via time-allocation, where the objective function of Eq. (5.15) is a linear appropriate transmission function of the time-slot factor $\beta_{l,k}$. The optimization problem of Eq. (5.15) can be decoupled with respect to two entries, namely M and T, which are two sub-problems:

$$\{M^{cen}, T^{cen}\} \quad = \quad \underbrace{\max_{T} \sum_{l=1}^{L_{PU}} \sum_{k=1}^{L_{CU}} W(\beta_{l,k})}_{\text{Sub-problem A}} \cdot \underbrace{\max_{M} \sum_{l=1}^{L_{PU}} \sum_{k=1}^{L_{CU}} m_{l,k}}_{\text{Sub-problem B}} \, . \tag{5.19}$$

At the first step, the optimum value of $\beta_{l,k}$ of sub-problem A in Eq. (5.19) may be found based on the condition (a), (b) and (c), where the computation of the sum rate of the PUs and CUs has been introduced in Section 5.2. Then the optimization of $\beta_{l,k}$ can be formulated as:

$$\beta_{l,k}^{cen} \quad = \quad \max_{\beta_{l,k}} \sum_{l=1}^{L_{PU}} \sum_{k=1}^{L_{CU}} W(\beta_{l,k}) \, . \tag{5.20}$$

Based on condition (a) of Eq. (5.15), the lower bound of $\beta_{l,k}$ is given by:

$$\beta_{l,k}^{\min} \geq \frac{R_{l,req}^{PU}}{C_{PU_{l,k}}} \, . \tag{5.21}$$

Moreover, the upper bound of $\beta_{l,k}$ based on condition (b) of Eq. (5.15) is given by:

$$\beta_{l,k}^{\max} \leq 1 - \frac{R_{k,req}^{CU}}{C_{CU_{l,k}}}. \tag{5.22}$$

There are three cases for setting $\beta_{l,k}^{cen}$ of Eq. (5.20):

- When considering the sum rate of the matched PUs as the optimization problem, we have:

$$\beta_{l,k}^{cen} = 1 - \frac{R_{k,req}^{CU}}{C_{l,k}^{CU}} . \tag{5.23}$$

- When maximizing the sum rate of the matched CUs, we derive at:

$$\beta_{l,k}^{cen} = \frac{R_{k,req}^{PU}}{C_{l,k}^{PU}} . \tag{5.24}$$

- When maximizing the total sum rate of the matched PU and CU, we get:

$$\beta_{l,k}^{cen} = \begin{cases} \frac{R_{PU_{req}}}{C_{PU}} & C_{CU} > C_{PU}; \\ 1 - \frac{R_{CU_{req}}}{C_{CU}} & C_{CU} < C_{PU}; \end{cases} \tag{5.25}$$

The derivation of Eq. (5.25) is detailed in Appendix A. After solving the Sub problem A of Eq. (5.19), the solution of the optimization problem of Eq. (5.15) can be re-derived as :

$$\{M^{cen}\} = \max_{M} \sum_{l=1}^{L_{PU}} \sum_{k=1}^{L_{CU}} W(\beta_{l,k}^{cen}) m_{l,k} , \tag{5.26}$$

$$s.t. \quad (d) \sum_{l=1}^{L_{PU}} m_{l,k} \leq 1 , \forall k$$
$$(e) \sum_{k=1}^{L_{CU}} m_{l,k} \leq 1 , \forall l ,$$

where the condition (d) and (e) is a binary one.

Lemma 5.1.: The solution of Eq. (5.15) is a feasible solution of Eq. (5.26) [208].

Proof: Let us denote $(\beta_{l,k}^{cen}, m_{l,k}^{cen})$ as the solution of the optimization problem of Eq. (5.15). The weight $W(\beta_{l,k}^{cen})$ depends on conditions (a), (b) and (c) of Eq. (5.15), which may be solved according to the terms $R_{l,k}^{PU}(\beta_{l,k}^{cen})$, $R_{l,req}^{PU}$, $R_{l,k}^{CU}(\beta_{l,k}^{cen})$ and $R_{k,req}^{CU}$. These four terms can be calculated based on the known channel conditions. This follows from the fact that the weight $W(\beta_{l,k})$ only depends on the variable $\beta_{l,k}$. Specifically, the maximum value of the $W(\beta_{l,k})$ can be obtained by maximizing the variable $\beta_{l,k}$. Note that, the optimal objective of Eq. (5.26) is $W(\beta_{l,k}^{cen})m_{l,k}$, which is a specific instance of the formulation of Eq. (5.15), since $W(\beta_{l,k})$ of Eq (5.15) is substituted by $W(\beta_{l,k}^{cen})$ of Eq. (5.26). Therefore, the solution of Eq. (5.26) is a feasible solution of Eq. (5.15). Hence, the lemma establishes the procedure of solving the original optimization problem of Eq. (5.15).

5.4 Coding and Modulation Design

In our proposed system, we will make use of this power- and bandwidth-efficient TTCM scheme which was discussed in Chapter 2. Employing TTCM has the advantage that the system's effective throughput can be increased upon increasing the code rate, when the channel-quality improves.

Additionally, the BER performance of the system may be improved when TTCM is used [95–97]. The TTCM encoder comprises two identical parallel-concatenated TCM encoders [99] linked by a symbol interleaver. The first TCM encoder directly processes the original input bit sequence, while the second TCM encoder manipulates the interleaved version of the input bit sequence. Then the bit-to-symbol mapper maps the input bits to complex-valued symbols using the SP-based labelling method [96]. The structure of the TTCM decoder is similar to that of binary turbo codes, but each decoder alternately processes its corresponding encoder's channel-impaired output symbol, and then the other encoder's channel-impaired output symbol [p.764] [96]. More details on the TTCM principles may be found in [96]. We have employed a ATTCM scheme for protecting the SR and the RD links, where the effective throughput (or information Bit Per Symbol (BPS)) range is given by iBPS$=\{0,1,2,3,5\}$ BPS when no transmission, QPSK, 8PSK, 16QAM and 64QAM are considered, respectively. Moreover, the TTCM mode switching thresholds Y=$[\gamma_0,\gamma_1,\gamma_2,\gamma_3]$ were determined based on the BER performance curves of each of the four TTCM schemes in a Rayleigh fading channel, which is shown in Figure 5.3. Specifically, the ATTCM mode switching operation and the throughput of the modes are specified by the following algorithm:

$$\text{MODE} = \begin{cases} \gamma_3 \leq \gamma_R, & \text{TTCM-64QAM, iBPS=5 ;} \\ \gamma_2 \leq \gamma_R < \gamma_3, & \text{TTCM-16QAM, iBPS=3;} \\ \gamma_1 \leq \gamma_R < \gamma_2, & \text{TTCM-8PSK, iBPS=2 ;} \\ \gamma_0 \leq \gamma_R < \gamma_1, & \text{TTCM-4PSK, iBPS=1 ;} \\ \gamma_R < \gamma_0, & \text{No transmission, iBPS=0 .} \end{cases}$$

In contrast to the idealistic CCMC based AAF design discussed in Section 5.2, we investigate a practical design of the CCR scheme advocated using an ATTCM based DAF scheme. As shown in Figure 5.1, all Cts/RN operate in the half-duplex DAF mode and it is assumed that each Ct/RN only knows its own channel, but that the Pr estimates all channels with the aid of training. The signal received via the direct (Pt-Pr) link is also detected. We use the notation γ_{ab} to refer to the instantaneous receive SNR of the link between node a and node b. The receive SNR at node b is given by:

$$\gamma_R = \frac{\varrho |h_{ab}|^2}{N_0}, \tag{5.27}$$

where h_{ab} represents the quasi-static Rayleigh fading channel between nodes a and b. The channel gains are independent of each other. The quasi-static Rayleigh fading channels between the Pts and the Cts/RN are denoted as $[h_{Pt_1,Ct_1},\ldots,h_{Pt_l,Ct_k}]_{L_{PU}\times L_{CU}}$, while those between the Cts/RNs and the Prs are represented by $[h_{Ct_1,Pr_1},\ldots,h_{Ct_l,Pr_k}]_{L_{CU}\times L_{PU}}$. As seen from Figure 5.1, we have $(l \times k)$ links spanning from the Pts to the Ct/RNs supported by K Cts/RN and also $(k \times l)$ links spanning from the Cts/RN to the Prs.

Each of the communication links will be assisted by the ATTCM scheme. We note that Shannon's CCMC capacity is only restricted by the SNR and the bandwidth. The CCMC and DCMC

based schemes have been discussed in Section 3.4.1.1. More specifically, we have specifically chosen the switching thresholds to ensure that the BER at the RN is lower than 10^{-5}. The corresponding switching thresholds of the ATTCM, as well the perfect CCMC and DCMC-achieving scenario were shown in Table 5.1. The reason why we have chosen the BER at the RN to be

Channel	Y[dB] at BER= 10^{-5}			
	Uncorrelated Rayleigh			iBPS
Coding/ Modulation	ATTCM	DCMC	CCMC	
4PSK	4.8	2	1.75	1
8PSK	12	8	6	2
16QAM	16	12.5	11	3
64QAM	24	20	17	5

Table 5.1: The SNR thresholds of TTCM, DCMC and CCMC schemes when communicating over AWGN and uncorrelated Rayleigh fading channels. The values are tabulated based on Figure 5.3.

lower than 10^{-5} is that the error floor emerging at BER$< 10^{-5}$ can be removed by using a long outer code, such as a Reed Solomon Code (RSC), albeit no RS code was used here. For quasi-static

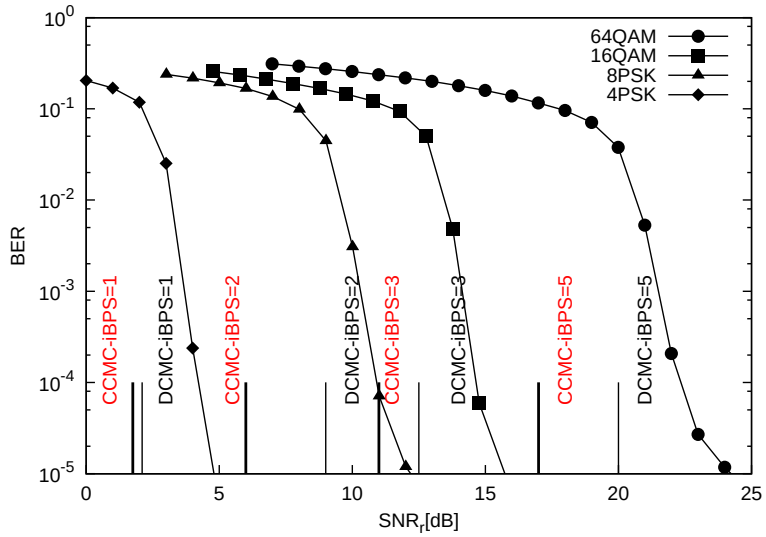

Figure 5.3: The BER versus SNR$_r$ performance of TTCM using a frame length of 120,000 symbols, when communicating over Rayleigh channels. Four TTCM iterations were invoked.

fading channels, the achievable rates over different links become random and vary as the channel changes. We have considered two different methods of evaluating the total system rate R_{total} between the communication link Pt-Ct and Ct-Pr, namely both the lower-bound and upper-bound of the system's total rate R_{total}. The lower bound assumes that the DAF based RN/Ct forwards the received signal to Pr directly and the corresponding rate is the minimum of the rates in the Pt-Ct

and Ct-Pr links [219, 220]:

$$R_{l,k}^{lower} = \frac{1}{t} \min\{R_{Pt_l - Ct_k}, R_{Ct_k - Pr_l}\} , \tag{5.28}$$

where t is the number of TSs in the cooperative relay transmission. We consider the classical $t = 2$ TSs based cooperative relaying channel. We ensured that the specific hop associated with the lower sum rate would convey its message successfully, while the other hop having the higher sum rate would give up some of its capacity. Moreover, we have also considered the upper-bound of the total achievable rate based on the average of the achievable sum-rates of both the Pt-Ct and Ct-Pr links as [221]:

$$R_{l,k}^{upper} = \frac{1}{t} \left(R_{Pt_l - Ct_k} + R_{Ct_k - Pr_l}\right) . \tag{5.29}$$

More specifically, the upper bound assumes that the DAF based RN/Ct always has enough data for transmission to the Pr and that its memory is always sufficient for storing the data arriving from the Pt.

5.5 Maximizing the Sum Rate of Matched Primary Users

In this section, we considered the optimization problem discussed in Section 5.3, which aims for maximizing the sum rate of matched PUs, and the corresponding weight are shown in Eq. (5.16). Then, the optimization problem of Eq. (5.15) can be rewritten as :

$$\max_{M,T} \sum_{l=1}^{L_{PU}} \sum_{k=1}^{L_{CU}} \beta_{l,k} C_{l,k}^{PU} m_{l,k} , \tag{5.30}$$

$$\begin{aligned} s.t. \quad & (a) \beta_{l,k} C_{l,k}^{PU} \geq R_{l,req}^{PU} , \forall l \forall k \\ & (b)(1 - \beta_{l,k}) C_{l,k}^{CU} \geq R_{k,req}^{CU} , \forall l \forall k \\ & (c) 0 \leq \beta_{l,k} \leq 1 , \forall l \forall k \\ & (d) \sum_{l=1}^{L_{PU}} m_{l,k} \leq 1 , \forall k \\ & (e) \sum_{k=1}^{L_{CU}} m_{l,k} \leq 1 , \forall l . \end{aligned} \tag{5.31}$$

The purpose of this section is twofold. First, we proposed a distributed algorithm, namely the PDA, for efficient spectrum access, invoking cooperation amongst the PUs for obtaining an improved performance for all PUs. Additionally, this PDA is formulated as a punishment based repeated game for attaining equilibrium. Secondly, we extended the repeated game concept to both the idealized perfect capacity-achieving coding scheme and to an attractive practical adaptive coded modulation scheme. The simulation results will show that our proposed PDA algorithm is a sub-optimal solution of Eq. (5.30) by comparing it to the optimal solution, which is obtained by the centralized algorithm.

5.5.1 The Matching Algorithm

In this section, we briefly highlight the matching algorithm [98] invoked for determining the spectral access for each (Pt, Pr) and (Ct, Cr) pair.

5.5.1.1 Preference Lists

Before any offer is made to the CUs, the PUs construct a preferred list of CUs, which can satisfy the PU's rate requirement. Specifically, each Pt has a preference list of Cts/RN that may assist in relaying its message, so that its achievable sum rate becomes higher than its minimum sum-rate requirement. Thus, the preference list for Pt_l is given by:

$$PULIST_l = \left\{ (Ct_{\kappa(k)}, Cr_{\kappa(k)}) \right\}_{k=1}^{L_{CU}}, \tag{5.32}$$

where the function $\kappa(k)$ satisfies the following conditions:

$$R^{PU}_{l,\kappa(k)}(\beta_{l,\kappa(k)}) > R^{PU}_{l,req},\ k \in (1,\ldots,L_{CU}). \tag{5.33}$$

The index of the CUs may be recorded in the PULIST, while their corresponding rate has satisfied the PU's rate requirement. Additionally, we have assumed that the first $\mathrm{Ct}_\kappa(k)$ at the top of the $PULIST_l$ provides the highest rate $R^{PU}_{l,\kappa(k)}(\beta_{l,\kappa(k)})$. Similarly, each CU also has its preferred PU list, and if it transmits in the spectral band occupied by the preferred PUs then its achievable transmission rate is higher than its minimum sum-rate requirement, $R^{CU}_{k,req}$. Thus, the preference list for Ct_k is given by:

$$CULIST_k = \left\{ (Pt_{\iota(l)}, Pr_{\iota(l)}) \right\}_{l=1}^{L_{PU}}, \tag{5.34}$$

where the function $\iota(l)$ satisfies the following conditions:

$$R^{CU}_{\iota(l),k}(\beta_{\iota(l),k}) > R^{CU}_{k,req},\ l \in (1,\ldots,L_{PU}). \tag{5.35}$$

Again, the ordering of the CULIST_k also range from the highest to the lowest.

5.5.1.2 Centralized Algorithm

In the Centralized Algorithm (CA), we consider all possible matching of the (Pt, Pr) and (Ct, Cr) pairs, and then select that particular matched pair, which has the maximum sum rate refer to Eq. (5.30). In our system, we aim for ensuring that each PU pair and CU pair has satisfied its minimum rate requirement. By referring to Eq. (5.30), it becomes plausible that the optimization problem is non-linear and requires an exhaustive search over all possible matching pairs and TS allocation combinations. If the PUs and CUs always want to maximize their own utilities, then the outcome of the optimization problem may not be in the best interests of at least one of those users, hence the centralized approach may not be ideal. When the optimization problem is solved, the

resultant matching information relating the PUs and CUs to each other will have to be transmitted to the corresponding users. The amount of overhead required for this side-information increases with the number of users, which may become excessively high, rendering it impractical. More specifically, the centralized algorithm relies on an exhaustive search method that imposes the highest number of operations for the sake of finding the optimum solution. Therefore, the centralized algorithm imposes the highest complexity. In this section, we give higher priority to the PUs and focus our attention on maximizing the PUs' utility. Let us consider a specific example which has $L = 2$ PUs and $K = 3$ CUs. Note that we have listed all possible matching pairs between these two PUs and three CUs in Table CA-1 as shown in Figure 5.4. The notation $m_{l,k}$ represents the matching pair between the lth PU and the kth CU. The notation P_i of Figure 5.4 defines the sum rate of matched PUs among the corresponding matching pairs. For example, P_1 is the corresponding sum rate of PU_1 and PU_2, while PU_1 is matched to CU_1 and PU_2 is matched to CU_2. In the CA algorithm, we would select the final matched pair, which has the highest value of P_i according to Table CA-1 of Figure 5.4.

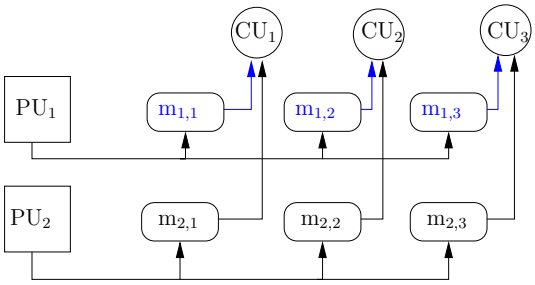

P_1	$m_{1,1}$	$m_{2,2}$
P_2	$m_{1,1}$	$m_{2,3}$
P_3	$m_{1,2}$	$m_{2,1}$
P_4	$m_{1,2}$	$m_{2,3}$
P_5	$m_{1,3}$	$m_{2,1}$
P_6	$m_{1,3}$	$m_{2,2}$

Table CA−1 all possible matching pairs

Figure 5.4: An example to illustrate the CA algorithm.

5.5.1.3 Conventional Distributed Algorithm

The key idea of CDA algorithm is that each (Pt, Pr) pair trades with a particular (Ct, Cr) pair for the sake of attaining mutual benefits in the context of cooperative relaying. This trading will be carried out by negotiating the specific number of TSs allocated, namely the value of $\beta_{l,k}$. The PUs are willing to allow the CUs to transmit using the PU-resources in exchange for the CUs' assistance in transmitting the PUs' message within the number of TSs allocated, namely $\beta_{l,k}$. This would reduce the transmission duration and save power for the PU, while the CU may be granted a time-slot duration of $(1-\beta_{l,k})$ for transmitting its own information. The specific details of the algorithm are summarized in Figure 5.5. The first step is initialization, where we initialize the number of TSs allocated as $\beta_{l,k} = \beta_{init}$. Then we set the value of the TS step counter to τ. We construct $PULIST_l$ and $CULIST_k$ based on the initialized value β_{init}. Step 2 and Step 3 in Figure 5.5 aim for finding a CU pair suitable for each PU pair. As an example, a $\beta_{l,k}$ offer is given by Pt_l to the top Ct_k in its preference list $PULIST_l$, which grants for the Ct_k a TS of $(1-\beta_{l,k})T$ duration for the CU's own transmission. When this Ct_k received an offer, it has two options, namely either to reject the offer, if the Pt_l is not in Ct_k's $CULIST_k$ or to accept, provided that this Pt_l is in the $CULIST_k$, which leads

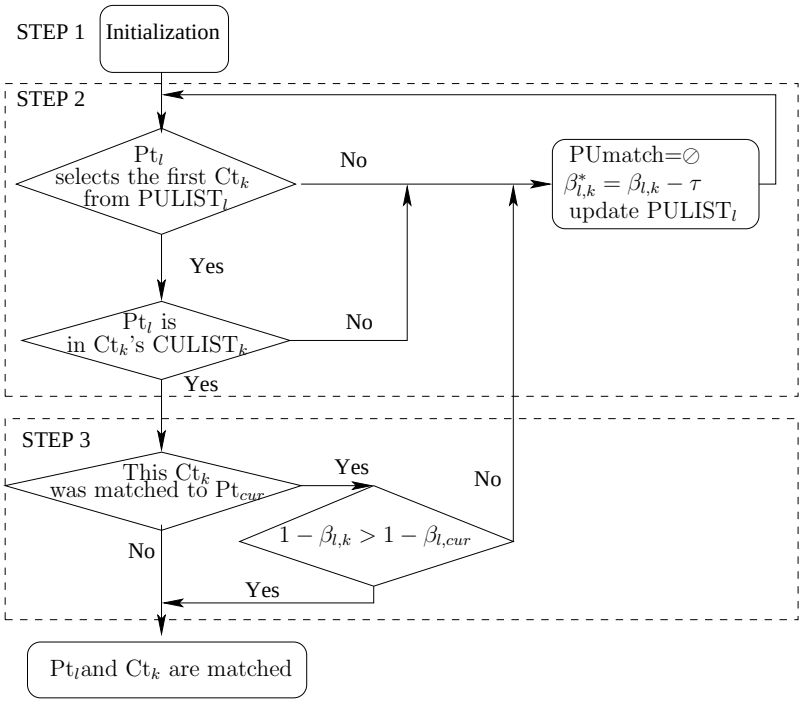

Figure 5.5: The flow-chart of CDA

to the matching of (Pt_l, Pr_l) and (Ct_k, Cr_k). If this intended Ct_k has already been matched to Pt_{cur}, and this Pt_{cur} failed to provide a higher rate for Ct_k, i.e. in terms of Eq. (5.9), if we have

$$R^{CU}_{l,cur}(\beta_{l,cur}) < R^{CU}_{l,k}(\beta_{l,k}) \,, \tag{5.36}$$

then the Ct_k will discard its current matching in favour of the new matching. Moreover, the rejected Pt_{cur} will update the number of TSs allocated by setting it to

$$\beta^*_{l,cur} \;\; = \;\; \beta_{l,cur} - \tau \,. \tag{5.37}$$

and then it will reconstruct its preference list based on $\beta^*_{l,cur}$ and repeat the matching. This algorithm aims for finding the specific number of TSs to be allocated, which can be accepted both by the (Pt_l, Pr_l) as well as by the (Ct_k, Cr_k) pairs, and the algorithm will be terminated when each PU pair has found its appropriate matched pair, provided that both their rate requirements can be satisfied. More specifically, the CDA constitutes a non-cooperative scheme, where none of the PUs cooperates. Instead, they compete with each other, with the selfish objective of maximizing their own rate. Let us denote the average rate of PU_l in CDA as:

$$r^S_l = E\left[R^S_l\right] \,, \tag{5.38}$$

where $E[.]$ is the expected value of $[.]$, the superscript S indicates the selfish nature of the CDA and R^S_l is the instantaneous rate of PU_l during a particular transmission. In order to explicitly portray the process of this algorithm, we conceived a simple example, which has two PUs and two CUs as shown in Figure 5.6. Each PU has its preference list and its minimum rate requirement

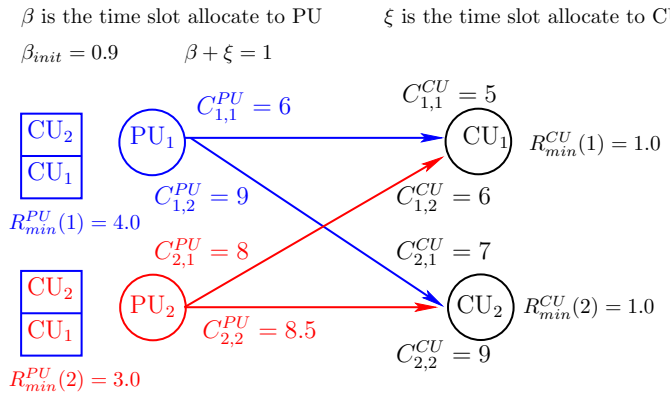

$\tau = 0.1$		R^{PU}	R^{CU}	
Step1	$PU_1 \longrightarrow CU_2$	$8.1 > 4$	$0.7 < 1$	✗
Step2	$PU_2 \longrightarrow CU_2$	$7.65 > 3$	$0.9 < 1$	✗
Step3	$PU_1 \longrightarrow CU_2$	$7.2 > 4$	$1.4 > 1$	✓
Step4	$PU_2 \longrightarrow CU_2$	$6.8 > 3$	$1.8 > 1$	✓
Step5	$PU_1 \longrightarrow CU_2$	$6.3 > 4$	$2.1 > 1$	✓
Step6	$PU_2 \longrightarrow CU_2$	$5.95 > 3$	$2.7 > 1$	✓
Step7	$PU_1 \longrightarrow CU_2$	$5.4 > 4$	$2.8 > 1$	✓
Step8	$PU_2 \longrightarrow CU_2$	$5.1 > 3$	$3.6 > 1$	✓
Step9	$PU_1 \longrightarrow CU_1$	$5.4 > 4$	$0.5 < 1$	✗
Step10	$PU_1 \longrightarrow CU_1$	$4.8 > 4$	$1 >= 1$	✓

Table A

Final matched pairs

$PU_1 \longrightarrow CU_1$	$R^{PU} = 4.8$	$R^{CU} = 1.0$
$PU_2 \longrightarrow CU_2$	$R^{PU} = 5.1$	$R^{CU} = 3.6$

Table B

$r^S_l = 4.95$

Figure 5.6: A example to illustrate the CDA algorithm.

$R^{PU}_{min}(l)$, $l \in L$. Note that the PU's achievable sum rate would not be satisfied, if it is lower than the minimum rate requirement. Each PU makes an offer to its most favored CU. If a CU receives two offers, it would select the one that may provide a higher TS for itself. The TS allocated to the CU of Figure 5.6 is denoted by ξ, where we have $\xi = 1 - \beta$. In our example, CU_2 is the top candidate in the PULISTs of PU_1 and PU_2. As shown in Table A of Figure 5.6, during Step1 and Step2 both PU_1 and PU_2 make their offers to CU_2 with the initial TS allocation of $\beta_{init} = 0.9$. Additionally, CU_2 chose PU_2 at Step8 by rejecting its initial match to PU_1 during Step7. This is because choosing PU_2 may provide $R^{CU}_{2,2} = C^{CU}_{2,2}\xi = 9 \times (1 - 0.6) = 3.6$ (which is higher than $R^{CU}_{2,1} = C^{CU}_{2,1}\xi = 7 \times (1 - 0.6) = 2.8$ gleaned from PU_1) for CU_2. Specifically, the value of β would be reduce to 0.6 (where $\beta_{init} - 3\tau = 0.9 - (3 \times 0.1) = 0.6$) if the first offer in the previous step is not accepted. In the CDA, PU_1 and PU_2 will compete with each other by increasing the TS of ξ and by reducing the value of β, until one of them loses out, when its TS offers would result in $R^{PU}_{l,k} < R^{PU}_{min}$. Hence, if two PUs are in favor of the same CU, the competition would fail to bring about any benefits for the competing PUs. The final matched pairs are shown in Table B of Figure 5.6. Hence the average rate of PU_l of this example is $r^S_l = \frac{4.8+5.1}{2} = 4.95$.

5.5.1.4 The Proposed Pragmatic Distributed Algorithm

As mentioned in the CDA of Section 5.5.1.3, the selected Ct will reject its current matching in favour of a new matching, whenever the new matching pair is capable of providing a higher rate for the Ct. We found that there is a drawback associated with this procedure. Assuming that there are two PUs in the system, namely Pt_1 and Pt_2 and that Ct_k is capable of satisfying the minimum PU rate requirements of both Pt_1 as well as Pt_2, then both Pt_1 and Pt_2 would list Ct_k in their preference lists of PULIST_1 and PULIST_2. Then Pt_1 and Pt_2 will both make offers to this Ct_k. Following this, there is a competition between Pt_1 and Pt_2. Assuming that Pt_1 won and hence Pt_2 was discarded. Then Pt_2 will update the number of allocated TS in order to offer a higher rate for the CU at the cost of a lower rate for Pt_2 according to the updated TS, $\beta^*_{l,cur} = \beta_{l,cur} - \tau$. Furthermore, it is possible that the two Pts would still be in favour of the same Ct_k after they have updated their preference lists. After the competition, the final matched (Pt_l, Pr_l) and (Ct_k, Cr_k) pair will grant a lower TS allocation to Pt_l resulting in a lower rate for the matched PU.

For the sake of ameliorating this particular situation in order to achieve higher total and individual profits for the matched PUs, we have proposed the PDA that aims for maximizing the utility of the matched PU. More specifically, our PDA is a cooperative scheme, where all PUs forms a grand coalition [218]. A *game unit* is constituted by L_{PU} rounds and each round has L_{PU} transmissions, where the PUs take turns to select the best available CU according to a round-robin type priority access list. The priority access list of the ith round is given by:

$$ALIST_i \quad = \quad \{Pt_i, Pt_{i\oplus 1}, \ldots, Pt_l, \ldots, Pt_{i\oplus(L_{PU}-1)}\}\,, \tag{5.39}$$

where $i = \{1, 2, \ldots, L_{PU}\}$ and the subscript of Pt_l for the jth transmission ($j = \{1, 2, \ldots, L_{PU}\}$) in the ith round is based on the modulo-L_{PU} summation:

$$l = i \oplus (j-1) = (i + (j-1)) \mod L_{PU}\,. \tag{5.40}$$

Hence, we have $ALIST_1 = \{Pt_1, Pt_2, Pt_3 \ldots, Pt_{L_{PU}}\}$ and $ALIST_2 = \{Pt_{L_{PU}}, Pt_1, Pt_2, \ldots, Pt_{L_{PU}-1}\}$. The first Pt in the $ALIST_i$ has the first priority to select its best CU. Then the second Pt in the list selects the best available CU from the remaining set of CUs, while the third Pt in the list selects its best available CU afterwards and the same procedure is invoked for the rest of the Pts in the list. During the next round, the first Pt in $ALIST_i$ will become the second Pt in $ALIST_{i+1}$, while the last Pt in $ALIST_i$ is now the first Pt in $ALIST_{i+1}$ according to the round-robin scheduling. Hence, after L_{PU} rounds each PU is guaranteed to have access to $\min\{L_{PU}, L_{CU}\}$ CUs amongst the top CUs in its PULIST[3], but is has no access to any CUs for the remaining $(L_{PU} - L_{CU})$ transmissions. In this way, the PUs give up any futile competition and cooperatively take turns, one at a time, to access the available CUs, which is expected to yield the most benefits for themselves. If none of the CUs in the current list may be satisfied, then only this specific Pt will update its TS allocation and then produces a new preference list. The proposed PDA has a low complexity because it does not require any exchange of information amongst the PUs, such as their rates. The first access list

[3]Provided that the rate requirements in Eq. (5.33) and Eq. (5.35) are satisfied.

$ALIST_1$ can be distributed at the beginning of the game by the base-station or by a PU acting as a cluster-head and the remaining lists can be computed locally by each PU. Then the PDA can be repeated automatically as many times as needed. Hence, each PU is guaranteed to have access to its top CU at least $1/L_{PU}$ times[4] on average. Let us now consider the specific example as shown in Figure 5.7, which has the same parameters as those of Figure 5.6, where we have two PUs and

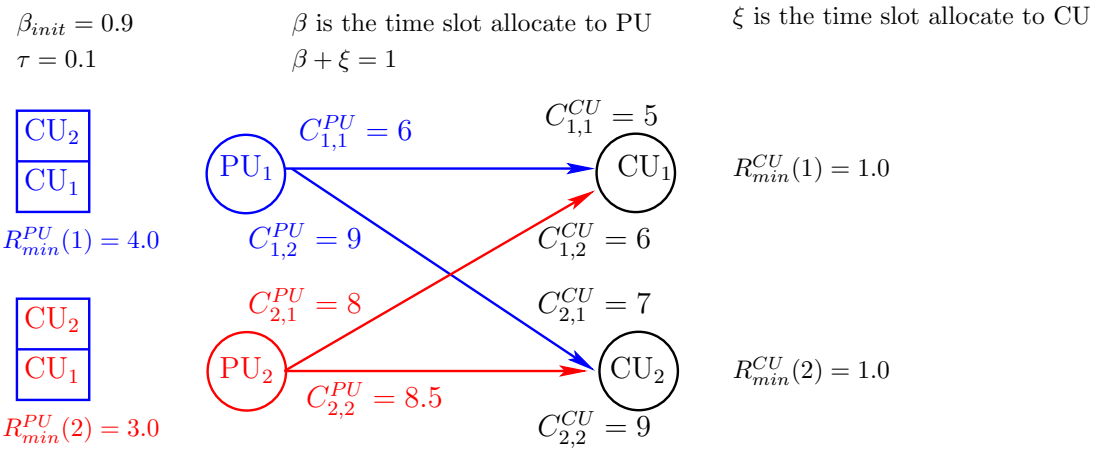

Round 1

		R^{PU}	R^{CU}	
Step1	$PU_1 \longrightarrow CU_2$	$8.1 > 4$	$0.7 < 1$	×
Step2	$PU_1 \longrightarrow CU_2$	$7.2 > 4$	$1.4 > 1$	✓
Step3	$PU_2 \longrightarrow CU_1$	$7.2 > 3$	$0.6 < 1$	×
Step4	$PU_2 \longrightarrow CU_1$	$6.4 > 3$	$1.2 > 1$	✓

Table A

Round 2

		R^{PU}	R^{CU}	
Step1	$PU_2 \longrightarrow CU_2$	$7.65 > 3$	$0.9 < 1$	×
Step2	$PU_2 \longrightarrow CU_2$	$6.8 > 3$	$1.8 > 1$	✓
Step3	$PU_1 \longrightarrow CU_1$	$5.4 > 4$	$0.5 > 1$	×
Step4	$PU_1 \longrightarrow CU_1$	$4.8 > 4$	$1 >= 1$	✓

Table B

Matched pairs of Round 1

$PU_1 \longrightarrow CU_2$	$R^{PU} = 7.2$	$R^{CU} = 1.4$
$PU_2 \longrightarrow CU_1$	$R^{PU} = 6.4$	$R^{CU} = 1.2$

$R^C_l = 6.8$

$r^C_l = 6.3$

Matched pairs of Round 2

$PU_2 \longrightarrow CU_2$	$R^{PU} = 6.8$	$R^{CU} = 1.8$
$PU_1 \longrightarrow CU_1$	$R^{PU} = 4.8$	$R^{CU} = 1$

$R^C_l = 5.8$

Figure 5.7: A example to illustrate our proposed PDA algorithm.

two CUs. Hence the CDA and PDA of Figure 5.6 and Figure 5.7 can be directly compared. Our game unit has $L_{PU} = 2$ rounds and each round has $L_{PU} = 2$ transmissions. The first round of our game is shown in Table A of Figure 5.7. At Step 1 of Round 1, PU_1 has a higher priority to select its best candidate CU_2, which allows PU_1 to update its TS allocation, until they become matched at Step 2 of Round 1 of Figure 5.7. After that, PU_2 selects its best candidate from the CUs which are not matched, thus the unmatched CU_1 has been chosen and the Round 1 match was successfully carried out at step 4. Now, at Round 2, PU_2 acquired a higher priority to select its top candidate CU_2 at Step 1 of Table B in Figure 5.7. Meanwhile, PU_1 selects the remaining CU_1 at Step 3 of Table B. Moreover, the expectation of the average rate of the PUs for these two rounds is $r^C_l = \frac{6.8+5.8}{2} = 6.3$, which higher than that of the CDA of Figure 5.6. Hence we have $r^C_l > r^S_l$.

[4]The PU would have access to its top CU in all L_{PU} rounds, if this CU is not sought after by other PUs.

Note that with reference to Eq. (5.23), the maximum TS allocation representing the maximum transmission period for the PU can be derived from Eq. (5.35) as:

$$\beta_{l,k}^{\max} = 1 - \frac{R_{k,req}^{CU}}{\log_2\left[1+\gamma_{CU}|h_{Ct_k,Cr_k}^{(l)}|^2\right]}, \tag{5.41}$$

while the minimum TS allocation can be computed from Eq. (5.4) and Eq. (5.5) as:

$$\beta_{l,k}^{\min} = \frac{R_{l,req}^{PU}}{C_{PU_{l,k}}}. \tag{5.42}$$

Referring to the flow chart of our PDA in Figure 5.8, the specific details of the algorithm can be

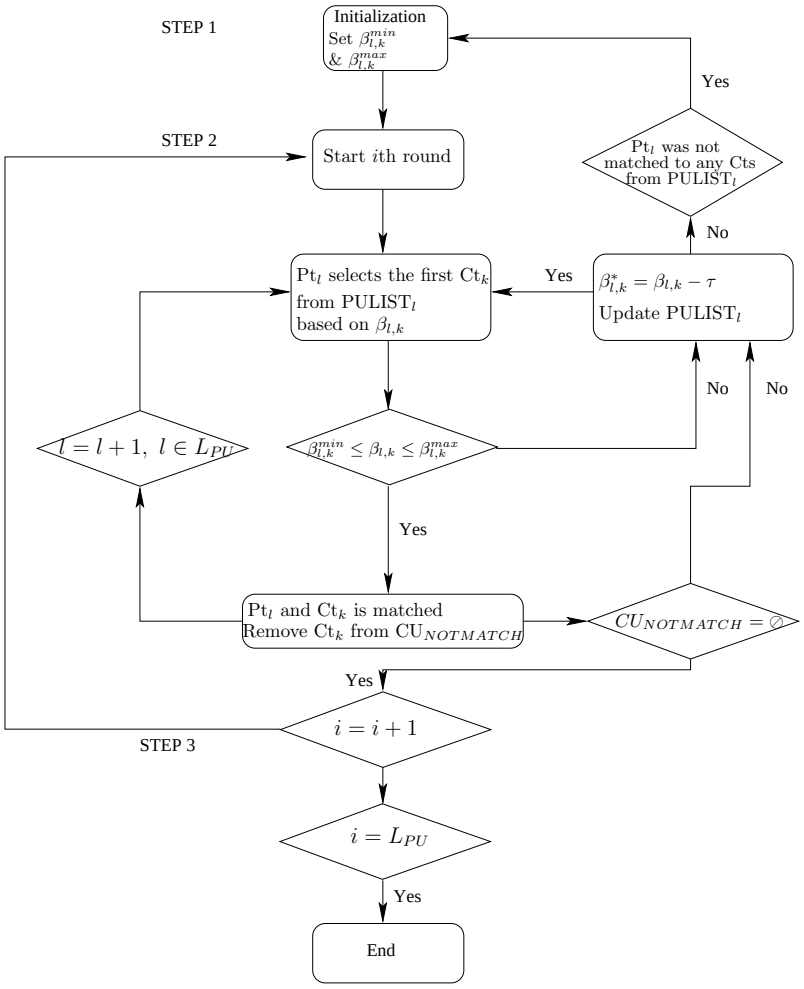

Figure 5.8: The flow chart of PDA

summarized as follows:

1. Initialization:
   (a) Set up the first priority list $ALIST_1 = \{Pt_1, Pt_2, \ldots, Pt_{L_{PU}}\}$ and broadcast it to all PUs.
   (b) Each Pt computes the remaining priority lists $ALIST_i$ for $i = \{2, 3, \ldots, L_{PU}\}$, based on the round-robin method given in Eq. (5.39).
   (c) Compute $\beta_{l,k}^{\min}$ and $\beta_{l,k}^{\max}$.

(d) Set $i = 1$ for the first round.

2. Do the matching for the ith round:

(a) Set the initial TS allocations to β_{init}, and set the step size of TS increment to τ.

(b) Construct PULIST$_l$ according to Section 5.5.1.1 based on β_{init}, where $l = \{1, \ldots, L_{PU}\}$.

(c) Construct CU$_{NOTMATCH} = \{Ct_1, \ldots, Ct_{L_{CU}}\}_{l=1}^{L_{CU}}$ to list all participating Cts.

(d) Set $j = 1$ for the first transmission.

(e) Do the matching for the jth transmission:

i. Find the corresponding Pt$_l$ for transmission, where $l = (i + (j-1)) \mod L_{PU}$.

ii. Pt$_l$ selects the best available Ct$_k$ from CU$_{NOTMATCH}$ based on PULIST$_l$:

- Pt$_l$ offers $\beta_{l,k}$ to Ct$_k$.
- If $\beta_{l,k}^{\min} \leq \beta_{l,k} \leq \beta_{l,k}^{\max}$, then (Pt$_l$, Pr$_l$) and (Ct$_k$, Cr$_k$) are matched. Remove Ct$_k$ from CU$_{NOTMATCH}$. If CU$_{NOTMATCH} \in \emptyset$ go to Step 3, else go to Step 2f.
- Otherwise, reduce the TS allocation to $\beta_{l,k} = \beta_{l,k} - \tau$ and update PULIST$_l$.
- If PULIST$_l$ is empty then Pt$_l$ is left unmatched and proceed to Step 2f.
- Otherwise, find another match at Step 2(e)ii.

(f) Set $j = j + 1$ and go to Step 2e for the next transmission, until $j = L_{PU}$.

3. Set $i = i + 1$ and go to Step 2 for the next round, until $i = L_{PU}$.

4. Terminate the game or repeat the game from Step 1 until no more transmission is needed.

The rate of PU$_l$ averaged over L_{PU} transmissions in the ith round can be computed as:

$$R_l^C = \frac{1}{L_{PU}} \sum_{i=1}^{L} R_{l,\kappa(i)}^{PU}(\beta_{l,\kappa(i)}) \,, \tag{5.43}$$

where the superscript C signifies the cooperative nature in PDA, $L = \min\{L_{PU}, L_{CU}\}$ and $\kappa(i)$ is the index of the best available Ct which satisfies the rate conditions of Eq. (5.33) and Eq. (5.35) during the ith round, while $R_{l,\kappa(i)}^{PU}(\beta_{l,\kappa(i)}) = 0$ if $\kappa(i) \in \emptyset$. Hence, the average rate of PU$_l$ after many repetitions is given by:

$$r_l^C = E\left[R_l^C\right] \,. \tag{5.44}$$

The proposed PDA does not require any exchange of the PU's rate information and we assume a practical time-varying wireless channel, which may change for each transmission round and the users are also allowed to move. According to the law of large numbers, once the PDA has been repeated a sufficiently high number of times, all PUs will achieve the same average PU rate due to having random channel conditions[5]. More explicitly, Figure 5.9 shows that when the PDA is repeated $N \geq 100$ times, the individual rates of PU$_1$ and PU$_8$ in the CCR scheme would converge to the same value. This was verified for a range of scenarios having different numbers of CUs, while the number of PUs is fixed to $L_{PU} = 8$. Similar trends were also observed for the other 6 PUs. Hence, the PDA is fair to all PUs, because their individual rates converged to the same value of r_l^C after a sufficient number of repetitions.

[5]User mobility is considered in the channel.

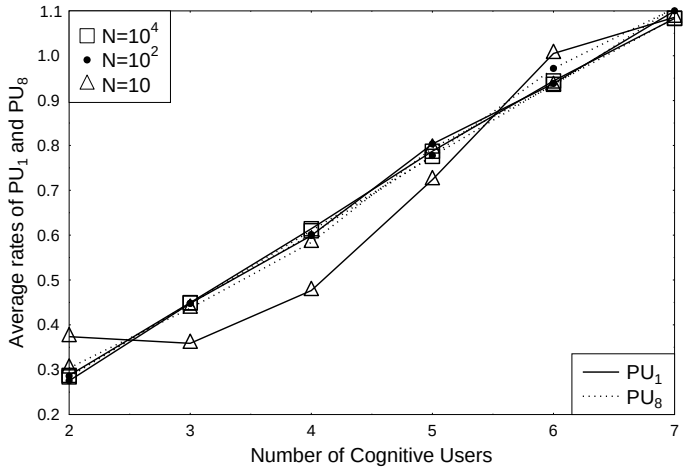

Figure 5.9: Performance of PU_1 and PU_8 in the **CCMC** aided **AAF based** CCR scheme when the PDA is invoked. The transmit SNRs of PU and CU are $\gamma_{PU} = 10$ dB and $\gamma_{CU} = 25$ dB, respectively. The number of PUs is $L_{PU} = 8$ and the Rayleigh fading channel condition changes for each transmission round. The number of repetitions considered in the game are $N = \{10, 10^2, 10^4\}$.

5.5.1.5 Random Algorithm

For the Random Algorithm (RA), each Pt will make an offer β to a Ct, which is randomly selected from its preference list. The selected Ct will choose that specific matching pair, which provides an increased CU sum rate, whilst discarding the one having a lower sum rate. More specifically, we followed the approach adopted in [98], where this β value is fixed for all PU and SU pairs and it was chosen experimentally for the sake of maximizing the average PU sum-rate. This RA is used for benchmarking both the CDA and the proposed PDA. Note that the CA and the RA represent the two extremes in terms of their overhead and the complexity imposed.

5.5.2 Repeated Game

The CDA was shown in [98] to create a stable matching, which exhibits a *competitive equilibrium*, when all the PUs are non-cooperative. If we consider a 'single-shot' game, where each PU only cares about its current payoff, then no individual PU would have the incentive to deviate from the CDA strategy. Hence, the CDA may be deemed to be a strategy that arrives at an equilibrium for the one-shot non-cooperative game, having an expected one-shot payoff of R_l^S given in Eq. (5.38). However, spectrum sharing between PUs and CUs may last for a long period of time, which may be viewed as a game repeated for many rounds, in which the PUs can cooperate based on their individual reputation and their mutual trust. More specifically, the proposed PDA is capable of guaranteeing a higher individual average PU rate compared to that of the CDA due to the avoidance of competition among the PUs. As shown in Section 5.5.3, the PDA outperforms the CDA, especially when the number of CUs is lower than that of the PUs. However, a PU using the PDA

may be tempted to abandon cooperation for the sake of gaining a higher instantaneous rate. Hence, we considered a penalty/punishment based repeated game [84, 215, 216], where the PUs (players) have incentives to cooperate for the sake of achieving a higher expected payoff (average PU rate), while any non-cooperative behavior can be avoided by appropriate punishment over a carefully selected limited period. Although the PDA may not converge to a stable equilibrium in a single-shot game, it does converge to an equilibrium in the repeated game enforced by the threat of punishment. If any of the PUs opts out of cooperation in the PDA, all PUs would revert to the non-cooperative CDA for a period of sufficiently long duration. This punishment would discourage opting out and would help to maintain cooperation.

More explicitly, the payoff of PU$_l$ in a repeated game is defined as the sum of payoffs of PU$_l$ discounted over time according to [215]:

$$U_l = (1-\delta)\sum_{i=1}^{\infty}\delta^i R_l^C[i]\,, \tag{5.45}$$

where δ ($0<\delta<1$) is the discount factor and $R_l^C[i]$ is the average rate of PU$_l$ defined in Eq. (5.43) for the ith round. When we have $\delta \to 1$, the PU is more patient and hence any future reward is weighed identically to the current payoff. Hence, the PU will constrain its current behavior in the interest of maintaining a good reputation. Let us denote the discounted payoff for cooperation in the PDA as U_l^C and that for opting out of cooperation (deviation) in the CDA as U_l^D. Then the following proposition[6] suggests that both U_l^C and U_l^D would converge to their means. Hence, it is better to maintain cooperation for each PU's benefit, as long as, we have $r_l^C > r_l^S$.

Proposition 1. As we have $\delta \to 1$, the instantaneous payoff U_l^C would converge to the expected payoff r_l^C while the current payoff U_l^D would converge to the averaged payoff r_l^S.

On the other hand, imposing an infinite-duration punishment is not efficient for all PUs, because all of them would be punished and would only result in a reduced PU rate of r_l^S. Explicitly, a *limited-duration punishment* [215] is a more efficient way of preventing non-cooperation, as long as the punishment is long enough to negate the one-time non-cooperation gain. If any PU deviates from cooperation in the PDA, then all PUs would revert to the non-cooperative CDA for the next T_p instances. Next, we show in the following proposition[7] that the limited-duration punishment based cooperation in PDA also has a perfect subgame equilibrium, which ensures optimality for subgames starting from any round of the entire repeated game.

Proposition 2. Provided that $r_l^C > r_l^S$ for all l, $l \in \{1,2,\ldots,L_{PU}\}$, we have $\tilde{\delta} < 1$, so that for a sufficiently large discount factor $\delta > \tilde{\delta}$, the game has a perfect subgame equilibrium with a discounted utility of r_l^C, provided that all players are governed by the limited-punishment strategy.

The punishment period duration T_p can be determined by analysing the conditions under which a PU would abandon cooperation at instant T^*. Consider the extreme case, where the payoff of PU$_l$ at instant T^* would be $R_{l,req}^{PU} = C_{PU}^*$ of Eq. (5.8), when no CU was matched to PU$_l$ under the PDA,

[6] The proof is given in Appendix A.

[7] The proof is given in Appendix B.

while the deviation gain[8] would be $\tilde{R}_l^D$. The expected discounted payoff for PU_l derived for their non-cooperative actions is bounded by:

$$u_l^D = E[U_l^D] \leq (1-\delta) \times \left(\overbrace{\sum_{i=1}^{T^*-1} \delta^i r_l^C}^{\text{All PUs are in a cooperation}} + \overbrace{\delta^{T^*} \tilde{R}_l^D}^{\text{PU}_l \text{ abandon's cooperation}} + \overbrace{\sum_{i=T^*+1}^{T^*+T_p} \delta^i r_l^S}^{\text{Deviated PUs are in punishment}} + \overbrace{\sum_{i=T^*+T_p+1}^{\infty} \delta^i r_l^C}^{\text{PUs are in cooperation after punishment}} \right), \quad (5.46)$$

while that in case of cooperation is bounded by:

$$u_l^C = E[U_l^C] \geq (1-\delta) \times \left(\overbrace{\sum_{i=1}^{T^*-1} \delta^i r_l^C}^{\text{All PUs are in a cooperation}} + \overbrace{\delta^{T^*} R_{l,req}^{PU}}^{\text{Direct transmission}} + \overbrace{\sum_{i=T^*+1}^{T^*+T_p} \delta^i r_l^C}^{\text{PUs are in cooperation}} + \overbrace{\sum_{i=T^*+T_p+1}^{\infty} \delta^i r_l^C}^{\text{PUs are in cooperation}} \right). \quad (5.47)$$

A selfish PU would prefer a strategy that can provide an increased payoff. It can be shown based on Eq. (5.46) and Eq. (5.47) that the requirement of $u_l^C > u_l^D$ for all l can be satisfied by:

$$\begin{aligned} &\max_l (1-\delta) \times \left(\sum_{i=1}^{T^*-1} \delta^i r_l^C + \delta^{T^*} R_{l,req}^{PU} + \sum_{i=T^*+1}^{T^*+T_p} \delta^i r_l^C + \sum_{i=T^*+T_p+1}^{\infty} \delta^i r_l^C \right) \\ &> \min_l (1-\delta) \times \left(\sum_{i=1}^{T^*-1} \delta^i r_l^C + \delta^{T^*} \tilde{R}_l^D + \sum_{i=T^*+1}^{T^*+T_p} \delta^i r_l^S + \sum_{i=T^*+T_p+1}^{\infty} \delta^i r_l^C \right). \quad (5.48) \end{aligned}$$

After removing the identical terms from Eq. (5.48), we arrive at:

$$\frac{\sum_{i=T^*+1}^{T^*+T_p} \delta^i}{\delta^{T^*}} > \max_l \frac{\tilde{R}_l^D - R_{l,req}^{PU}}{r_l^C - r_l^S}, \quad (5.49)$$

where the term $\frac{\sum_{i=T^*+1}^{T^*+T_p} \delta^i}{\delta^{T^*}}$ can be transformed to: $\sum_{i=T^*+1}^{T^*+T_p} \delta^{(i-T^*)} = \sum_{i=1}^{T_p} \delta^i$, which would further lead to the following condition

$$\sum_{i=1}^{T_p} \delta^i > \max_l \frac{\tilde{R}_l^D - R_{l,req}^{PU}}{r_l^C - r_l^S}, \quad (5.50)$$

where we have $\sum_{i=1}^{T_p} \delta^i \to T$, when $\delta \to 1$. Hence, the punishment period is bounded by:

$$T_p > \max_l \frac{\tilde{R}_l^D - R_{l,req}^{PU}}{r_l^C - r_l^S}. \quad (5.51)$$

[8]We assume a hypothetical scenario, where PU_l is capable of predicting its payoff (PU_l rate) under CDA, although the PU rate is only available at the end of the PU competition in the CDA.

In other words, as long as T_p satisfies Eq. (5.51), PU_l would not deviate from the cooperative strategy, since the one-time payoff under the non-cooperative strategy has been negated by punishment, so that we have $u_l^C > u_l^D$.

Hence, the repeated game based on the PDA is capable of providing higher individual PU rates as well as a higher PU sum-rate on average. Hence it is an attractive and stable game, even when no information is available about PU rates.

5.5.3 Performance Results

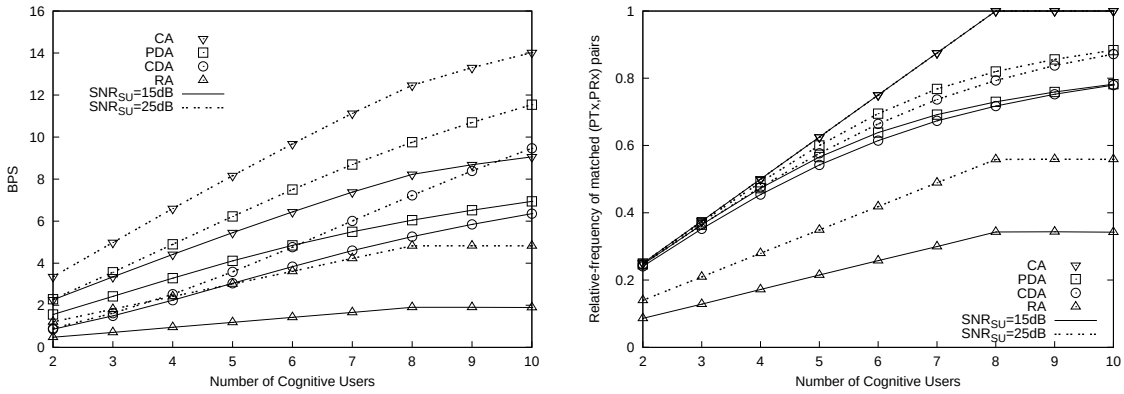

(a) R_{match}^{PU} versus L_{CU}

(b) P_{match} versus the L_{CU}

Figure 5.10: Performance of the **CCMC** aided **AAF based** CCR **benchmark [98]** scheme communicating over block-fading Rayleigh fading channel. A BER below 10^{-5} is maintained. The "CA", "PDA", "CDA" and "RA" techniques were detailed in Section 5.5.1. The transmit SNR of the CU, γ_{CU}, is represented by SNR_{CU}. The parameters are shown in Table 5.2.

Figure 5.10a shows the average total sum-rate of the matched (Pt, Pr) pairs versus the total number of CUs, $L_{CU} = \{2, 3, \ldots, 10\}$, for the proposed CCR scheme, when we have $L_{PU} = 8$. In our evaluation of Eq. (5.5), Eq. (5.8) and Eq. (5.9), we assumed that the transmit SNRs of all CUs are equal, yielding $\gamma_{CU_1} = \cdots = \gamma_{CU_l} = \gamma_{CU}$. We also assumed that the SNR of all PUs are $\gamma_{PU_1} = \gamma_{PU_2} = 10$ dB. The remaining simulation parameters are shown in Table 5.2. We investigate our scheme in conjunction with two different transmit SNRs of the CU, namely for $\gamma_{CU} = 15$ dB and $\gamma_{CU} = 25$ dB. When γ_{CU} is increased, the average total sum-rate of the matched (Pt, Pr) pairs is also increased. We have considered the CDA, the PDA, the CA and the RA of Section 5.5.1.5 in Figure 5.10a. The CA achieves the highest average total sum-rate among these four algorithms, while the RA achieves the lowest sum rate in Figure 5.10a. It is observed in Figure 5.10a that our PDA achieves a higher sum-rate than that of the CDA at the same L_{CU} and γ_{CU}. The PDA consistently attains a higher rate than the CDA for all scenarios. Furthermore, when we have $\gamma_{CU} = 25$ dB and $L_{CU} \leq 3$, the CDA scheme performs slightly worse than the RA

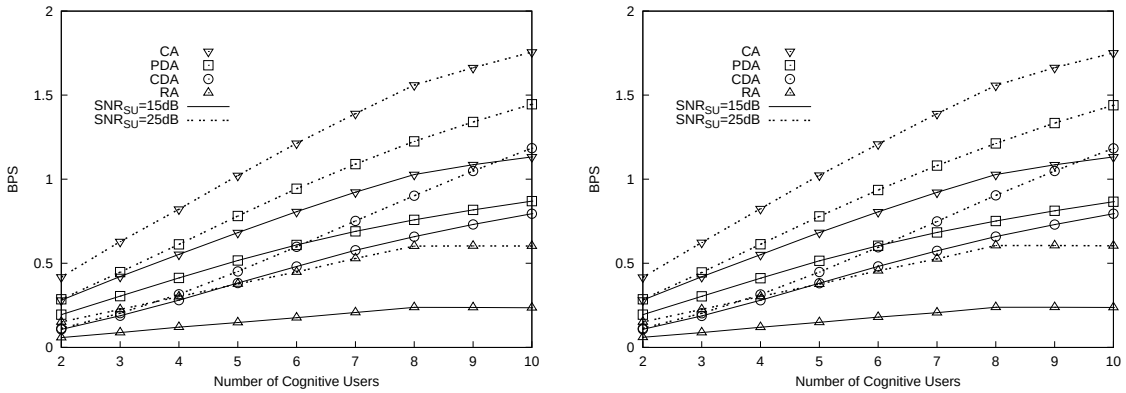

(a) Average Rate of PU_1 (b) Average Rate of PU_8

Figure 5.11: R_{match}^{PU} versus L_{CU} performance of the **CCMC** aided **AAF based** CCR **benchmark [98]** scheme communicating over block-fading Rayleigh fading channel, which has shown two specific PUs' performance of Figure 5.10a. A BER below 10^{-5} is maintained. The "CA", "PDA", "CDA" and "RA" techniques were detailed in Section 5.5.1. The transmit SNR of the CU, γ_{CU}, is represented by SNR_{CU}. The parameters are shown in Table 5.2.

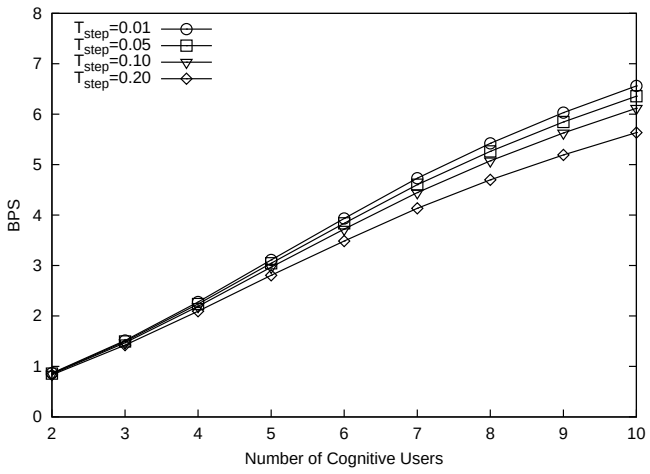

Figure 5.12: Performance of the CDA aided CCR scheme for the **CCMC** capacity. "T_{step}" is the step size τ of the TS-increment. **The transmit SNR of the CU is** $\gamma_{CU} = 15$ **dB**. Additionally, this CDA obeys Figure 5.10a ad the corresponding parameters are shown in Table 5.2.

Modulation	4-PSK, 8-PSK, 16-QAM, 64-QAM
Coding	TTCM
Number of frames	10^5
Channel	Rayleigh fading channel
Total number of CU	$L_{CU} = 10$
Total number of PU	$L_{PU} = 8$
Initialization of β for CDA	$\beta_{init} = 0.99$
Initialization of β for PDA	$\beta_{init} = \beta_{\max}$
Step size of β	$\tau = 0.05$
Pathloss exponent	$\alpha = 4$
Requirement of CU	$R_{req}^{CU} = 2.0$
Requirement of PU	$R_{req}^{PU} = C_{PU}^{*}$
Pathloss	$\varrho = \frac{1}{d^{\alpha}}$

Table 5.2: The parameters of our proposed ATTCM aided CCR scheme.

scheme, due to the competition loss encountered.

Figure 5.10b portrays the expected relative frequency of successfully matched PUs versus the number of CUs, which is evaluated as:

$$P_{match} = \frac{1}{L_{PU}} E\left[\sum_{l}^{L_{PU}} \sum_{k}^{L_{CU}} m_{l,k}\right] . \tag{5.52}$$

It is observed in Figure 5.10b that P_{match} increases upon increasing γ_{CU} and L_{CU}, because a higher sum-rate was achieved by the matched (Pt, Pr) pairs with the aid of cooperative relaying, when there are more CUs available and the channel quality improves. As shown in Figure 5.10b, the P_{match} of the CA is the highest, followed by that of the PDA, CDA and RA. Hence, the rate-improvement observed in Figure 5.10a is linked to a higher P_{match}, resulting from a better matching.

Figure 5.11a and Figure 5.11b show the average total sum-rate of the matched PU_1 and PU_8, versus the total number of CUs, L_{CU}, for the various CCR schemes. As seen from Figure 5.11a, the average individual rate of PU_1 and PU_8 (and of all other PUs as well) has converged to the same curve after a longer simulation consisting of 10^5 transmissions. We observe that the performance of PU_l (for $l \in \{1, \ldots, L_{PU}\}$) is close to that of the CA, when invoking the proposed PDA. By contrast, the rate of PU_l is lower, when employing the CDA because it has to make further sacrifices by reducing its TS $\beta_{l,k}$, when competing with other PUs for the same CU. Furthermore, the rate of PU_l operating under our PDA is lower than that of the CA, but much higher than that of the CDA. Hence, the proposed PDA outperforms the CDA in terms of both the total PU sum rate and the individual PU rate. Moreover, we also consider the corresponding average total sum-rate of all matched (PT, PR) pairs as a function of the step size τ in Figure 5.12. As expected, the total sum-rate decreases upon increasing τ. However, a small τ would lead to a longer matching period.

Hence, we have chosen $\tau = 0.05$ as a compromise.

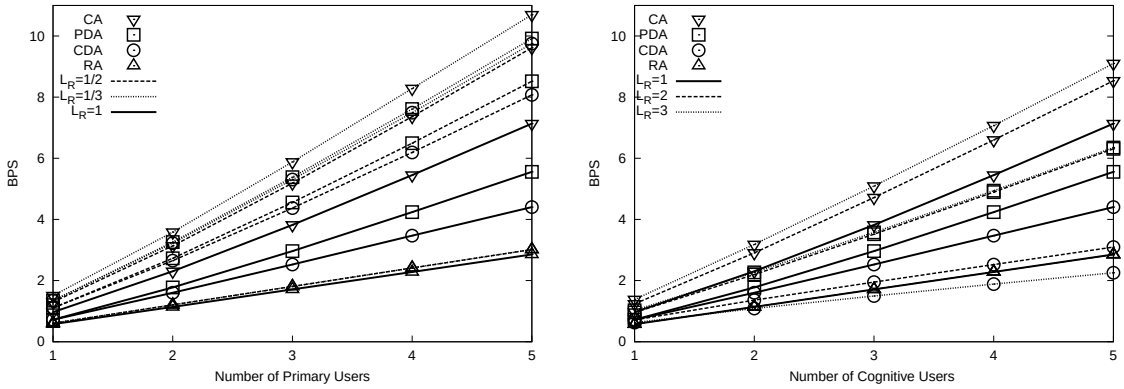

(a) R^{PU}_{match} versus L_{PU} (b) R^{PU}_{match} versus L_{CU}

Figure 5.13: Performance of the **CCMC** aided **AAF based** CCR **benchmark [98]** scheme communicating over quasi-static Rayleigh fading channel. The "CA", "PDA", "CDA" and "RA" techniques were detailed in Section 5.5.1. The initial TS allocation is $\beta_{init} = 0.99$, the step size of TS is $\tau = 0.05$ and $L_R = L_{PU}/L_{CU}$. The parameters are shown in Table 5.2.

Additionally, Figure 5.13 shows the average total sum-rate of the matched (Pt, Pr) for the proposed CCR scheme. We have considered the CDA, the PDA, the CA and the RA in Figure 5.13. The CU's rate is kept to the minimum of $R^{CU}_{k,req} = 2$ bps and the fraction L_R is given by: $L_R = L_{PU}/L_{CU}$. Explicitly, the number of PUs and CUs is identical for $L_R = 1$, while the number of CUs is higher than that of the PUs for $L_R < 1$, and vice versa. The CA achieves the highest average total sum-rate among these four algorithms, while the RA achieves the lowest sum rate in Figure 5.13a. It is observed in Figure 5.13a that our PDA achieves a higher sum-rate than that of the CDA at the same L_{PU}. The PDA consistently attains a higher rate than the CDA for the scenario, where the number of CUs is higher than that of the PUs. As shown in Figure 5.13b, we observe that the rate of PU_l operating under our PDA is lower than that of the CA, but much higher than that of the CDA, when the number of PUs is higher than that of the CUs. Furthermore, when we have $L_R = 3$, the CDA scheme performs slightly worse than the RA scheme, which is a consequence of the competition loss encountered. Moreover, observe in Figure 5.13a and Figure 5.13b, the performance curves of RA are overlapped, since increasing the number of PUs or CUs does not influence its random selection. Additionally, the average individual PU rate was found to be exactly a fraction of $\frac{1}{L_{PU}}$ of the total PU sum rate for all PUs. Thus the trend of the individual PU rate follows the trend of the total PU sum rate. Hence, the proposed PDA outperforms the CDA in terms of both the total PU sum rate and the individual PU rate, especially when the number of PUs is higher than that of the CUs, i.e. for $L_R > 1$.

Furthermore, we investigate the performance of the CCMC, DCMC and ATTCM aided DAF based CCR schemes for four different matching algorithms when aiming for spectral access. The

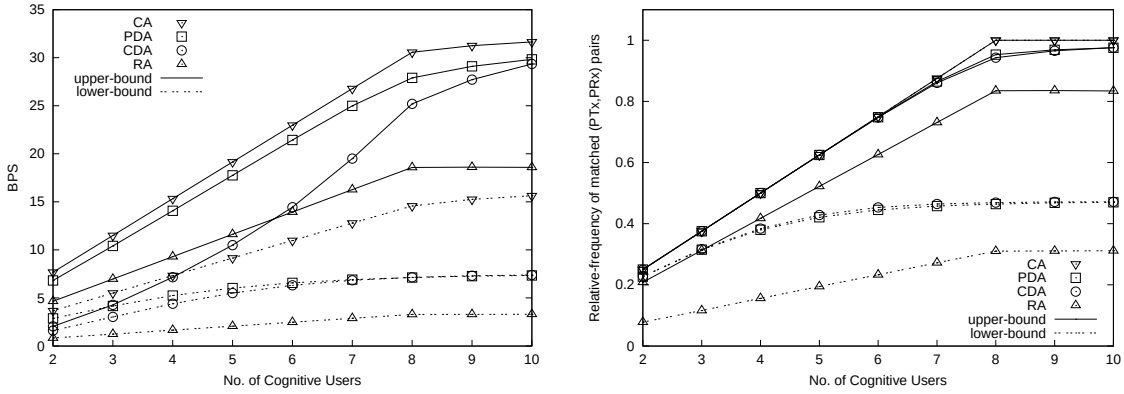

(a) R_{match}^{PU} versus L_{CU} (b) P_{match} versus the L_{CU}

Figure 5.14: Performance of the **CCMC** aided **DAF based** CCR scheme communicating over block-fading Rayleigh fading channel. The "CA", "PDA", "CDA" and "RA" techniques were discussed in Section 5.5.1. The "upper-bound" and "lower-bound" refer to the upper-bound and lower-bound of the total system's throughput for transmission over the cooperative relay channel of Section 5.4. A BER below 10^{-5} is maintained and **the transmit SNR of PU** $\gamma_{PU} = 20dB$ **and the transmit SNR of CU** $\gamma_{CU} = 35$ **dB is used**. The parameters are shown in Table 5.2.

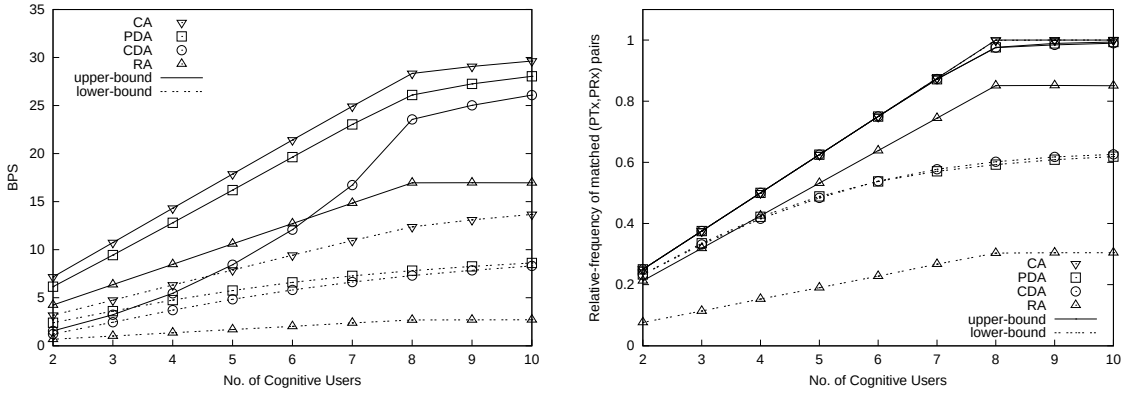

(a) R_{match}^{PU} versus L_{CU} (b) P_{match} versus the L_{CU}

Figure 5.15: Performance of the **DCMC** aided **DAF based** CCR scheme communicating over block-fading Rayleigh fading channel. The "CA", "PDA", "CDA" and "RA" techniques were discussed in Section 5.5.1. The "upper-bound" and "lower-bound" refer to the upper-bound and lower-bound of the total system's throughput for transmission over the cooperative relay channel of Section 5.4. A BER below 10^{-5} is maintained and **the transmit SNR of PU** $\gamma_{PU} = 20dB$ **and the transmit SNR of CU** $\gamma_{CU} = 35$ **dB is used**. The parameters are shown in Table 5.2.

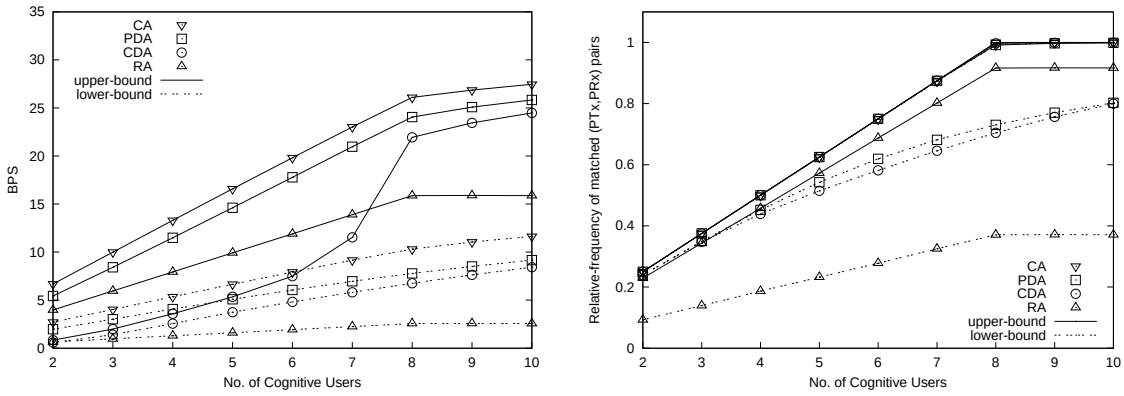

(a) R_{match}^{PU} versus L_{CU}

(b) P_{match} versus the L_{CU}

Figure 5.16: Performance of the **ATTCM** aided **DAF based** CCR scheme communicating over block-fading Rayleigh fading channel. The "CA", "PDA", "CDA" and "RA" techniques were discussed in Section 5.5.1. The "upper-bound" and "lower-bound" refer to the upper-bound and lower-bound of the total system's throughput for transmission over the cooperative relay channel of Section 5.4. A BER below 10^{-5} is maintained and **the transmit SNR of PU** $\gamma_{PU} = 20dB$ **and the transmit SNR of CU** $\gamma_{CU} = 35$ **dB is used**. The parameters are shown in Table 5.2.

average total sum-rate of all matched (Pt, Pr) pairs versus L_{CU} curves of the CCMC, DCMC and ATTCM aided CCR schemes when $L_{PU} = 8$, are shown in Figure 5.14a, Figure 5.15a and Figure 5.16a, respectively. As seen from Figure 5.14a, the total sum-rate of all matched (Pt, Pr) pairs is higher, when we consider the CA of Section 5.5.1.2. We have considered both the upper-bound and lower-bound performance seen in Figure 5.14a. For the lower-bound performance, we considered the lowest transmission rate among the Pt-Ct and Ct-Pr links in order to ensure that the information of both links can be transmitted successfully. However in this case the link associated with the higher rate generously surrenders some of its unused rate for ensuring that the one with a lower rate can also transmit successfully. Additionally, the upper bound is derived, when considering the sum rate of both the Pt-Ct and Ct-Pr links, which gives a higher average total sum rate. Furthermore, as L_{CU} increases, the sum-rate of all matched (Pt, Pr) pairs also increases. This is because when the total number of CUs is high, each Pt will have a high number of choices for selecting better CUs. Thus, the probability of successful matching of PUs and CUs also increases. Additionally, the final matched (Pt, Pr) pairs are the ones with the higher sum-rate. Some unmatched CUs will not be able to transmit. However, when we have $L_{CU} < L_{PU}$, the CDA-based scheme suffers from severe competition loss. More specifically, as seen for the ATTCM aided scheme in Figure 5.16a, the upper bound PU rate of the CDA scheme is even lower than that of the RA scheme, when $L_{CU} \leq 7$. As expected, the system-rate of the matched PUs relying on the CCMC aided CCR scheme is better in comparison to that of the DCMC and of the ATTCM aided schemes, as revealed in Figure 5.14a, Figure 5.15a and Figure 5.16a. It is observed from these figures that the performance

of our PDA is close to that of the CA. However, the achievable rate of matched PUs four our PDA was $(17.69\text{ BPS} - 7.48\text{ BPS}) = 10.21$ BPS higher than that of the CDA as shown in Figure 5.16a, when we have $L_{CU} = 6$. Observe in Figure 5.16a that there is a substantial gap between the PDA and CDA for $L_{CU} < L_{PU}$. Moreover, the CDA performs poorer than the RA scheme in terms of its upper-bound for $L_{CU} < L_{PU}$, since the competition in the CDA is more intense, while the number of CUs is low. Additionally, the trend of RA does not change too much, when the number of CUs is increased, because the matching of RA is randomly distributed. The percentage P_{match} of matched PUs versus the number of CUs, L_{CU}, is investigated in Figure 5.14b, Figure 5.15b and Figure 5.16b. The idealistic CCMC aided CCR scheme achieves the highest matching percentage. Additionally, the percentage of matched users found by the CA is seen to be significantly higher than that of the RA. Interestingly, the upper bound P_{match} curves seen in Figure 5.14b for all CA, PDA and CDA schemes are quite close to each others, although the PU rate of CDA is much lower, when $L_{CU} < L_{PU}$. This indicates that the CDA suffers from competition loss, despite having a similar P_{match}.

5.6 Chapter Conclusions

In this section, we have presented four PU/CU matching algorithms conceived for spectral access in our CCR scheme, which aims for maximizing the utility of matched PUs. In our proposed PDA, the PUs trade with the CUs by negotiating the appropriate TS allocation, capable of guaranteeing that the rate requirements of the matched PUs and CUs are satisfied. Our PDA scheme may be broadly viewed as a *repeated game* [84, 215, 216], where the PUs are the players. The PUs and CUs are not cooperating in a game theoretical sense, although they do cooperate in the sense of relaying. More explicitly, the CDA proposed in [98] was shown to create a stable matching, which exhibits a *competitive equilibrium*, when all PUs and CUs are non-cooperative. If we consider a 'single-shot' game, where each PU only cares about its own current payoff, then no individual PU would have the incentive to deviate from the CDA strategy. Hence, the CDA may be deemed to be a strategy that arrives at an equilibrium for the single-shot non-cooperative game. However, spectrum sharing between the PUs and CUs may be sustained for a long period of time, which may be viewed as a game repeated for numerous rounds, in which the PUs can cooperate based on their individual reputation and their mutual trust. More specifically, the proposed PDA may be classified as a repeated game, where all PUs are capable of cooperating with each other. They are motivated to form a grand coalition for achieving an increased expected PU rate by discouraging the PUs from competing with each other for the same CU's assistance. Although the PDA may not converge to a stable equilibrium in a single-shot game, it does converge to an equilibrium in the repeated game enforced by the threat of punishment. More specifically, if any of the PUs opts out of cooperation in the PDA, all PUs would revert to the non-cooperative CDA for a period of sufficiently long duration. Since the expected payoff in PDA is higher than that of the CDA,

this punishment would discourage opting out and hence would help to maintain cooperation. Our numerical analysis revealed that the proposed PDA achieved a better performance than the CDA benchmark scheme, especially when the number of CUs is lower than that of the PUs, as shown in Table 5.3 and Table 5.4. Furthermore, the proposed PDA has a low complexity, because it does not require the sharing of information regarding the PUs' rates amongst the PUs.

$L_{CU} = 6 < L_{PU} = 8$	Average total sum-rate of matched PUs (R^{PU}_{match})					
	Upper-bound			Lower-bound		
	ATTCM	DCMC	CCMC	ATTCM	DCMC	CCMC
CA	19.81	21.41	22.96	7.92	9.42	10.96
PDA	17.11	19.63	21.43	6.60	6.70	6.57
CDA	7.48	12.08	14.13	5.81	5.80	6.30
RA	11.89	12.71	13.93	2.02	2.02	2.46

Table 5.3: The comparison of the average total sum-rate of matched PUs based on our four matching algorithms, which may extracted from Figure 5.14a, Figure 5.15a and Figure 5.16a.

$L_{CU} = 6 < L_{PU} = 8$	Relative frequency of matched PUs (P_{match}))					
	Upper-bound			Lower-bound		
	ATTCM	DCMC	CCMC	ATTCM	DCMC	CCMC
CA	75%	75%	75%	74.9 %	74.9%	74%
PDA	74.9%	74.9%	74.8%	61.9%	53.7%	44.5%
CDA	74.9%	74.9%	74.7%	58.2%	53.8%	45.3%
RA	68.7%	63.8%	62.5%	27.8%	22.7%	23.2%

Table 5.4: The comparison of the relative frequency of matched PUs based on our four matching algorithms, which may extracted from Figure 5.14b, Figure 5.15b and Figure 5.16b.

Chapter 6

Conclusions and Future Research

In this chapter, we will conclude all our Cooperative Cognitive Radio (CCR) designs in Section 6.1, before suggesting a range of promising future research topics in Section 6.2.

6.1 Conclusions

Chapter 2 : In this chapter, we first reviewed the principle of the fixed-mode TTCM in Section 2.2. We have conceived a novel TTCM aided SDMA scheme based on the two-way relaying system of Section 2.3.2 by employing the classic 4PSK modulation scheme. The power sharing aided scheme is capable of achieving an approximately 1.8 dB SNR gain, when compared to the non-power sharing scheme as shown in Figure 2.17. This allows us to minimize the overall transmit power. Our proposed ML-detected SDMA-based two-way relaying scheme is capable of outperforming the non-cooperative TTCM benchmark scheme by approximately 5.3 dB at a BER of 10^{-6} as seen from Figure 2.18. The MMSE based SDMA scheme offers the best compromise in terms of the detection complexity imposed and the performance gain attained. In Figure 2.18 we have also quantified that the modulo-two addition method of Section 2.3.2.1 is capable of providing an approximately 1 dB of SNR gain compared to that employed the concatenation method, where both schemes employ the ML MUD and the power sharing mechanism is activated. Furthermore, in Section 2.3.3, a 4PSK-TTCM-aided SDMA-based two-way relaying scheme was implemented based on imperfect channel estimation. As seen in Figure 2.22 and Figure 2.23, the BER and throughput of the imperfect channel estimation based scheme is worse than that of the perfect channel estimation based scheme of Figure 2.17 and Figure 2.18. Furthermore, we have studied an adaptive TTCM (ATTCM) scheme in Section 2.3.4. The applications of ATTCM were discussed in Chapter 3, Chapter 4 and Chapter 5.

Chapter 3 : We have considered an overlay scheme in our active CCR system, as shown in Fig-

ure 3.1. In Section 3.2, we found that the optimum ratios of the relay power over the total power budget in our proposed system were higher, when Amplified-and-Forward (AAF) relaying was employed compared to that using the Decode-and-Forward (DAF) protocol, as shown in Figure 3.3 and Figure 3.4. Additionally, the four fixed transmission modes of Figure 3.5 in Section 3.3 were compared in Table 3.1, where System D is the most practical system that is capable of reducing the original bandwidth by 12% for the CU's benefit, while the PU enjoys a 20% higher bit rate. Moreover, in Section 3.4.2 we have proposed a practical ATTCM aided one-way relaying (OWR) CCR scheme , where adaptive coding and modulation were invoked according to the near-instantaneous channel conditions. With reference to Figure 3.23 we found that the proposed OWR-CCR scheme would release 81% bandwidth at an SNR of 5 dB. Furthermore, in Section 3.4.3 we have also investigated the ATTCM aided two-way relay (TWR) scheme based on our CCR system. Specifically, we found in Figure 3.23 that the bandwidth reduction can be increased by 7% upon employing the Time Division Broadcast Channel (TDBC) based scheme of Section 3.4.3 compared to the OWR scheme. Additionally, observe in Figure 3.23 that an 11% bandwidth reduction can be attained by employing the Multiple-Access Broadcast Channel (MABC) based scheme of Section 3.4.3 in comparison to the OWR system. Therefore, at a given SNR, the TWR-CCR system always attains a higher bandwidth reduction than that of the corresponding OWR-CCR system. More specifically, the idealistic Discrete-input Continuous-output Memoryless Channel (DCMC) and Continuous-input Continuous-output Memoryless Channel (CCMC) capacity based systems were also employed in our proposed OWR-CCR and TWR-CCR schemes as the benchmark schemes.

Chapter 4 : We have studied the family of Generalized Dynamic Network Codes (GDNC) [182, 183] in this chapter. In order to increase the average transmission rate of GDNC without reducing its diversity order, in Section 4.2.3, we have considered an Adaptive Dynamic Network Code (ADNC) based design, which feeds back the transmission state of PUs from the BS to the CUs. More specifically, the BS would feed back a flag to the CUs concerning the success or failure of the transmission from each PU to the BS. In our system, all transmission links have employed the ATTCM scheme. Additionally, the combination of the ATTCM and ADNC schemes was specifically configured according to the near-instantaneous channel conditions in our CCR system. We have selected the Min-Max scenario of Section 4.3 to transmit information frames from the PU to the BS via the CUs, in order to minimize the potential error propagation from the CUs to the BS. More specifically, we have considered two systems of our simulations. In System 1, the 'no transmission mode' was invoked, when we have encountered an SNR lower than the threshold to be exceeded for activating one of the ATTCM mode switching operation. By contrast, the 4PSK modulation mode is used under the same conditions in System 2. We found that our proposed ATTCM-ADNC-CCR scheme based on System 1 is capable of releasing up to 40% of bandwidth for exploitation by the

CUs, as shown in Figure 4.16.

Chapter 5 : In this chapter, we have presented the four PU/CU matching algorithms conceived for spectral access in our CCR scheme, where the PUs trade with the CUs by negotiating the appropriate trust time-slot (TS) allocation, which is capable of guaranteeing that the rate requirements of the matched PUs and CUs are satisfied. Based on the formulation of the optimization problem in Section 5.3, we focused on maximizing the total utility of matched PUs, where the PUs always have a higher priority than the CUs. More specifically, the main purpose is to reduce the transmission time and to improve the sum rate of PUs. Specifically, the Centralized Algorithm (CA) of Section 5.5.1.2 and the Random Algorithm (RA) of Section 5.5.1.5 constitute the upper and lower bounds for the solution of the optimization problem, as discussed in Eq. (5.30). The Conventional Distributed Algorithm (CDA) of Section 5.5.1.3 proposed in [98] was shown to create a stable PU-CU matching, which exhibits a *competitive equilibrium*, when all PUs and CUs are non-cooperative. Our Pragmatic Distributed Algorithm (PDA) of Section 5.5.1.4 may be broadly viewed as a *repeated game* [84, 215, 216] among the PUs. Explicitly, spectrum sharing between the PUs and CUs may be sustained for a long period of time in PDA, which may be viewed as a game repeated for numerous rounds, in which the PUs can cooperate based on their individual reputation and their mutual trust. However, the PUs and CUs are not cooperating in a game-theoretical sense, although they do cooperate in the sense of relaying as detailed in Section 5.5.2. The PUs are motivated to form a grand coalition for achieving an increased expected PU rate by discouraging the PUs from competing with each other for the same CU's assistance. Although the PDA may not converge to a stable equilibrium in a single-shot game, it does converge to an equilibrium in the repeated game enforced by the threat of punishment in case of defection from cooperation.

Additionally, both the proposed PDA and CDA have a low complexity compared to the CA. Furthermore, our numerical analysis based in Section 5.5.3 revealed that the proposed PDA achieved a better performance than the CDA benchmark scheme, especially when the number of CUs is lower than that of the PUs, as shown in Table 5.3 and Table 5.4.

6.2 Future Research

6.2.1 Successive Relay aided Cooperative Cognitive Radio Networks

The concept of successive relaying was first suggested in [222] and a generalized mode was proposed in [22], which offers a further insights into the achievable rates and also into the associated diversity-multiplexing trade-off. Moreover, the successive relaying scheme is capable of achieving both cooperative diversity and a high bandwidth efficiency in order to improve the spectrum efficiency [20, 22]. In [223], spectrum sharing based on two-path successive relaying has been con-

sidered. Specifically, two CUs act as the RNs to help the PUs' transmission in a successive fashion, meanwhile they also sending their own information to the intended destination. Additionally, the superposition coding technique was employed by the CUs and the so-called successive decoding was used at the primary's receiver. Additionally, an adaptive spectrum leasing scheme based both on two-path successive relaying as well as Decode and forward (DAF) protocol has been advocated in [224], in order to improve the system throughput.

In Chapter 2 and Chapter 3, we have employed the two-way relaying regime in our proposed CCR systems. By employing the MABC or TDBC scheme, our system attained an additional bandwidth reduction compared to the one-way relaying system for the CUs' secondary transmissions. Hence, we would like to incorporate the above-mentioned ideas into our cooperative CR scheme proposed in this thesis. Specifically, we may consider two groups of CUs and two PUs as a basic example. Each group of CUs would receive the information from the PUs, and would also be interfered by the other CUs, who remained silent during a transmission period or phase. Explicitly, investigating the interferences imposed by the CUs may be a promising topic for our future research. We may assume that each PU and/or CU equipped with a single antenna operating in half-duplex mode. As we investigated in Section 2.3.2.1.2, the IC MUD may be employed. To elaborate further, the network coding technique discussed in Section 4 may be employed instead of the superposition coding scheme for combining the information received from the PUs and also their own information gleaned from the CUs. Furthermore, with the aid of a well-designed transmission arrangement, we may be able to exploit the bandwidth band for the CUs and meanwhile reduce the PUs' transmission time.

6.2.2 Increase both the number of PUs and CUs in our ADNC Aided CCR Scheme

In Chapter 4, we have employed the $\mathcal{M}_{2\times4}$ and $\mathcal{M}_{4\times8}$ matrix aided schemes based on our ATTCM-ADNC-CCR system. A further extension of this design could employ a larger transfer matrix in our system, such as the transfer matrix $\mathcal{M}_{6\times12}$ [195]. With reference to Eq. (4.10), the identity matrix associated with the transfer matrix $\mathcal{M}_{6\times12}$ is given by:

$$\hat{\mathcal{I}_{6\times12}} = \begin{bmatrix} 1 & 0 & 0 & 0 & 0 & 0 \\ 0 & 1 & 0 & 0 & 0 & 0 \\ 0 & 0 & 1 & 0 & 0 & 0 \\ 0 & 0 & 0 & 1 & 0 & 0 \\ 0 & 0 & 0 & 0 & 1 & 0 \\ 0 & 0 & 0 & 0 & 0 & 1 \end{bmatrix}. \tag{6.1}$$

Additionally, the corresponding parity matrix is defined as [195]:

$$\hat{\mathcal{P}_{6\times 12}} = \begin{bmatrix} 11 & 2 & 4 & 6 & 14 & 12 \\ 1 & 11 & 13 & 10 & 14 & 10 \\ 2 & 4 & 2 & 10 & 5 & 9 \\ 6 & 13 & 12 & 11 & 8 & 12 \\ 4 & 12 & 12 & 2 & 6 & 6 \\ 11 & 13 & 10 & 14 & 10 & 4 \end{bmatrix}. \tag{6.2}$$

More specifically, the number of PUs becomes $L = 6$ and number of CUs is $K = 6$, when employing the $\mathcal{M}_{6\times 12}$ based ADNC-CCR scheme. Additionally, by increasing the number of PUs and CUs, the corresponding transfer matrix will be changed. Therefore, the transmission arrangement of a new system has to be produced. The coding arrangement in the broadcast phase of this specific example can be summarized as follows:

$$(BP_1): PU_1 \xrightarrow[(=0/1)]{\mathcal{I}_1} CU_1/CU_2/CU_3/CU_4/CU_5/CU_6,\ PU_1 \xrightarrow[(=0/1)]{\mathcal{I}_1} BS\,; \tag{6.3}$$

$$(BP_2): PU_2 \xrightarrow[(=0/1)]{\mathcal{I}_2} CU_1/CU_2/CU_3/CU_4/CU_5/CU_6,\ PU_2 \xrightarrow[(=0/1)]{\mathcal{I}_2} BS\,; \tag{6.4}$$

$$(BP_3): PU_3 \xrightarrow[(=0/1)]{\mathcal{I}_3} CU_1/CU_2/CU_3/CU_4/CU_5/CU_6,\ PU_3 \xrightarrow[(=0/1)]{\mathcal{I}_3} BS\,; \tag{6.5}$$

$$(BP_4): PU_4 \xrightarrow[(=0/1)]{\mathcal{I}_4} CU_1/CU_2/CU_3/CU_4/CU_5/CU_6,\ PU_4 \xrightarrow[(=0/1)]{\mathcal{I}_4} BS\,; \tag{6.6}$$

$$(BP_5): PU_5 \xrightarrow[(=0/1)]{\mathcal{I}_5} CU_1/CU_2/CU_3/CU_4/CU_5/CU_6,\ PU_5 \xrightarrow[(=0/1)]{\mathcal{I}_5} BS\,; \tag{6.7}$$

$$(BP_6): PU_6 \xrightarrow[(=0/1)]{\mathcal{I}_6} CU_1/CU_2/CU_3/CU_4/CU_5/CU_6,\ PU_6 \xrightarrow[(=0/1)]{\mathcal{I}_6} BS. \tag{6.8}$$

Additionally, the corresponding coding arrangement of the cooperative phase may be formulated as:

$$(CP_1): CU_1 \xrightarrow[(=0/1)]{\overbrace{\mathcal{M}_{6\times 12}(1,7)\cdot\mathcal{I}_1}^{PU_1\to CU_1} \oplus \overbrace{\mathcal{M}_{6\times 12}(1,8)\cdot\mathcal{I}_2}^{PU_2\to CU_1} \oplus \overbrace{\mathcal{M}_{6\times 12}(1,9)\cdot\mathcal{I}_3}^{PU_3\to CU_1} \oplus \overbrace{\mathcal{M}_{6\times 12}(1,10)\cdot\mathcal{I}_4}^{PU_4\to CU_1} \oplus \overbrace{\mathcal{M}_{6\times 12}(1,11)\cdot\mathcal{I}_5}^{PU_5\to CU_1} \oplus \overbrace{\mathcal{M}_{6\times 12}(1,12)\cdot\mathcal{I}_6}^{PU_6\to CU_1}} BS\,; \tag{6.9}$$

$$(CP_2): CU_2 \xrightarrow[(=0/1)]{\overbrace{\mathcal{M}_{6\times 12}(2,7)\cdot\mathcal{I}_1}^{PU_1\to CU_2} \oplus \overbrace{\mathcal{M}_{6\times 12}(2,8)\cdot\mathcal{I}_2}^{PU_2\to CU_2} \oplus \overbrace{\mathcal{M}_{6\times 12}(2,9)\cdot\mathcal{I}_3}^{PU_3\to CU_2} \oplus \overbrace{\mathcal{M}_{6\times 12}(2,10)\cdot\mathcal{I}_4}^{PU_4\to CU_2} \oplus \overbrace{\mathcal{M}_{6\times 12}(2,11)\cdot\mathcal{I}_5}^{PU_5\to CU_2} \oplus \overbrace{\mathcal{M}_{6\times 12}(2,12)\cdot\mathcal{I}_6}^{PU_6\to CU_2}} BS\,; \tag{6.10}$$

$$(CP_3): CU_3 \xrightarrow[(=0/1)]{\overbrace{\mathcal{M}_{6\times 12}(3,7)\cdot\mathcal{I}_1}^{PU_1\to CU_3} \oplus \overbrace{\mathcal{M}_{6\times 12}(3,8)\cdot\mathcal{I}_2}^{PU_2\to CU_3} \oplus \overbrace{\mathcal{M}_{6\times 12}(3,9)\cdot\mathcal{I}_3}^{PU_3\to CU_3} \oplus \overbrace{\mathcal{M}_{6\times 12}(3,10)\cdot\mathcal{I}_4}^{PU_4\to CU_3} \oplus \overbrace{\mathcal{M}_{6\times 12}(3,11)\cdot\mathcal{I}_5}^{PU_5\to CU_3} \oplus \overbrace{\mathcal{M}_{6\times 12}(3,12)\cdot\mathcal{I}_6}^{PU_6\to CU_3}} BS\,; \tag{6.11}$$

$$(CP_4): CU_4 \xrightarrow[(=0/1)]{\overbrace{\mathcal{M}_{6\times 12}(4,7)\cdot\mathcal{I}_1}^{PU_1\to CU_4} \oplus \overbrace{\mathcal{M}_{6\times 12}(4,8)\cdot\mathcal{I}_2}^{PU_2\to CU_4} \oplus \overbrace{\mathcal{M}_{6\times 12}(4,9)\cdot\mathcal{I}_3}^{PU_3\to CU_4} \oplus \overbrace{\mathcal{M}_{6\times 12}(4,10)\cdot\mathcal{I}_4}^{PU_4\to CU_4} \oplus \overbrace{\mathcal{M}_{6\times 12}(4,11)\cdot\mathcal{I}_5}^{PU_5\to CU_4} \oplus \overbrace{\mathcal{M}_{6\times 12}(4,12)\cdot\mathcal{I}_6}^{PU_6\to CU_4}} BS\,; \tag{6.12}$$

$$(CP_5): CU_5 \xrightarrow[(=0/1)]{\overbrace{\mathcal{M}_{6\times 12}(5,7)\cdot\mathcal{I}_1}^{PU_1\to CU_5} \oplus \overbrace{\mathcal{M}_{6\times 12}(5,8)\cdot\mathcal{I}_2}^{PU_2\to CU_5} \oplus \overbrace{\mathcal{M}_{6\times 12}(5,9)\cdot\mathcal{I}_3}^{PU_3\to CU_5} \oplus \overbrace{\mathcal{M}_{6\times 12}(5,10)\cdot\mathcal{I}_4}^{PU_4\to CU_5} \oplus \overbrace{\mathcal{M}_{6\times 12}(5,11)\cdot\mathcal{I}_5}^{PU_5\to CU_5} \oplus \overbrace{\mathcal{M}_{6\times 12}(5,12)\cdot\mathcal{I}_6}^{PU_6\to CU_5}} BS\,; \tag{6.13}$$

$$(CP_6): CU_6 \xrightarrow[(=0/1)]{\overbrace{\mathcal{M}_{6\times 12}(6,7)\cdot\mathcal{I}_1}^{PU_1\to CU_6} \oplus \overbrace{\mathcal{M}_{6\times 12}(6,8)\cdot\mathcal{I}_2}^{PU_2\to CU_6} \oplus \overbrace{\mathcal{M}_{6\times 12}(6,9)\cdot\mathcal{I}_3}^{PU_3\to CU_6} \oplus \overbrace{\mathcal{M}_{6\times 12}(6,10)\cdot\mathcal{I}_4}^{PU_4\to CU_6} \oplus \overbrace{\mathcal{M}_{6\times 12}(6,11)\cdot\mathcal{I}_5}^{PU_5\to CU_6} \oplus \overbrace{\mathcal{M}_{6\times 12}(6,12)\cdot\mathcal{I}_6}^{PU_6\to CU_6}} BS\,. \tag{6.14}$$

The challenge of employing a larger transfer matrix is to consider a complex network encoder and decoder. It is expected that the system based on a larger transfer matrix or higher number of PUs and CUs, would benefit from a higher diversity order and a higher detection reliability. Therefore, the system throughput achieved may increase, which leads to more bandwidth being released from the PUs. The new system would enable the PUs to transmit more Bit-per Symbol (BPS) at a given SNR.

6.2.3 Optimising the Spectrum Trading Between PUs and CUs in CR

As discussed in Chapter 5, we have maximized the total sum rate of matched PUs. The potential further research may consider to solve two problems, namely that of optimizing the total sum rate of the matched CUs and optimizing the total sum rate of all matched PUs and CUs. More specifically, when considering to optimize the total sum rate of the matched CUs, the CUs may be the 'seller' auctioning the opportunities to support the primary communication of PUs. In contrast to Chapter 5, the CUs have the right to make decisions to select the PUs, which could bring about the most benefits to themselves. In this situation, the competitive behaviors among the CUs are not supported. We may construct a new scheme in which two CUs will cooperate with each other to achieve a higher group profit and then distribute it equally for fairness. Meanwhile, the PUs need help from the CUs, since their transmission power may be decreased, when using the CUs as RNs.

By contrast, the assumptions may be changed, when we aim for maximizing the total sum rate between the matched PUs and CUs. In our previous research, a higher sum rate of the matched PUs would lead to a lower sum rate of the matched CUs, if the PUs have a higher priority than the CUs. When we consider maximizing the total sum rate of both the PUs and CUs, we should guarantee equilibrium or fairness among them. Specifically, they may need cooperation between the PUs and CUs. However, due to aiming for maximizing their own benefit, some of the CUs may defect from cooperation and may even cheat, by reporting false information in order to gain a higher pay-off. Therefore, a cheat-proof strategy [84] should be employed for CUs which ensures that the CUs are always cooperative. Additionally, the cheat-proof strategy of [84] is based on the concept of *transfer*, which is referred to the Bayesian design theory [88]. More specifically, a CU with the highest channel quality will be selected to help the PU's transmission in a particular time-slot. Hence, when a CU reports a high channel quality, it will be asked to pay a tax. The tax is increased as the reported channel quality is increased.

Appendix A

Appendix

Appendix of Chapter 5

Appendix A: the derivation of Eq. (5.25).

As discussed in Section 5.3, based on Eq. (5.18) and Eq. (5.20), the objective function of $\beta_{l,k}$ that maximizes the total sum rate of matched PU and CU can be rewritten as:

$$\max \sum_{l=1}^{L_{PU}} \sum_{k=1}^{L_{CU}} W(\beta_{l,k}^{cen}) \quad = \quad \max \sum_{l=1}^{L_{PU}} \sum_{k=1}^{L_{CU}} \left(\beta_{l,k} C_{l,k}^{PU} + (1-\beta_{l,k}) C_{l,k}^{CU} \right) . \tag{A.1}$$

The problem of Eq. (A.1) is a convex function and has three linear constrains which are the condition (a), (b), and (c) of Eq (5.15) and as follows:

$$s.t. \quad (a) \beta_{l,k} C_{PU_{l,k}} \geq R_{l,req}^{PU} , \forall l \forall k \tag{A.2}$$

$$(b)(1-\beta_{l,k}) C_{CU_{l,k}} \geq R_{k,req}^{CU} , \forall l \forall k \tag{A.3}$$

$$(c) 0 \leq \beta_{l,k} \leq 1 , \forall l \forall k. \tag{A.4}$$

Hence the Lagrangian function for Eq. (A.1) using the corresponding constrains of Eq. (A.2), Eq. (A.3), and Eq. (A.4) can be expressed as:

$$\begin{aligned} \mathcal{L}(\beta_{l,k}^{cen}, \lambda, \mu) = & \quad \sum_{l=1}^{L_{PU}} \sum_{k=1}^{L_{CU}} W(\beta_{l,k}) \\ & + \sum_{l=1}^{L_{PU}} \sum_{k=1}^{L_{CU}} \lambda_{l,k} \left(\beta_{l,k} C_{l,k}^{PU} - R_{l,req}^{PU} \right) \\ & + \sum_{l=1}^{L_{PU}} \sum_{k=1}^{L_{CU}} \mu_{l,k} \left(C_{l,k}^{CU} - \beta_{l,k} C_{l,k}^{CU} - R_{k,req}^{CU} \right) . \end{aligned} \tag{A.5}$$

where the weight $W(\beta_{l,k})$ as seen in Eq. (5.18) aims to maximize the sum rate of PU and CU. The $\lambda = (\lambda_{l,k} : l \in L,\ k \in K)$ is a matrix of Lagrange multipliers corresponding to the PUs' rate requirement constraint of Eq (A.2) with $\lambda_{l,k} \geq 0$. Then the vector $\mu = (\mu_{l,k} : l \in L,\ k \in K)$ of Lagrange multipliers corresponds to the CUs' rate constraint of Eq (A.3) with $\mu_{l,k} \geq 0$. The dual function can be expressed as:

$$\mathcal{H}(\beta_{l,k}^{cen}, \lambda, \mu) \quad = \quad \max_{0 \leq \beta_{l,k} \leq 1} \mathcal{L}(\beta_{l,k}^{cen}, \lambda, \mu) . \tag{A.6}$$

The dual problem corresponding to the primal problem of Eq. (A.1) is formulated as:

$$\min \mathcal{H}(\beta_{l,k}^{cen}, \lambda, \mu) \, . \tag{A.7}$$

The primal problem of Eq. (A.1) is a convex function problem where a strong duality[1] exits [225, 226]. Hence the optimal values for the primal and dual problems are equal. Consequently, the optimal value of Eq. (A.1) can be solved through its dual problem of Eq. (A.6). The maximization problem of Eq. (A.6) can be simpled as:

$$\begin{aligned} \mathcal{H}(\beta_{l,k}^{cen}, \lambda, \mu) \quad &= \sum_{l=1}^{L} \sum_{k=1}^{K} \max_{l,k} \left(\beta_{l,k} C_{l,k}^{PU} + C_{l,k}^{CU} - \beta_{l,k} C_{l,k}^{CU} \right) \\ &\quad + \lambda_{l,k} \left(\beta_{l,k} C_{l,k}^{PU} - R_{l,req}^{PU} \right) \\ &\quad + \mu_{l,k} \left(C_{l,k}^{CU} - \beta_{l,k} C_{l,k}^{CU} - R_{k,req}^{CU} \right) \, . \end{aligned} \tag{A.8}$$

The optimization allocation of $\beta_{l,k}^{cen}$ for fixed values of $\lambda_{l,k}$ and $\mu_{l,k}$ can be calculated for each PU and CU by applying the Karush-Luhn-Tucker (KKT) conditions [226], such that we have:

$$\frac{\partial \mathcal{H}(\beta_{l,k}^{cen}, \lambda, \mu)}{\partial \beta_{l,k}} = C_{l,k}^{PU} - C_{l,k}^{CU} + \lambda_{l,k} C_{l,k}^{PU} - \mu_{l,k} C_{l,k}^{CU} = 0 \, . \tag{A.9}$$

Then the calculation of Lagrange multipliers corresponding to the constraint of Eq (A.2) is given by:

$$\frac{\partial \mathcal{H}(\beta_{l,k}^{cen}, \lambda, \mu)}{\partial \lambda_{l,k}} = C_{l,k}^{PU} \beta_{l,k} - R_{l,req}^{PU} = 0 \Rightarrow \beta_{l,k} = \frac{R_{l,req}^{PU}}{C_{l,k}^{PU}} \, . \tag{A.10}$$

Additionally, the calculation of Lagrange multiplies $\mu_{l,k}$ corresponds to the constraint of Eq (A.3) may be expressed as:

$$\frac{\partial \mathcal{H}(\beta_{l,k}^{cen}, \lambda, \mu)}{\partial \mu_{l,k}} = C_{l,k}^{CU} - \beta_{l,k} C_{l,k}^{CU} - R_{k,req}^{CU} = 0 \Rightarrow \beta_{l,k} = 1 - \frac{R_{k,req}^{CU}}{C_{l,k}^{CU}} \, . \tag{A.11}$$

Hence, we could obtain two bounds of optimization value for $\beta_{l,k}^{cen}$. Based on Eq (A.9), λ and μ may be expressed as:

$$\lambda_{l,k} = \frac{(1 + \mu_{l,k}) C_{l,k}^{CU}}{C_{l,k}^{PU}} - 1 \quad \text{and} \quad \mu_{l,k} = \frac{1 + \lambda_{l,k} C_{l,k}^{PU}}{C_{l,k}^{CU}} - 1 \, . \tag{A.12}$$

Since $\lambda_{l,k} > 0$ and $\mu_{l,k} > 0$, Eq. (A.12) may be further derived as:

$$\mu_{l,k} > \frac{C_{l,k}^{PU}}{C_{l,k}^{CU}} - 1 \quad \text{and} \quad \lambda_{l,k} > \frac{C_{l,k}^{CU}}{C_{l,k}^{PU}} - 1 \, . \tag{A.13}$$

Moreover, when the conditions in Eq. (A.13) are satisfied, we could obtain the bounds related to Eq. (A.10) and Eq. (A.11). Finally, the optimization value of $\beta_{l,k}^{cen}$ that maximizes the total sum rate of PU and CU is given by:

$$\beta_{l,k}^{cen} = \begin{cases} \frac{R_{l,req}^{PU}}{C_{l,k}^{PU}} & C_{CU} > C_{PU}; \\ 1 - \frac{C_{l,k}^{CU}}{R_{k,req}^{CU}} & C_{CU} < C_{PU}. \end{cases} \tag{A.14}$$

[1] The optimal duality gap of strong duality is zero. It means that the best bound that can be obtained form the Lagrange dual function is tight [225].

Based on the solution defined in Eq. (A.14), we could obtained the optimization value of $\beta_{l,k}^{cen}$ directly. Then we aim to solve the optimization problem as shown in Eq. (5.26). The centralized solution of Eq. (5.26) can be solved by using the centralized algorithm as discussed in Section 5.5.1.2. The corresponding simulation results are shown in Figure A.1.

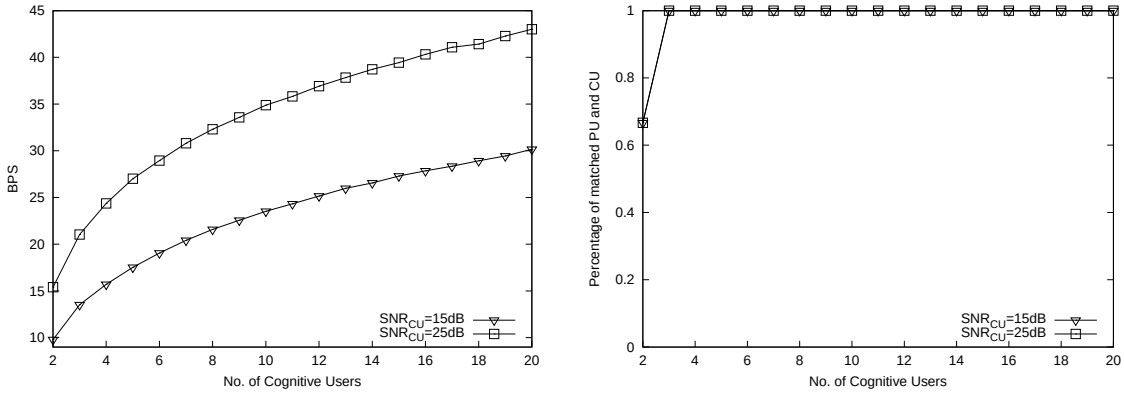

(a) R_{match}^{total} versus L_{CU}

(b) P_{match}^{total} versus the L_{CU}

Figure A.1: Performance of the **CCMC** aided **AAF based** cooperative CR scheme communicating over block-fading Rayleigh fading channel while considering maximize the total utility of matched PUs and CUs. The parameters are shown in Table 5.2.

Appendix B: Proof of Proposition 1

Proof. The discounted payoff in Eq. (5.45) can be shown to be asymptotically equivalent to the average of the one-time payoffs, when δ approaches unity as follows:

$$\begin{aligned}\lim_{\delta\to 1} U_l &= \lim_{\delta\to 1}\lim_{N\to\infty}\frac{1-\delta}{1-\delta^N}\sum_{i=1}^{N}\delta^i R_l^C[i] \\ &= \lim_{N\to\infty}\sum_{i=1}^{N}\left(\lim_{\delta\to 1}\frac{\delta^i-\delta^{i+1}}{1-\delta^N}\right)R_l^C[i]\,, \end{aligned} \tag{A.15}$$

The last equality of Eq. (A.15) can be derived based on the L'Hôpital's rule, where the term in the round bracket of Eq. (A.15) can be derived as:

$$\begin{aligned}\lim_{\delta\to 1}\frac{\delta^i-\delta^{i+1}}{1-\delta^N} &= \lim_{\delta\to 1}\frac{\partial(\delta^i-\delta^{i+1})}{\partial(1-\delta^N)} \\ &= \lim_{\delta\to 1}\frac{i\delta^{i-1}-(i+1)\delta^i}{0-N\delta^{N-1}} \\ &= \lim_{\delta\to 1}\frac{1}{N}\,. \end{aligned} \tag{A.16}$$

Then refer to Eq. (A.16), Eq. (A.15) can be rewrite as:

$$\lim_{\delta\to 1} U_l = \lim_{N\to\infty}\frac{1}{N}\sum_{i=1}^{N}R_l^C[i] = r_l^C\,. \tag{A.17}$$

Furthermore, if PU_l opts out of cooperation at instant T^*, then its payoff would be given by $\{R_l[i], i = 0, 1, \ldots, T^* - 1\}$, which are i.i.d. random variables due to i.i.d. random channel variations and its mean is given by r_l^C of Eq. (5.44). The payoff after the deviation is given by $\{R_l[i], i = T^* + 1, T^* + 2, \ldots\}$ which is an i.i.d. random variable with the mean r_l^S of Eq. (5.38). The payoff after abandoning cooperation converges to its mean, $U_l^D \to r_l^S$, due to the law of large numbers. Hence, abandoning cooperation only benefits PU_l at instant T^*. Similarly, the payoff $\{R_l[i], i = 0, 1, \ldots\}$ would converge to its mean, $U_l^C \to r_l^C$ if abandoning cooperation never happens.

Appendix C: Proof of Proposition 2

Proof. Since the CDA has an equilibrium for the one-shot game, all PUs would not disagree to adopt the CDA strategy for the punishment stage. Since the CDA would result in r_l^S, which is lower than r_l^C, the threat of using the CDA strategy as the punishment after any non-cooperation would result in only a one-time gain for the 'defector', which can be readily negated by limited-duration punishment, when we have $\delta \to 1$. Hence, all PUs are motivated to adopt the cooperative strategy of the PDA throughout the game, which is also the optimal behaviour for any subgame[2].

[2]This proof is adopted from Section 14.8 of [215].

Bibliography

[1] X. Chen, H. Chen, and W. Meng, "Cooperative communications for cognitive radio networks: From theory to applications," *IEEE Communications Surveys Tutorials*, vol. 16, pp. 1180–1192, March 2014.

[2] H. Ogawa, D. Polifko, and S. Banba, "Millimeter-wave fiber optics systems for personal radio communication," *IEEE Transactions on Microwave Theory and Techniques*, vol. 40, pp. 2285–2293, Dec 1992.

[3] T. Komine, J. Lee, S. Haruyama, and M. Nakagawa, "Adaptive equalization system for visible light wireless communication utilizing multiple white led lighting equipment," *IEEE Transactions on Wireless Communications*, vol. 8, pp. 2892–2900, June 2009.

[4] R. Piesiewicz, C. Jansen, D. Mittleman, T. Kleine-Ostmann, M. Koch, and T. Kurner, "Scattering analysis for the modeling of thz communication systems," *IEEE Transactions on Antennas and Propagation*, vol. 55, pp. 3002–3009, Nov 2007.

[5] T. Yucek and H. Arslan, "A survey of spectrum sensing algorithms for cognitive radio applications," *IEEE Communications Surveys Tutorials*, vol. 11, pp. 116 –130, Quarter 2009.

[6] J. Mitola and G. Q. Maguire, "Cognitive radio: making software radios more personal," *IEEE Personal Communications*, vol. 6, pp. 13 –18, Aug 1999.

[7] A. Goldsmith, S. Jafar, I. Maric, and S. Srinivasa, "Breaking spectrum gridlock with cognitive radios: An information theoretic perspective," *Proceedings of the IEEE*, pp. 894 –914, May 2009.

[8] S. Haykin, "Cognitive radio: brain-empowered wireless communications," *IEEE Journal on Selected Areas in Communications*, vol. 23, pp. 201 – 220, Feb. 2005.

[9] F. C. Commission, "Spectrum policy task force," *Rep. ET Docket no. 02-135*, Nov 2002.

[10] W. Zhang and K. Letaief, "Cooperative spectrum sensing with transmit and relay diversity in cognitive radio networks - [transaction letters]," *IEEE Transactions on Wireless Communications*, pp. 4761 –4766, December 2008.

[11] G. Ganesan and Y. Li, "Cooperative spectrum sensing in cognitive radio, Part i: Two user networks," *IEEE Transactions on Wireless Communications*, vol. 6, pp. 2204 –2213, June 2007.

[12] A. Baker, S. Ghosh, A. Kumar, and M. Bayoumi, "Notice of Violation of IEEE Publication Principles LDPC decoder: A cognitive radio perspective for next generation (XG) communication," *IEEE Circuits and Systems Magazine*, vol. 7, pp. 24–37, March 2007.

[13] K. J. R. Liu, A. K. Sadek, W. Su and A. Kwasinski, *Cooperative Communications and Networking*. Cambridge University Press , New York, 2009.

[14] A. Sendonaris, E. Erkip, and B. Aazhang, "User cooperation diversity. Part I: System description," *IEEE Transactions on Communications*, vol. 51, pp. 1927 – 1938, Nov 2003.

[15] A. Sendonaris, E. Erkip, and B. Aazhang, "User cooperation diversity. Part II. Implementation aspects and performance analysis," *IEEE Transactions on Communications*, vol. 51, pp. 1939–1948, Nov 2003.

[16] K. Azarian, H. E. Gamal, and P. Schniter, "On the achievable diversity-multiplexing tradeoff in half-duplex cooperative channels," *IEEE Transactions on Information Theory*, vol. 51, pp. 4152–4172, Dec 2005.

[17] A. Bletsas, A. Khisti, D. Reed, and A. Lippman, "A simple cooperative diversity method based on network path selection," *IEEE Journal on Selected Areas in Communications*, vol. 24, pp. 659–672, March 2006.

[18] A. Host-Madsen and J. Zhang, "Capacity bounds and power allocation for wireless relay channels," *IEEE Transactions on Information Theory*, vol. 51, pp. 2020–2040, June 2005.

[19] T. Hunter and A. Nosratinia, "Diversity through coded cooperation," *IEEE Transactions on Wireless Communications*,, vol. 5, pp. 283–289, Feb 2006.

[20] B. Rankov and A. Wittneben, "Spectral efficient protocols for half-duplex fading relay channels," *IEEE Journal on Selected Areas in Communications*, vol. 25, pp. 379–389, February 2007.

[21] B. Rankov and A. Wittneben, "Achievable rate regions for the two-way relay channel," in *2006 IEEE International Symposium on Information Theory*, pp. 1668–1672, July 2006.

[22] Y. Fan, C. Wang, J. Thompson, and H. Poor, "Recovering multiplexing loss through successive relaying using repetition coding," *IEEE Transactions on Wireless Communications*, vol. 6, pp. 4484–4493, December 2007.

[23] Y. Han, A. Pandharipande, and S. Ting, "Cooperative decode-and-forward relaying for secondary spectrum access," *IEEE Transactions on Wireless Communications*, vol. 8, pp. 4945 –4950, October 2009.

[24] Q. Zhang, J. Jia, and J. Zhang, "Cooperative relay to improve diversity in cognitive radio networks," *IEEE Communications Magazine*, vol. 47, pp. 111–117, February 2009.

[25] O. Simeone, Y. Bar-Ness, and U. Spagnolini, "Stable throughput of cognitive radios with and without relaying capability," *IEEE Transactions on Communications*, vol. 55, pp. 2351–2360, Dec 2007.

[26] Y. Chen, G. Yu, Z. Zhang, H. Chen, and P. Qiu, "On cognitive radio networks with opportunistic power control strategies in fading channels," *IEEE Transactions on Wireless Communications*, vol. 7, pp. 2752–2761, July 2008.

[27] Y. Zou, J. Zhu, B. Zheng, and Y. Yao, "An adaptive cooperation diversity scheme with best-relay selection in cognitive radio networks," *IEEE Transactions on Signal Processing*, vol. 58, pp. 5438–5445, Oct 2010.

[28] Y. Zou, Y. Yao, and B. Zheng, "Cognitive transmissions with multiple relays in cognitive radio networks," *IEEE Transactions on Wireless Communications*, vol. 10, pp. 648–659, February 2011.

[29] L. Li, X. Zhou, H. Xu, G. Li, D. Wang, and A. Soong, "Simplified relay selection and power allocation in cooperative cognitive radio systems," *IEEE Transactions on Wireless Communications*, vol. 10, pp. 33–36, January 2011.

[30] P. Ubaidulla and S. Aissa, "Optimal relay selection and power allocation for cognitive two-way relaying networks," *IEEE Wireless Communications Letters*, vol. 1, pp. 225–228, June 2012.

[31] G. Zhao, C. Yang, G. Li, D. Li, and A. Soong, "Power and channel allocation for cooperative relay in cognitive radio networks," *IEEE Journal of Selected Topics in Signal Processing*, vol. 5, pp. 151–159, Feb 2011.

[32] R. Zhang, Y. Liang, and S. Cui, "Dynamic resource allocation in cognitive radio networks," *IEEE Signal Processing Magazine*, vol. 27, pp. 102–114, May 2010.

[33] J. Liang and J. Chen, "Resource allocation in cognitive radio relay networks," *IEEE Journal on Selected Areas in Communications*, vol. 31, pp. 476–488, March 2013.

[34] Y. Tachwali, B. Lo, I. Akyildiz, and R. Agusti, "Multiuser resource allocation optimization using bandwidth-power product in cognitive radio networks," *IEEE Journal on Selected Areas in Communications*, vol. 31, pp. 451–463, March 2013.

[35] Q. Li, S. H. Ting, A. Pandharipande, and Y. Han, "Cognitive spectrum sharing with two-way relaying systems," *IEEE Transactions on Vehicular Technology*, vol. 60, pp. 1233–1240, March 2011.

[36] H. Mu and J. Tugnait, "Interference alignment-like precoder design in multi-pair two-way relay cognitive radio networks," in *IEEE Global Communications Conference (GLOBECOM)*, pp. 1471–1476, Dec 2012.

[37] Q. Zhang, S. Kota, V. Lau, W. Su, and A. Kwasinski, "Introduction to the issue on cooperative communication and signal processing in cognitive radio systems," *IEEE Journal of Selected Topics in Signal Processing*, vol. 5, pp. 1–4, Feb 2011.

[38] N. Devroye, P. Mitran, and V. Tarokh, "Achievable rates in cognitive radio channels," *IEEE Transactions on Information Theory*, vol. 52, pp. 1813 – 1827, May 2006.

[39] W.F. Su and J.D. Matyjas and S. Batalama, "Active cooperation between primary users and cognitive radio users in cognitive ad-hoc networks," in *2010 IEEE International Conference on Acoustics Speech and Signal Processing (ICASSP)*, pp. 3174 –3177, March 2010.

[40] W. Su, J. Matyjas, and S. Batalama, "Active cooperation between primary users and cognitive radio users in heterogeneous ad-hoc networks," *IEEE Transactions on Signal Processing,*, vol. 60, pp. 1796 –1805, April 2012.

[41] B. Cao, Q. Zhang, J. W. Mark, L. Cai, and H. Poor, "Toward efficient radio spectrum utilization: user cooperation in cognitive radio networking," *IEEE Network*, vol. 26, pp. 46–52, July 2012.

[42] O. Simeone, J. Gambini, Y. B. Ness, and U. Spagnolini, "Cooperation and cognitive radio," in *IEEE International Conference on Communications (ICC '07)*, pp. 6511 –6515, June 2007.

[43] S. Mallick, R. Devarajan, R. Loodaricheh, and V. Bhargava, "Robust resource optimization for cooperative cognitive radio networks with imperfect CSI," *IEEE Transactions on Wireless Communications*, vol. 14, pp. 907–920, Feb 2015.

[44] E. C. V. D. Meulen, "Three-terminal communication channels," *Advances in Applied Probability*, vol. 3, no. 1, pp. 120–154, 1971.

[45] T. Cover and A. Gamal, "Capacity theorems for the relay channel," *IEEE Transactions on Information Theory*, pp. 572 – 584, Sep 1979.

[46] S. X. Ng, Y. Li, and L.Hanzo, "Distributed turbo trellis coded modulation for cooperative communications," in *IEEE International Conference on Communications*, pp. 1 –5, June 2009.

[47] S. X. Ng, K. Zhu, and L. Hanzo, "Distributed source-coding, channel-coding and modulation for cooperative communications," in *IEEE 72nd Vehicular Technology Conference Fall (VTC 2010-Fall)*, pp. 1 –5, Sept. 2010.

[48] Y.-C. Liang and R. Zhang, "Optimal analogue relaying with multi-antennas for physical layer network coding," in *IEEE International Conference on Communications*, pp. 3893 – 3897, May 2008.

[49] I. Hammerstrom, M. Kuhn, C. Esli, J. Zhao, A. Wittneben, and G. Bauch, "MIMO two-way relaying with transmit CSI at the relay," in *IEEE 8th Workshop on Signal Processing Advances in Wireless Communications, 2007. SPAWC 2007*, pp. 1 –5, June 2007.

[50] K. Lee and L. Hanzo, "MIMO-assisted hard versus soft decoding-and-forwarding for network coding aided relaying systems," *IEEE Transactions on Wireless Communications*, vol. 8, pp. 376 –385, Jan. 2009.

[51] T. Unger and A. Klein, "On the performance of two-way relaying with multiple-antenna relay stations," in *16th IST Mobile and Wireless Communications Summit*, pp. 1 –5, July 2007, Budapest, Hungary.

[52] M. Chen and A. Yener, "Multiuser two-way relaying: detection and interference management strategies," *IEEE Transactions on, Wireless Communications*, vol. 8, pp. 4296 –4305, Aug 2009.

[53] J. aneman, D. Tse, and G. Wornell, "Cooperative diversity in wireless networks: Efficient protocols and outage behavior," *IEEE Transactions on Information Theory*, vol. 50, pp. 3062 – 3080, Dec 2004.

[54] R. Madan, N. Mehta, A. Molisch, and J. Zhang, "Energy-efficient cooperative relaying over fading channels with simple relay selection," *IEEE Transactions on Wireless Communications*, vol. 7, pp. 3013–3025, August 2008.

[55] Y. Jing and H. Jafarkhani, "Single and multiple relay selection schemes and their achievable diversity orders," *IEEE Transactions on Wireless Communications*, vol. 8, pp. 1414–1423, March 2009.

[56] C. Shannon, "Two-way communication channels," *in Proceedings of Foth Berkeley Symposium on Math. Statist. and Prob.*, vol. 1, pp. 611–644, 1961.

[57] R. H.Y.Louie, Y. Li, and B. Vucetic, "Practical physical layer network coding for two-way relay channels: performance analysis and comparison," *IEEE Transactions on Wireless Communications*, vol. 9, pp. 764–777, February 2010.

[58] P. Larsson, N.Johansson, and K. Sunell, "Coded bi-directional relaying," in *IEEE 63rd Vehicular Technology Conference (VTC 2006-Spring)*, vol. 2, pp. 851–855, May 2006.

[59] L.Hanzo, J.Akhtman, M.Jiang, and L.Wang, *MIMO-OFDM for LTE, WIFI and WIMAX: coherent verus no-coherent and cooperative Turbo-Tranceivers*. John wiley-IEEE Press, 2011.

[60] L. Wang, L. Kong, S. Ng, and L. Hanzo, "Code-rate-optimized differentially modulated near-capacity cooperation," *IEEE Transactions on Communications*, pp. 2185 –2195, August 2011.

[61] L. Wang and L. Hanzo, "Optimum time resource allocation for tdma-based differential decode-and-forward cooperative systems: a capacity perspective," *IEEE Communications Letters*, no. 6, pp. 506 –508, 2010.

[62] G. Kramer, M. Gastpar, and P. Gupta, "Cooperative strategies and capacity theorems for relay networks," *IEEE Transactions on Information Theory,*, pp. 3037 – 3063, Sept. 2005.

[63] Y. Zeng and Y.-C. Liang, "Spectrum-sensing algorithms for cognitive radio based on statistical covariances," *IEEE Transactions on Vehicular Technology*, vol. 58, pp. 1804 –1815, May 2009.

[64] S. Haykin, D. Thomson, and J. Reed, "Spectrum sensing for cognitive radio," *Proceedings of the IEEE*, pp. 849 –877, May 2009.

[65] Z. Tian and G. B. Giannakis, "A wavelet approach to wideband spectrum sensing for cognitive radios," in *1st International Conference on Cognitive Radio Oriented Wireless Networks and Communications*, pp. 1 –5, June 2006.

[66] Z. Quan, S. Cui, A. Sayed, and H. Poor, "Optimal multiband joint detection for spectrum sensing in cognitive radio networks," *IEEE Transactions on Signal Processing*, pp. 1128 –1140, March 2009.

[67] R. Niu, B. Chen, and P. Varshney, "Fusion of decisions transmitted over rayleigh fading channels in wireless sensor networks," *IEEE Transactions on Signal Processing*, pp. 1018 – 1027, March 2006.

[68] I. Akyildiz, W.-Y. Lee, M. Vuran, and S. Mohanty, "A survey on spectrum management in cognitive radio networks," *IEEE Communications Magazine*, vol. 46, pp. 40–48, April 2008.

[69] C. He, Z. Feng, Q. Zhang, Z. Zhang, and H. Xiao, "A joint relay selection, spectrum allocation and rate control scheme in relay-assisted cognitive radio system," in *IEEE 72nd Vehicular Technology Conference Fall (VTC 2010-Fall)*, pp. 1–5, Sept 2010.

[70] H. Wang, L. Gao, X. Gan, X. Wang, and E. Hossain, "Cooperative spectrum sharing in cognitive radio networks: A game-theoretic approach," in *2010 IEEE International Conference on Communications (ICC)*, pp. 1–5, May 2010.

[71] X. Qiao, Z. Tan, S. Xu, and J. Li, "Combined power allocation in cognitive radio-based relay-assisted networks," in *2010 IEEE International Conference on Communications Workshops (ICC)*, pp. 1–5, May 2010.

[72] B. Wang, Z. Han, and K. Liu, "Distributed relay selection and power control for multiuser cooperative communication networks using stackelberg game," *IEEE Transactions on Mobile Computing*, vol. 8, pp. 975–990, July 2009.

[73] Y. Xiao, G. Bi, and D. Niyato, "Game theoretic analysis for spectrum sharing with multi-hop relaying," *IEEE Transactions on Wireless Communications*, vol. 10, pp. 1527–1537, May 2011.

[74] G. Scutari, D. Palomar, and S. Barbarossa, "Optimal linear precoding strategies for wideband non-cooperative systems based on game theory part II: Algorithms," *IEEE Transactions on Signal Processing*, vol. 56, pp. 1250–1267, March 2008.

[75] Z. Han, Z. Ji, and K. Liu, "Non-cooperative resource competition game by virtual referee in multi-cell OFDMA networks," *IEEE Journal on Selected Areas in Communications*, vol. 25, pp. 1079–1090, August 2007.

[76] L. Zhao, J. Zhang, and H. Zhang, "Using incompletely cooperative game theory in wireless mesh networks," *IEEE Network*, vol. 22, pp. 39–44, Jan 2008.

[77] E. Larsson and E. Jorswieck, "Competition versus cooperation on the miso interference channel," *IEEE Journal on Selected Areas in Communications*, vol. 26, pp. 1059–1069, September 2008.

[78] M. Naeem, A. Anpalagan, M. Jaseemuddin, and D. Lee, "Resource allocation techniques in cooperative cognitive radio networks," *IEEE Communications Surveys Tutorials*, vol. 16, pp. 729–744, Second 2014.

[79] G. Bansal, O. Duval, and F. Gagnon, "Joint overlay and underlay power allocation scheme for ofdm-based cognitive radio systems," in *IEEE 71st Vehicular Technology Conference (VTC 2010-Spring)*, pp. 1–5, May 2010.

[80] A. Marques, L. Lopez-Ramos, G. Giannakis, and J. Ramos, "Resource allocation for interweave and underlay crs under probability-of-interference constraints," *IEEE Journal on Selected Areas in Communications*, vol. 30, pp. 1922–1933, November 2012.

[81] Q. Zhao and B. Sadler, "A survey of dynamic spectrum access," *IEEE Signal Processing Magazine*, vol. 24, pp. 79–89, May 2007.

[82] R. Manna, R. H. Louie, Y. Li, and B. Vucetic, "Cooperative spectrum sharing in cognitive radio networks with multiple antennas," *IEEE Transactions on Signal Processing*, vol. 59, pp. 5509–5522, Nov 2011.

[83] D. Niyato, E. Hossain, and Z. Han, "Dynamic spectrum access in ieee 802.22- based cognitive wireless networks: a game theoretic model for competitive spectrum bidding and pricing," *IEEE Wireless Communications*, vol. 16, pp. 16–23, April 2009.

[84] Y. Wu, B. Wang, K. J. R. Liu, and T. C. Clancy, "Repeated open spectrum sharing game with cheat-proof strategies," *IEEE Transactions on Wireless Communications*, vol. 8, pp. 1922–1933, April 2009.

[85] M. Haddad, S. Elayoubi, E. Altman, and Z. Altman, "A hybrid approach for radio resource management in heterogeneous cognitive networks," *IEEE Journal on Selected Areas in Communications*, vol. 29, pp. 831–842, April 2011.

[86] D. Li, Y. Xu, X. Wang, and M. Guizani, "Coalitional game theoretic approach for secondary spectrum access in cooperative cognitive radio networks," *IEEE Transactions on Wireless Communications*, vol. 10, no. 3, pp. 844–856, 2011.

[87] A. Attar, M. Nakhai, and A. Aghvami, "Cognitive radio game for secondary spectrum access problem," *IEEE Transactions on Wireless Communications*, vol. 8, pp. 2121–2131, April 2009.

[88] Z. Han, D. Niyato, W. Saad, T. Basar, and A. Hjorungnes, *Game Theory in Wireless and Communication Networks: Theory, Models and Applications*. Cambridge University Press , 2012.

[89] K. Akkarajitsakul, E. Hossain, D. Niyato, and D. I. Kim, "Game theoretic approaches for multiple access in wireless networks: A survey," *IEEE Communications Surveys Tutorials*, vol. 13, pp. 372–395, Third 2011.

[90] L. Gavrilovska, V. Atanasovski, I. Macaluso, and L. DaSilva, "Learning and reasoning in cognitive radio networks," *IEEE Communications Surveys Tutorials*, vol. 15, pp. 1761–1777, April 2013.

[91] Y. Xu, A. Anpalagan, Q. Wu, L. Shen, Z. Gao, and J. Wang, "Decision-theoretic distributed channel selection for opportunistic spectrum access: Strategies, challenges and solutions," *IEEE Communications Surveys Tutorials*, vol. 15, pp. 1689–1713, April 2013.

[92] D. Niyato and E. Hossain, "Competitive pricing for spectrum sharing in cognitive radio networks: Dynamic game, inefficiency of nash equilibrium, and collusion," *IEEE Journal on Selected Areas in Communications*, vol. 26, pp. 192–202, Jan 2008.

[93] M. L. Treust and S. Lasaulce, "A repeated game formulation of energy-efficient decentralized power control," *IEEE Transactions on Wireless Communications*, vol. 9, pp. 2860–2869, September 2010.

[94] P. Zhou, Y. Chang, and J. Copeland, "Reinforcement learning for repeated power control game in cognitive radio networks," *IEEE Journal on Selected Areas in Communications*, vol. 30, pp. 54–69, January 2012.

[95] P. Robertson and T. Wörz, "Bandwidth-Efficient Turbo Trellis-Coded Modulation Using Punctured Component Codes," *IEEE Journal on Selected Areas in Communications*, vol. 16, pp. 206–218, Feb 1998.

[96] L. Hanzo and S. X. Ng and T. Keller and W. Webb, *Quadrature Amplitude Modulation:From Basics to Adaptive Trellis-Coded, Turbo-Equalised and Space-Time Coded OFDM, CDMA and MC-CDMA Systems*. Wiley-IEEE Press, 2004.

[97] S. X. Ng and O. R. Alamri and Y. Li and J. K. liewer and L. Hanzo , "Near-capacity turbo trellis coded modulation design based on EXIT charts and union bounds," *IEEE Transactions on Communications*, vol. 56, no. 12, pp. 2030–2039, 2008.

[98] S. Bayat, R. Louie, Y. Li, and B. Vucetic, "Cognitive radio relay networks with multiple primary and secondary users: Distributed stable matching algorithms for spectrum access," in *2011 IEEE International Conference on Communications (ICC)*, pp. 1 –6, June 2011.

[99] G. Ungerböck, "Channel coding with multilevel/phase signals," *IEEE Transactions on Information Theory*, vol. 28, pp. 55–67, January 1982.

[100] S. T. Brink, "Convergence behaviour of iteratively decoded parallel concatenated codes," *IEEE Transactions on Communications*, vol. 49, pp. 1727–1737, October 2001.

[101] J. Kliewer and S. X. Ng and L. Hanzo, "Efficient computation of EXIT functions for non-binary iterative decoding," *IEEE Transactions on Communications*, vol. 54, pp. 2133–2136, December 2006.

[102] S. X. Ng and T. H. Liew and L. L. Yang and L. Hanzo, "Comparative study of TCM, TTCM, BICM and BICM-ID schemes," in *IEEE Vehicular Technology Conference, (VTC 2001 Spring)*, vol. 4, pp. 2450–2454, 2001.

[103] C. Shannon, "A mathematical theory of communication," *The Bell System Technical Journal*, vol. 27, pp. 379–423, July 1948.

[104] L. Hanzo and T. H. Liew and B. L. Yeap and R. Y. S.Tee and S. X. Ng, *Turbo Coding, Turbo Equalisation and Space-Time Coding: EXIT-Chart-Aided Near-Capacity Designs for Wireless Channels-Second Edition*. John Wiley and Sons ltd, 2011.

[105] S. X. Ng, *Coded modulation schemes for wireless channels*. PHD thesis, 2002.

[106] T. S. Rappaport, *Wireless Communications, Principles and Practice, second edition*. NJ: Prentice Hall, 1996.

[107] D. D. Liang, *Coherent and non-coherent Coded Modulation for Cooperative Communications*. PHD thesis, 2013.

[108] B. Sklar, "Rayleigh fading channels in mobile digital communication systems .I. characterization," *IEEE Communications Magazine*, vol. 35, pp. 90–100, Jul 1997.

[109] M. Jiang, S. Ng, and L. Hanzo, "TCM, TTCM, BICM and BICM-ID assisted MMSE multiuser detected SDMA-OFDM using Walsh-Hadamard spreading," in *IEEE 59th Vehicular Technology Conference (VTC 2004-Spring)*, pp. 1129 – 1133 Vol.2, May 2004.

[110] S. Verdu, *Multiuser Detection*. Cambridge University Press, 1998.

[111] H. Ochiai, P. Mitran and V. Tarokh, "Design and analysis of collaborative diversity protocols for wireless sensor networks," in *Proceedings of IEEE VTC Fall*, (Los Angeles, USA), pp. 4645 – 4649, 26-29 September 2004.

[112] P. Wolniansky, G. Foschini, G. Golden, and R. Valenzuela, "V-BLAST: an architecture for realizing very high data rates over the rich-scattering wireless channel," in *1998 URSI International Symposium on Signals, Systems, and Electronics*, pp. 295 –300, 1998.

[113] S. Duff Iain , A. Erisman , J. K. Reid, *Direct methods for sparse matrices (Monographs on numerical analysis) Oxford: Clarendon*. Oxford University Press ,1986.

[114] S. Benedetto, D. Divsalar, G. Montorsi, and F. Pollara, "A soft-input soft-output app module for iterative decoding of concatenated codes," *IEEE Communications Letters*, vol. 1, pp. 22–24, Jan 1997.

[115] Y. Huang and J. Ritcey, "16-QAM BICM-ID in fading channels with imperfect channel state information," *IEEE Transactions on Wireless Communications*, vol. 2, pp. 1000 – 1007, Sept. 2003.

[116] T. Weber, A. Sklavos, and M. Meurer, "Imperfect channel-state information in MIMO transmission," *IEEE Transactions on Communications*, vol. 54, pp. 543 – 552, March 2006.

[117] S. Yang, T. Lv, and L. Hanzo, "Base Station Cooperation in MIMO-Aided Multi-User Multi-Cell Systems Employing Distributed Probabilistic Data Association Based Soft Reception," in *2011 IEEE International Conference on Communications (ICC)*, June 2011.

[118] S. Alamouti, "A simple transmit diversity technique for wireless communications," *IEEE Journal on Selected Areas in Communications*, vol. 16, pp. 1451–1458, Oct 1998.

[119] X. guo Tang and Z. Ding, "Error propagation in blind sequence estimation," *IEEE Communications Letters*, vol. 6, pp. 265–267, June 2002.

[120] A. R. A.J.Gines, E.J. Peralias, "Blind adaptive estimation of integral nonlinear errors in adcs using arbitrary input stimulus," *IEEE Transactions on Instrumentation and Measurement*, vol. 60, pp. 452–461, Feb 2011.

[121] J. F. X. Mestre, "Spatial filtering for pilot-aided wcdma systems: a semi-blind subspace approach," *IEEE Transactions on Signal Processing*, vol. 51, pp. 2665–2678, Oct 2003.

[122] J. Hayes, "Adaptive Feedback Communications," *IEEE Transactions on Communication Technology*, vol. 16, pp. 29–34, February 1968.

[123] J. Torrance and L. Hanzo, "Optimisation of switching levels for adaptive modulation in slow Rayleigh fading," *Electronics Letters*, vol. 32, pp. 1167–1169, Jun 1996.

[124] A. Goldsmith and S.-G. Chua, "Adaptive coded modulation for fading channels," *IEEE Transactions on Communications*, vol. 46, pp. 595–602, May 1998.

[125] S. X. Ng, C. Wong, and L. Hanzo, "Burst-by-burst adaptive decision feedback equalized TCM, TTCM, BICM and BICM-ID," in *IEEE International Conference on Communications (ICC 2001)*, vol. 10, pp. 3031–3035, 2001.

[126] L. hanzo and C. H. Wong and and M. S. Yee, *Adaptive Wireless Transceivers: Turbo-Coded, Turbo-Equalized and Space-Time Coded TDMA, CDMA and OFDM Systems*. John Wiley Sons, Ltd, 2002.

[127] J. K. Cavers, "Variable-Rate Transmission for Rayleigh Fading Channels," *IEEE Transactions on Communications*, vol. 20, pp. 15–22, Feb 1972.

[128] V. Hentinen, "Error Performance for Adaptive Transmission on Fading Channels," *IEEE Transactions on Communications*, vol. 22, pp. 1331–1337, Sep 1974.

[129] S. Massoumi and S. Kallel, "Adaptive trellis coded modulation for mobile communications," in *IEEE Pacific Rim Conference on Communications, Computers and Signal Processing*, pp. 538–541 vol.2, May 1991.

[130] S. Otsuki, S. Sampei, and N. Morinaga, "Square-QAM adaptive modulation/TDMA/TDD systems using modulation level estimation with Walsh function," *Electronics Letters*, vol. 31, pp. 169–171, Feb 1995.

[131] J. Torrance and L. Hanzo, "Optimisation of switching levels for adaptive modulation in slow Rayleigh fading," *Electronics Letters*, vol. 32, pp. 1167–1169, Jun 1996.

[132] A. Goldsmith and S.-G. Chua, "Variable-rate variable-power MQAM for fading channels," *IEEE Transactions on Communications*, vol. 45, pp. 1218–1230, Oct 1997.

[133] C. H. Lim and J. K. Jeong, "Adaptive modulation using multipath fading compensation," *Electronics Letters*, vol. 34, pp. 940–942, May 1998.

[134] M. Alouini and A. Goldsmith, "Capacity of Rayleigh fading channels under different adaptive transmission and diversity-combining techniques," *IEEE Transactions on Vehicular Technology* , vol. 48, pp. 1165–1181, Jul 1999.

[135] C. Wong and L. Hanzo, "Upper-bound performance of a wideband burst-by-burst adaptive modem," in *1999 IEEE 49th Vehicular Technology Conference*, vol. 3, pp. 1851–1855 vol.3, Jul 1999.

[136] A. Duel-Hallen, S. Hu, and H. Hallen, "Long-range prediction of fading signals," *IEEE Signal Processing Magazine*, vol. 17, pp. 62–75, May 2000.

[137] K. Hole, H. Holm, and G. Oien, "Adaptive multidimensional coded modulation over flat fading channels," *IEEE Journal on Selected Areas in Communications*, vol. 18, pp. 1153–1158, July 2000.

[138] C. Wong and L. Hanzo, "Upper-bound performance of a wide-band adaptive modem," *IEEE Transactions on Communications*, vol. 48, pp. 367–369, Mar 2000.

[139] V. Lau, "Design of adaptive bit interleaved tcm for rayleigh fading channels," in *2000 IEEE International Conference on Communications*, vol. 3, pp. 1188–1192 vol.3, 2000.

[140] B. Choi and L. Hanzo, "Optimum mode-switching-assisted constant-power single- and multicarrier adaptive modulation," *IEEE Transactions on Vehicular Technology*, vol. 52, pp. 536–560, May 2003.

[141] Y. J. Zhang and K. Letaief, "Single- and multi-user adaptive pragmatic trellis coded modulation for OFDM systems," in *IEEE Wireless Communications and Networking*, vol. 1, pp. 9–14 vol.1, March 2003.

[142] Z. Zhou, B. Vucetic, M. Dohler, and Y. Li, "MIMO systems with adaptive modulation," *IEEE Transactions on Vehicular Technology* , vol. 54, pp. 1828–1842, Sept 2005.

[143] D. Duong, G. Oien, and K. Hole, "Adaptive coded modulation with receive antenna diversity and imperfect channel knowledge at receiver and transmitter," *IEEE Transactions on Vehicular Technology*, vol. 55, pp. 458–465, March 2006.

[144] G. Caire and K. Kumar, "Information Theoretic Foundations of Adaptive Coded Modulation," *Proceedings of the IEEE*, vol. 95, pp. 2274–2298, Dec 2007.

[145] X. Wang, Q. Liu, and G. Giannakis, "Analyzing and Optimizing Adaptive Modulation Coding Jointly With ARQ for QoS-Guaranteed Traffic," *IEEE Transactions on Vehicular Technology*, vol. 56, pp. 710–720, March 2007.

[146] A. Svensson, "An Introduction to Adaptive QAM Modulation Schemes for Known and Predicted Channels," *Proceedings of the IEEE*, vol. 95, pp. 2322–2336, Dec 2007.

[147] X. Huang, H.-C. Wu, and Y. Wu, "Novel Pilot-Free Adaptive Modulation for Wireless OFDM Systems," *IEEE Transactions on Vehicular Technology*, vol. 57, pp. 3863–3867, Nov 2008.

[148] H. Jiang, L. Lai, R. Fan, and H. Poor, "Optimal selection of channel sensing order in cognitive radio," *IEEE Transactions on Wireless Communications*, vol. 8, pp. 297–307, Jan 2009.

[149] R. Fantacci, D. Marabissi, D. Tarchi, and I. Habib, "Adaptive modulation and coding techniques for OFDMA systems," *IEEE Transactions on Wireless Communications*, vol. 8, pp. 4876–4883, September 2009.

[150] I. Djordjevic, "Adaptive Modulation and Coding for Free-Space Optical Channels," *IEEE/OSA Journal of Optical Communications and Networking*, vol. 2, pp. 221–229, May 2010.

[151] J. Jiang, J. Thompson, and H. Sun, "A Singular-Value-Based Adaptive Modulation and Cooperation Scheme for Virtual-MIMO Systems," *IEEE Transactions on Vehicular Technology*, vol. 60, pp. 2495–2504, July 2011.

[152] G. Piro, L. Grieco, G. Boggia, F. Capozzi, and P. Camarda, "Simulating LTE Cellular Systems: An Open-Source Framework," *IEEE Transactions on Vehicular Technology*, vol. 60, pp. 498–513, Feb 2011.

[153] P. Li, H. Zhang, B. Zhao, and S. Rangarajan, "Scalable Video Multicast With Adaptive Modulation and Coding in Broadband Wireless Data Systems," *IEEE/ACM Transactions on Networking*, vol. 20, pp. 57–68, Feb 2012.

[154] N. Mastronarde and M. van der Schaar, "Joint Physical-Layer and System-Level Power Management for Delay-Sensitive Wireless Communications," *IEEE Transactions on Mobile Computing*, vol. 12, pp. 694–709, April 2013.

[155] J. Yoon, H. Zhang, S. Banerjee, and S. Rangarajan, "Video Multicast With Joint Resource Allocation and Adaptive Modulation and Coding in 4G Networks," *IEEE/ACM Transactions on Networking*, vol. 22, pp. 1531–1544, Oct 2014.

[156] L. Wan, H. Zhou, X. Xu, Y. Huang, S. Zhou, Z. Shi, and J.-H. Cui, "Adaptive modulation and coding for underwater acoustic ofdm," *IEEE Journal of Oceanic Engineering*, vol. 40, pp. 327–336, April 2015.

[157] A. Goldsmith, S. Jafar, I. Maric, and S. Srinivasa, "Breaking spectrum gridlock with cognitive radios: An information theoretic perspective," *Proceedings of the IEEE*, vol. 97, pp. 894 –914, May 2009.

[158] R. Manna, R. Louie, Y. Li, and B. Vucetic, "Cooperative spectrum sharing in cognitive radio networks with multiple antennas," *IEEE Transactions on Signal Processing*, vol. 59, pp. 5509 –5522, Nov. 2011.

[159] L. Hanzo, O. Alamri, M. El-Hajjar, and N. Wu, *Near-Capacity Multi-Functional MIMO Systems*. Wiley-IEEE Press, 2009.

[160] K. Ben Letaief and W. Zhang, "Cooperative communications for cognitive radio networks," *Proceedings of the IEEE*, vol. 97, pp. 878 –893, May 2009.

[161] Y. Li, "Distributed coding for cooperative wireless networks: An overview and recent advances," *IEEE Communications Magazine*, vol. 47, pp. 71 –77, August 2009.

[162] O. Simeone, I. Stanojev, S. Savazzi, Y. Bar-Ness, U. Spagnolini, and R. Pickholtz, "Spectrum leasing to cooperating secondary ad hoc networks," *IEEE Journal on Selected Areas in Communications*, vol. 26, pp. 203 –213, Jan. 2008.

[163] M. Ju and I.-M. Kim, "Relay selection with anc and tdbc protocols in bidirectional relay networks," *IEEE Transactions on Communications*, vol. 58, pp. 3500 –3511, December 2010.

[164] S. Ng and L. Hanzo, "On the MIMO channel capacity of multidimensional signal sets," *IEEE Transactions on Vehicular Technology*, vol. 55, pp. 528 – 536, March 2006.

[165] L. Hanzo, T. Liew, B. Yeap, R. Tee, and S. Ng, *Turbo Coding, Turbo Equalisation and Space-Time Coding for Transmission over Fading Channels*. Wiley-IEEE Press, 2011.

[166] A. Goldsmith, *Wireless Communication*. Cambridge University Press, England, 2005.

[167] T. Fouad, A. Hira, and M. Mukesh, "Joint optimization of physical layer parameters and routing in wireless mesh networks," in *The 9th IFIP Annual Mediterranean, Ad Hoc Networking Workshop (Med-Hoc-Net)*, pp. 1 –8, June 2010.

[168] L. K. Kong, S. Ng, R. Maunder, and L. Hanzo, "Maximum-throughput irregular distributed space-time code for near-capacity cooperative communications," *IEEE Transactions on Vehicular Technology* , vol. 59, pp. 1511 –1517, March 2010.

[169] H. Ochiai, P. Mitran, and V. Tarokh, "Design and analysis of collaborative diversity protocols for wireless sensor networks," in *IEEE 60th Vehicular Technology Conference, 2004 (VTC2004-Fall)*, vol. 7, pp. 4645 – 4649 Vol. 7, Sept. 2004.

[170] J. G. Proakis, *Digital communications*. New York: McGraw-Hill, 1995.

[171] H. Sun, S.X.Ng, and L. Hanzo, "Turbo trellis-coded hierarchical modulation assisted decode-and-forward cooperation," *IEEE Transactions on Vehicular Technology*, vol. PP, pp. 1–1, October 2014.

[172] G. Li, Z. Xu, C. Xiong, C. Yang, S. Zhang, Y. Chen, and S. Xu, "Energy-efficient wireless communications: tutorial, survey, and open issues," *IEEE Wireless Communications*, vol. 18, pp. 28 –35, December 2011.

[173] D. Michalopoulos, H. Suraweera, G. Karagiannidis, and R. Schober, "Amplify-and-forward relay selection with outdated channel estimates," *IEEE Transactions on Communications*, vol. 60, pp. 1278 –1290, May 2012.

[174] I. Krikidis, "Relay selection for two-way relay channels with mabc df: A diversity perspective," *IEEE Transactions on Vehicular Technology*, vol. 59, pp. 4620 –4628, Nov. 2010.

[175] R. Ahlswede, N. Cai, S.-Y. Li, and R. Yeung, "Network information flow," *IEEE Transactions on Information Theory,*, vol. 46, no. 4, pp. 1204–1216, 2000.

[176] R. Yeung, "Network coding: A historical perspective," *Proceedings of the IEEE*, vol. 99, no. 3, pp. 366–371, 2011.

[177] S.-Y. Li, Q. Sun, and Z. Shao, "Linear network coding: Theory and algorithms," *Proceedings of the IEEE*, vol. 99, no. 3, pp. 372–387, 2011.

[178] X. Zhang, A. Ghrayeb, and M. Hasna, "On relay assignment in network-coded cooperative systems," *IEEE Transactions on Wireless Communications,*, vol. 10, pp. 868 –876, March 2011.

[179] X. Li, T. Jiang, S. ui, J. An, and Q. Zhang, "Cooperative communications based on rateless network coding in distributed mimo systems [coordinated and distributed mimo]," *IEEE Wireless Communications,*, vol. 17, pp. 60 –67, June 2010.

[180] S. Sharma, Y. Shi, J. Liu, Y. Hou, S. Kompella, and S.F.Midkiff, "Network coding in cooperative communications: Friend or foe?," *IEEE Transactions on Mobile Computing*, vol. 11, no. 7, pp. 1073–1085, 2012.

[181] M. Xiao and M. Skoglund, "Multiple-user cooperative communications based on linear network coding," *IEEE Transactions on Communications,*, vol. 58, no. 12, pp. 3345–3351, 2010.

[182] J.L.Rebelatto, B. Uchoa-Filho, Y. Li, and B. Vucetic, "Adaptive distributed network-channel coding," *IEEE Transactions on Wireless Communications*, vol. 10, no. 9, pp. 2818–2822, 2011.

[183] J. Rebelatto, B. Uchoa-Filho, Y. Li, and B. Vucetic, "Multiuser cooperative diversity through network coding based on classical coding theory," *IEEE Transactions on Signal Processing*, vol. 60, no. 2, pp. 916–926, 2012.

[184] M. Xiao, J. Kliewer, and M. Skoglund, "Design of network codes for multiple-user multiple-relay wireless networks," *IEEE Transactions on Communications*, vol. 60, no. 12, pp. 3755–3766, 2012.

[185] L. Li, L. Wang, and L. Hanzo, "Generalized adaptive network coding aided successive relaying for noncoherent cooperation," *IEEE Transactions on Communications,*, vol. 61, pp. 1750–1763, May 2013.

[186] S.-Y. Li, R. Yeung, and N. Cai, "Linear network coding," *IEEE Transactions on Information Theory*, vol. 49, pp. 371–381, Feb 2003.

[187] R. Koetter and M. Medard, "An algebraic approach to network coding," *IEEE/ACM Transactions on Networking*, vol. 11, pp. 782–795, Oct 2003.

[188] R. Dougherty, C. Freiling, and K. Zeger, "Insufficiency of linear coding in network information flow," *IEEE Transactions on Information Theory*, vol. 51, pp. 2745–2759, Aug 2005.

[189] P. Popovski and H. Yomo, "hysical Network Coding in Two-Way Wireless Relay Channels," in *IEEE International Conference on Communications (ICC '07)*, pp. 707–712, June 2007.

[190] S. Katti, H. Rahul, W. Hu, D. Katabi, M. Medard, and J. Crowcroft, "XORs in the Air: Practical Wireless Network Coding," *IEEE/ACM Transactions on Networking*, vol. 16, pp. 497–510, June 2008.

[191] R. Koetter and F. Kschischang, "Coding for Errors and Erasures in Random Network Coding," *IEEE Transactions on Information Theory*, vol. 54, pp. 3579–3591, Aug 2008.

[192] R. Zhang and L. Hanzo, "Coding schemes for energy efficient multi-source cooperation aided uplink transmission," *IEEE Signal Processing Letters,*, vol. 16, pp. 438 –441, May 2009.

[193] D. Nguyen, T. Tran, T. Nguyen, and B. Bose, "Wireless broadcast using network coding," *IEEE Transactions on Vehicular Technology*, vol. 58, pp. 914–925, Feb 2009.

[194] H. V. Nguyen, S. X. Ng, and L. Hanzo, "Performance bounds of network coding aided cooperative multiuser systems," *IEEE Signal Processing Letters,*, vol. 18, pp. 435 –438, July 2011.

[195] H. Nguyen, S. Ng, and L. Hanzo, "Irregular convolution and unity-rate coded network-coding for cooperative multi-user communications," *IEEE Transactions on Wireless Communications*, vol. 12, pp. 1 –13, January 2013.

[196] A. Keshavarz-Haddad and R. Riedi, "Bounds on the Benefit of Network Coding for Wireless Multicast and Unicast," *IEEE Transactions on Mobile Computing*, vol. 13, pp. 102–115, Jan 2014.

[197] Y. J. Chun, M. Hasna, and A. Ghrayeb, "Adaptive network coding for spectrum sharing systems," *IEEE Transactions on Wireless Communications*, vol. 14, pp. 639–654, Feb 2015.

[198] M. Xiao and M. Skoglund, "Multiple-user cooperative communications based on linear network coding," *IEEE Transactions on Communications,*, vol. 58, pp. 3345 –3351, December 2010.

[199] SAGE, *Open source mathematics software*. Available: http://wwwsagemath.org/.

[200] L. Hanzo and L. L. Yang and E. L. Kuan and K. Yen, *Single- and Multi-Carrier DS-CDMA: Multi-User Detection, Space-Time Spreading, Synchronisation, Networking and Standards*. IEEE Wiley Press, 2003.

[201] H. V. Nguyen, Z. barbar, S. X. Ng, M. Mazzotti, L. Iacobelli and L. Hanzo, "Network coded MIMO aided cooperative communications in the ambulance-and-emergency area," in *MoWNet'2014*, September 2014.

[202] W. Liang, S. X. Ng, and L. Hanzo, "Cooperative communication between cognitive and primary users," *IET Communications*, vol. 7, no. 17, pp. 1982–1992, 2013.

[203] S. Bayat, R. Louie, Z. Han, Y. Li, and B. Vucetic, "Distributed stable matching algorithm for physical layer security with multiple source-destination pairs and jammer nodes," in *2012 IEEE Wireless Communications and Networking Conference (WCNC)*, pp. 2688 –2693, April 2012.

[204] L. Jayasinghe, N. Rajatheva, and M. Latva-aho, "Optimal power allocation for pnc relay based communications in cognitive radio," in *2011 IEEE International Conference on Communications (ICC)*, pp. 1–5, June 2011.

[205] L. Zhang, Y.-C. Liang, and Y. Xin, "Joint beamforming and power allocation for multiple access channels in cognitive radio networks," *IEEE Journal on Selected Areas in Communications*, vol. 26, pp. 38–51, Jan 2008.

[206] M. Tao and Y. Liu, "Spectrum leasing and cooperative resource allocation in cognitive ofdma networks," *Journal of Communications and Networks*, vol. 15, pp. 102–110, Feb 2013.

[207] Y. Pei and Y. Liang, "Cooperative spectrum sharing with bidirectional secondary transmissions," *IEEE Transactions on Vehicular Technology*, vol. 64, pp. 108–117, Jan 2015.

[208] M. Shamaian, S. H. Lee, S. Vishwanath, and H. Vikalo, "Distributed algorithms for spectrum access in cognitive radio relay networks," *IEEE Journal on Selected Areas in Communications*, vol. 30, pp. 1947 –1957, November 2012.

[209] J. Tadrous, A. Sultan, M. Nafie, and A. El-Keyi, "Power control for constrained throughput maximization in spectrum shared networks," in *IEEE Global Telecommunications Conference (GLOBECOM 2010)*, pp. 1–6, Dec 2010.

[210] H. Zhou, B. Liu, Y. Liu, N. Zhang, L. Gui, Y. Li, X. Shen, and Q. Yu, "A cooperative matching approach for resource management in dynamic spectrum access networks," *IEEE Transactions on Wireless Communications*, vol. 13, pp. 1047–1057, February 2014.

[211] P. Lin, J. Jia, Q. Zhang, and M. Hamdi, "Dynamic spectrum sharing with multiple primary and secondary users," *IEEE Transactions on Vehicular Technology,*, vol. 60, pp. 1756 –1765, may 2011.

[212] D. P. Bertsekas, "A distributed asynchronous relaxation algorithm for the assignment problem," in *24th IEEE Conference on Decision and Control,*, vol. 24, pp. 1703 –1704, Dec. 1985.

[213] C. An, L. Zhang, and W. Liu, "A spectrum allocation algorithm based on matching game," in *WiCom '09. 5th International Conference on Wireless Communications, Networking and Mobile Computing*, pp. 1 –3, Sept. 2009.

[214] V. Asghari and S. Aissa, "Resource management in spectrum-sharing cognitive radio broadcast channels: Adaptive time and power allocation," *IEEE Transactions on Communications*, vol. 59, no. 5, pp. 1446–1457, 2011.

[215] M. J. Osborne, *An Introduction to Game Theory*. Oxford University Press, 2004.

[216] R. J. Aumann and M. Maschler, *Repeated games with incomplete information*. The MIT Press, 1995.

[217] R.B. Myerson, *Game Theory Analysis of Conflict*. Harvard University Press, 1997.

[218] W. Saad, Z. Han, M. Debbah, A. Hjorungnes, and T. Basar, "Coalitional game theory for communication networks," *IEEE Signal Processing Magazine*, vol. 26, no. 5, pp. 77–97, 2009.

[219] O. Oyman, N. Laneman, and S. Sandhu, "Multihop relaying for broadband wireless mesh networks: From theory to practice," *IEEE Communications Magazine*, vol. 45, pp. 116 –122, November 2007.

[220] O. Simeone, Y. Bar-Ness, and U. Spagnolini, "Stable throughput of cognitive radios with and without relaying capability," *IEEE Transactions on Communications*, vol. 55, no. 12, pp. 2351–2360, 2007.

[221] H. N. Vu and H.-Y. Kong, "Joint subcarrier matching and power allocation in ofdm two-way relay systems," *Journal of Communications and Networks*, vol. 14, pp. 257 –266, June 2012.

[222] T. Oechtering and A. Sezgin, "A new cooperative transmission scheme using the space-time delay code," in *2004. ITG Workshop on Smart Antennas*, pp. 41–48, March 2004.

[223] C. Zhai, W. Zhang, and P. Ching, "Cooperative spectrum sharing based on two-path successive relaying," *IEEE Transactions on Communications*, vol. 61, pp. 2260–2270, June 2013.

[224] C. Zhai and W. Zhang, "Adaptive spectrum leasing with secondary user scheduling in cognitive radio networks," *IEEE Transactions on Wireless Communications*, vol. 12, pp. 3388–3398, July 2013.

[225] H. Hindi, "A tutorial on convex optimization," in *Proceedings of the 2004 American Control Conference*, vol. 4, pp. 3252–3265 vol.4, June 2004.

[226] H. Hindi, "A tutorial on convex optimization II: duality and interior point methods," in *American Control Conference*, pp. 11 pp.–, June 2006.

Subject Index

Author Index

Z